Master's thesis

NTNU
Norwegian University of Science and Technology
Faculty of Engineering
Department of Geoscience and Petroleum

Sander Boger Øren
Eskil Klingenberg

# Subsea System for CO2 Injection

Master's thesis in Subsea Technology
Supervisor: Tor Berge Stray Gjersvik
Co-supervisor: Sigbjørn Sangesland, Audun Faanes, Bernt Johan Leira

June 2024

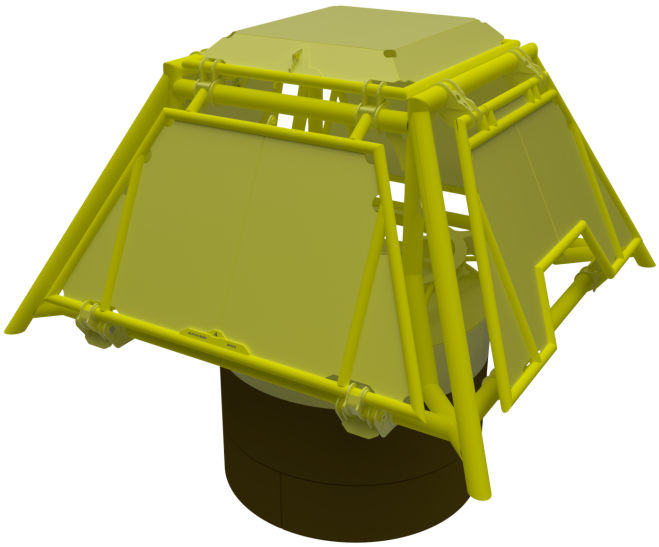

NTNU
Norwegian University of
Science and Technology

Sander Boger Øren
Eskil Klingenberg

# Subsea System for CO2 Injection

Master's thesis in Subsea Technology
Supervisor: Tor Berge Stray Gjersvik
Co-supervisor: Sigbjørn Sangesland, Audun Faanes, Bernt Johan Leira
June 2024

Norwegian University of Science and Technology
Faculty of Engineering
Department of Geoscience and Petroleum

NTNU
Norwegian University of
Science and Technology

# Preface

This master thesis has been conducted at the Department of Geoscience and Petroleum in cooperation with the Department of Marine Technology at the Norwegian University of Science and Technology (NTNU). The thesis is written in the spring semester of 2024, where the projects aim is to develop a conceptual subsea system to challenge conventional solutions utilized in today's industry.

# Acknowledgment

We would like to express our gratitude to our supervisors at the Department of Geoscience and Petroleum, Tor Berge Stray Gjersvik and Sigbjørn Sangesland, for their invaluable guidance and support throughout the course of the project. Additionally, we extend our thanks to Audun Faanes from Equinor for his insights on the concept and to Bernt Johan Leira for his advice during the project's scope and his expertise in strength analysis.

# Summary

Interest and investments in carbon capture and storage (CCS) are increasing, creating a need for specialized solutions to streamline the process. Currently the industry utilizes equipment designed for production purposes. This thesis explores possible design solutions for subsea systems used for CO2 injection, focusing on developing a modularized concept for the template structure. The goal is to achieve a compact design with reusable modules to reduce both cost as emissions.

To investigate the potential of this design concept, a CAD model is created based on industry standards and requirements. The model is divided into 3 modules with the outer protective frame, inner frame and suction anchor. Alternative material such as aluminum alloy 5083 has been incorporated for the outer protective shell to lower the weight and emissions for the template. The model is subjected to a series of standardized load cases required for installation on the Norwegian continental shelf to assess the behavior and structural integrity of the structure. This assessment is performed using FEM analysis of the complete template structure. Based on the analysis results, necessary design changes and optimizations is made before a final model is presented.

Additionally, the thesis includes an early design phase for the x-mas tree intended for installation within the template. No CAD model or structural analysis is conducted for the tree design, but a possible configuration is discussed to showcase the potential of a well-integrated template and x-mas tree system.

The final concept demonstrates strong performance under various loading conditions and offers competitive properties in terms of weight, size and cost. The total weight of the final template design excluding the suction anchor is 24.596 kilograms, which is approximately 75% lighter than the integrated template structure used for the injection well in the Northern Lights project. Despite primarily using an aluminum alloy for the template frame, the material cost is also reduced with an estimated 15% due to the lower mass. The concepts production phase, installation phase, and part reusability is also discussed and compared to existing solution.

# Sammendrag

Interessen og investeringene i karbonfangst og lagring øker, og det skaper et behov for spesialiserte løsninger for å effektivisere prosessen. For øyeblikket benytter industrien utstyr som er designet for produksjonsformål. Denne oppgaven utforsker mulige designløsninger for undervannssystemer brukt til CO2-injeksjon, med fokus på å utvikle et modul basert konsept for templatestrukturen. Målet er å oppnå et kompakt design med gjenbrukbare moduler for å redusere både kostnader og utslipp.

For å undersøke potensialet i dette konseptet, er det konstruert en CAD-modell basert på industristandarder og krav. Modellen er delt inn i tre moduler: den ytre beskyttelsesrammen, den indre rammen og sugeankeret. Alternative materialer som aluminiumlegering 5083 er blitt brukt i den ytre beskyttelsesskallet for å redusere vekten og utslippene fra templaten. Modellen ble utsatt for en rekke standardiserte lasttilfeller som kreves for installasjon på den norske kontinentalsokkelen for å vurdere strukturens oppførsel og integritet. Denne vurderingen er utført ved hjelp av FEM-analyser av hele templatestrukturen. Basert på analyse resultatene blir nødvendige designendringer og optimaliseringer gjennomført før den endelige modellen er presentert.

I tillegg inkluderer oppgaven en tidlig designfase for juletreet som er ment for installasjon i templaten. Ingen CAD-modell eller strukturanalyse er utført for juletreets design, men en mulig konfigurasjon er diskutert for å vise potensialet i et godt integrert ramme- og juletre system.

Det endelige konseptet viser gode verdier under forskjellige lastforhold og tilbyr konkurransedyktige egenskaper når det gjelder størrelse og vekt. Den totale vekten av den endelige templatestrukturen ekskludert sugeankeret er 24.596 kilogram, som er omtrent 75% lettere enn den integrerte templatestrukturen som brukes for injeksjonsbrønnen i Northern Lights prosjektet. Selv om det hovedsakelig er bruk av en aluminiumslegering for konstruksjonen, er materialkostnadene også redusert med omtrent 15% på grunn av den lavere massen. Konseptets produksjonsfase, installasjonsfase og delenes gjenbrukbarhet blir også diskutert og sammenlignet med eksisterende løsninger.

# Table of Contents

Preface ..... i
Summary ..... ii
Sammendrag ..... iv
Table of Contents ..... iv
List of Figures ..... ix
List of Tables ..... xii
List of Equations ..... xiii
List of Abbreviations ..... xiv
1. Introduction ..... 1
1.1 Background ..... 1
1.2 Objective ..... 1
1.3 Limitations ..... 2
1.4 Report structure ..... 3
2. Previous Published Knowledge ..... 4
2.1 Carbon Capture and Storage - CCS ..... 4
2.1.1 The Three Phases of CCS ..... 5
2.1.1.1 Capture Phase ..... 5
2.1.1.2 Transportation Phase ..... 6
2.1.1.3 Storage Phase ..... 6
2.2 Northern Lights ..... 10
2.2.1 Northern Lights Template Structure ..... 11
2.2.2 Vertical X-mas Tree ..... 11
2.2.3 Tie-in Systems ..... 12
2.2.4 Suction Anchor ..... 13
2.2.5 Trawl Protection ..... 14
2.2.6 Installation, Operation and Removal ..... 15
2.3 SMEAHEIA ..... 16
2.3.1 Infrastructure ..... 16
2.3.2 Reservoirs ..... 17
2.3.2.1 The Viking Group ..... 17
2.3.2.2 Dunlin Groups ..... 18
2.3.3 Potential ..... 18
2.4 CO2 Injection Environment Oil vs. Gas Production ..... 19
2.4.1 Injection Environment ..... 19

2.4.2 Production Environment ..... 21
2.4.3 Reservoir ..... 21
2.5 Aluminum ..... 23
2.5.1 Aluminium Alloys ..... 23
2.5.1.1 5083-H116 Aluminium Alloy ..... 24
2.5.2 Welding of Aluminium ..... 26
2.5.2.1 Certificates and Approval ..... 26
2.5.2.2 Challenges of Aluminium Welding ..... 26
2.5.2.3 Arc Welding – Mig and Tig ..... 27
2.5.2.4 Laser Welding - LW ..... 33
2.5.2.5 Friction Stir Welding ..... 35
2.6 Steel ..... 37
2.6.1 Steel Alloys ..... 37
2.6.1.1 Stainless Steel: ..... 37
2.6.1.2 Carbon Steel: ..... 37
2.6.1.3 Tool Steel: ..... 38
2.6.1.4 Alloy Steel: ..... 38
2.6.2 Structural Steel ..... 38
2.6.2.1 S355G ..... 39
2.7 Corrosion ..... 41
2.7.1 Galvanic Corrosion ..... 41
2.7.2 Passive Cathodic Protection ..... 43
2.7.3 Active Cathodic Protection ..... 44
2.7.4 Protective Coating ..... 45
3. Concept Presentation ..... 46
3.1 Choice of Direction ..... 46
3.1.1 Modularization of Layout ..... 46
3.1.2 Single Centered Suction Anchor ..... 47
3.1.3 Material Choices ..... 48
3.1.3.1 Outer Frame ..... 49
3.1.3.2 Inner Frame ..... 49
3.1.3.3 Suction Anchor ..... 50
3.2 Design Criterion ..... 51
3.2.1 Design for Overtrawability ..... 51
3.2.2 Hatch Design ..... 52
3.3 Presentation of Model ..... 53
3.3.1 Aluminum Frame ..... 53

3.3.1.1 Side Hatch ..... 54
3.3.1.2 Top Hatch ..... 56
3.3.1.3 Hinges ..... 57
3.3.1.4 Complete Aluminum Module ..... 61
3.3.2 Steel Module ..... 64
3.3.3 Suction Anchor ..... 67
3.3.4 Complete Model ..... 68
4. Structural Analysis ..... 71
4.1 Loads ..... 71
4.1.1 Static Loads ..... 72
4.1.2 Trawling Loads ..... 73
4.1.3 Dropped Objects ..... 74
4.2 Set-up ..... 75
4.2.1 Simplified Model ..... 76
4.2.2 Symmetry ..... 76
4.2.3 Meshing ..... 77
4.2.4 Constraints ..... 77
4.2.5 Material Choice and Properties ..... 78
4.3 Aluminum Module ..... 80
4.3.1 Welding of Aluminum ..... 80
4.3.2 Main Frame ..... 82
4.3.1.1 Trawlnet Friction ..... 82
4.3.1.2 Trawlboard Overpull ..... 84
4.2.2 Side Hatches ..... 85
4.2.2.1 Crane Ship Heave ..... 85
4.2.2.2 Parked ROV ..... 86
4.2.2.3 Dropped Objects ..... 88
4.2.3 Top Hatch ..... 90
4.2.3.1 Crane Ship Heave ..... 90
4.2.3.2 Dropped Objects ..... 92
4.3 Steel Module ..... 94
4.3.1 Trawlnet Friction ..... 94
4.4 Corrosion Protection ..... 97
4.4.1 Steel Module Protection ..... 97
4.4.2 Aluminum Module Protection ..... 98
4.4.3 Isolating Gasket ..... 99
4.4.3.1 Bolts and Washers: ..... 99

4.4.3.2 Insulation Gasket: ..... 100
4.5 Design of Flange and Bolts ..... 101
4.5.1 Complete Design of Flanges ..... 102
5. Presentation and Comparison of Final Model ..... 104
5.1 Presentation of Final Model Concept ..... 104
5.1.1 Aluminum Frame ..... 104
5.1.2 Front and Rear Hatch ..... 106
5.1.3 Top Hatch ..... 107
5.1.4 Steel Module ..... 108
5.1.5 Complete Final Model ..... 110
5.2 Installation Process ..... 113
5.2.1 Installation of Suction Anchor ..... 113
5.2.2 Installation of Template Frame ..... 114
5.3 Subsea X-mas Tree ..... 118
5.3.1 Size Reduction ..... 118
5.3.2 Module Based Design ..... 118
5.4 Economical Drivers ..... 121
5.4.1 Material Cost ..... 121
5.4.2 Installation Phase ..... 122
5.4.3 Manufacturing Phase ..... 123
5.4.4 Reuse of Components ..... 123
6. Discussion ..... 124
6.1 Possibilities Within the Concept Design ..... 124
6.2 Choice of Material ..... 126
6.3 Limitations of FEM Analysis ..... 128
6.4 Alternative Configurations ..... 129
6.4.1 Simplification and Material Considerations ..... 129
6.4.2 Design Benefits ..... 129
6.4.3 Weight Considerations ..... 129
6.4.4 Conclusion ..... 130
7. Conclusion ..... 131
8. Future work ..... 133
Bibliography ..... 134
Appendix A ..... 144
A.1 Penetration Depth Suction Anchor ..... 144
A.2 Required Suction Pressure for Anchor ..... 148

A.3 Horizontal Drift of Anchor During Installation ..... 149
Appendix B ..... 152
B.1 Aluminum Frame - Trawlnet Friction ..... 152
B.2 Aluminum Frame - Trawlboard Overpull ..... 154
B.3 Front Hatch - Heave Motion ..... 156
B.4 Front Hatch – ROV Parking ..... 159
B.5 Front Hatch – Dropped Object 100 mm ..... 161
B.6 Top Hatch – Heave Motion ..... 164
B.7 Top Hatch – Dropped Object 100 mm ..... 167
B.8 Top Hatch – Trawlnet Friction ..... 170
B.9 Steel frame – Trawlnet Friction ..... 172
Appendix C ..... 175
C.1 Aluminum Frame – Trawlnet Friction ..... 175
C.2 Aluminum Frame – Trawlboard Overpull ..... 177
C.3 Front Hatch – Heave Motion ..... 178
C.4 Front Hatch – ROV Parking ..... 179
C.5 Front Hatch – Dropped Object 500 mm ..... 180
C.6 Front Hatch – Dropped Object 100 mm ..... 181
C.7 Top Hatch – Heave Motion ..... 182
C.8 Top Hatch – Dropped object 100 mm ..... 183
C.9 Top Hatch – Trawlnet Friction ..... 184
C.10 Steel Frame – Trawlnet Friction ..... 185

# List of Figures

Figure 1: Storage Overview and Core Sample [8] ..... 7
Figure 2: CO2 Trapping. [9] ..... 9
Figure 3: Langskip and Northern Lights Project Scope [11]. ..... 10
Figure 4: Northern Lights Template Structure. [10] ..... 11
Figure 5: Aker Solution Vertical X-mas Tree used in NL Project [10]. ..... 12
Figure 6: Aker Solution Horizontal Connection System (HCS) [10]. ..... 13
Figure 7: NL Project Sealine Protection Cover (SPC). [10] ..... 14
Figure 8: Glass Reinforced Plastic- and Steel Protection Covers. [10]..... 15
Figure 9: Smeaheia Project Scope [14]. ..... 16
Figure 10: Viking Group Geography [15]..... 17
Figure 11: P-T Diagram. [18]..... 19
Figure 12: MIG Welding [34]. ..... 28
Figure 13: TIG Welding [34]. ..... 29
Figure 14: Extent of HAZ in Welds [35]. ..... 31
Figure 15: Melt Pool Formation, a) Conduction b) Keyhole c) Keyhole with Porosity [39]. . 34
Figure 16: Microstructures in FSW [46]. ..... 36
Figure 17: Passive Cathodic Protection [59]..... 43
Figure 18: Active Cathodic Protection [59]. ..... 44
Figure 19: Subsea Coating [61]..... 45
Figure 20: Illustration of Stability for a Four-Anchor Config. Compared to a Single Anchor.48
Figure 21: CAD Model - Aluminum Frame..... 53
Figure 22: CAD Model - Front and Rear Hatches. ..... 54
Figure 23: CAD Model - Front Hatch with Illustration of Parked ROV [66]..... 55
Figure 24: CAD Model - Side Hatches. ..... 56
Figure 25: CAD Model - Top Hatch. ..... 56
Figure 26: CAD Model - Front Hinge with Hatch Closed..... 57
Figure 27: CAD Model - Front Hinge with Hatch Open. ..... 58
Figure 28: CAD Model - Side Hinge Closed. ..... 59
Figure 29: CAD Model - Side Hinges Opened. ..... 60
Figure 30: CAD Model - Side Hatch Locking Mechanism. ..... 60
Figure 31: CAD Model - Top Hinge in Open Position. ..... 61
Figure 32: CAD Model - Complete Aluminum Module with Dimensions..... 62

Figure 33: CAD Model - Steel Module. ..... 64
Figure 34: CAD Model - Steel Module with Connection Point and Locking Bolt. ..... 65
Figure 35: CAD Model - Suction Anchor. ..... 67
Figure 36: CAD Model - Fully Assembled Concept with Front, Rear and Top Hatch Open. . 68
Figure 37: CAD Model - Fully Assembled Concept Installed at Seabed - Closed Hatches. ... 69
Figure 38: Building the Mathematical and FE Model [69]. ..... 75
Figure 39: Ansys Model - Friction Load with Resulting Von-Mises Stresses. ..... 82
Figure 40: Ansys Model - Friction Load with Resulting von Mises Stresses in Top Corner. . 83
Figure 41: Ansys Model - Trawlboard Overpull Load with Resulting von Mises Stresses. .... 84
Figure 42: Ansys Model - Front Hatch - Heave Motion and Resulting von Mises Stresses. ... 85
Figure 43: Ansys Model - Bracket for the Front Hatch During Heave Motion. ..... 86
Figure 44: Ansys Model - Front Hatch with Parked ROV. ..... 87
Figure 45: Ansys Model - Hinge Area on Front Hatch During ROV Touchdown. ..... 87
Figure 46: Ansys Model - Front Hatch with von Mises Stresses - 100 mm Dropped Object.. 89
Figure 47: Ansys Model - Front Hatch with Closeup of Dropped Object 100 mm. ..... 90
Figure 48: Ansys Model - Top Hatch with Resulting von Mises Stress from Heave Motion. 91
Figure 49: Ansys Model - Detailed view of Top Hatch with Heave Motion. ..... 92
Figure 50: Ansys Model - Top Hatch with von Mises stresses for 100 mm Dropped Object. 92
Figure 51: Ansys Model - Detailed Impact Area with 100 mm Dropped Object. ..... 93
Figure 52: Ansys Model - Steel Frame with Corresponding Loads from Trawlnet Friction. .. 95
Figure 53: Ansys Model - Steel Module for Trawlnet Friction Load ..... 95
Figure 54: Ansys Model - Deformation of Steel Module for Trawlnet Friction Load. ..... 96
Figure 55: Aluminum and Carbon Steel Separation [73]. ..... 100
Figure 56: CAD Model - Flange Design Between the Steel- and Aluminum Module. ..... 102
Figure 57: CAD Model - Finished Aluminum Frame. ..... 105
Figure 58: CAD Model - Finished Front and Rear Hatch. ..... 106
Figure 59: CAD Model - Finished Top Hatch. ..... 107
Figure 60: CAD Model - Inside of Finished Top Hatch. ..... 108
Figure 61: CAD Model - Finished Steel Module. ..... 108
Figure 62: CAD Model - Finished Template Structure in its Closed Position. ..... 110
Figure 63: CAD Model - Finished Template Structure in its Fully Open Position. ..... 111
Figure 64: Illustration - Template Frame During the Lifting Phase of the Installation. ..... 115
Figure 65: Illustration - Template Frame Positioned Correctly Above the Suction Anchor. 116
Figure 66: Illustration - Template Frame Installed at Anchor with Attached Locking Bolt.. 117

Figure 67: Illustration - Module-based X-mas Tree Concept [62], page 26. ..... 119
Figure 68: Installation Vessel Size [81]. ..... 122
Figure 69 - A.3: Raynolds Number with Corresponding Drag Coefficient [83]. ..... 150

# List of Tables

Table 1: Aluminium Alloy Composition [25]. ..... 24
Table 2: Chemical Composition of Alloy 5083 [26]. ..... 24
Table 3: Physical Properties of Alloy 5083-H116 [28]. ..... 25
Table 4: Aluminium Preheating and Intermediate Pass Temperature [36]. ..... 30
Table 5: HAZ Factor 5083-H116 Plate [35]. ..... 30
Table 6: HAZ Factor 5083-H116 Tube [35]. ..... 31
Table 7: Weld Filler Material for Alloy 5083 [35]. ..... 32
Table 8: EU vs. US Structural Steel Notation [50]. ..... 38
Table 9: Chemical Composition - S355 [53]. ..... 39
Table 10: Mechanical Properties - S355G [52]. ..... 40
Table 11: Galvanic Series Table [58]. ..... 42
Table 12: Overview of Properties of Aluminum Module. ..... 63
Table 13: Overview of Properties of Steel Module. ..... 66
Table 14: Overview of Properties of Full Concept Model. ..... 70
Table 15: Static Loads [65]. ..... 72
Table 16: Trawling Loads [64]. ..... 73
Table 17: Dropped Objects. [64] ..... 74
Table 18: Strength Characteristics for 5083 [35] and S355 [52] incl. SF. ..... 79
Table 19: Yield Strength for Welding Filler Material incl. SF [35]. ..... 81
Table 20: Yield Strength in HAZ for 5083-H116 incl. SF. [35] ..... 81
Table 21: Reaction Forces Obtained from Aluminum Module Flange ..... 94
Table 22: Surface Preparation and Coating - Carbon Steel [70]. ..... 97
Table 23: Surface Preparation and Coating - Stainless Steel [70]. ..... 98
Table 24: List of Variables for Bolt Design [75]. ..... 101
Table 25: Nominal Stress Areas with Thread Diameters from ISO-898-1-2013 [76]. ..... 102
Table 26: Component Overview First vs. Final Model ..... 112
Table 27: Material Costs ..... 121
Table 28 - A.1: Undrained Shear Strength at Specific Penetration Depths. ..... 144
Table 29 - A.1: Data Properties - Calculations of Penetration Depth for Suction Anchor. ..... 145
Table 30 - A.3: Component and Data Properties - Calculations of Horizontal Drift. ..... 149

# List of Equations

Equation 1: External Pressure. ..... 20
Equation 2: Mass Flow through Injection Tubing. ..... 20
Equation 3: Cross Section Area of 6-inch Tubing. ..... 20
Equation 4: Injection Velocity. ..... 20
Equation 5: Oil Reservoir Pressure. ..... 21
Equation 6: Estimated Conversion of Joules to Newton Force. ..... 74
Equation 7: Calculation of Bolt Dimensions from EN 1993-1-8 [74]. ..... 101
Equation 8 - A.1: Buoyancy factor for aluminum and steel. ..... 145
Equation 9 - A.1: Total Wet Weight. ..... 145
Equation 10 - A.1: Area of top section. ..... 145
Equation 11 - A.1: Area of tip section. ..... 146
Equation 12 - A.1: Area of outer wall section. ..... 146
Equation 13 - A.1: Area of wall section. ..... 146
Equation 14 - A.1: Wet weight of suction anchor. ..... 146
Equation 15 - A.1: Average undrained shear strength. ..... 146
Equation 16 - A.1: Total wet weight. ..... 146
Equation 17 - A.1: Total penetration resisting force. ..... 147
Equation 18 – A.2: Additional Penetration Force. ..... 148
Equation 19 - A.2: Required Suction Pressure. ..... 148
Equation 20 - A.3: Reynolds Number for Anchor and Wireline. ..... 149
Equation 21 - A.3: Drag Force for Wireline (WL) and Anchor (A). ..... 150
Equation 22 - A.3: Equilibrium of Crane Tip. ..... 151

# List of Abbreviations

**CCS** – Carbon Capture and Storage
**CO2** – Carbon Dioxide
**MTPA** – Million Tons per Annum
**EOR** – Enhanced Oil Recovery
**LCO2** – Liquid Carbon Dioxide
**NL** – Northern Lights
**NCS** – Norwegian Continental Shelf
**VXT** – Vertical X-mas Tree
**BOP** – Blowout Preventer
**TH** – Tubing Hanger
**WH** – Wellhead
**VMX** – Vertical Manifold to XT
**ROV** – Remote Operated Vehicle
**HCS** – Horizontal Connection System
**ITS** – Integrated Template Structure
**GRP** – Glass Reinforced Plastic
**LWI** – Light Well Intervention
**HAZ** – Heat Affected Zone
**MIG** – Metal Inert Gas
**TIG** – Tungsten Inert Gas
**FSW** – Friction Stir Welding
**LW** – Laser Welding
**TMAZ** – Thermos-Mechanically Affected Zone
**NZ** – Nugget Zone
**GACP** – Galvanic Anode Cathodic Protection
**ICCP** – Impressed Current Cathodic Protection
**TSA** – Thermal Sprayed Aluminum
**PLS** – Progressive Collapse Limit State
**ULS** – Ultimate Limit State
**OD** – Outside Diameter
**SF** – Safety Factor
**YS** – Yield Strength
**TS** – Tensile Strength
**FEM** – Finite Element Method
**CPS** – Coating Procedure Specification
**CPT** – Coating Procedure Test
**MDFT** – Minimum Dry Film Thickness
**PTFE** – Polytetrafluoroethylene
**PMV** – Production Master Valve
**DHSV** – Downhole Safety Valve
**PWV** – Production Wing Valve

# 1. Introduction

## 1.1 Background

The interest in carbon capture and storage (CCS) has increased in recent years due to rising concerns about global warming. Recognizing the potential of CCS to significantly reduce emissions on a global scale, Norway has positioned itself at the forefront of the technological developments in this field. The economic benefits are compelling, particularly as the cost of emitting carbon dioxide (CO2) directly into the atmosphere steadily increases. This cost is driven by emission-trading and taxation policies that has seen a significant rise in recent years [1]. This trend will inevitably render CCS as an increasingly attractive option for major corporations seeking to manage their excess CO2 emissions.

To maintain its leadership in this market, Norway must adopt an early investment strategy that prioritizes industry-leading solutions for efficient CO2 injection. The current approach primarily relies on equipment optimized for production wells, which can result in excessive use of materials and overall cost. This master thesis will therefore focus on exploring new design options and possibilities for a pure subsea system for CO2 injections.

## 1.2 Objective

The objective of this study is to identify new design opportunities for a single satellite well optimized for pure CO2 injection on the Norwegian continental shelf (NCS). This is done to explore potential cost reductions associated with minimized material usage, simplified installation procedures, reduced footprint, and opportunities for component reusability. The main advantage of achieving this will be to make CCS a serviceable operation in an earlier stage, regarding the steady rise of emissions trading prices for CO2.

To accomplish this a model will be constructed with a focus on the qualities mentioned above. The model will represent a complete subsea system to showcase the potential benefits compared to the solutions used today. Particularly, it will be compared to the Northern Lights project, which currently hosts the only completed CCS well on the NCS.

The main objectives of the study is described below in chronological order.

- Explore and understand the industry standards and solution used today regarding CCS systems.
- Gather data on relevant material properties and operability to better access the design opportunities of alternative materials.
- Construct a conceptual model representing new design philosophies with potential improvements regarding the footprint, weight, material selection, installation proses and reusability.
- Define a set of loading cases relevant for the subsea system according to industry standards and regulations.
- Preform a structural analysis on the conceptual model to establish an understanding of the behavior and structural integrity of the system during loading.
- Redesign and dimension the model according to the data obtained in the structural analysis.
- Compare the final concept model to the solution used today regarding cost, operability and emissions.

## 1.3 Limitations

The main limitation in this study is the scope of work associated with designing a complete subsea system. As there is a vast range of standards and design details to be considered, some limitations must be set to limit the time use. The goal here is to establish the primary design criterions to ensure a sensible solution where only minor changes must be made to the structure in order to complete the requirements. This limitation will somewhat reduce the accuracy of the associated costs, dimensions and footprint regarding the complete structure.

Another limitation for the structural analysis is the student license for the Ansys program. This limits the maximum number of elements and nodes that can be used in one single analysis. As the model represents a big system this can result in a decreased accuracy for the simulation work. The effect of this will be reduced by utilizing symmetry and tactical division of the model structure.

## 1.4 Report structure

The structure of this report is designed to first gather relevant information, laying the groundwork for the subsequent design phase. It then discusses design solutions, incorporating the resulting data from the structural analysis and cost estimations. The work done in each chapter is outlined below:

- Chapter one will introduce the theses, discussing the background and objective.
- Chapter two begins by exploring the necessary data regarding current solutions and the structural properties of relevant materials. This information will lay the groundwork for the subsequent chapters.
- Chapter tree focuses on the discussion of design choices and criteria, before a conceptual model of the template structure is then presented.
- Chapter four introduces the chosen load cases and set-up process. The results of the structural analysis are then presented and discussed to assess the structural integrity of the design.
- Chapter five presents the required design optimalization based on the findings from Chapter four. This chapter also discusses the installation process and compares the concept model with the existing solution for the Northern Lights project.
- Chapter six discusses the data obtained throughout the thesis regarding the provided solutions and results.
- Chapter seven presents the conclusions of the thesis.
- Chapter eight outlines potential future of the study, suggesting areas for further research and development to further enhance the design of the subsea system.

# 2. Previous Published Knowledge

The following chapter will explore the Carbon Capture and Storage industry and the factors that make this technology advantageous. Additionally, it will examine various projects within the industry to provide insights into the current state of the technology and gather data on relevant materials that will be used later in the thesis.

## 2.1 Carbon Capture and Storage - CCS

Carbon Capture and Storage is a process that involves capturing carbon dioxide emissions from industrial plants and other sources of CO2 emissions. The captured CO2 is then transported to a storage facility and subsequently injected underground for secure, long-term storage. This approach will play an important role in ensuring a sustainable future by preventing these gases from entering the earth's atmosphere and contributing to global warming.

The Norwegian government has greenlit an ambitious CCS project known as Langskip. This initiative presents a CO2 handling project, covering the entire process from capture to permanent storage. Aligned with the Paris Agreement, which mandates a 55 percent reduction in emissions compared to 1990 levels, Langskip is a strategic response to Norway's commitment. The estimated cost of Langskip is approximately 30 billion NOK, with the government pledging to cover two-thirds of the total investments, while the remaining portion is supported by the industry [2].

Norway's total emissions amounted to 48.9 million tons of CO2 in 2022. Equinor, demonstrating its dedication to CCS, has partnered in multiple CCS projects, such as Northern Lights and Smeaheia. Their ambitious objective by 2035 is to capture and store between 30-60 million tons per annum (MTPA) [3]. This commitment is done to effectively capture the entirety of Norway's CO2 discharge, leading towards a net zero emission scenario [4].

### 2.1.1 The Three Phases of CCS

In the global commitment to mitigate carbon emissions and address the challenges of climate change, Carbon Capture and Storage technology has emerged as a promising direction. The CCS process involves three primary phases. First, the Capture Phase involves encapsulating CO2 before its release into the atmosphere. Subsequently, the captured CO2 undergoes transportation to designated storage facilities. Lastly, in the Storage Phase, CO2 is injected into reservoirs, ensuring secure and permanent storage. This approach highlights the role of CCS technology in transitioning towards a more sustainable and environmentally conscious future.

#### *2.1.1.1 Capture Phase*

When fossil fuels are converted to energy, CO2 is generated as a by-product of combustion. The impact of CO2 emissions on the environment and its role as a contributor to global warming are well-established. In response, CCS processes have been developed to address this issue. The CCS process begins with a capturing phase, where the gas is encapsulated before it enters the atmosphere. The capture of CO2 involves three primary methods: Pre-combustion process, post-combustion process and a combination of Oxyfuel combustion and post-combustion process [5].

1. Pre-combustion Process:

   The pre-combustion process involves converting fuel into a gaseous mixture of hydrogen and CO2. Through this method, hydrogen is separated and can be utilized as fuel without producing CO2 as a by-product. The resultant CO2 is then compressed and prepared for transportation, contributing to reduction of emissions [5].

2. Post-combustion Process:

   In the post-combustion process, CO2 is separated after combustion from the exhaust gases. This separation is achieved through an absorption-based approach, utilizing a liquid solvent to react and extract CO2 from the medium. Subsequently, the CO2-absorbing liquid can be heated to produce pure CO2 steam, facilitating its capture and following transportation [5].

3. Oxyfuel Combustion:

   Oxyfuel combustion involves the use of oxygen instead of air for fuel combustion. This method primarily produces water as a by-product, significantly reducing CO2 emissions. A combination of oxyfuel combustion with a post-combustion process streamlines CO2 separation, enhancing the efficiency of carbon capture and storage initiatives [5].

*2.1.1.2 Transportation Phase*

Ensuring the safe and reliable transportation of CO2 is important for the effective implementation of CCS projects. While the transportation of CO2 is a routine practice in many regions worldwide, substantial investments in expansive infrastructure are necessary to facilitate large-scale CCS initiatives.

The transportation of CO2 relies on various methods including tanks, pipelines, and ships capable of accommodating both gaseous and liquid CO2. Given that liquid CO2 occupies considerably less volume than its gaseous counterpart, compression is employed before transportation to optimize efficiency. Pipeline transportation stands out as the dominant method for conveying large quantities of CO2, while ship transportation is utilized in areas lacking access to storage facilities. For shorter distances, trucks and railroads could be economically viable alternatives for CO2 transportation.

Efforts to enhance and diversify transportation infrastructure for CO2 are crucial for advancing global CCS endeavors, showing the importance of continued investment and innovation in this aspect of CCS technology.

Transporting CO2 is generally perceived as safer compared to other substances due to its non-flammable and non-explosive nature. Nevertheless, strict safety measures and regulation is still applied for the transportation phase. It is essential that all CO2 transportation methods adhere to international standards and operate under closely monitored conditions [6].

In 2017, new standards for CO2 transportation and storage were established by Oljedirektoratet in collaboration with Standard Norge and Gassnova. These standards set criteria for the design, construction, and operation of pipelines utilized in CCS transportation. By implementing these standards, the industry ensures the highest level of safety and reliability throughout the CO2 transportation process, thereby mitigating potential risks and establishing confidence in CCS initiatives [7].

*2.1.1.3 Storage Phase*

The concept of injecting and storing CO2 underground has been a well-established technology for several years. Underground reservoirs offer the most logical and expansive solution for storage. These geological systems are widespread across the globe and have the capacity to store centuries worth of CO2 emissions.

These storage reservoirs exhibit sedimentary characteristics similar to oil and gas reservoirs, making them suitable for long-term CO2 storage, an example is illustrated in Figure 1. With their high-volume capacity and widespread distribution, underground reservoirs represent a pivotal component in the mission to reduce carbon emissions and combat climate change through CCS initiatives [8].

The permanent injection and storage of CO2 into reservoirs necessitate specific geological characteristics to ensure efficiency:

1. Pore Size

   The rock formations within the reservoir must possess adequately sized pores, typically in the millimeter range, to accommodate the volume of CO2 intended for storage.

2. Permeability

   These pores in the rock must also exhibit sufficient permeability, allowing the CO2 to disperse and distribute itself uniformly within the formation at the desired injection rate.

3. Cap Rock

   The reservoir must feature a cap rock or barrier positioned at the top of the formation. This cap rock acts as a complete seal, ensuring the containment and permanent storage of the injected CO2 within the reservoir [8].

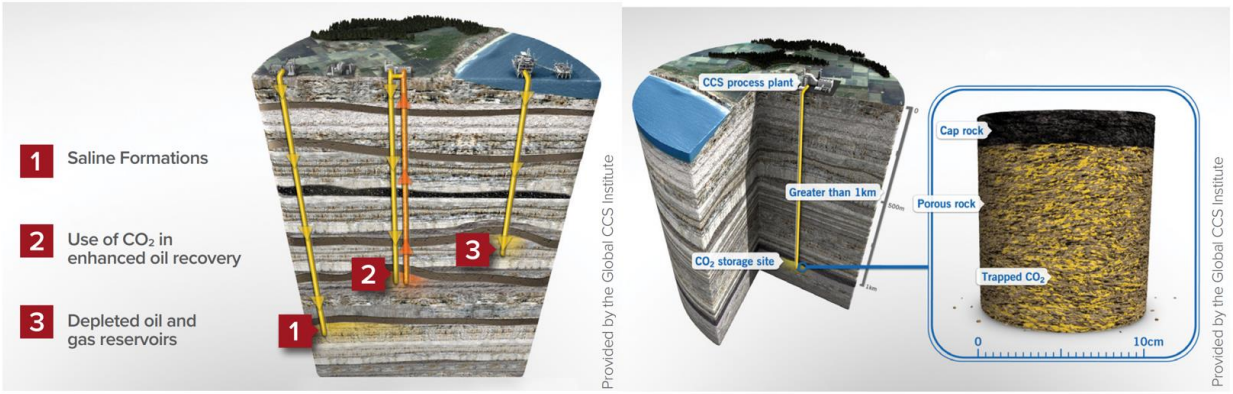


*Figure 1: Storage Overview and Core Sample [8].*

The Storage Overview illustration in Figure 1 provides insight into the various types of storage utilized in today's industry:

1. Saline Formations:

   Saline formations refer to deep water-bearing reservoirs that feature a caprock, offering secure and permanent storage for CO2. These formations, characterized by their geological structure, serve as key storage reservoirs for carbon capture and storage initiatives.

2. Enhanced Oil Recovery (EOR):

   Certain industries employ an EOR technique, which involves injecting CO2 into oil-producing reservoirs to enhance production rates. By utilizing CO2 in this manner, not only can oil extraction be increased, but CO2 can be effectively injected simultaneously, contributing to CO2 emission management.

3. Depleted Oil Fields and Gas Reservoirs:

   Depleted oil fields and gas reservoirs are sites that have exhausted their economic potential for production. Despite this, they possess excellent trapping and storage capabilities, making them suitable candidates for CO2 storage. Leveraging these depleted fields and reservoirs for CO2 storage represents a practical and sustainable approach to carbon management [8].

Saline Formations are highly sought after for CO2 injection on a global scale, particularly in contexts where emission reduction is a primary concern. Upon injection into the well, CO2 interacts with various components of the geological system, leading to multiple forms of encapsulation, all of which are included in Figure 2:

- **Structural Trapping:** Due to its buoyancy compared to saltwater existing within the reservoir, CO2 tends to migrate towards the surface where it becomes structurally trapped within the formation by the cap rock, ensuring long-term containment.

- **Solution Trapping:** A portion of the injected CO2 dissolves into the saline water, undergoing solution trapping, where it remains indefinitely trapped within the solution, contributing to permanent storage.

- **Residual Trapping:** CO2 can also become trapped in tiny pore spaces within the rock formation, a phenomenon known as residual trapping. This mechanism further enhances the long-term storage of CO2 within the reservoir.

- **Mineral Trapping:** Through interactions with the rock formation, CO2 reacts with the rock formation itself, resulting in the formation of new minerals that encapsulate the CO2 indefinitely. This process solidifies the carbon capture, ensuring its permanent storage within the geological structure [8].

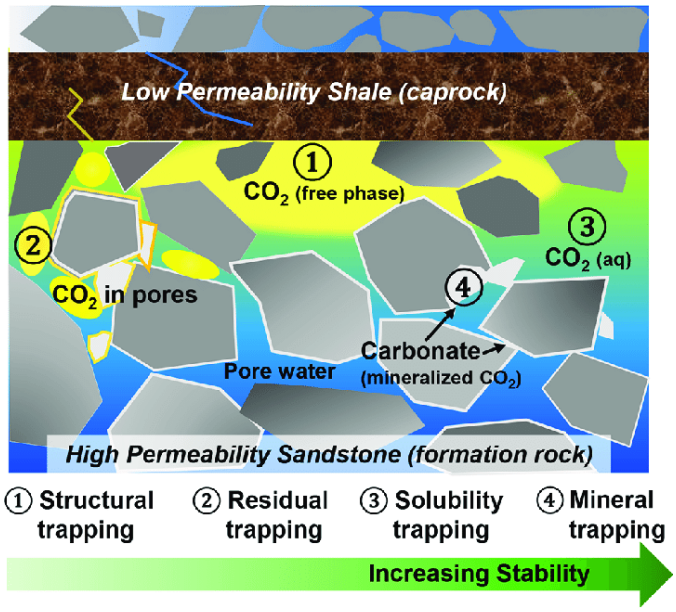


*Figure 2: CO2 Trapping [9].*

## 2.2 Northern Lights

The Northern Lights project is a collaborative effort between Equinor, Shell, and Total Energies, and is a significant component of the carbon capture and storage (CCS) initiative known as Langskip. Designed to mitigate carbon emissions from industrial sources, Langskip aims to store CO2 securely and permanently. The project's primary objective is to capture CO2, then transport it as liquid CO2 (LCO2) to an onshore terminal situated on Norway's west coast. From there, the CO2 will be conveyed via pipeline to a designated storage reservoir in the North Sea [10], as showcased in Figure 3.

The 2019 project report from Northern Lights has laid the groundwork for shaping the concept development outlined in this thesis. It is clear that the future of CCS is dependent on the development of a specialized injection system tailored specifically for CO2. This will involve the creation of more streamlined components, innovative template structures, and a reconfiguration of well designs. Unlike the operational framework of traditional production systems currently used for CO2 injection, the injection environment significantly diverges from that of a production well. Consequently, this thesis aims to formulate a conceptual template structure for a more compact system, using the approaches outlined in the Northern Lights project as a base point.

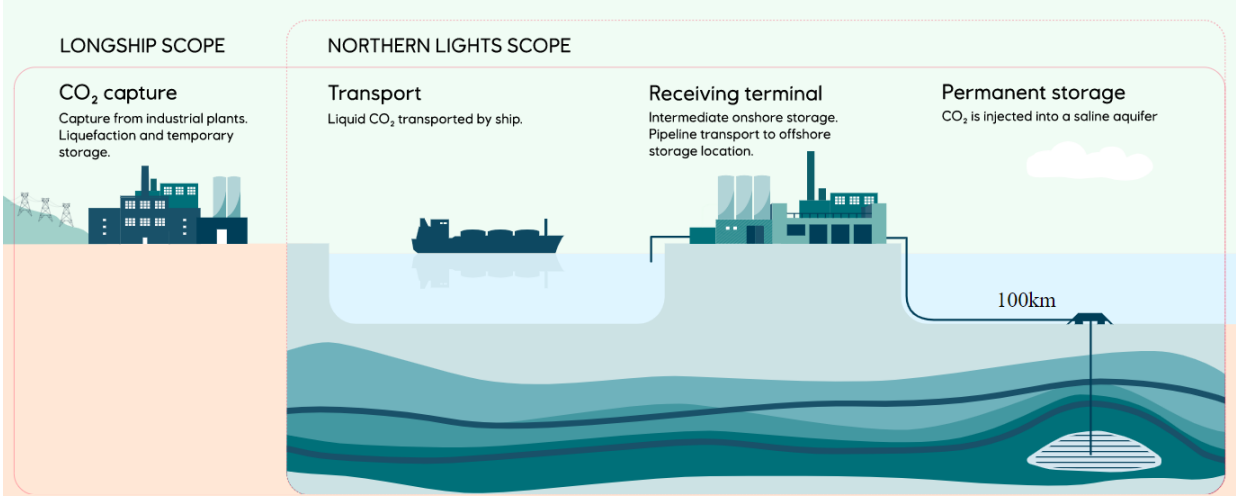


*Figure 3: Langskip and Northern Lights Project Scope [11].*

### 2.2.1 Northern Lights Template Structure

The Northern Lights project has adopted a single well satellite structure incorporating an integrated protection structure and structural support for the wellhead, illustrated in Figure 4. This template draws upon the standard portfolio for subsea development on the Norwegian Continental Shelf (NCS), aligning with Equinor's frame agreement NSC2017+ where relevant. The selection criteria for this template structure prioritize support for a vertical X-mas tree (VXT), the wellhead system, blowout preventer (BOP), and the separately retrievable CO2 injection header flowbase [10].

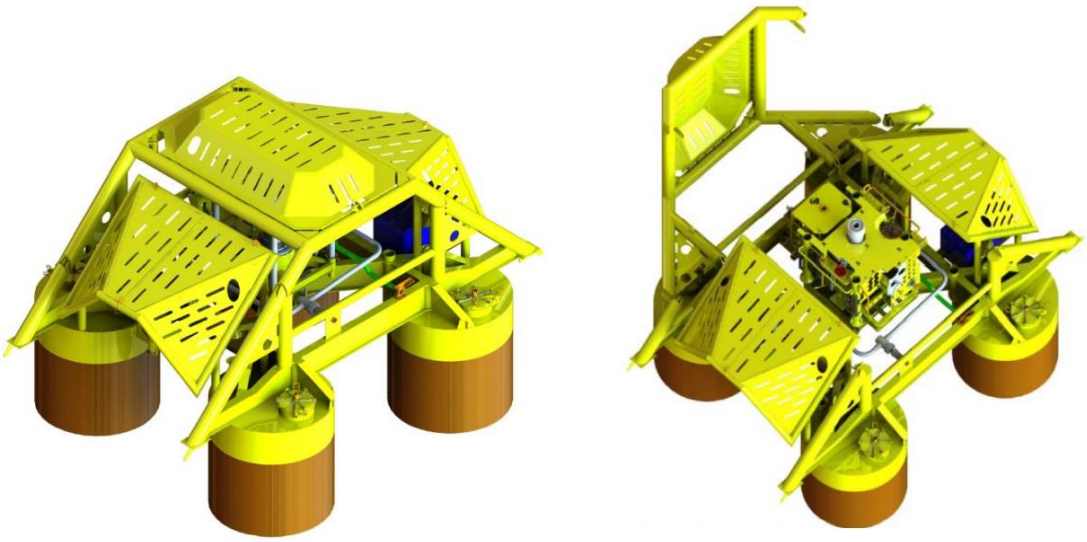

*Figure 4: Northern Lights Template Structure [10].*

### 2.2.2 Vertical X-mas Tree

The Vertical X-mas Tree (VXT) selected for the Northern Lights project adheres to the standard NCS 2017+ specifications, featuring a 7 x 5-inch production tree design provided by Aker Solutions, featured in Figure 5. Configured with a concentric bore layout, the tubing hanger (TH) is conventionally installed in the wellhead (WH) beneath the tree. Wet-mate communication between the top of the TH and the bottom face of the VXT is provided by production and annulus stabs, alongside electrical/hydraulic stingers.

The connection from the VXT to the flowbase is secured through a Vertical Manifold to XT connection (VMX) system, which will be operated using a remote operated vehicle (ROV). Consequently, the template structure must incorporate designs parameters to ensure access to these interfacing components [10].

By utilizing a VXT traditionally employed in oil production for the injection project, the need for extensive design modifications within the industry is underscored. The development of a streamlined X-mas tree tailored specifically for CO2 injection would achieve a smaller component, thereby reducing the weight considering the required size of the template structure and suction anchor.

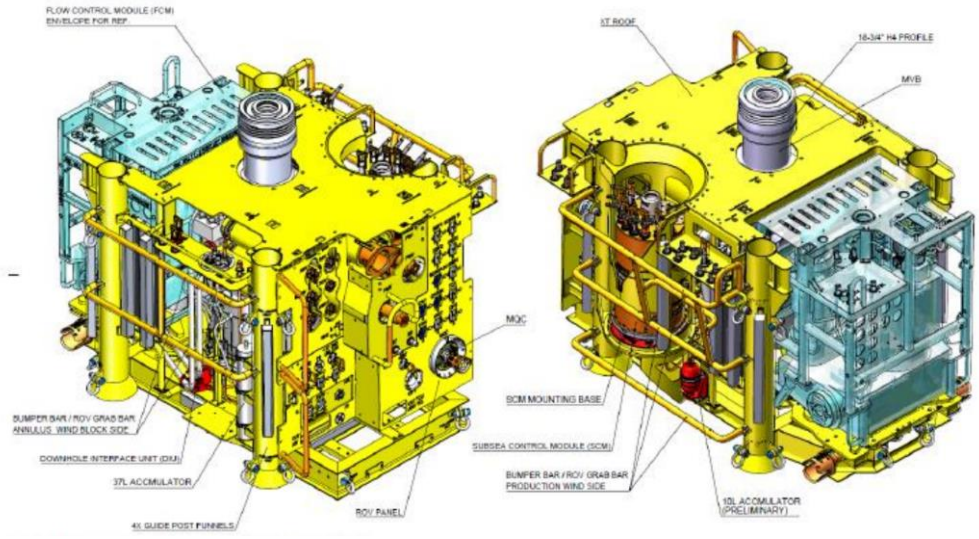


*Figure 5: Aker Solution Vertical X-mas Tree used in NL Project [10].*

### 2.2.3 Tie-in Systems

The tie-in system for the injection spool employs a standard horizontal connection system (HCS) provided by Aker Solutions, showcased in Figure 6. This technology is proven reliable in oil production and suitable for the set water depth parameter for the Northern Lights field at 300 meters. The HCS facilitates installation without guide wires, utilizing a remote operated vehicle (ROV) for connection [10].

Ensuring seamless integration with the X-mas Tree upon connection underscores the need to provide sufficient space on the template structure's trawl protection. This space must accommodate all components without interference, allowing the ROV to access the necessary connection points.

The absence of a specific X-mas Tree designed for injection in today's industry poses a challenge within this thesis regarding where these accommodations are to be designed. However, it emphasizes the importance of considering such design parameters should the concept progress to a development phase.

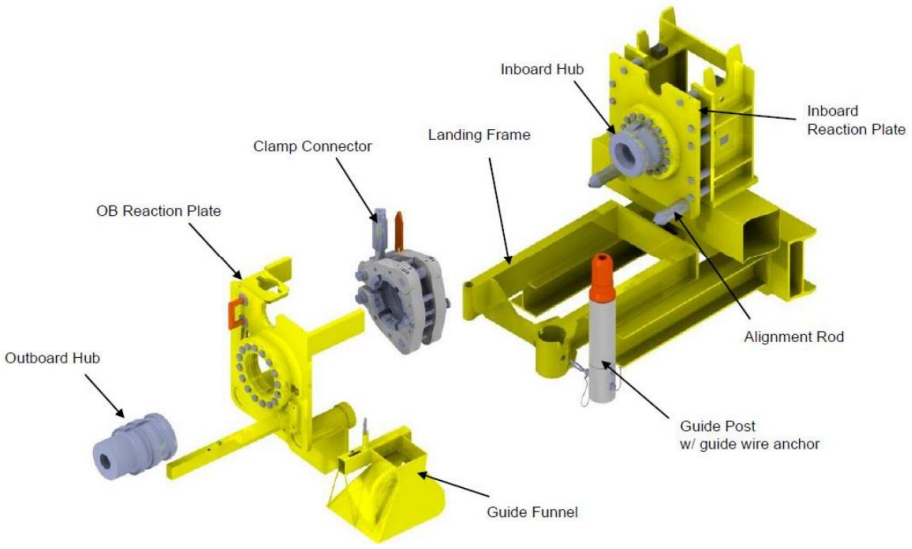


*Figure 6: Aker Solution Horizontal Connection System (HCS) [10].*

### 2.2.4 Suction Anchor

Northern Lights has opted for a satellite-type structure, featuring a typical Integrated Template Structure (ITS) configuration equipped with four suction anchors for secure installation at the seabed. The selected template, along with its supporting suction anchors, comply to standard specifications designed to accommodate the X-mas tree, BOP, and wellhead system defined within the NCS2017+ frame agreement [10].

As industry parameters progress towards specialized compact injection systems, the necessity for larger suction anchors can be reduced. This evolution would result in a reduction in both suction anchor size and formation, helping to streamlining the system into a tailored injection system. The current estimated weight of the project's template frame is at least 103 tons, excluding the anchors [10]. Exploring opportunities to minimize the size and height of the X-mas tree and BOP installed on the template presents a pathway towards a more compact template and suction anchor design.

### 2.2.5 Trawl Protection

The placement of subsea facilities and pipelines in the North Sea will intersects with fishing activities, where general authority agreements must be followed. This agreement states that all subsea facilities must be engineered to withstand trawling activities, as outlined in the framework regulations, section 45, paragraph 2 [10].

*"Subsea facilities and pipeline systems shall also be designed and installed such that the facilities can withstand mechanical damage caused by other activity, and such that they do not damage fishing gear or obstruct fishery activity to an unreasonable extent."* [12]

The design criteria specify that the system must be overtrawlable, necessitating the satellite's design to incorporate hatches covering the VXT, flowbase, and umbilical interface. The Northern Lights template structure integrates two Sealine Protection Covers (SPC) and an overtrawlable hatch to guarantee safe overtrawlability and provide protection against dropped objects. Figure 7 illustrates the SPC cover for the NL template structure.

*Figure 7: NL Project Sealine Protection Cover (SPC) [10].*

Given that fishing activity spans over significant portions of the entire subsea field, any seabed-placed component must also be shielded by an overtrawlable structure, offering protection against dropped objects, illustrated in Figure 8. This necessitates the utilization of Glass Reinforced Plastic (GRP), or steel protection covers, which can be stabilized with rocks if necessary [10].

*Figure 8: Glass Reinforced Plastic- and Steel Protection Covers [10].*

### 2.2.6 Installation, Operation and Removal

For the NL project, the single satellite structure will be installed from a construction vessel with a minimum crane capacity of 250 tons, while the X-mas tree installation will be handled by a Light Well Intervention vessel (LWI). Utilizing a smaller construction vessel for the remainder of the subsea equipment, spool fabrication, protection covers, and tie-in operations is deemed sufficient, considering factors such as availability and cost estimations [10].

At the conclusion of a field's life and completion of injection operations, decommissioning becomes a critical phase. All subsea equipment and infrastructure must be removed and disposed of if not suitable for reuse, adhering to guidelines outlined in resources such as the Oil and Gas Decommissioning Toolkit provided by The Commonwealth [13]. The seabed must be left in a safe and environmentally acceptable condition, with no obstructions to fishing by trawling. Therefore, all equipment must be designed to facilitate a removal procedure.

## 2.3 SMEAHEIA

Smeaheia represents a CO2 development initiative aimed at supporting Europe in achieving its climate objectives. The project's primary goal is to establish a transport and storage infrastructure dedicated to capturing and injecting between 30 to 50 million tons of CO2 annually by 2035. Upon completion, this licensed venture seeks to establish a robust CO2 transportation network spanning Northwestern Europe to connect with expansive storage reservoirs in the North Sea [14]. Smeaheia's project scope from 1996 to 2030 is included in Figure 9.

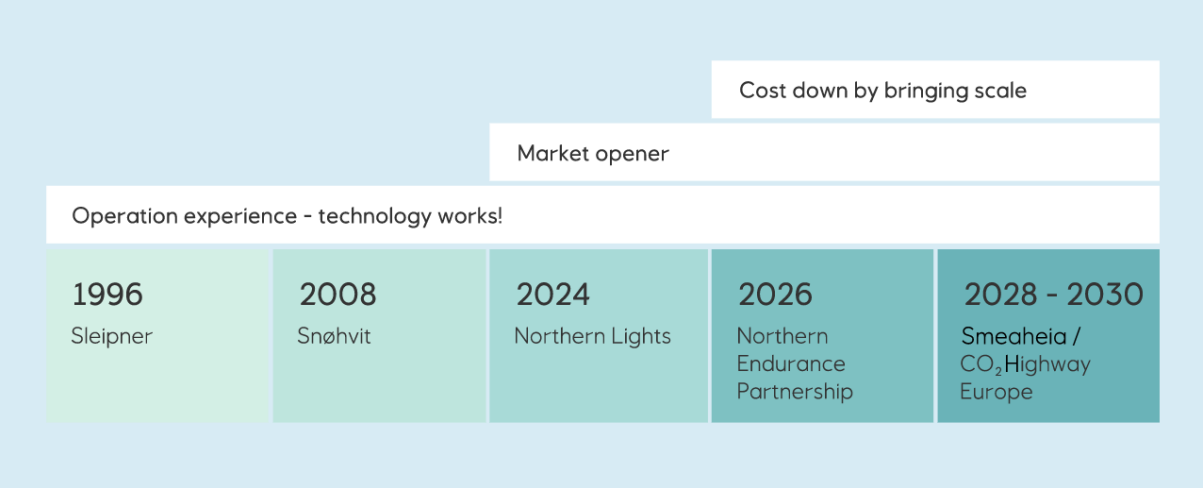


*Figure 9: Smeaheia Project Scope [14].*

### 2.3.1 Infrastructure

For this project two main transportation concepts are discussed, CO2 ship transport and pipeline. Both of which are being developed in parallel. The CO2 ship transport concept is known as the Norwegian Hub. This involves an onshore receiving terminal on Norway's west coast, linked by a CO2 pipeline directly to wells and reservoirs in the North Sea.

The second concept is named the CO2 Highway Europe. This advocates for a direct CO2 pipeline route connecting Northwestern Europe to the Smeaheia wells and other North Sea reservoirs, as the CCS technology and collaboration develops further.

Compared to ship transport, the CO2 Highway Europe is projected to reduce transport costs by over 50%. While pipeline implementation entails a significant upfront investment, it aligns with a more sustainable CCS strategy over the long term. Additionally, a pipeline approach promises enhanced operational consistency and reduced lifecycle emissions [14].

### 2.3.2 Reservoirs

Two reservoirs within the Jurassic Viking and Dunlin Groups are discussed for the CO2 injection process. Equinor is currently in the development phase, requiring data through the drilling of two appraisal wells in 2024 [14]. Existing analyses of the fields indicate promising potential for further development of storage reservoirs at Smeaheia.

#### *2.3.2.1 The Viking Group*

The Viking Group, illustrated in Figure 10, is divided into three formations; Melke, Rogn and Spekk Formations located in the North Sea near the Trøndelag Platform. Characterized by mudstones and siltstones, the lithology of the Viking Group makes it a viable candidate for CO2 injection [15].

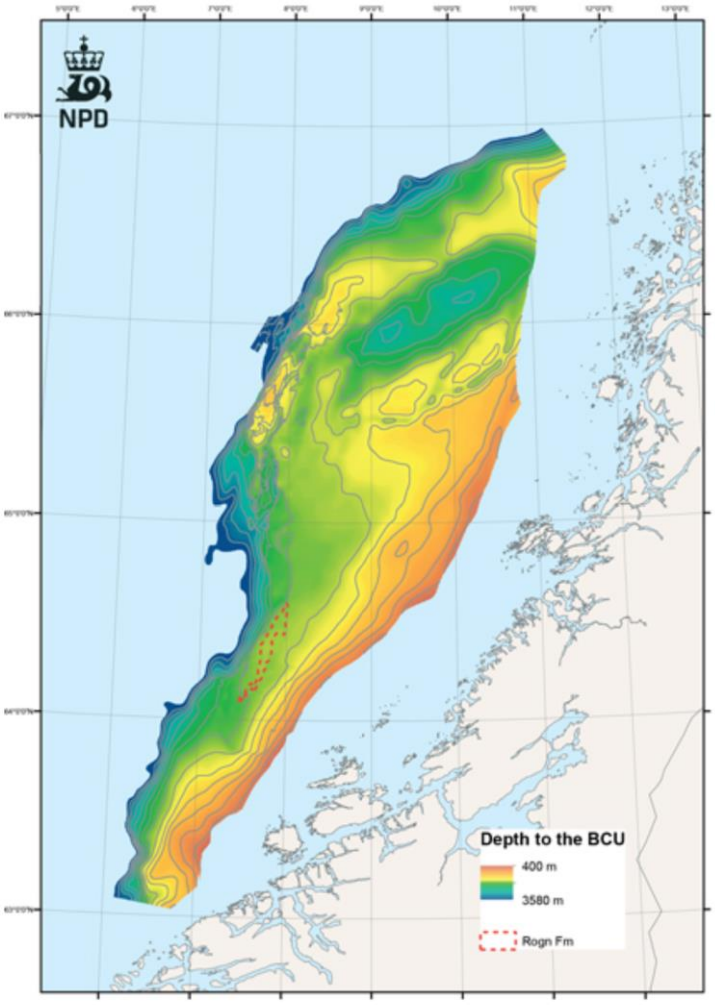


*Figure 10: Viking Group Geography [15].*

#### *2.3.2.2 Dunlin Groups*

The Dunlin Group consists of five wells in five formations, Amundsen, Johansen, Burton, Cook and Drake. Four of them is owned by Norwegian companies and one is based out of the UK. The lithology of the area tends to be more calcareous in the Norwegian sector and in some places limestone beds are in place [16].

Both candidates have shown good capabilities for serving as CO2 storage reservoirs, but further investigations and data gatherings are needed to assess them more carefully and reach a conclusion for their intended purpose. The tests are set to take place for both groups within the year 2024 [14].

### 2.3.3 Potential

The CCS market is experiencing rapid growth and development. As highlighted in the CCS seminar hosted by ETN in February 2024, industry stakeholders recognize the importance of establishing a strategic partnership [17]. This underscores the necessity of implementing streamlined concepts for CO2 injection to enhance efficiency, reduce costs, and render the CCS industry more globally attractive. Such efforts are important in combating global warming and its corresponding effects.

## 2.4 CO2 Injection Environment Oil vs. Gas Production

This chapter will examine the differences between a CO2 injection well and a conventional gas/oil producing environment. The environmental and operational distinctions between the two will be discussed, where the dimensions for CO2 injection purposes will be evaluated and compared to a production well. The observations align with the theme of this thesis, emphasizing the need for the development of specialized solutions tailored specifically for CO2 injection systems.

### 2.4.1 Injection Environment

The pressure and temperature environment experienced at the wellhead of any subsea site is dependent on the specific reservoir conditions. For a reservoir to be suitable for CO2 injection the reservoir must consist of large amount of clear space, which an oil or gas producing reservoir is not.

Maintaining CO2 in its liquid state during injection and transport to the reservoir is crucial. The wellhead temperature is influenced by the ambient temperature at the seabed, resulting in a temperature range of the injected fluid to be approximately 4-8 degrees Celsius [10]. Utilizing a P-T diagram enables estimation of the operational pressure required to ensure that CO2 remains in its liquid state throughout the descent into the storage reservoir. As illustrated in Figure 13, the red line reads a minimum pressure of approximately 30 bars necessary to sustain the temperature of LCO2 at 6 degrees Celsius.

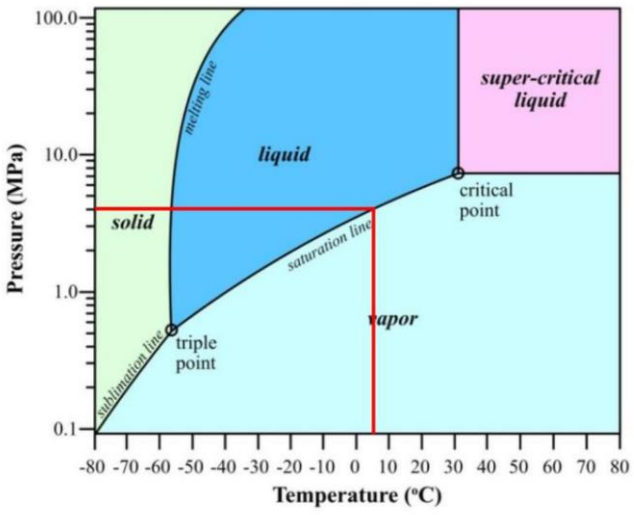


*Figure 11: P-T Diagram [18].*

Using the Northern Lights project as an example, where an injection well has been completed at a water depth of approximately 300 meters [10]. This results in an external pressure at the wellhead of:

$$P = \rho g h = 1025 \frac{kg}{m^3} * 9{,}8065 \frac{m}{s^2} * 300\ m = 30{,}2\ bar$$

*Equation 1: External Pressure.*

The injection velocity of LCO2 through a 6-inch diameter injection tubing can be computed. Assuming the injection of pure LCO2 without contamination and considering an ambient temperature of 6 degrees Celsius as well as an injection pressure of 50 bar, the density of LCO2 is estimated to be 897.6 kg/m3 [19]. According to the Northern Lights report, each well is projected to inject approximately 1 to 1.5 million tons of LCO2 per annum [11].

$$1{,}5MTPA = 47{,}55\ \frac{kg}{s}$$

$$Flow = Q = \frac{mass/_s}{density} = \frac{47{,}55\ \frac{kg}{s}}{897{,}3\ \frac{kg}{m^3}} = 0{,}05299\ {}^{m^3}/_s$$

*Equation 2: Mass Flow through Injection Tubing.*

$$A = \pi * r^2 = \pi * 0{,}0762^2 = 0{,}01824\ m^2$$

*Equation 3: Cross Section Area of 6-inch Tubing.*

$$V = \frac{Q}{A} = \frac{0{,}05299\ \frac{m^3}{s}}{0{,}01824\ m^2} = 2{,}9\ {}^{m}/_s$$

*Equation 4: Injection Velocity.*

### 2.4.2 Production Environment

A production wellhead is exposed to far more environmental strain due to the initial pressure built up in the reservoir. One can exert a bottomhole pressure of about 0,47 psi/ft of depth, this would yield a pressure of approximately 588,12 bar for an oil producing reservoir similar to the Northern Lights storage site at 2600 meters below the seabed [20]. In comparison the Northern Lights reservoir is subject to about 200-300 bars [10].

$$0{,}47\ \frac{psi}{ft} = 0{,}2262\ \frac{bar}{m}$$

$$0{,}2262\ \frac{bar}{m} * 2600\ m = 588{,}12\ bar$$

*Equation 5: Oil Reservoir Pressure.*

While these calculations are simplified, they underscore the significant differences between a CO2 injection well and an oil-producing well, highlighting the distinct environmental stresses which the components are subjected to.

### 2.4.3 Reservoir

Reservoir conditions is mainly dependent on the site location and the time frame of an injection process. The main differences when comparing an injection reservoir with a producing reservoir is the initial reservoir pressure. When selecting a storage location for CO2 it is required that the reservoir is mainly filled with open voids so that the injected medium can spread across the volume and fill the open space. This means that the initial reservoir pressure will gradually increase in parallel with the injection of the medium, but it will never reach a pressurization equal to that off a production reservoir. For CO2 injection it is also important that the temperature of the storage site is adequate to maintain the CO2 in its liquid phase through the whole descent into the reservoir.

The injection well Eos completed by Equinor for the Northern Lights project have an estimated temperature and reservoir pressure of 100 degrees Celsius and 200-300 bar, respectively [10]. These parameters yield the well sufficient and suitable for CO2 injection and storage.

A production reservoir is not occupied by large voids, instead these voids are filled with oil or gas that are to be produced. These reservoirs will therefore be pressurized before production starts, and the pressure drawdown starts in parallel with the production of the medium. This subsequently means that such reservoirs will have much higher initial pressures and ultimately a higher environmental strain on the well and subsea equipment.

## 2.5 Aluminum

Aluminum is one of the most common manufacturing metals in the world. It has proven itself as a preferable choice in the automobile, aerospace, and naval industry for its great strength-to-weight ratio [21]. The metal offers a huge combination of valuable properties, including corrosion resistance, it does not magnetize and works as a great electrical conductor.

Aluminum can easily be processed with pressure, rolling, pulling, and stamping. The ductile properties of aluminum makes it extremely adaptable where the metal can be processed into extremely thin foils, as low as 4 microns thick, which equals to three times thinner than a human hair. In addition to these capabilities the metal is a lot more cost efficient than other materials, and the use of aluminum could drastically reduce costs of utilizing other materials [22].

### 2.5.1 Aluminum Alloys

One of the many abilities that aluminum possess is the ability to easily bond with other chemical elements. By doing so it creates the opportunity to create a vast variety of aluminum alloys. Small amounts of admixtures can change the mechanical properties of the metal, which makes for the endless area of use for aluminum [22].

An aluminum alloy usually consists of two chemical elements, where aluminum acts as the main metal of the mixture, and the second part is dependent on the desired application of which the alloy is to be used [23]. As an example, when combining aluminum with magnesium the blend-alloy gains strength while maintaining its light weight, this type of alloy is often used in the automobile industry.

NORSOK M-121 states that there are only two aluminum alloys approved for immersed application. This includes 5083 and 6082 [24]. For the basis on this thesis the 5083 with applicable temper H116 is used. Table 1 shows the different aluminum alloy compositions for both wrought and cast alloys.

*Table 1: Aluminum Alloy Composition [25].*

| WROUGTH ALLOYS | | | | CASTED ALLOYS | | |
|---|---|---|---|---|---|---|
| **SERIES** | **Composition** | **Alloy** | **Heat Treatable** | **SERIES** | **Alloy** | **Heat Treatable** |
| **1XXX** | Al | Aluminum | | **1XX.X** | Aluminum | |
| **2XXX** | AlCu | Copper | **x** | **2XX.X** | Copper | **x** |
| **3XXX** | AlMn | Manganese | | **3XX.X** | Silicon and/or Copper | **x** |
| **4XXX** | AlSi | Silicon | | **4XX.X** | Silicon | **x** |
| **5XXX** | AlMg | Magnesium | | **5XX.X** | Magnesium | |
| **6XXX** | AlMgSi | Magnesium + Silicon | **x** | **6XX.X** | - | |
| **7XXX** | AlMgZn | Magnesium + Zinc | **x** | **7XX.X** | Zinc | **x** |
| **8XXX** | Other | Iron or Tin | | **8XX.X** | Tin | **x** |
| **9XXX** | - | - | | **9XX.X** | Other | |

*2.5.1.1 5083-H116 Aluminum Alloy*

5083 is an aluminum alloy consisting of magnesium, manganese and chromium. It is most commonly used in harsh environments due to its exceptional strength characteristics. The alloy has the highest strength of all non-heat-treatable alloys and is often utilized as plates for ship building.

The 5083 is proven to be easier to weld than any 6xxx-series alloy. The heat affected zones (HAZ) are much stronger and the material is more predictable in terms of post-weld strength. 5083 is one of two aluminum alloys approved for immersed application by NORSOK M-121, due to its corrosion resistance in saltwater [24]. The chemical composition of alloy 5083 is tabulated in Table 2**.**

*Table 2: Chemical Composition of Alloy 5083 [26].*

| **5083** | **Mn** | **Fe** | **Cu** | **Mg** | **Si** | **Zn** | **Cr** | **Ti** | **Al** |
|---|---|---|---|---|---|---|---|---|---|
| **%** | 0,40 - 1,0 | 0 - 0,40 | 0 - 0,1 | 4,0 - 4,9 | 0 - 0,4 | 0 - 0,25 | 0,05 - 0,25 | 0,15 | Balance |

The H116 temper applies to all aluminum products in the 5xxx-series where the magnesium content is 3% or more. H116 is a non-heat treatment, meaning that the metal is strain hardened to specified tensile property limits [27]. This involves heating the metal at relatively low temperature and subject the alloy strain beyond the yield point. When the treatment is done, the metal recovers and an increased stress is required to produce plastic deformations. The metal becomes stronger and is more difficult to deform [26]. The physical properties of a complete hardened 5083-H116 alloy are tabulated over the varying thickness.

*Table 3: Physical Properties of Alloy 5083-H116 [28].*

| ALLOY | THICKNESS | ULTIMATE | YIELD | ELONGATION |
|---|---|---|---|---|
| | [mm] | [MPa] | | [%] |
| **5083-H116** | 6 - 12,5 | 305 | 215 | 12 |
| | 12,5 - 40 | 305 | 215 | 10 |
| | 40 - 80 | 305 | 200 | 10 |

### 2.5.2 Welding of Aluminum

There are several different methods for welding aluminum, with the most commonly practiced and applicable ones being Metal Inert Gas (MIG), Tungsten Inert Gas (TIG), friction stir- (FSW), and laser welding (LW). Each method has its own set of advantages and disadvantages, all of which will be explored in this chapter. MIG and TIG welding are widely utilized and extensively documented, whereas FSW and LW methods are considered alternative approaches.

#### *2.5.2.1 Certificates and Approval*

To obtain industry approval, any welded structure must be fabricated by a certified welder within an approved welding shop. If circumstances necessitate work outside such a facility, additional approvals must be obtained [29].

All welds must undergo examination to verify the weld quality to mitigate chance of cracks or crevices, which could potentially result in corrosion, weld fatigue, or material failure. Documentation of these weld inspections must accompany the structure upon delivery, signed by both the responsible fabrication personnel and a certified welding inspector.

#### *2.5.2.2 Challenges of Aluminum Welding*

Welding aluminum presents unique challenges compared to welding materials such as steel. This is primarily due to the chemical composition of the alloy, which tends to crack. The most significant challenges arise from issues like porosity, hot cracking, and thermal conductivity.

Porosity:

Porosity poses a significant challenge in aluminum welding due to the solubility of hydrogen in liquid aluminum. During welding, the aluminum alloy and filler metal liquefy, potentially absorbing the hydrogen. As the metals cool and solidify, it is no longer able to retain the hydrogen in solution, leading to its entrapment within the weld and the formation of hydrogen bubbles, resulting in porosity [30].

Hot Cracking:

Hot cracking is characterized by cracks forming at elevated temperatures near the solidus-point of the alloy. The reduced ductility of the metal at high temperatures, often caused by impurities in the alloy, making it brittle near the solidus. Cracks forms from tensile stresses induced during the heating and cooling phases of the weld, particularly at the grain boundaries of the alloy. This phenomenon can be minimized by reducing the heat input, employing a larger groove radius during welding, or selecting a filler material that is more compatible with aluminum [31].

Thermal Conductivity:

Aluminum alloys has a high thermal conductivity, causing cold areas of the metal to constantly distribute heat away from welds. This presents a challenge for achieving weld penetration. One solution is to increase the heat input to reach the critical temperature necessary for penetration, although excessive temperatures may induce hot cracking [30].

Consequently, welding aluminum poses significant challenges, emphasizing the importance of skilled welders to achieve satisfactory results. Proper selection of welding equipment, input settings, and experience are crucial to produce good welds and minimize the risk of contamination and failures.

#### *2.5.2.3 Arc Welding – Mig and Tig*

Arc welding utilizes an electric voltage applied to two separated electrodes. When the voltage applied to the electrodes increases the air insulation breaks and a current flow between the two, causing bright light and high amounts of heat to emit simultaneously. This generated arc-shaped light is called an electric arc and the welding technique builds upon the usage of the arcs heat to melt the welded medium. In arc welding the positive voltage is subjected to the welding rod acting as an electrode, the negative voltage is supplied to the base material [32]. There are two commonly used welding techniques that utilize arc welding, MIG and TIG.

Metal Inert Gas – MIG

Metal Inert Gas (MIG) welding is a welding technique where the base materials are joined together through a current, also called an arc. A continuous feed of filler material, serving as the positive electrode, is supplied through the welding gun, as showcased in Figure 12.

As the electric arc melts the electrode wire, it fuses together with the base material. Simultaneously, a shielding gas, typically argon and/or helium, flows through the gun to prevent the weld from any atmospheric contaminations [33].

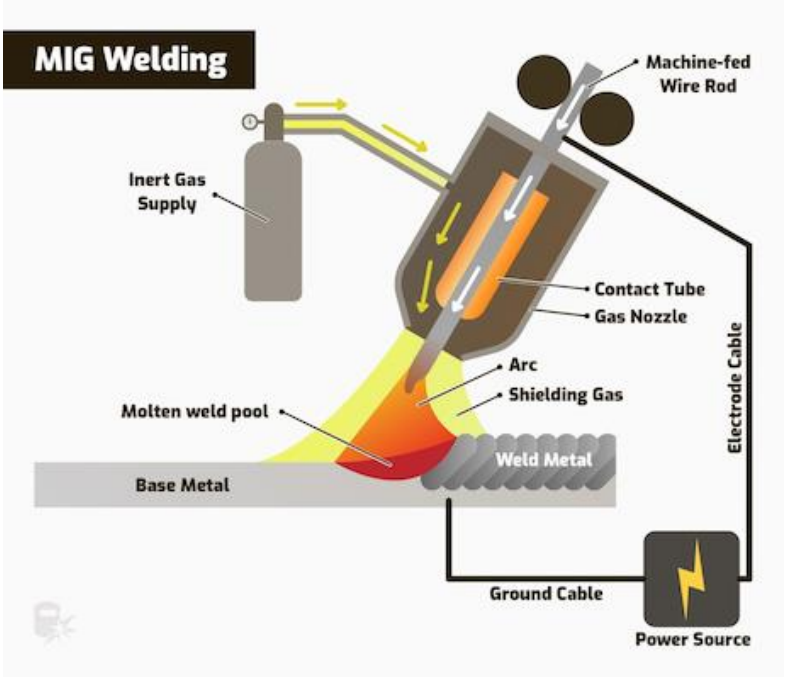


*Figure 12: MIG Welding [34].*

Tungsten Inert Gas – TIG

Tungsten Inert Gas (TIG) welding is similar to MIG welding which also utilize the electric arc as a heat source. The shielding gas, typically 100% Argon for TIG, flows through the welding torch to protect the welds and metals from contaminations [34]. Unlike the MIG welding, TIG is equipped with a tungsten metal rod on the torch, which acts as the electrode, illustrated in Figure 14. This means that for TIG welding the filler material must be added separately. TIG welding is often used for thin material welding procedures as it offers a lower heat input and is less likely to harm the welded medium.

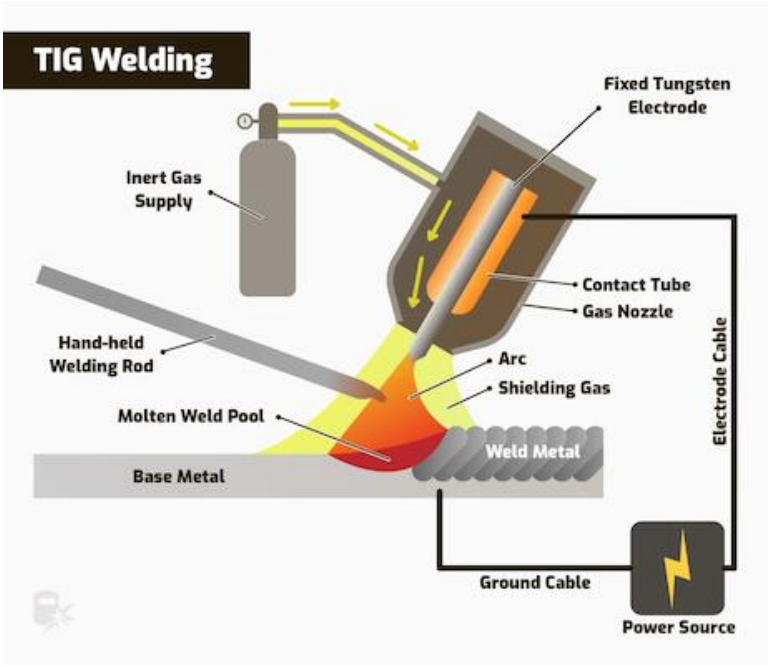


*Figure 13: TIG Welding [34].*

Strength and Quality

In order to get a sufficient weld, Eurocode state that thick members must be preheated due to a requirement of the medium to possess efficient local heat [35]. The preheating of the material must be done within a controlled environment and manner. If aluminum where to be exposed to high temperatures over time it could alter the material properties of the alloy. Welding structures often employ preheating tables for arc welding over thick members, providing welders with information such as maximum temperature, exposure time, and limits for multi-layer welds.

*Table 4: Aluminum Preheating and Intermediate Pass Temperature [36].*

| BASE METAL | MAX PRE HEAT TEMP. [°C] | MAX INTER-PASS TEMP. [°C] |
|---|---|---|
| **1XXX** | 120 | 120 |
| **2XXX** | 120 | 100 |
| **3XXX** | 120 | 120 |
| **4XXX** | 120 | 120 |
| **5XXX** | 120 | 120 |
| **6XXX** | 120 | 100 |
| **7XXX** | 100 | 80 |

The tensile and yield strength of aluminum structures can be highly affected by heat affected zones (HAZ). These zones experience cycles of heating and cooling, which can alter material properties, diverging from the original base alloys. Eurocode 9 provides tables detailing the strength reduction in the HAZ for various aluminum alloys. The design of any structure must take these factors into account, as the welds often exhibits lower strength compared to the base material [35].

*Table 5: HAZ Factor 5083-H116 Plate [35].*

| | | | MIG | | TIG | |
|---|---|---|---|---|---|---|
| **PLATE** | Thickness | Yield | HAZ Factor | HAZ Factor | HAZ Factor | HAZ Factor |
| | [mm] | [MPa] | TS | YS | TS | YS |
| **5083-H116** | t ≤ 6 | 215 | 0,90 | 0,72 | 0,90 | 0,72 |
| | 6 < t ≤ 15 | 215 | 0,90 | 0,72 | 0,81 | 0,65 |

*Table 6: HAZ Factor 5083-H116 Tube [35].*

| | | | MIG | | TIG | |
|---|---|---|---|---|---|---|
| **DRAWN TUBE** | Thickness | Yield | HAZ Factor | HAZ Factor | HAZ Factor | HAZ Factor |
| | [mm] | [MPa] | TS | YS | TS | YS |
| **5083-H116** | t ≤ 6 | 215 | 0,96 | 0,68 | 0,96 | 0,68 |
| | 6 < t ≤ 15 | 215 | 0,96 | 0,68 | 0,87 | 0,61 |

The extent of the HAZ varies for different geometric welds. Generally, thicker weld beads result in more pronounced HAZ [35]. Figure 14 showcase various geometric welds, illustrating the extent of HAZ across different weld scenarios.

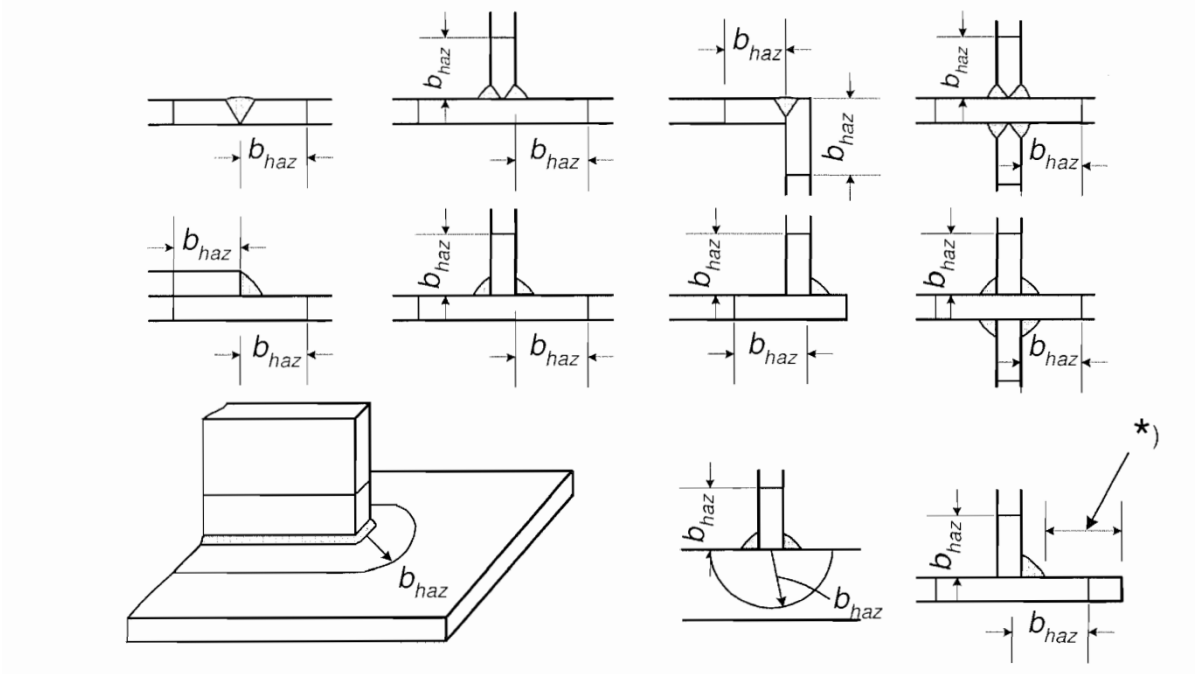


*Figure 14: Extent of HAZ in Welds [35].*

The choice of filler material can contribute to the strength, corrosion resistance, cracks and ultimately the quality of the weld. Recommended filler materials for different aluminum alloys are tabulated in Table 7, referencing Eurocode 9 to accommodate for such effects. The determination of which material is best suited should be made from specified tables in prEN 1011-4, as referenced in the Eurocode and shall be in conjunction with the design requirements for such joints [35].

*Table 7: Weld Filler Material for Alloy 5083 [35].*

| 1ST PART | 2ND PART | STRENGTH |
|---|---|---|
| | **5083** | |
| **5083** | Filler Material: | [MPa] |
| | 5056A | 240 |
| | 5356 | 240 |
| | 5556A | 240 |
| | 5183 | 240 |

*2.5.2.4 Laser Welding - LW*

Laser welding is a precise and delicate welding technique that utilize a strong light beam to fuse metals together. The light beam is generated from a freestanding laser and directed to the weld torch, where the focused energy will heat up and melt the workpieces, leading to the joining of two welded mediums without the need for a filler material.

This technique offers a significant advantage in terms of high precision and control over the applied energy, as it can be targeted directly at the wanted location without any spread. The resulting welds exhibit reduced heat-affected zones compared to conventional arc welding methods. Gas shielding, similar to arc welding, involves the use of helium and/or argon to prevent contamination and porosity [37].

CO2 Lasers:

CO2 lasers are widely adopted in laser welding due to their high-power output and minimal weld bead spread. The laser excites carbon dioxide molecules, forcing them to emit radiation. This radiation is then directed through a reflective pipe and concentrated by the welding torch, which form the laser beam. These types of tools are relatively inexpensive, effective and versatile, capable of welding a wide range of materials [38].

Neodymium-doped Yttrium Aluminum Garnet Lasers – Nd:YAG

Nd:YAG lasers generate high power infrared light with a wavelength of 1,064 micrometers. The method serves as a good candidate for welding because metallic materials absorb this wavelength more efficiently than other infrared spectrums. The setup combines high energy output and precision while requiring low maintenance, making it a practical alternative for aluminum welding [38].

Fiber Lasers:

This method utilizes a laser diode that transmits through a fiber optic which focuses the laser through the welding torch. The fiber laser serves as a good tool for automated welding equipment with a long-life expectancy and minimal maintenance needs [38].

Conduction and Keyhole Welding:

There are two main types of laser welding utilized in today's industry, conduction- and keyhole welding. They work differently but offers their own advantages.

Conduction welding is a soft process where a laser beam gradually melts the metal beyond its fusion point, transitioning it into a liquid phase to form a weld. Although this process is slow, it yields high quality results with minimal to no spread, thereby limiting the HAZ.

In contrast, keyhole welding is a fast and more aggressive process that melts and vaporizes the metal by penetrating deeper into the medium, creating a characteristic "keyhole". This method employs a high heat, allowing the melting pool to transition into a gaseous phase, which may result in spattering. Keyhole welding is suitable for high-volume production due to its efficiency, but is limited by weld porosity and higher HAZ [38], as illustrated in Figure 15.

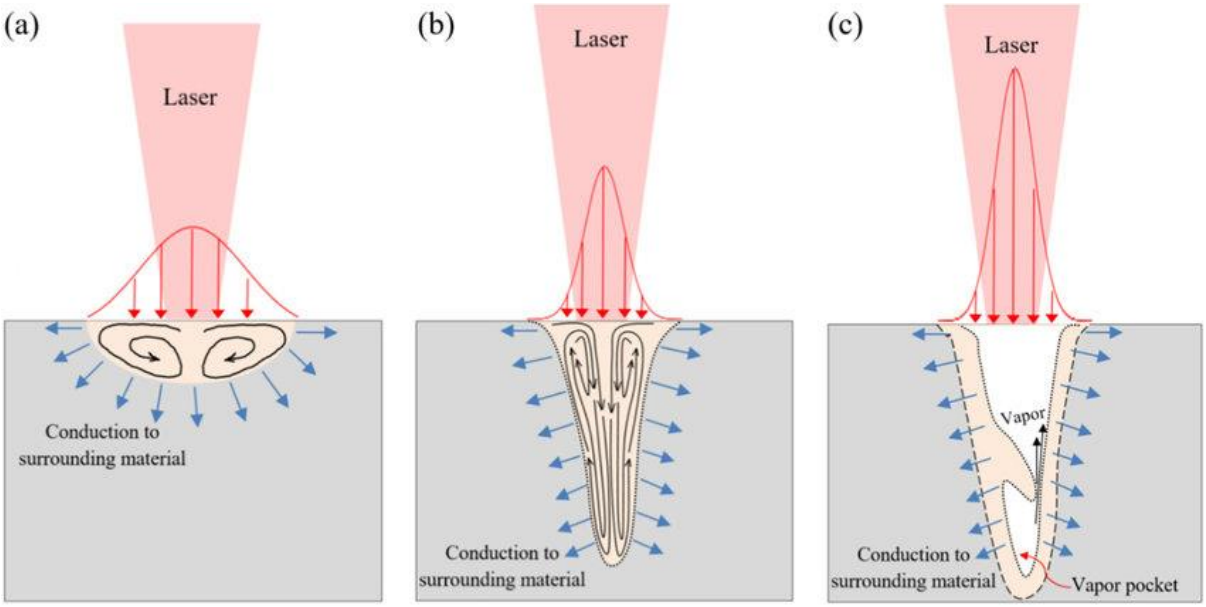


*Figure 15: Melt Pool Formation, a) Conduction b) Keyhole c) Keyhole with Porosity [39].*

Strength and Quality:

Laser welding offers numerous advantages that enhance the strength and quality of the weld. Similar to arc welding methods, it is important to clean and prepare the surface before welding to prevent any contaminations and porosity. Unlike some arc welding techniques, laser welding lack the capability to remove oxides during the welding process, underscoring the importance of thorough surface cleaning for laser welding to be beneficial [40].

When welding aluminum it is noteworthy that the alloy acts as a capable light reflector, which can complicate the welding process as the aluminum will have a low power and heat absorption [41]. A higher power output must therefore be used in order to ensure weld quality when welding aluminum. One effective option to address reflection issues is to utilize the Nd:YAG method.

Laser welding require a lower temperature input as supposed to arc welding and utilize a much highly concentrated and precise weld with the laser's accuracy. This characteristic minimizes the affected HAZ on the workpiece and results in a smaller strength reduction in the welds.

To ensure a proper quality weld when employing deep penetration method, controlling the power output is crucial to establish a stable and secure keyhole. A proper keyhole penetration can reduce both the width and strength losses in the HAZ, eliminating the risk of vapor entrapment and porosity.

#### *2.5.2.5 Friction Stir Welding*

Friction Stir Welding (FSW) is a welding process that uses frictional heat combined with a precise and controlled pressure to create high-strength welding joints with minimal HAZ, low mechanical distortion and excellent surface finish. The FSW method forces the metal into a plasticized state where the two bonding metals are stirred together under pressure to forge a fully penetrated weld [42].

The tool utilized in FSW is a cylindrical extraction called the shoulder. This shoulder rotates on the seam between the two bonding metals creating friction and heat. While the metal does not reach its melting point, the heat and friction facilitate the fusion of atoms for the two metals in the plastic state [43]. This allows the welded region to maintain its grain structure integrity and mechanical properties.

Microstructures:

The mechanical properties of FSW have been proven better than for traditional welding methods. Three main properties of FSW are to be discussed; weld nugget, thermos-mechanically affected zone (TMAZ) and HAZ.

Both the weld nugget and TMAZ are thermos mechanical affected zones, but they are to be considered separately within the scope of microstructure. This is due to the fact that the weld nugget experience dynamic recrystallization while the TMAZ does not [44].

During the welding process the nugget zone (NZ) is in direct contact with the rotating tool, illustrated in Figure 16. Therefore, it will experience a thermal cycle and severe plastic deformations. During the process the metals grains disintegrate and dynamically recrystallize, producing even finer grains.

The TMAZ is located next to the NZ and will also undergo a thermal cycle and some plastic deformations. However, the plastic strain is not sufficient to result in dynamic recrystallization. The HAZ is then located near the TMAZ, and will only experience a thermal cycle but no plastic strain [45].

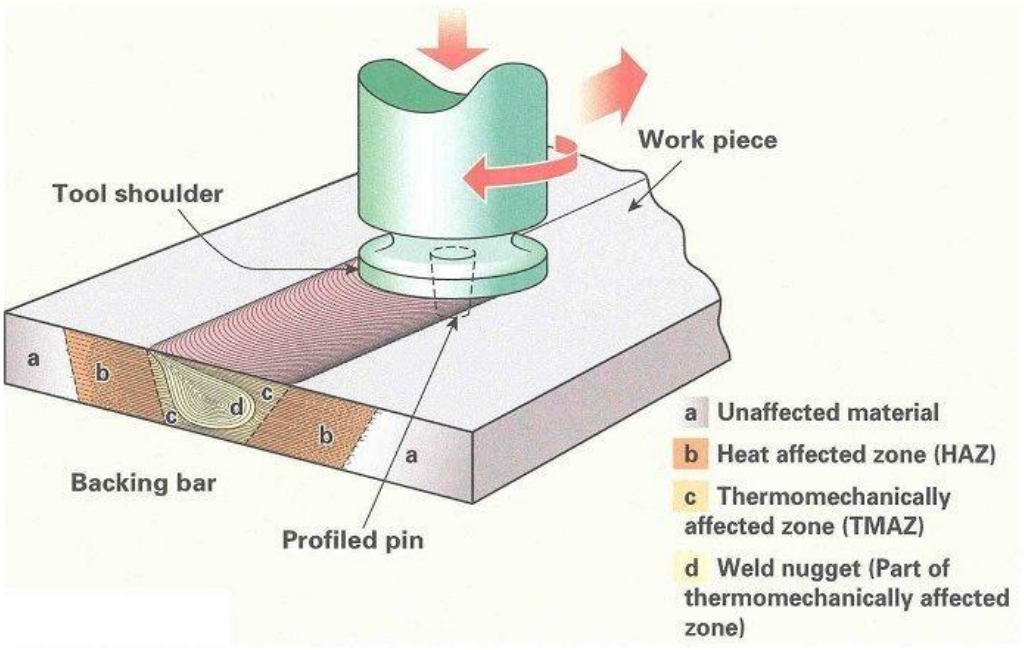


*Figure 16: Microstructures in FSW [46].*

Advantages:

The FSW method offers numerous advantages over conventional welding processes. Unlike traditional methods, FSW eliminates issues such as hot cracking, porosity, and solidification. Additionally, the low temperatures involved result in minimal shrinkage and distortion of the material. FSW requires no filler material, flux, or shielding gas for aluminum welding, as it leverages the material's plastic state to create a secure bond. This also ensures a clean welding process, as no spatter or fumes are generated during welding. FSW has demonstrated excellent mechanical properties, often equaling or exceeding those achievable by other welding methods, particularly for aluminum [44].

## 2.6 Steel

Steel alloy primarily composed of iron and small amounts of carbon, is the most used material in constructing the world's infrastructure and industries. Its versatility is showcased through a huge variety of alloys, where various elements are introduced to the material to create desired properties like abrasion- and corrosion resistance.

The production of steel is done by a smelting process, typically executed through either a blast furnace or an electric arc furnace. Following smelting, the molten steel undergoes casting via a hot strip mill. The steel is then formed by a variety of techniques, usually hot- or cold rolling, shaping the alloy into plates, bars, pipes, or any desired configuration. The finished product is then tempered to attain the desired steel grade [47].

### 2.6.1 Steel Alloys

The alloying process and material composition is highly dependent on the desired application for the steel. Typically, the elements are fused together in a furnace operating at temperatures exceeding 1600 degrees Celsius for several hours. Following, the alloy undergoes an annealing process at temperatures around 500 degrees to eliminate impurities and alter both physical- and chemical properties [48].

On average carbon makes for around 2% if the steels composition and plays an important role in the materials properties. Increasing the carbon content will increase the strength and hardness of the alloy. Steel alloys are categorized in four primary groups: Stainless Steel, Carbon Steel, Tool Steel and Alloy Steel [49].

#### *2.6.1.1 Stainless Steel:*

Stainless steel is an alloy known for its corrosion resistance. This emerges from the chromium content within the alloy which forms a thin, invisible layer of oxide on the surface of the material. This oxide-layer acts as a shield against corrosion and preserves the integrity of the metal.

#### *2.6.1.2 Carbon Steel:*

Carbon steel encompasses an alloy spectrum with carbon content ranging from 0,05 to 2,1%. The level of carbon within the alloy directly affects its strength and hardness, with higher carbon concentrations yielding a harder material. However, high carbon content also renders the material less flexible and more challenging to weld.

*2.6.1.3 Tool Steel:*

Tool steel is tailored specifically for crafting tools, and industrial work environments. The alloy is introduced to elements such as tungsten, chromium, and vanadium, which makes the material heat resistant and durable, qualities essential for tools engineered for prolonged use and rough environments.

*2.6.1.4 Alloy Steel:*

While all steels are technically alloys, when discussing alloy steels, one typically refers to carbon steel augmented with additional alloying elements beyond iron and carbon. The inclusion of these elements fortifies the steel, enhancing its strength, corrosion resistance, and hardens the metal when heat treated. These alloy steels are mostly represented in pipelines, building beams and heavy machinery parts [49].

### 2.6.2 Structural Steel

A specific subgenre of steel alloys is structural steel. Engineered in a variety of industry-standard cross-sectional shapes, these steels are crafted with specific chemical compositions and mechanical properties to suit their designated applications.

Structural steel encompasses a diverse library of grades, each distinguished by a prefix 'S' denoting it a structural steel. It's noteworthy that while there are numerous grades, the classification systems, particularly the European standards, may not be universally adopted. Consequently, the numerical identification of structural steel might vary across different regions, even when the material composition remains consistent [50], this is showcased in the following table.

*Table 8: EU vs. US Structural Steel Notation [50].*

| EU | US |
|---|---|
| **S235** | A283C |
| **S275** | A570Gr40 |
| **S355** | A572Gr50 |

The precise chemical composition of structural steel holds high importance, as even minor alterations can significantly affect its properties. The mechanical properties of any structural steel is fundamental for its intended application. Optimized for construction, structural steel

shows numerous advantages over alternative materials. Its cost-effectiveness and producibility make it a preferred choice for large-scale projects [51].

Structural steel exhibits exceptional load-bearing capacity relative to its dimensions, combined with good ductility, enabling it to absorb energy and support substantial weights without undergoing plastic deformation. Furthermore, its remarkable versatility allows for shaping and molding to suit diverse applications.

#### *2.6.2.1 S355G*

S355, adhering to the European standard, signifies a structural steel where the 'S' denotes its structural designation, while the subsequent number denotes its yield strength [50]. Widely embraced in both onshore and offshore construction, the S355 grade is a proven versatile construction material.

Structural steel requirements for offshore applications are dependent upon the specific application and geographic location. Conforming to standards such as prEN 10225, BS 7191, and utilizing material specifications outlined by NORSOK, the S355 alloy emerges as a suitable candidate for North Sea applications [52].

As previously noted, the mechanical properties of structural steel are linked to its chemical composition. The chemical composition of S355 may vary depending on factors such as tempering, thickness, and delivery conditions. A standard chemical composition for the EU-grade S355 steel is detailed in Table 9.

*Table 9: Chemical Composition - S355 [53].*

| EU GRADE | C | Mn | P | S | Si |
|---|---|---|---|---|---|
| | [%] | | | | |
| **S355** | 0,23 | 1,60 | 0,05 | 0,05 | 0,05 |

Subsequently, S355G demonstrates good strength and load-bearing capabilities due to its high-quality mechanical properties. Characterized as a low carbon manganese steel, it provides excellent weldability and impact resistance in diverse environments. Furthermore, its commendable machinability renders it a compelling choice for this thesis. The mechanical properties of the alloy is presented in Table 10 where “N” represent normal delivery conditions.

*Table 10: Mechanical Properties - S355G [52].*

| | S355G + N | |
|---|---|---|
| **THICKNESS** | TS | YS |
| **[MM]** | [MPa] | |
| **T ≥ 16** | 470 - 630 | 355 |
| **16 > T ≥ 25** | 470 - 630 | 345 |
| **25 > T ≥ 40** | 470 -630 | 345 |
| **40 > T ≥ 100** | 470 - 630 | 325 |

## 2.7 Corrosion

Corrosion is a naturally destructive phenomenon that occurs when some metals are exposed to the environment. The reaction between air, moisture and metal can result in chemical reactions where the metal converts to its more chemically stable oxide, hydroxide or sulfide form, resulting in rusting and strength losses in the reacting metal [54]. For the bases of this thesis where two different metal alloys are used to form one structure, the phenomenon of Galvanic Corrosion will be studied in detail.

Subsea structures and equipment submerged in seawater are particularly vulnerable to corrosion, as the interaction with the marine environment accelerates oxidation. Protecting metals used in subsea applications is crucial to prevent damage and maintain material integrity. Failure to do so can lead to strength loss and compromise the longevity of the equipment.

In today's subsea industry, corrosion protection is a standard practice, with various methods employed to protect components. These methods include passive cathodic-, active cathodic protection, and protective coating corrosion resistance, each offering distinct advantages [55].

### 2.7.1 Galvanic Corrosion

Galvanic corrosion occurs when two dissimilar metals are in contact with each other and immersed in an electrolyte, such as seawater. In this phenomenon, one metal acts as the cathode while the other serves as the anode. Essentially, the cathode draws electrons from the anode, accelerating the anode corrosion process. Consequently, the corrosion rates of both metals are altered, with the cathode “feeding” from the anode [56].

Bimetallic corrosion arises from the difference in electrode-potentials between two metals, illustrated in Table 11. When submerged in seawater, each metal develops an electrode-potential reflecting its ability for oxidation or reduction. When assessing the galvanic series table, metals positioned higher on the table are deemed anodic, while those lower down are cathodic. The greater the separation between the metals in the series, the more pronounced the potential difference is, leading to an accelerated corrosion rate [57].

*Table 11: Galvanic Series Table [58].*

| | No. | MATERIAL | VOLTAGE RANGE | RELATIVE POSITION |
|---|---|---|---|---|
| ↑ LEAST NOBAL (ANODIC) | 1 | Magnesium | -1.60 to -1.67 | |
| | 2 | Zinc | -1.00 to -1.07 | |
| | 3 | Beryllium | -0.93 to -0.98 | |
| | 4 | Aluminum Alloys | -0.76 to -0.99 | |
| | 5 | Cadmium | -0.66 to -0.71 | |
| | 6 | Mild Steel | -0.58 to -0.71 | |
| | 7 | Cast Iron | -0.58 to -0.71 | |
| | 8 | Low Alloy Steel | -0.56 to -0.64 | |
| | 9 | Austenitic Cast Iron | -0.41 to -0.54 | |
| | 10 | Aluminum Bronze | -0.31 to -0.42 | |
| | 11 | Brass (Naval, Yellow, Red) | -0.31 to -0.40 | |
| | 12 | Tin | -0.31 to -0.34 | |
| | 13 | Copper | -0.31 to -0.40 | |
| | 14 | 50/50 Lead/Tin Solder | -0.29 to -0.37 | |
| | 15 | Admiralty Brass | -0.24 to -0.37 | |
| | 16 | Aluminum Brass | -0.24 to -0.37 | |
| | 17 | Manganese Bronze | -0.24 to -0.34 | |
| | 18 | Silicon Bronze | -0.24 to -0.30 | |
| | 19 | Stainless Steel (410, 416) | -0.24 to -0.37 (-0.45 to -0.57) | |
| | 20 | Nickel Silver | -0.24 to -0.30 | |
| | 21 | 90/10 Copper/Nickel | -0.19 to -0.27 | |
| | 22 | 80/20 Copper/Nickel | -0.19 to -0.24 | |
| | 23 | Stainless Steel (430) | -0.20 to -0.30 (-0.45 to -0.57) | |
| | 24 | Lead | -0.17 to -0.27 | |
| | 25 | 70/30 Copper Nickel | -0.14 to -0.25 | |
| | 26 | Nickel Aluminum Bronze | -0.12 to -0.25 | |
| | 27 | Nickel Chromium Alloy 600 | -0.09 to -0.15 (-0.35 to -0.48) | |
| | 28 | Nickel 200 | -0.09 to -0.20 | |
| | 29 | Silver | -0.09 to -0.15 | |
| | 30 | Stainless Steel (302, 304, 321, 347) | -0.05 to -0.13 (-0.45 to -0.57) | |
| | 31 | Nickel Copper Alloys (400, K500) | -0.02 to -0.13 | |
| | 32 | Stainless Steel (316, 317) | 0.00 to -0.10 (-0.35 to -0.45) | |
| | 33 | Alloy 20 Stainless Steel | 0.04 to -0.12 | |
| | 34 | Nickel Iron Chromium Alloy 825 | 0.02 to -0.10 | |
| | 35 | Titanium | 0.04 to -0.12 | |
| | 36 | Gold | 0.20 to 0.07 | |
| | 37 | Platinum | 0.20 to 0.07 | |
| ↓ MOST NOBAL (CATHODIC) | 38 | Graphite | 0.36 to 0.19 | |

### 2.7.2 Passive Cathodic Protection

In a passive cathodic protection system, a sacrificial anode is coupled with a dissimilar metal with a lower voltage range. This connection creates an electrical potential difference between the two metals, creating electricity, initiating the galvanic corrosion. As a result, the original anode is shielded from corrosion, as it would otherwise corrode at a significantly accelerated rate without the passive protection system [57].

The utilization of galvanic corrosion phenomenon has led to the development of comprehensive Galvanic Anode Cathodic Protection (GACP) systems, showcased in Figure 17. These systems produced as a series of aluminum or zinc-based alloy anodes, often installed on submerged offshore steel structures, and serves as sacrificial cathodes. This arrangement effectively shields the structural steel from corrosion. However, it's important to note that these anode materials have a limited lifespan and require periodic replacement to maintain effective protection levels. Additionally, GACP systems must adhere to specific standards outlined in DNV-RP-B401 and ISO 24656 [55].

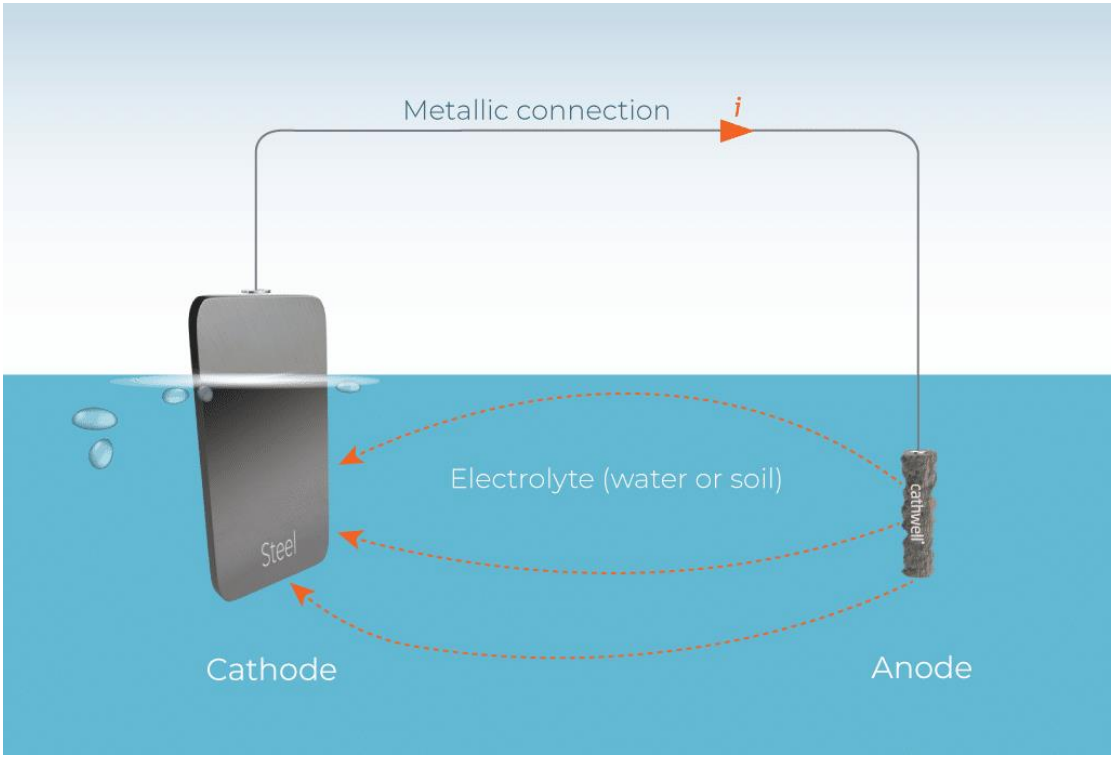


*Figure 17: Passive Cathodic Protection [59].*

### 2.7.3 Active Cathodic Protection

Implementing a passive cathodic protection method becomes impractical for large structures due to the unrealistic quantity of sacrificial anodes needed to supply adequate current for complete protection. To ensure sufficient protection, an external power source is employed to assist the electrochemical reactions. This technique is known as impressed current cathodic protection (ICCP) [57], illustrated in Figure 18.

Compared to GACP systems, ICCP systems are significantly lighter and impose less drag in water. They rely on a dependable power supply, instrumentation and are typically secured to the structure using bolts and flanges [55]. ICCP systems are commonly used for long stretches of pipelines [57].

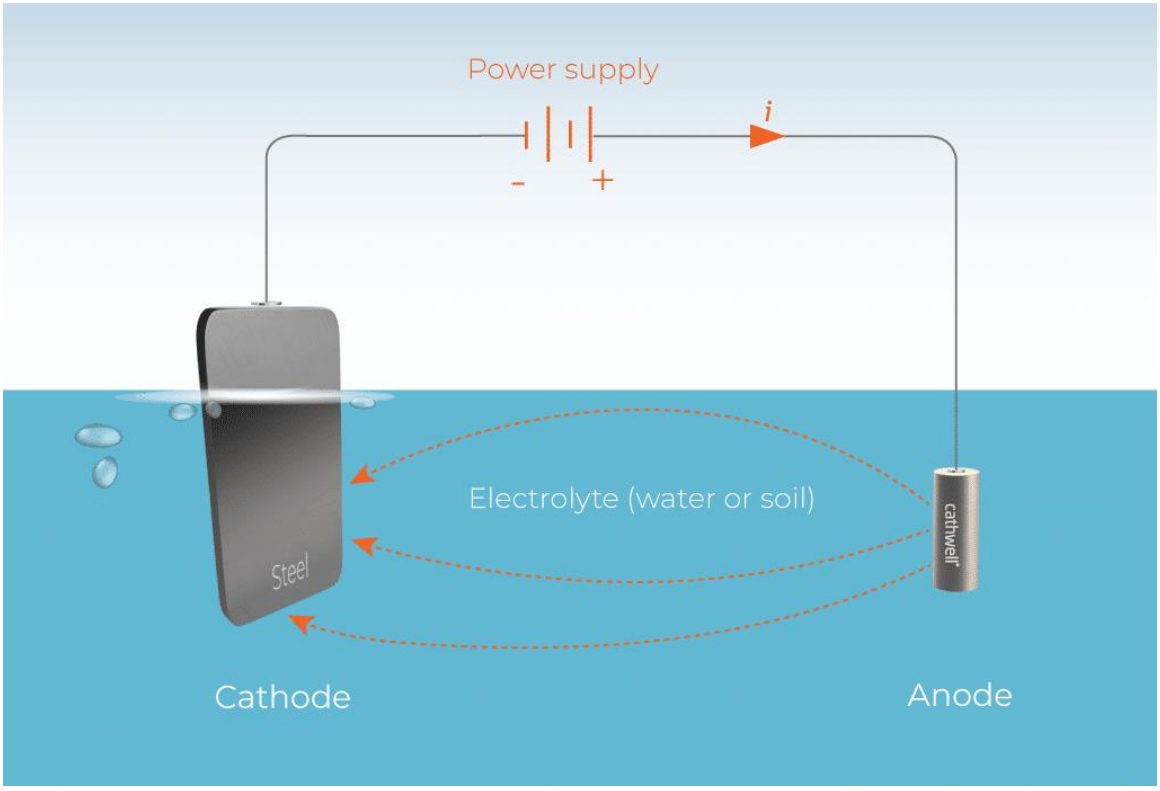


*Figure 18: Active Cathodic Protection [59].*

### 2.7.4 Protective Coating

Subsea equipment operates in environments of extreme temperatures, pressures, and corrosive conditions. With a life expectancy often exceeding 20 years, it is important to protect materials against corrosion throughout their lifespan. Protective coatings are essential for ensuring the corrosion resistance of subsea structures.

These coatings are designed to endure harsh conditions to protect equipment, structures, and entire infrastructures from corrosion, salinity, abrasion, and biological growth. The coatings are specifically formulated to serve as corrosion barriers for exposed surfaces, preserving the integrity of metal properties. Additionally, these coatings possess antifouling abilities to prevent any attachment from marine growth [60].

Generally, these coatings are made from an epoxy resin, which can either be zinc or non-zinc containing. Thermal sprayed aluminum (TSA) has for many years proved itself as a viable option, however this is being phased out with a Non-Zinc-Based epoxy resin, as this provides advantages in fewer required coats and integrity [55].

For the coatings to be effective, thorough surface preparation is required and the coatings must be selected based on the specific environmental conditions of the subsea field [60]. The choice of coating protection for the given equipment or structure must follow applicable standards from NORSOK M501 and ISO 23944 [55].

*Figure 19: Subsea Coating [61].*

# 3. Concept Presentation

In this chapter a concept model will be presented based on the design criteria outlined in the previous chapter for a pure CO2 injection well. The model aims to meet the design criteria necessary for installation on the Norwegian continental shelf, while also offering a more specialized design tailored specifically for pure CO2 injection. To achieve this the model adopts a modularized approach allowing for greater flexibility in design, material selection, and component reusability. The model is created using Autodesk Inventor where the structure is initially modelled with production-ready parts to mimic a fully developed structure. The various design choices will be discussed in detail to showcase the opportunities present within the design.

## 3.1 Choice of Direction

The early design phase and layout of the structure is based on the preparational work established in the specialization project for the master theses [62]. This report discusses potential layouts of the template structure and subsea x-mas tree specifically tailored for CO2 injection. As the report presents different ideas, the concept model will encompass the most promising solutions with the biggest interest for further development and analysis. The main focus will be on a new design layout for the template structure, as this showed promising results. An evaluation of the potential subsea x-mas tree will be discussed later in chapter 5 to fully showcase the complete subsea system.

### 3.1.1 Modularization of Layout

Adopting a modularized design can be an essential step in allowing for new possibilities regarding reusability of parts, individual replacement, new material options and an optimized installation and operational process. For this to be beneficial the layout of the modularized parts will have to adopt a streamlined solution allowing for an individual lifespan of each module. An essential step in achieving this is to adopt standardized fastening points between each module and a careful consideration of division points.

The modules of the template structure are divided into 3 main modules with a separate suction anchor, inner frame, and outer trawl protection. This configuration allows for a separate installation of the suction anchor prior to the template frame, where the complete installation

process will be discussed in more detail later. The layout also opens the opportunity to use individual materials for specific modules according to desired needs.

Using a modularized layout will lead to a more complex structure since each of the modules will need to have its own structural integrity. The design of the template will have to accommodate for this by utilizing strong connection points that is capable of handling any loading scenario. The goal here is to achieve a functional way for the forces to travel between the outer frame down to the anchor and soil. To achieve this, special consideration regarding the exposed parts have been prioritized, where the intension is to construct a clean design which builds natural strength for the exposed loading.

As a result of the more complex structure the templates weight will be somewhat larger compared to a similarly designed fully integrated option, where the benefit of designing the template as one system is considered. The increased number of parts will also lead to increased fabrication work. This cost increase will be deemed irrelevant if the goal of reusability of modules is achieved, where the need for an entirely new template structure for later projects is eliminated. The exception to this will be the suction anchor, as the varying soil conditions can make it difficult to find a suitable installation site for later use.

### 3.1.2 Single Centered Suction Anchor

Utilizing a single suction anchor compared to a four-anchor solution will have clear benefits regarding the footprint of the structure, installation process and achieving a cleaner design considering the modularization of the template structure. The challenge associated with this solution is a decreased stability during some loading scenarios, especially for softer soil conditions. The increased size of the single anchor can become a challenge for larger structures, making this a preferable option for an CO2 injection well which can utilize more compact solution regarding equipment and overall footprint.

Comparing the weight of a single anchor and four-anchor solution for the same load and soil conditions the weight is somewhat larger for the four-anchor configuration, as shown in the specialization project for the thesis at page 40. [62]. As the reduction of utilizing a single anchor is minor, the main contributing factor to the reduced weight will come down to achieving a more compact frame design with an overall smaller footprint. As the Template structure is modularized a single anchor will allow a much more compact inner frame design, as it

eliminates the need for a stiff frame combining the anchors. This yields a decrease in needed beam elements resulting in less fabrication work and overall material usage.

One of the design criterions for the anchor is that the connection points between it and the frame must be easy to operate subsea with limited maneuverability and equipment. A single anchor solution will allow for a simpler design of these connection points since it can be integrated into the anchor itself for added natural strength.

The main concern for the single anchor approach is the reduced stability of the complete structure, as illustrated in Figure 20 below. A horizontal load will cause a bending moment at the anchor, where the increased distance between the reaction forces of the four-anchor solution provides a more stable solution. This means that a single anchor solution will require careful consideration of the soil conditions at the installation sites to ensure a safe lifespan of the structure.

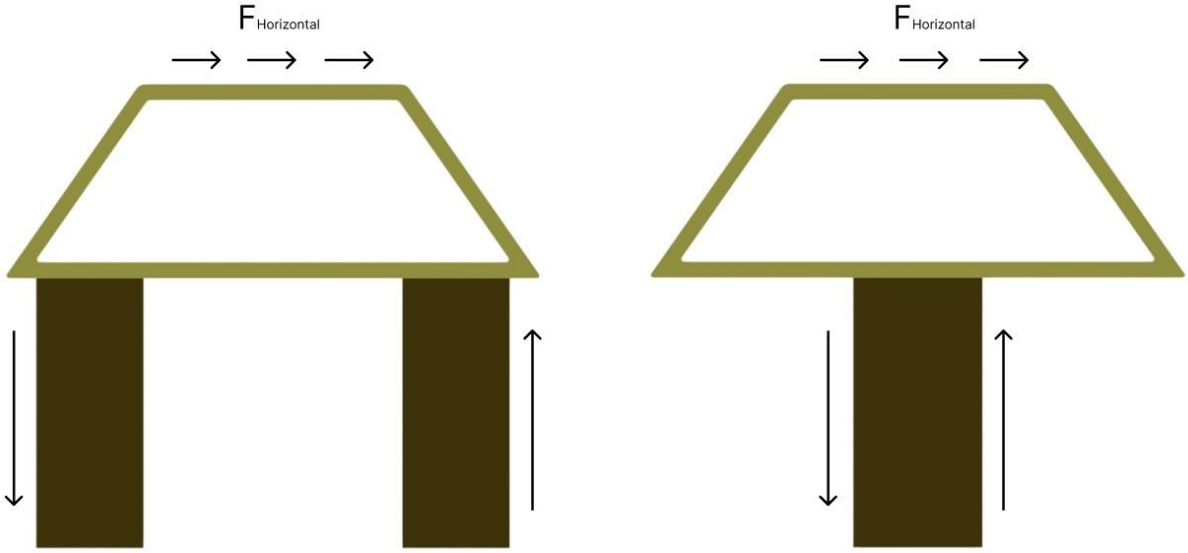


*Figure 20: Illustration of Stability for a Four-Anchor Config. Compared to a Single Anchor.*

### 3.1.3 Material Choices

The template structures unique modular design offers increased flexibility in material selection, enabling the customization of materials for individual modules to meet specific property requirements. Historically, structural steel has been the preferred material for subsea equipment due to its favorable qualities in terms of strength, durability, corrosion resistance, and cost-effectiveness.

In later years there has been a growing exploration of alternative materials within the industry. This exploration is driven in interest of reducing costs and minimizing the environmental impact of subsea structures. Promising alternatives regarding the template design are aluminum and fiberglass, as they offer compelling potential for implementation in specific modules which will be elaborated further below.

#### 3.1.3.1 Outer Frame

The outer frame of the template structure is designed as an individual structural component, where the only contact point will be four flanges anchoring it to the inner frame module. By utilizing isolated connection point between these two modules aluminum alloys will be viable option for the outer frame module. By opting for this solution, the weight of the outer frame can potentially be significantly reduced compared to a complete steel approach. Using aluminum will also help reduce the overall environmental footprint of the structure. As the outer frame will be seen as a reusable component the significance of the added material cost will also be reduced.

The main concern with this approach is the potential for galvanic corrosion, as discussed in section 2.7.1, between the aluminum and steel frame segments of the connecting flange. The different corrosion concerns as well as the structural differences between the chosen aluminum alloy and steel will be discussed in more detail in the structural analysis chapter. As the possibility of corrosion can be reduced through a carefully considered design this is still something that has to be considered from the start of the design process.

#### 3.1.3.2 Inner Frame

The inner frame of the template represents the connection points between the outer frame, suction anchor, and installed equipment. As the anchor and equipment installed is considered mainly steel constructions, opting for the same material will be favorable for the inner frame. This will help achieving a clean design, eliminating the need for isolating connection points towards other modules and equipment than the outer aluminum frame. The connection points between the inner frame and suction anchor will have to be operatable by an ROV for installation at the seabed. As the design process of such a connection point is already challenging, adding the need for insulation will not be seen as an optimal approach.

The inner frame sits in between the outer frame and anchor, which means it will also have to cope with forces transferred by the outer protective frame from varying loading cases. Considering the connection pins from the inner frame to the suction anchor, it is important that the frame does not deform significantly under loading. Significant deformation could cause the pins to wedge in place, resulting in difficulties during the retrieval process. Because of this the higher strength and Young's modulus associated with steel will be considered favorable.

#### 3.1.3.3 Suction Anchor

The template is constructed with one centered suction anchor resulting in large bending stresses during varying loading scenarios. The anchor will absorb forces from the frame modules with minimal flex and give. To ensure the structural strength of the anchor it is favorable to also use steel for the anchor. As mentioned above it is also important to use the same material for the anchor an inner frame module to eliminate the need for isolated mounting points.

One option is to construct a structural frame for the anchor using steel, with an alternative material used for the skirts and lid. This can be done in a measure to reduce the weight and cost of the anchor and is a concept Equinor has been experimenting with in recent years within the cap-x project [63]. This solution is not implemented into this project in an effort to simplify the anchor design. A complete steel anchor will allow for the mounting points to the inner frame to be more efficiently integrated into the anchor. It will also be easier to obtain the structural integrity needed without the need for excessive beam and plate elements, resulting in an overall reduction in fabrication costs.

## 3.2 Design Criterion

The template structure must follow the necessary standards for installation on the NCS. since the structure is in the conceptual stage, only the primary requirements stated in the NORSOK U-002 and NORSOK U-001 standards will be discussed in detail. As the template structure is intended to be overtrawlable, it will also have to meet specific requirements regarding this. The exception is a physical trawl model test, which is excluded to limit the scope of the master thesis.

### 3.2.1 Design for Overtrawlability

Choosing an overtrawlable design will result in a lighter frame with a smaller footprint. This is a result of overlooking PLS loads from fishing gears, as trawlboard snag, trawl ground rope snag and trawlboard snag on sealine [64]. The main requirements for the template structure to follow is listed below [65].

1. The protective structure shall deflect all fishing equipment.
2. The structure shall include corners, with the maximum true angle of 58º from the horizontal optimized to assist trawl and trawl wire deflection.
3. Corners, ramps and equivalent structures shall penetrate the seabed to avoid snagging from trawl warp lines and ground ropes. Effects from installation tolerances and expected souring shall be accommodated.
4. The overall geometry of the structure and the size of openings shall be such that trawl doors are prevented from entering into the structure.
5. If vertical side bracings are included, these shall be spaced to prevent intrusion and rotation of trawl equipment, without restricting subsea structures access for the intervention system.

For a template structure to be considered overtrawlable it must undergo physical testing to obtain the required documentation. The model test uses a scaled model placed in a towing tank which can drag a replicated trawl gear for the installation site. The test should simulate the trawl gear type, trawl speed, water depth, friction on seabed and structure, length, stiffness and angle of warp lines, minimum breaking strength in warp line, bobbins and ground rope [64]. As undergoing such a test is a comprehensive task this is not done for this project.

The cost and timespan required for such an approach have rendered it less appealing for previous projects. However, with the emphasis of the new template design on reusable modules and the increasing concern over emissions costs, such an alternative could become favorable. This is primarily due to the reduced material requirements resulting from lower stresses associated with an overtrawlable option.

### 3.2.2 Hatch Design

The main criterion for the hatch design is to allow for good accessibility during installation and interventional work. This can be done by assessing the distinct operations required during the lifespan of the template to ensure a good design. The requirements within NORSOK U-002 must also be followed and is listed below [65].

1. If applicable, the protective hatches shall withstand dynamic forces induced by wire (i.e. vessel heave) during opening/closing, maximum 7 tons.
2. The protective hatches shall be designed to fall freely in water during opening/closing but means of controlled lowering should be provided.
3. Any replacement of hatches or roof sections shall be performed according to the selected intervention strategy.
4. Any openings in grating on the roof hatches shall be sufficiently small to protect against objects that are lifted over the structure.

## 3.3 Presentation of Model

Using the materials previously discussed in this chapter, a full-scale model of a subsea template structure has been constructed using Autodesk Inventor. The model consists of plate elements and tube sections, complemented by selected casted parts where a more complex geometry is needed. This approach ensures a realistic construction using accessible and cost-effective components, while also considering an efficient assembly process. The model will be presented stepwise before the complete system is shown.

### 3.3.1 Aluminum Frame

To construct the main frame structure, tube sections are chosen for their versatile strength configurations. Additionally, they are easy to obtain and weld during the assembly process. The structure must endure various loading scenarios, necessitating a naturally stiff system. Located between the outer hatches and steel modules, the frame must also withstand transferred loads form the hatches to ensure the structural integrity of the complete system. These stresses are then distributed through the frame onto the steel and anchor modules. The modelled frame is shown in Figure 21 below.

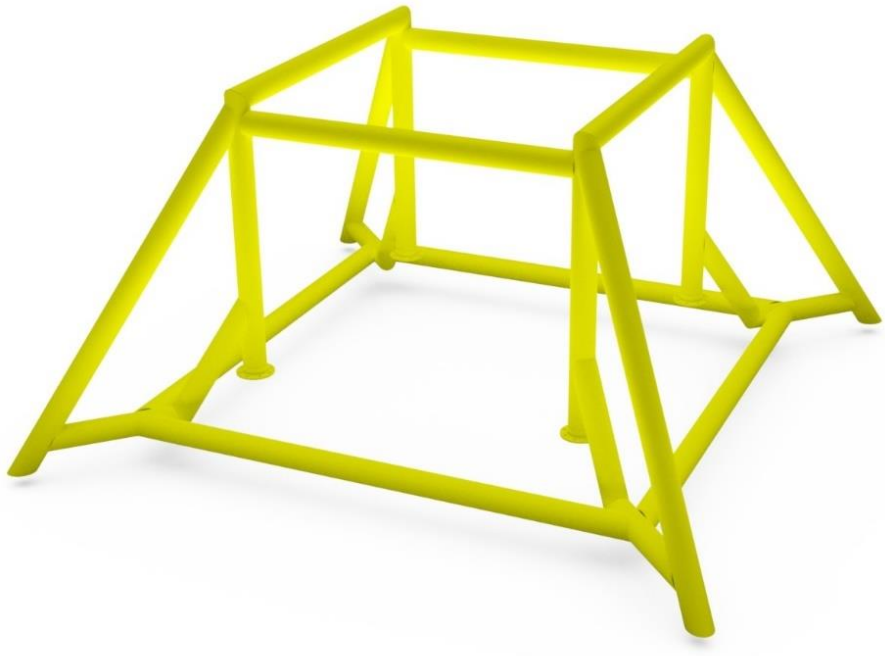

*Figure 21: CAD Model - Aluminum Frame.*

The frame consists of tube sections with an outside diameter (OD) of 360mm and a thickness of 20mm. It maintains symmetry across two midplanes, resulting in a predictable design for the varying loading cases throughout its lifespan. The shape is designed to keep the aluminum material at a safe distance from the steel modules and installed equipment to reduce the risk of galvanic corrosion. The only contact point will be the four flanges located in the center bottom section, where the frame will be bolted to the inner steel module. The complete design of the isolating flanges will be elaborated on further in chapter 4.5. To assist trawl deflection the true angle of the protruding corner pipes and the horizontal plane is set to 55 degrees, keeping the design within the limit presented in NORSOK U-002 [65].

#### *3.3.1.1 Side Hatch*

Installed on the aluminum frame is five hatches than can be operated independently. The hatches are constructed with a stiff outside frame using tube section with an OD of 200 mm and thickness of 20 mm. Plate elements with a thickness of 25mm are positioned between the pipe sections. This design choice minimizes the number of components required compared to alternative methods, reducing welding and construction time. The front and rear hatches are identical, where the model is shown in Figure 22.

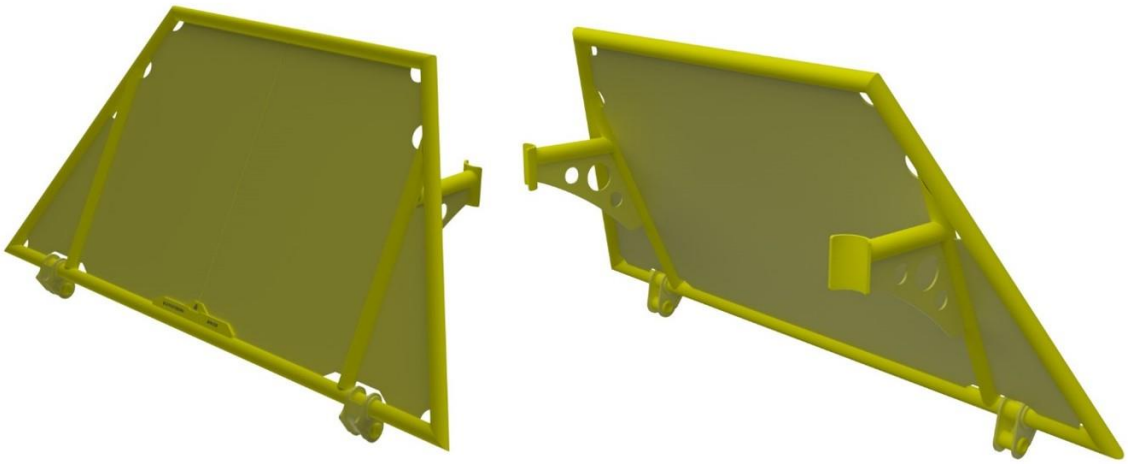

*Figure 22: CAD Model - Front and Rear Hatches.*

Each hatch features two protruding arms with reinforcing plates to ensure structural support when in the closed position. The hatch will rest securely on the vertical pipe sections of the main frame structure. The front and rear hatch is design to lay horizontally when in its open position, which will provide good accessibility for ROV entrance. The horizontal position and hatch shape will also allow for ROV parking during installation and maintenance work, as illustrated in Figure 23. The dimensions of the shown ROV are 2575 mm x 1550 mm (L x W), representing a typical workclass ROV.

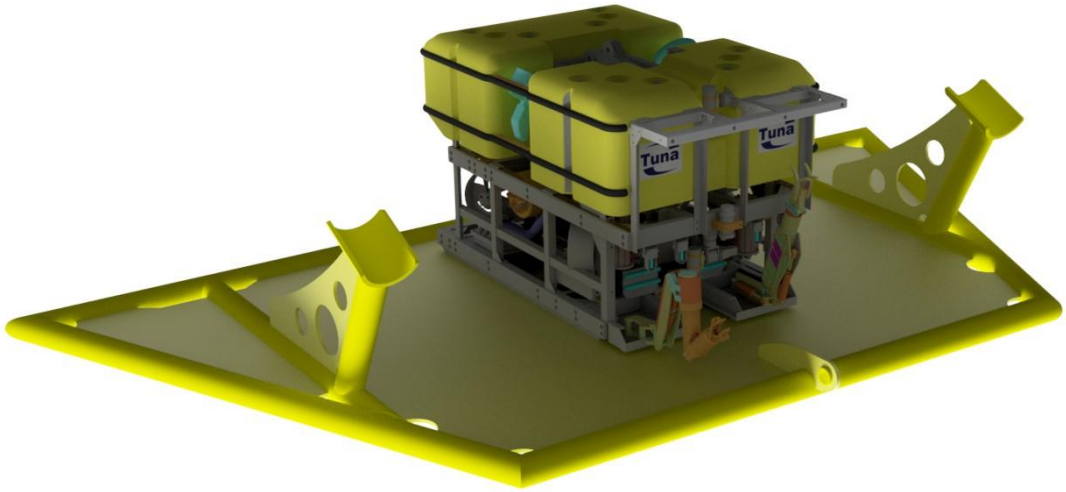


*Figure 23: CAD Model - Front Hatch with Illustration of Parked ROV [66].*

The side hatches of the template frame are designed in a similar way to the front and rear sections. Given that the flowline connections for the installed x-mas tree are situated on the sides, an opening is incorporated at the bottom to allow for easy flowline and cable entry. Additionally, to simplify the installation process they are equipped with top mounted hinges. This will allow for efficient placement of the horizontal tie-in system discussed in chapter 2.3 or comparable systems. The model of the side hatches is shown in Figure 24 below.

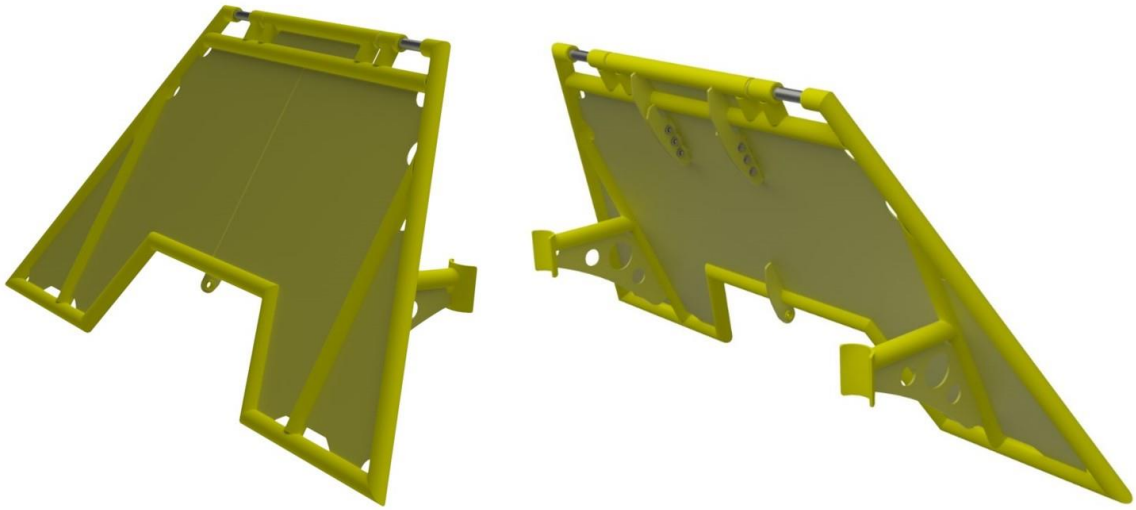

*Figure 24: CAD Model - Side Hatches.*

### *3.3.1.2 Top Hatch*

To construct the top hatch a sturdy frame consisting of tube sections is used for the foundation. Plate elements are placed at a 45º angle from the horizontal plane to gradually increase the height of the hatch towards the middle. This is done to make room for the guideposts utilized when installing the x-mas tree. The guideposts should be taller than the main frame to reduce the risk of collisions, simplifying the installation process. The hatch opens towards the rear with a resting position of 30º away from the frame structure with regards to the vertical plane. This is done to limit the intrusion of the hatch during installation of equipment on the template. The model of the top hatch is shown in Figure 25.

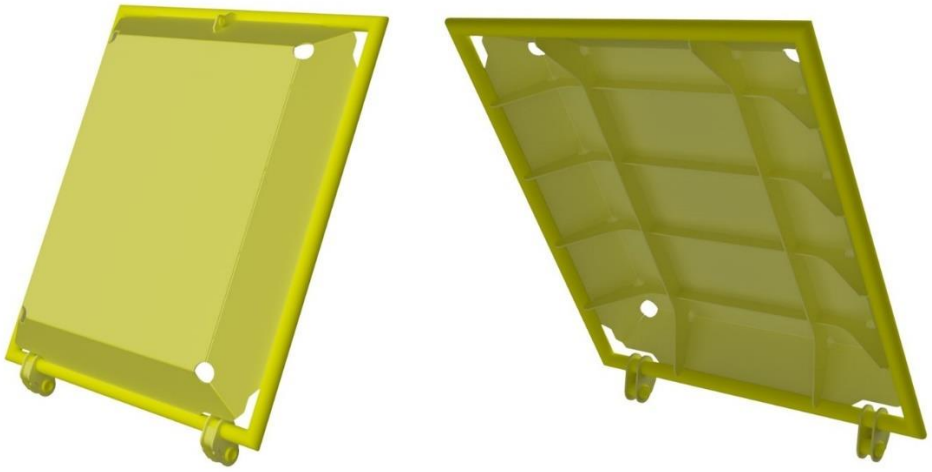

*Figure 25: CAD Model - Top Hatch.*

Below the plate elements a set of beam elements are welded in place to enhance the vertical load bearing capacity of the hatch. This will be especially important when considering loading from dropped objects near the center of the hatch. The beam elements are constructed using a well proven layout with girders in the transverse direction, complemented with smaller longitudinal stiffeners. This method is commonly used in ship construction for its versatile and efficient strength building capability, which easily can be dimensioned to handle the varying loading cases present for the hatch [67].

#### *3.3.1.3 Hinges*

To achieve an accessible template design, each hatch can be opened using a crane ship positioned at the water surface above. The design of the hinges varies according to the specific function and available space for the front/rear hatch, side hatches, and top-mounted hatch. For the front and rear hatch, the hinge is positioned at the lower horizontal tube section of the main frame structure, as illustrated in Figure 26.

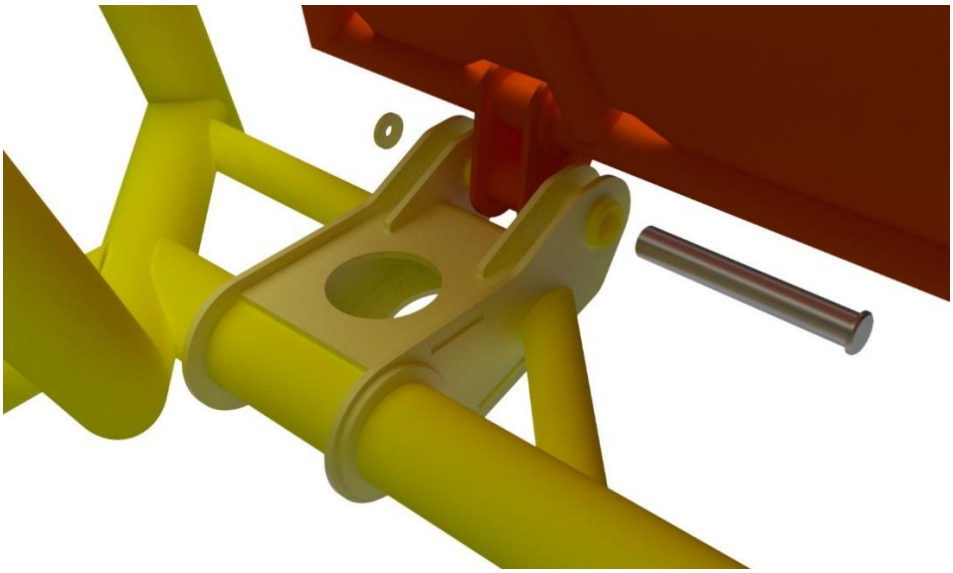

*Figure 26: CAD Model - Front Hinge with Hatch Closed.*

Separate brackets are welded to both the main frame and hatch, with the hatch highlighted in red in the previous figure. These brackets are connected by a bolt secured with a locking plate, achieving an easy installation and removal process. The bracket welded to the main frame is also reinforced by two tube sections to enhance the stiffness during varying loading cases.

To enable the hatch to lay horizontally when opened, the two brackets are designed to touch in this position as illustrated in Figure 27 below. To manage the stresses associated with ROV parking, the contact area of the two brackets is maximized without creating protruding parts that could increase the risk of snagging during over trawling.

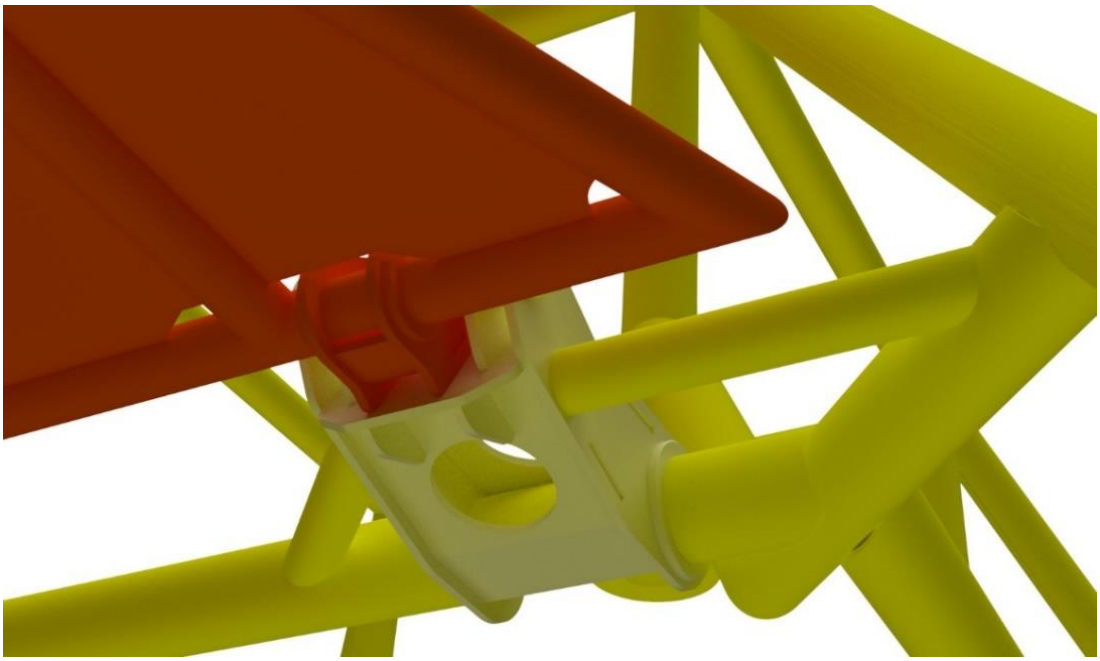

*Figure 27: CAD Model - Front Hinge with Hatch Open.*

The top mounted hinges for the side hatches require a different design than the front-mounted hinges due to spacing constraints. In this configuration, a single bracket is welded to the main frame structure. The bolt housing is integrated into the hatch frame itself, as illustrated in Figure 28. This design offers a compact solution with fewer plate elements, resulting in a clean and cost-effective design during the construction phase.

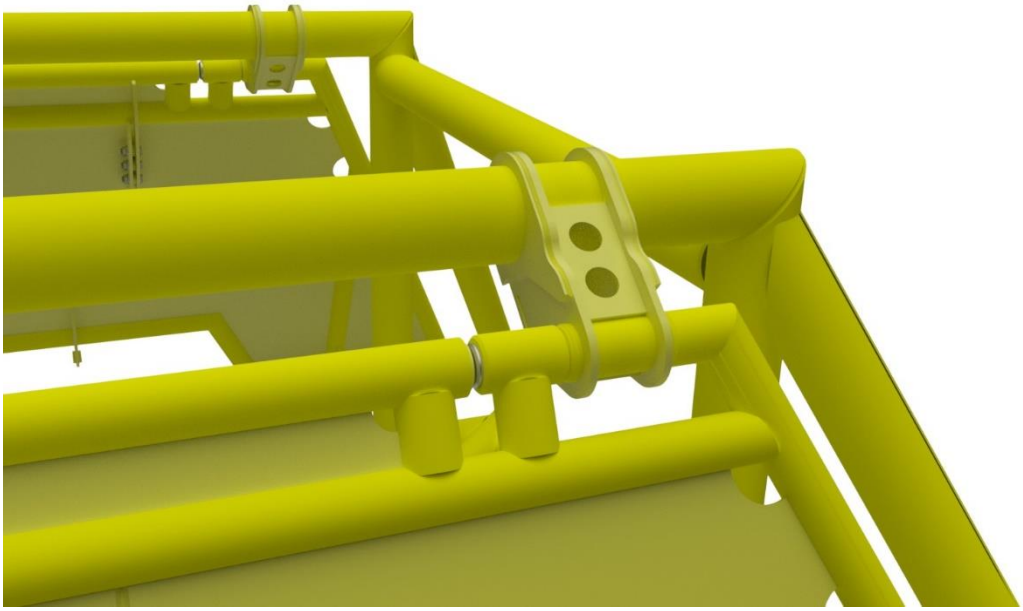

*Figure 28: CAD Model - Side Hinge Closed.*

Grooves are also positioned on the bracket to provide support for the hatch frame when in its fully opened position. The hatches rest at a 15º angle from the vertical plane towards the middle of the module, reducing the likelihood of accidental falls. To further mitigate this risk, the bracket should incorporate a locking option to secure the hatch in the opened position. An illustration of the side hatches in the open position is provided in Figure 29 below.

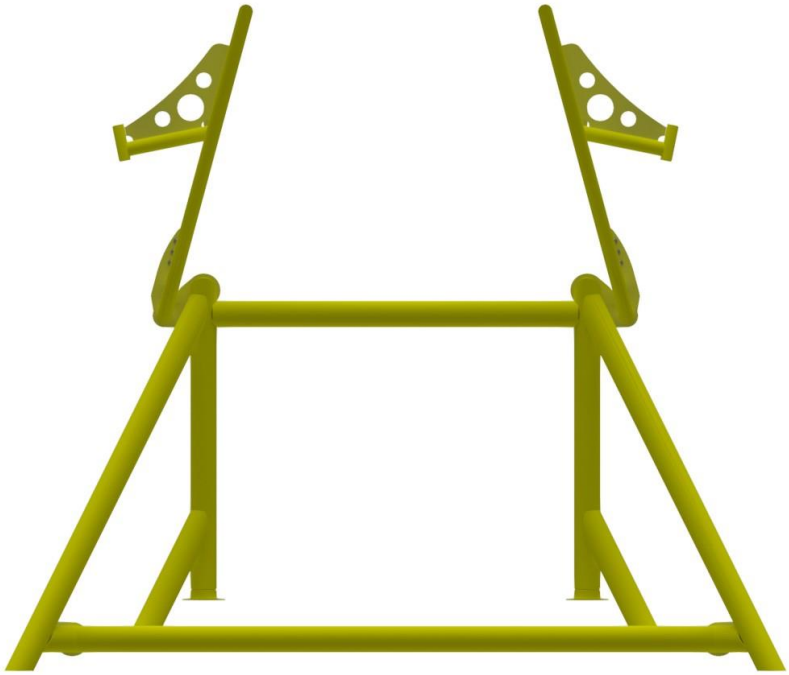

*Figure 29: CAD Model - Side Hinges Opened.*

Due to the integration of the bolt housing in the frame of the hatch, the bolt will require a different method of locking then the front hinges. To solve this problem the top centered part of the side hatch is made as a separate part, as showcased in red in Figure 30. This component is fastened to the hatches using six bolts, effectively locking it in place during normal operation and preventing the bolt from moving independently. When disassembling the hatch this part can easily be removed to access the bolt, facilitating maintenance and repair processes.

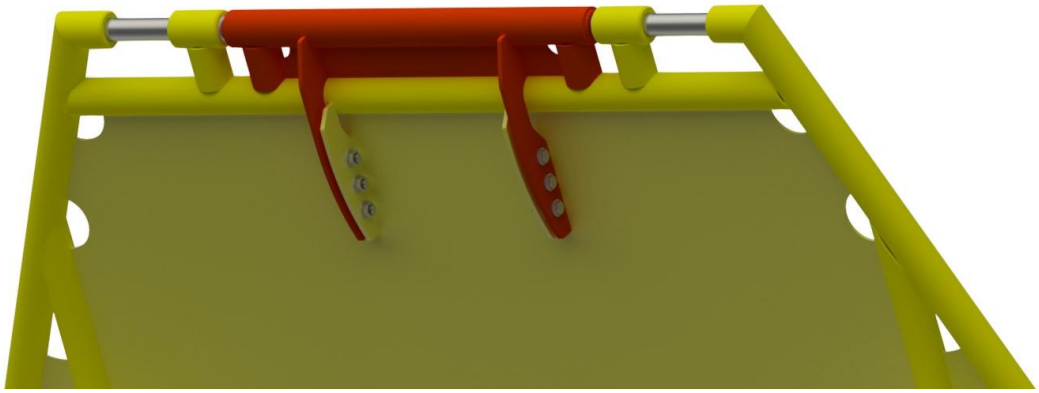

*Figure 30: CAD Model - Side Hatch Locking Mechanism.*

The hinges for the top hatch are designed similarly to the front and rear hinges, ensuring stability when fully open. Figure 31 illustrates this, highlighting the top hatch with its welded bracket in red, showcasing the contact areas that provide a stable resting position. The hatch is positioned at a 30º angle away from the vertical plane, extending from the central opening of the main frame. This angle is chosen to mitigate the risk of accidental falls and to create sufficient space for hanging equipment during installation, thereby reducing the risk of collisions.

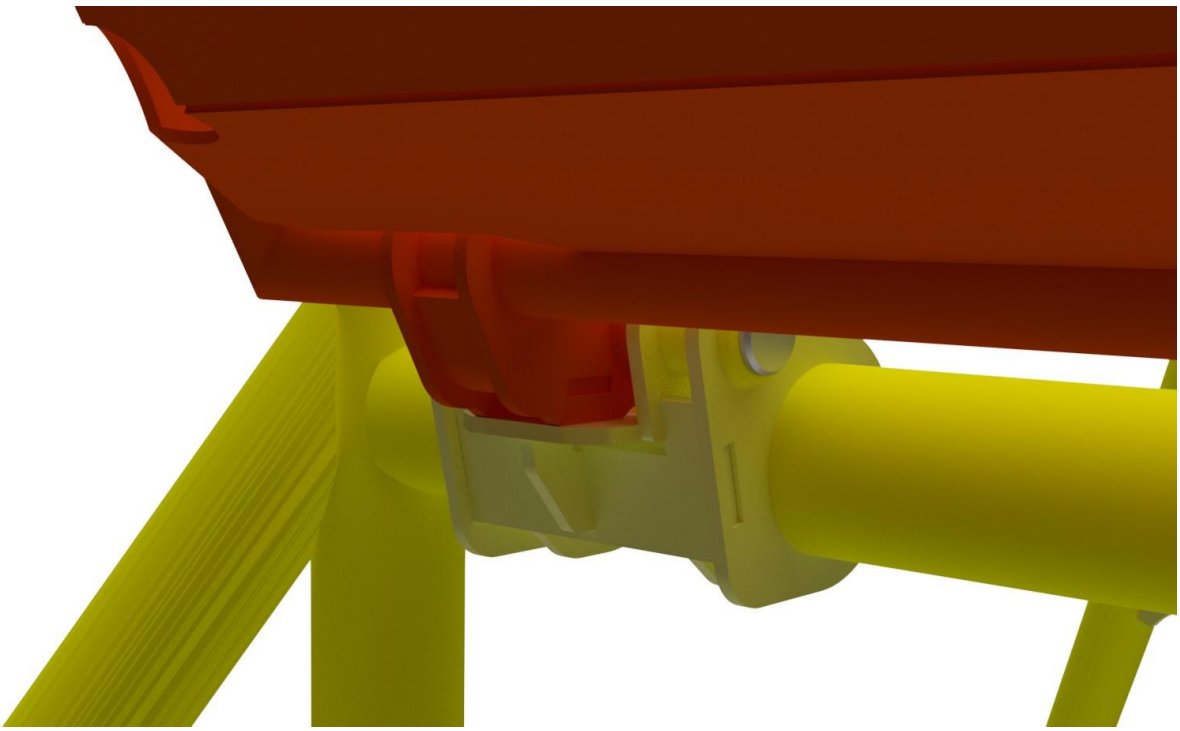

*Figure 31: CAD Model - Top Hinge in Open Position.*

### *3.3.1.4 Complete Aluminum Module*

To get the complete aluminum module all the previous parts are assembled. The dimensions of the module are displayed in Figure 32, where the length and width of the template is equal to 10500 mm and height 5810 mm, representing a compact design. The top opening is 4785 mm x 4785 mm, allowing for easy entry of a compact subsea x-mas tree. The dimensions of the module can easily be adjusted to suit the preferred installed equipment.

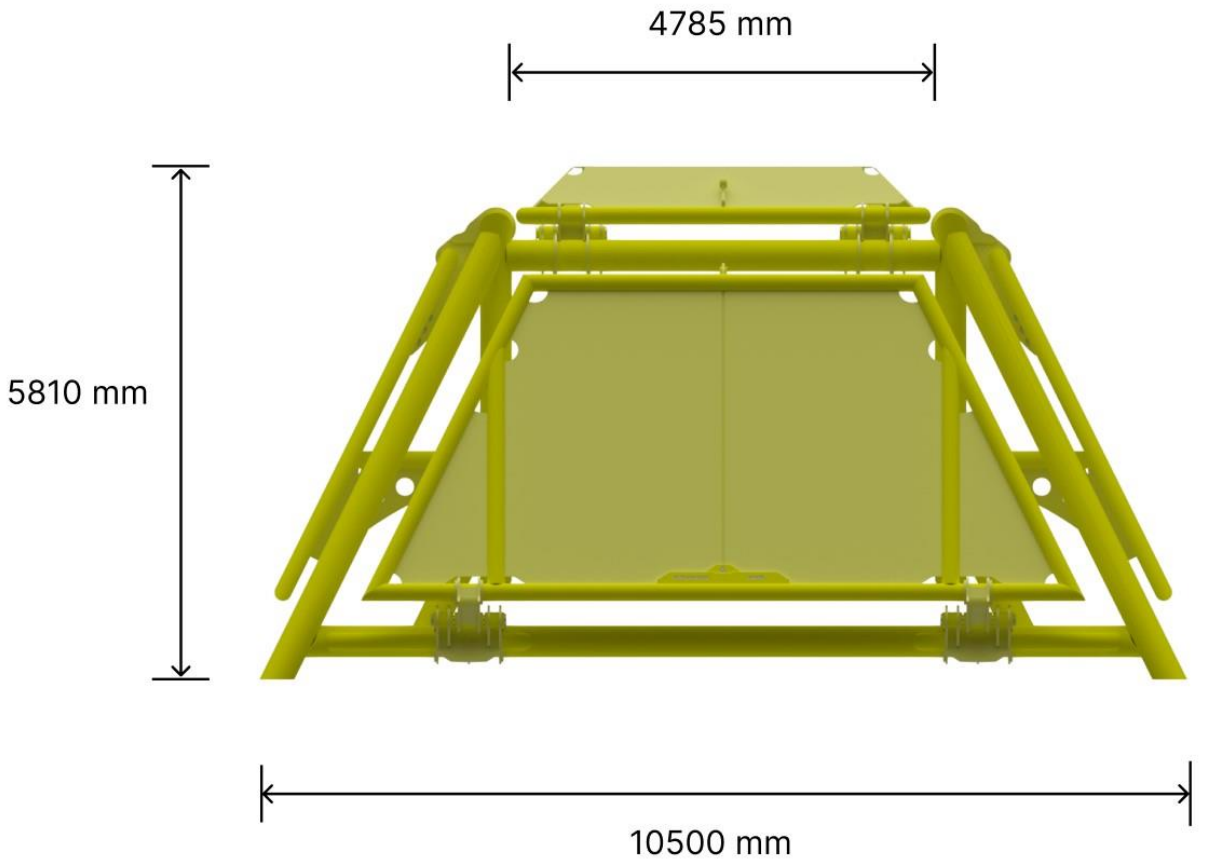


*Figure 32: CAD Model - Complete Aluminum Module with Dimensions.*

The complete assembly consists of a total of 309 parts, with a total weight of 20774 kilograms. Table 12 outlines each major component within the assembly with its associated weight, number of parts, and material selection.

*Table 12: Overview of Properties of Aluminum Module.*

| COMPONENT | MATERIAL | NUMBER OF PARTS | TOTAL WEIGHT [KG] | QUANTITY |
|---|---|---|---|---|
| **MAIN FRAME** | 5083-H116 | 24 | 6137 | 1 |
| **FRONT/REAR HATCH** | 5083-H116 | 30 | 2500 | 2 |
| **SIDE HATCH** | 5083-H116 | 38 | 2480 | 2 |
| **TOP HATCH** | 5083-H116 | 31 | 2754 | 1 |
| **FRONT/REAR HINGE** | 5083-H116 | 16 | 322 | 4 |
| **SIDE HINGE** | 5083-H116 | 8 | 108 | 4 |
| **TOP HINGE** | 5083-H116 | 11 | 101 | 2 |
| | | | | |
| **TOTAL** | - | 309 | 20773 | - |

### 3.3.2 Steel Module

The steel module will be positioned within the center of the aluminum module, serving as a connection point between the aluminum module and the suction anchor. The connection between the aluminum module and the steel module is facilitated by the isolated flange, highlighted in red in Figure 33. A detailed view of the flange design will be provided later in chapter 4.5. In the center of the module, there is a 965.2 mm (38 inch) hole designed to accommodate the installed wellhead.

*Figure 33: CAD Model - Steel Module.*

The construction primarily consists of plate elements that have been cut or bent to shape, resulting in cost-effective and accessible parts. The thickness varies between 15mm to 30mm, depending on the estimated strength requirements. These plate elements are utilized to fabricate I-beams with varying heights and thickness profiles, aiming to minimize overall height while ensuring the natural stiffness towards different loading scenarios. Additionally, the construction incorporates a circular I-beam between the four main beams to enhance stiffness against torsional flexing.

To make for an easy connection to the suction anchor four rods are welded to an integrated pipe section in the frame, as illustrated in gray in Figure 34. These rods are casted parts to allow for a more complex shape at the bottom to help center the rods easily in the receiving housing of the suction anchor. To secure the frame once it sits in place a bolt operated by an ROV is used. The bolt is meant to slide into a horizontal receiving housing welded to the suction anchor, achieving a secure connection point.

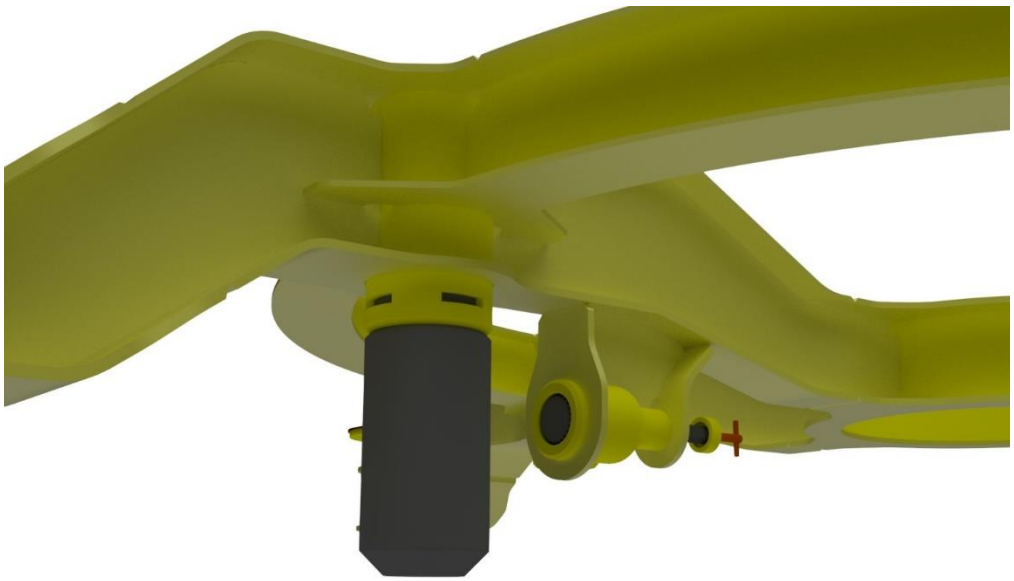

*Figure 34: CAD Model - Steel Module with Connection Point and Locking Bolt.*

The complete assembly consists of a total of 87 parts, with a total weight of 6397 kilograms. Table 13 below outlines each major component within the assembly with its associated weight, number of parts, and material selection.

*Table 13: Overview of Properties of Steel Module.*

| COMPONENT | MATERIAL | NUMBER OF PARTS | TOTAL WEIGHT [KG] | QUANTITY |
|---|---|---|---|---|
| **MAIN FRAME** | S355 | 55 | 5997 | 1 |
| **LOCKING BOLT** | S355 | 4 | 24 | 4 |
| **BRACKET FOR LOCKING BOLT** | S355 | 4 | 76 | 4 |
| | | | | |
| **TOTAL** | - | 87 | 6397 | - |

### 3.3.3 Suction Anchor

As the suction anchor is not the primary focus of this study, only a simplified model is created to illustrate the installation process and complete template system. Structurally the suction anchor operates similarly to a traditional one, with the exception of the connection points designed specifically for the installation of the steel module at the seabed. These four connection points, along with the horizontal housing for the locking bolt, are visible at the top of the anchor in Figure 35. A more detailed view of this will be provided in chapter 5.2, where an illustration of the installation process of the final model is described.

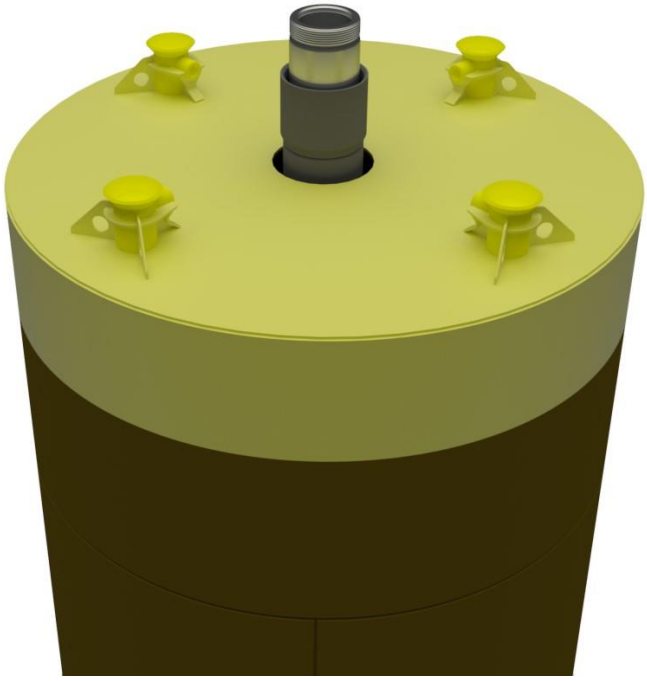

*Figure 35: CAD Model - Suction Anchor.*

The anchor is designed with a concentric hole to facilitate drilling and completion of the well through the anchor. This configuration results in a structurally independent well structure, which helps alleviate certain loads from both the anchor and the accompanying template structure. The diameter of the anchor is intentionally set to 6000 mm to allow for installation through a moonpool. The penetration depth used is estimated to 11000 mm. Final calculations regarding this will be conducted once the model is complete and the data for the system's total weight is available.

### 3.3.4 Complete Model

To obtain the complete template system the three previously presented modules are assembled, as illustrated in Figure 36 below. The model showcases the front, rear, and top hatches in their open positions. This solution presents a compact system with excellent accessibility for installation and maintenance work. Despite being divided into modules, the structure maintains an overall clean design with a limited number of production parts.

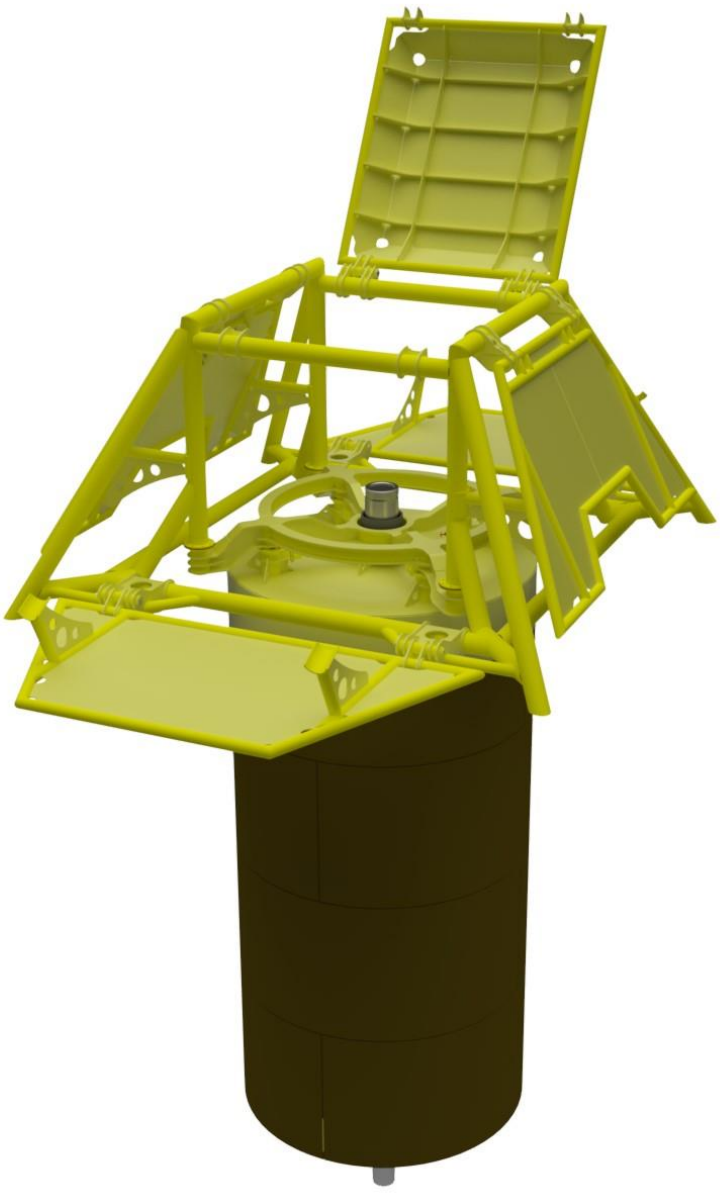

*Figure 36: CAD Model - Fully Assembled Concept with Front, Rear and Top Hatch Open.*

Figure 37**,** illustrates the template installed at the seabed with all the hatches in its closed position, showcasing the overall compact design of the structure. The structure has no protruding parts with an overall smooth finish on the outside to help build the groundwork for a completely overtrawlable template structure.

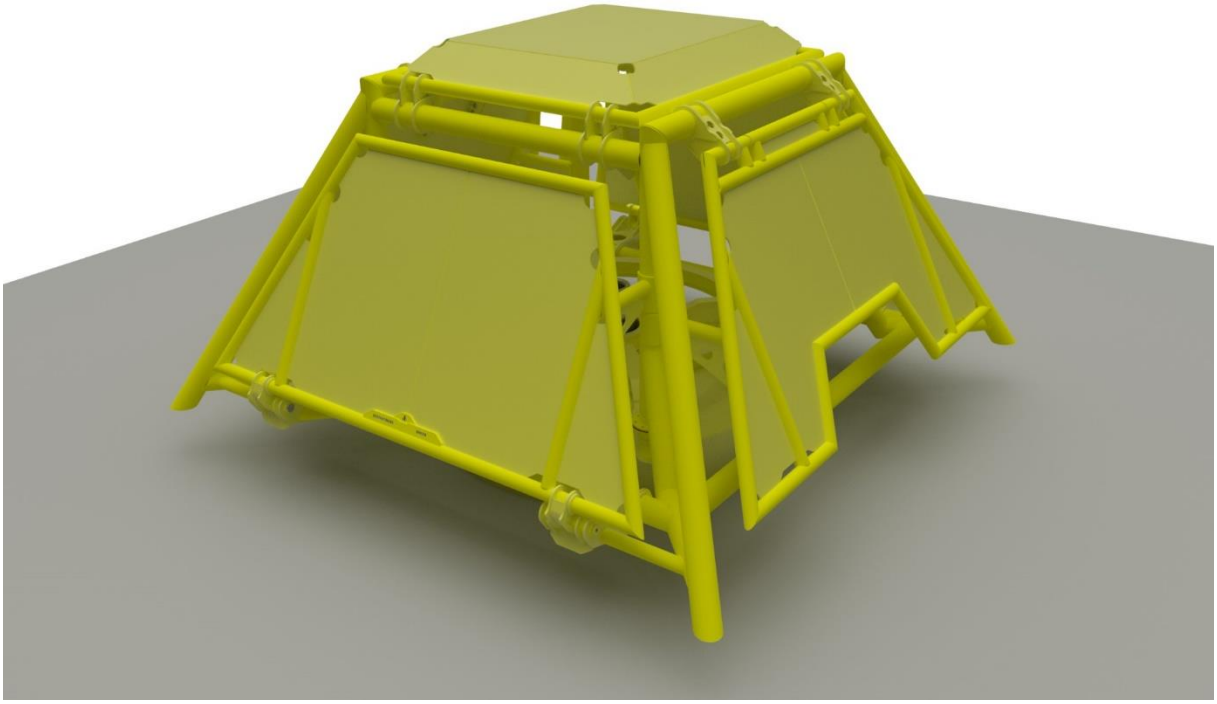

*Figure 37: CAD Model - Fully Assembled Concept Installed at Seabed - Closed Hatches.*

The complete template assembly consists of a total of 396 parts, with a total weight of 27170 kilograms. Table 14 outlines each module within the assembly with its associated weight, number of parts, and material selection. The suction anchor is excluded from the table as it has not yet been made a detailed model.

*Table 14: Overview of Properties of Full Concept Model.*

| COMPONENT | MATERIAL | NUMBER OF PARTS | TOTAL WEIGHT [KG] | QUANTITY |
|---|---|---|---|---|
| **ALUMINUM MODULE** | 5083-H116 | 309 | 20773 | 1 |
| **STEEL MODULE** | S355 | 87 | 6397 | 1 |
| | | | | |
| **TOTAL** | - | 396 | 27170 | - |

# 4. Structural Analysis

In this chapter, the conceptual model introduced in the previous chapter will be analyzed under various load scenarios to assess the structural integrity of the template structure. Based on the analysis results, modifications will be implemented to enhance the system's ability to withstand the varying loads encountered throughout its operational lifespan. The objective is to develop a subsea system that meets the qualifications for installation and operational use on the Norwegian continental shelf, providing a more accurate estimation of costs, weight and usability. The structural analysis will be caried out using the finite element method (FEM) within the ANSYS software, supplemented by hand calculations.

## 4.1 Loads

During its operational lifespan the structure will encounter diverse load cases with varying degrees of occurrence. The design loads utilized are primarily gathered from NORSOK standards, supplemented by information from lecture notes and user-defined loads specific to the structure. These load cases can be categorized into the following segments:

- Splash zone
- Static loads
- Trawl loads
- Tie-in loads
- Dropped objects

The hydrodynamic forces in the splash zone will not be analyzed in this study to narrow down the scope of work. The focus will be on detailed definitions of static loads, trawl loads and dropped objects concerning the template structure. Given that the subsea system represents a new concept, load cases from different template layouts will be selected to suit the model as needed. These cases will then undergo analysis using the finite element method, complemented by hand calculations for relevant load scenarios and components.

### 4.1.1 Static Loads

As the well structure is considered structurally independent of the suction anchor and accompanying template structure, the static loads exerted on the template structure are limited. Excluded loads includes tie-in loads and the weight of installed equipment during drilling and normal operation. The specific static loads that are to be considered for the template structure are listed in Table 15.

*Table 15: Static Loads [65].*

**STATIC LOADS**

| DESIGN LOAD TYPE | Design load | Design state |
|---|---|---|
| **CRANE SHIP HEAVE ON HATCHES DURING OPENING/CLOSING** | 7 tons | ULS |
| **HATCH FULLY OPEN WITH PARKED ROV** | 7502 N | ULS |

The static load for crane ship heave can be referenced from NORSOK U-002 rev 2, section 4.2.7. Given that the hatches are primarily intended to be operated by a crane ship, this load applies to every hatch on the template structure. The hatches will be most exposed to this load when positioned vertically while the crane ship undergoes heave motion. Consequently, a load of 7 tons will be applied to the lifting points on the hatches.

Both the front and rear hatch of the template structure are designed to lay horizontally in their open state to facilitate short-term parking of an ROV or unused equipment. This configuration results in a significant bending moment towards the hinge point, as the hatch is only supported at the hinge when open.

To simulate the potential impact of an ROV touchdown on the hatch, the weight of a typical workclass ROV is considered. For this load the Magnum Plus ROV from Oceaneering has been used as an example of a typical ROV. It has an air weight of 3060 kg but is buoyancy neutral in water [68]. An approximate force equivalent to 25% of the weight is selected to represent the

touchdown force of the ROV hitting the hatch. This force is then applied to the midpoint of the hatch to assess its structural integrity under such conditions.

### 4.1.2 Trawling Loads

Given the installation location of the template at the NCS, trawling loads become a critical factor to consider. In the early design phase, the template structure is deemed overtrawlable. Three relevant load cases will then be considered, as stated in NORSOK U-001 rev. 3, section 5.1 [64]. These loads are trawlnet friction, trawlboard overpull, and trawlboard impact, and can be found in Table 16 below.

*Table 16: Trawling Loads [64].*

**TRAWLING LOADS**

| DESIGN LOAD TYPE | Design load | | Design state |
|---|---|---|---|
| **TRAWLNET FRICTION** | 2 x 200 [kN] | Horizontal +/- 20 deg | ULS |
| **TRAWLBOARD OVERPULL** | 300 [kN] | Horizontal +/- 20 deg | ULS |
| **TRAWLBOARD IMPACT** | 13 [kJ] | | ULS |

The trawlnet friction load comes from the trawlnet being dragged over the template and can last for several seconds, dependent upon the size of the trawlnet and towing speed. The specific type of trawling equipment utilized will vary depending on the installation site. Since the template structure is intended for reuse at different locations, it will be necessary to test its resilience against the complete range of equipment it may encounter at a later stage.

In its conceptual state, the template is subjected to a standard value of 2 x 200 kN as a baseline to assess its capabilities. This friction force will be evenly distributed over the affected surface area of the template. To evaluate the structure for the worst-case scenario, the load is applied to the top hatch for this analysis.

The trawlboard overpull load represents a more localized force, dependent upon the size of the trawlboard. Like the friction load, the overpull load is most significant when applied to the top of the template. The load is therefore applied to the surface area of one of the top horizontal beams of the main frame structure. The load is set at 300 kN in the horizontal direction, with a range of +/- 20 degrees.

The trawlboard impact is the initial impact from the trawlboard when it first hits the structure. The impact energy will depend on the size, shape, mass and velocity of the trawlboard. With limited information of these parameters this analysis is left out of this study, but is something that should be investigated at a later stage.

### 4.1.3 Dropped Objects

During the equipment installation process following the template installation, various equipment will be lifted and operated over the template structure. To account for the possibility of accidental falls of these objects, the hatches must be tested against the impact energy for dropped objects. As specified in NORSOK U-001 rev. 3, section 5.1, there are two relevant loads for structures that are not multi well structures. These loads are presented in Table 17.

*Table 17: Dropped Objects [64].*

| **DESIGN LOAD TYPE** | DESIGN LOAD | | DESIGN STATE |
|---|---|---|---|
| **DROPPED OBJECT 500 MM** | 20 [kJ] | Point load | PLS |
| **DROPPED OBJECT 100 MM** | 5 [kJ] | Point load | PLS |

Loads from dropped objects will result in the template structure absorbing kinetic energy. To accurately simulate this scenario, a dynamic analysis should be conducted, incorporating detailed parameters of the potential objects that may fall on the structure. To simplify the analysis, this kinetic energy can be converted to a static point load using Equation 6. For this example, the first load of 20 kJ and an object diameter of 500 mm is used from Table 17.

$$20KJ = 20.000Nm$$

$$20.000Nm = F * 0.5m$$

$$F = 20.000Nm / 0.5m$$

$$F = 40kN$$

*Equation 6: Estimated Conversion of Joules to Newton Force.*

The force calculated using the equation will then be applied to a circular surface area on the hatch with the corresponding diameter of the dropped object. This will be an estimation, where the primary objective is to gain a better understanding of how the model will respond to such loading. Detailed dynamic simulations should be conducted at a later stage to ensure that the structural integrity of the template is not compromised.

As this scenario falls under a PLS case, conducting a plastic analysis allowing for permanent deformation in the material should also be considered at a later stage. By doing so, the complete strength profile of the material can be utilized, provided that the deformed areas do not cause damage to any nearby installed equipment. To streamline the scope of work and focus on developing a functional concept model, these analyses will not be conducted at this stage.

## 4.2 Set-up

To avoid redundancy a common setup procedure is presented. This will eliminate the need for individual figures and discussions for each analysis situation. Figures demonstrating this setup will instead be included in appendix B if further explanation is needed. The setup phase plays a critical role in ensuring realistic and reliable results during the analysis, where careful consideration has been given to each setup process across all analyses. The setup procedure follows the steps showcased in Figure 38.

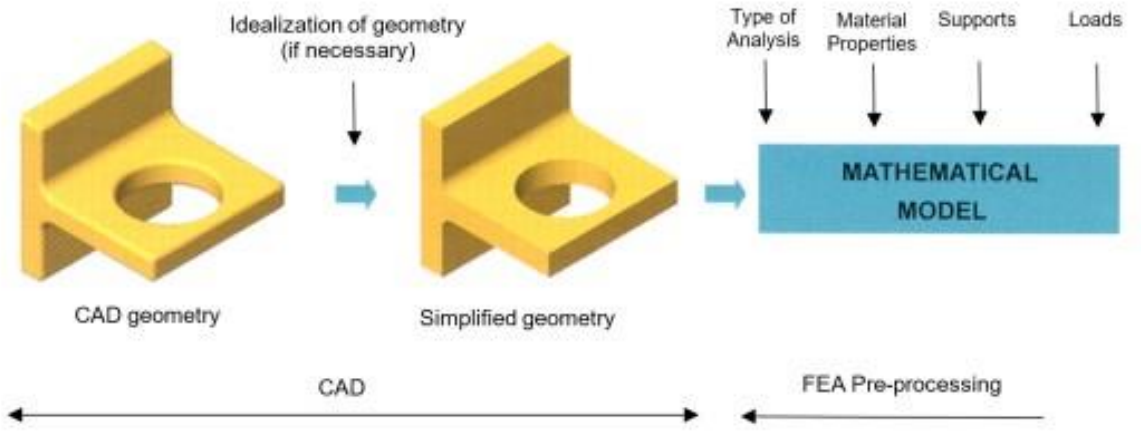


*Figure 38: Building the Mathematical and FE Model [69].*

### 4.2.1 Simplified Model

Before proceeding with an analysis, the geometry of the structure must be considered. To achieve an optimal geometry for a structural analysis, an individual model is created for each loading scenario. This model is simplified with fewer details and complex shapes, minimizing unnecessary clutter during both the meshing process and the analysis run.

Unlike the original concept model which includes production ready parts with room for weld material and joints, the analysis model removes this to ensure that the program simulates a full connection between each welded part. Unnecessary fillets or rounding effects on bolt housing or plate elements are also eliminated. For each scenario, parts that are not significant for the analysis are suppressed to reduce the total number of parts which helps streamlining the analysis process and improving computational efficiency.

### 4.2.2 Symmetry

To reduce the total number of elements and nodes in the analysis program, symmetry is utilized where possible. This involves cutting the model through a midplane to exploit symmetrical geometry and loading cases. If both the model and loading case exhibit symmetry, this method can significantly reduce the computational resources required. With a limit of 128,000 nodes and elements for the student license, using symmetry becomes a helpful tool for obtaining accurate results, especially for larger models. Employing symmetry planes can also substantially decrease the computational time required to run simulation on bigger systems. The impact of this limitation on running time is relatively minor within the maximum limit of 128 00 nodes and elements, as modern computers are capable of handling larger computational loads.

To utilize symmetry in the ANSYS program, the symmetry region feature is used. To do this the model is cut in the CAD program prior to importing it into ANSYS. The symmetry function is then applied by selecting the cut surface area along with its corresponding normal vector. This will indicate to the program that the model is symmetric through this plane and direction of the vector. To verify the results of the symmetry region function, a test is conducted on the front hatch where the loading case is run with both a full and cut model. If the results align, it confirms that the symmetry function is working correctly. Despite this, the deformed model of any analysis will be checked to ensure that the deformation appears appropriate and that the program properly accounts for the cut segment.

### 4.2.3 Meshing

The meshing of the model is a critical step in ensuring reliable analysis results. Considering the somewhat complex structure of the model with a combination of piping sections and plate elements, 3D solid elements are chosen to provide the overall best results. The program will provide a combination of hexahedral and tetrahedral elements to best suit the geometry of the model. Higher order quadratic elements are preferred due to their ability to accurately capture bending and provide higher accuracy due to their increased number of nodes [69]. While hexahedral quadratic elements require more computational work, the size limit of elements and nodes in the student license of the software means that the running time still remains low.

To accurately capture the distribution of von-Mises stress in critical areas, the body sizing feature in ANSYS is utilized. This function allows specific parts of the model to have smaller elements compared to the rest of the model. It's a valuable tool for achieving accurate results in localized regions without significantly increasing the total number of elements. Given the size limit of 128.000 elements or nodes in the student version of the ANSYS program, it becomes especially useful to concentrate more elements in exposed areas of the structure.

### 4.2.4 Constraints

Defining proper constraints for each loading scenario is necessary to ensure accurate analysis results where the model behaves realistically under the applied loads. Incorrectly defined constraints can lead to significant inaccuracies, causing the model to move in ways that do not reflect real-world behavior. Below are the typical constraints used throughout the analysis:

- **Fixed Support:** Applied to a surface where it can be considered structurally fixed, such as welded joints.
- **Displacement:** Applied to a surface to restrict movement in specific directions (x, y, or z) and rotations around specific axes (x, y, or z) relative to the model coordinate system.
- **Cylindrical Support:** Used to simulate support of a surface in radial, tangential, or axial directions.
- **Force:** Applied at a surface to define a static load in the x, y, and z directions of the model coordinate system.

- **Standard Earth Gravity:** Simulates the weight of the structure due to Earth's gravity. This function uses the weight of the structure in air, with fixed values that cannot be changed. As the model is submerged during loading this will result in a small difference, providing an additional safety factor.

By applying these constraints appropriately, the model can accurately simulate the behavior of the structure under various loading conditions.

### 4.2.5 Material Choice and Properties

The two materials selected for this concept is aluminum alloy 5083 H116 for the structural frame and structural steel grade S355 for the rigid mounting frame. Both materials have proven themselves for marine environments and are approved for immersed applications.

The strength characteristics of 5083 H116 has been assessed as noteworthy for the material choice, making it a suitable choice for applications discussed in this thesis. It is one of only two aluminum alloys approved for immersed applications by NORSOK M-121 [24]. The strength reduction in the HAZ for 5083-H116 are much less severe compared to the other immersible approved 6082 alloy, which suffers from more severe strength reduction around welds.

S355 Steel have for many years been utilized for offshore applications and serves as a great candidate for the structural component of the complete concept structure. It offers great strength characteristics, load-bearing capabilities and weldability. The following table outlines key strength characteristics, including a safety factor (SF) of 1,5 that are to be utilized in the analysis chapter of the thesis.

*Table 18: Strength Characteristics for 5083 [35] and S355 [52] incl. SF.*

| MATERIAL | THICKNESS [mm] | YIELD STRENGTH [MPa] | TENSILE STRENGTH [MPa] | YS (SF) [MPa] | TS (SF) [MPa] |
|---|---|---|---|---|---|
| **5083-H116** | t ≥ 16 | 215 | 305 | 143 | 203 |
| **S355G2** | | 355 | 470 - 630 | 237 | 313 - 420 |
| **5083-H116** | 16 > t ≥ 25 | 215 | 305 | 143 | 203 |
| **S355G2** | | 345 | 470 - 630 | 230 | 313 - 420 |
| **5083-H116** | 25 > t ≥ 40 | 215 | 305 | 143 | 203 |
| **S355G2** | | 345 | 470 - 630 | 230 | 313 - 420 |
| **5083-H116** | 40 > t ≥ 100 | 200 | 305 | 133 | 133 |
| **S355G2** | | 325 | 470 - 630 | 217 | 313 - 420 |

## 4.3 Aluminum Module

The aluminum module serves as a protective enclosure for the installed equipment, exposed to various loading scenarios such as trawling loads, static loads, and dropped objects. To accurately analyze its structural integrity, the module is divided into three separate models: the main frame, side hatches, and top hatch. This segmentation allows for focused analysis on each section, ensuring precise results during the FEM analysis. Following the assessment of individual sections under relevant loading conditions, an evaluation of the entire module will be conducted.

### 4.3.1 Welding of Aluminum

As stated in section 2.5.2 the most researched, available and applicable welding practice are arc welding methods such as MIG and TIG. The Eurocode provides guidelines for strength reductions in and around the welds, as well as applicable filler materials [35]. As the conceptual structure is to undergo an extensive static analysis it is important to assess any information about the strength integrity of the material. Therefore, it is decided that the components included in the complete structure shall be welded using MIG or TIG methods, so that accompanying strength tables can be presented and utilized through the entirety of the analysis.

For any aluminum welding, the filler material will exhibit a yield strength of 240 MPa according to Eurocode and detailed in Table 7 in section 2.5.2.3. This yield strength is higher than the initial strength of the aluminum alloy 5083 at 215 MPa. Consequently, the most compromised areas will be in the heat affected zones. Because of this it will be important to present the yield limits in these zones near the welded joints, including a safety factor of 1,5. Data utilized for calculating the yield strength characteristics showcased in the following tables are covered in section 2.5.2.3.

*Table 19: Yield Strength for Welding Filler Material incl. SF. [35].*

| 1ST PART | 2ND PART | STRENGTH | STRENGTH INCL. SF |
|---|---|---|---|
| | Filler Material: | [MPa] | |
| **5083** | 5056A | 240 | 160 |
| | 5356 | 240 | 160 |
| | 5556A | 240 | 160 |
| | 5183 | 240 | 160 |

*Table 20: Yield Strength in HAZ for 5083-H116 incl. SF. [35]*

| **DRAWN TUBE** | | | **YIELD STRENGTH** | | | |
|---|---|---|---|---|---|---|
| | | | HAZ | | HAZ incl. SF | |
| | Thickness | Yield | MIG | TIG | MIG | TIG |
| **5083-H116** | [mm] | | | [MPa] | | |
| | t ≤ 6 | 215 | 146,2 | 146,2 | 97,5 | 103,2 |
| | 6 < t ≤ 15 | 215 | 146,2 | 131,2 | 97,5 | 87,5 |

| **PLATE** | | | **YIELD STRENGTH** | | | |
|---|---|---|---|---|---|---|
| | | | HAZ | | HAZ incl. SF | |
| | Thickness | Yield | MIG | TIG | MIG | TIG |
| **5083-H116** | [mm] | | | [MPa] | | |
| | t ≤ 6 | 215 | 154,8 | 154,8 | 103,2 | 103,2 |
| | 6 < t ≤ 15 | 215 | 154,8 | 139,8 | 103,2 | 93,2 |

### 4.3.2 Main Frame

In this chapter, the main frame of the aluminum module is analyzed for the two primary load cases associated with trawling, excluding the trawlboard impact. To simplify the analysis and achieve more accurate results, the main frame is isolated to create a smaller and manageable model. Since the aluminum frame will transfer its stresses to the steel frame below, a probe function is employed at the flanges to obtain the reaction forces for both load cases. These reaction forces will later be used to analyze the steel frame module.

#### 4.3.1.1 Trawlnet Friction

The frictional force from the net during over trawling will be transmitted from the hatches through the hinges to the aluminum frame. The structure will be most compromised when the friction load is applied at the top of the structure. Therefore, the force is applied to the connection point for the hinges on the frame. As specified in Table 16, the force is 2 x 200 kN and is applied horizontally. The resulting von Mises stress distribution can be observed in Figure 39 below, where a probe function is utilized to highlight the most exposed areas.

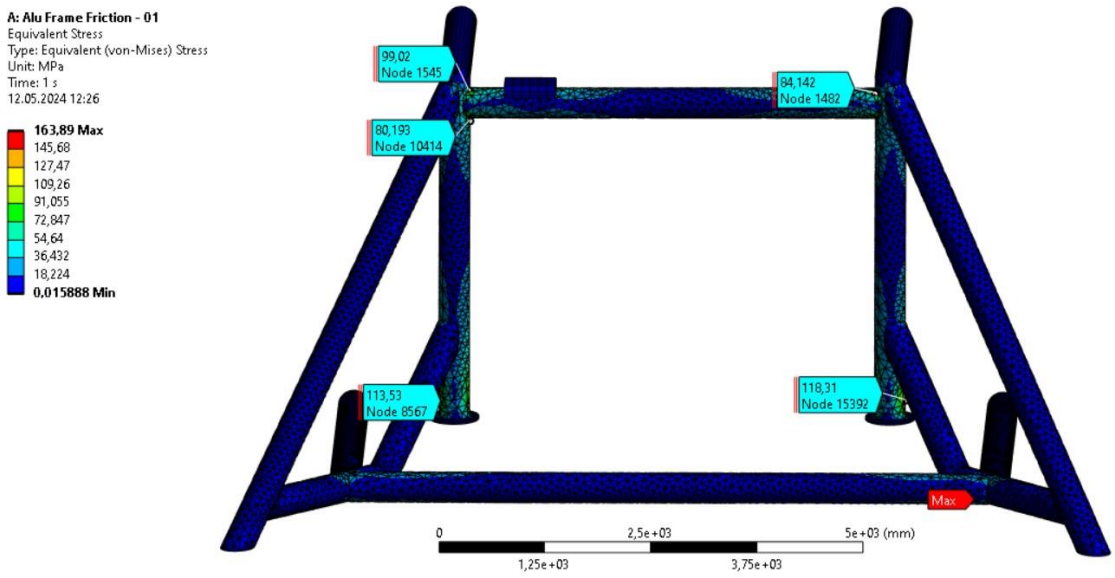


*Figure 39: Ansys Model - Friction Load with Resulting Von-Mises Stresses.*

From the figure, it is evident that the most affected areas are at the corner sections of the pipe connection. At the top central beam in Figure 39, a maximum stress of 99 MPa is observed. However, it's important to note that the model does not include the weld material present in the corners, which will simulate a smaller contact area between the pipe sections than what will occur in reality. Consequently, this leads to a higher local reading of stresses in these areas than what would be actually be experienced.

The weld material for the 5083 material has a yield strength of 160 MPa, including a safety factor of 1,5. As the stresses are well below this limit, the limiting factor for the frame is the material in the heat-affected zone (HAZ) areas, where the stresses are approximately at the defined limit of 97 MPa. This can also be observed in Figure 40 showcasing a detailed view of the connection point. Here a singularity spot of 135 MPa can also be seen. However, including the surface area of the welding material would reduce the local stresses due to the added material and contact area.

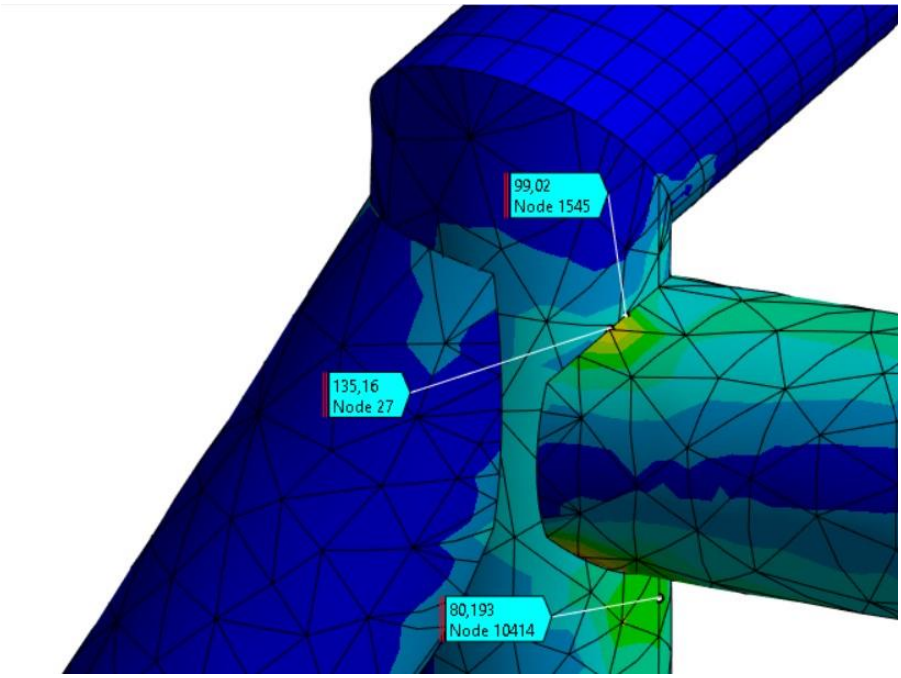


*Figure 40: Ansys Model - Friction Load with Resulting von Mises Stresses in Top Corner.*

From evaluating the results of the analysis, the model demonstrates good structural capabilities in handling this type of loading scenario. The frame effectively distributes stresses between its pipe elements and exhibits the desired system stiffness. The dimensions of the pipe sections have been estimated accurately, with little need for changes.

To address the higher stresses observed in the corners due to the lack of contact area between the pipe sections, incorporating plate elements in these areas can be beneficial. This addition would enhance stiffness and contact area, thereby improving stress distribution and reducing concentration in the corner sections. Overall, these adjustments would further optimize the structural integrity and performance of the template structure.

4.3.1.2 Trawlboard Overpull

To simulate the effect of overpull from a trawlboard, the force is applied directly to the surface area of one of the top beams of the main frame structure. This will result in a more localized load dependent on the size and shape of the trawlboard and ensures that the frame is subjected to the most exposed state of loading. The load applied is equal to 300 kN and is directed horizontally, as specified in Table 16.

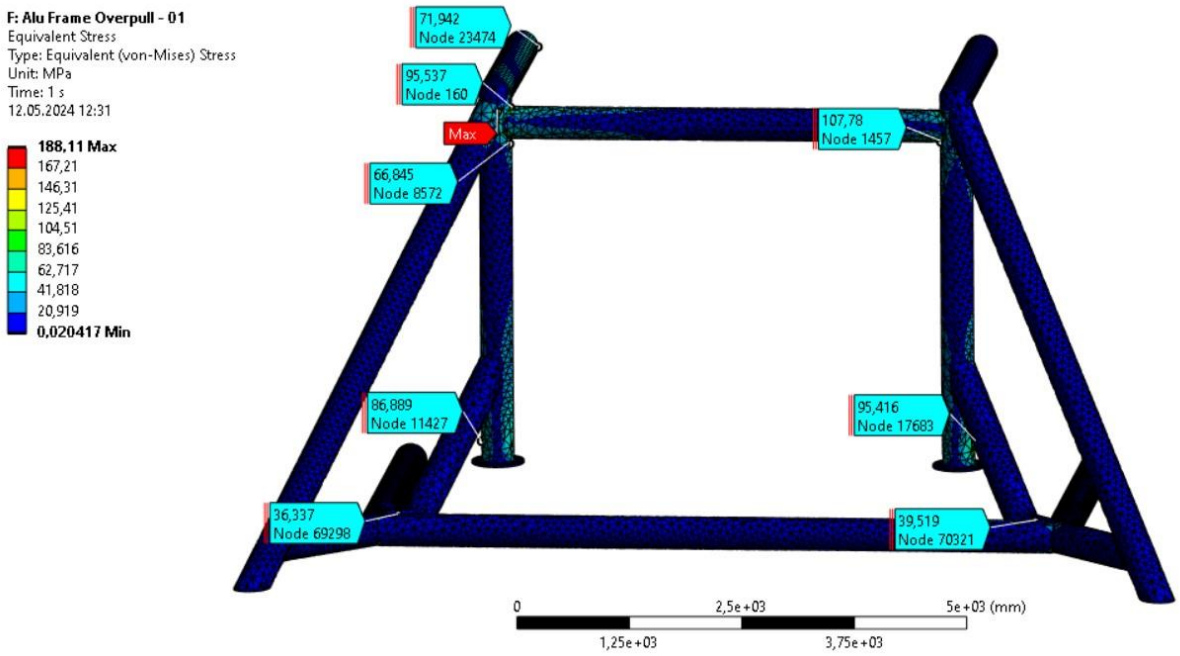


*Figure 41:* Ansys Model - Trawlboard Overpull Load with Resulting von Mises Stresses.

Similar to the friction load, the most affected areas under the overpull load are at the corners. The frame exhibiting stresses around to the HAZ yielding limit of 97 MPa including the SF of 1.5, with some singularity points present above the limit. The stresses near the flanges are lower compared to the friction load, which aligns with expectations as the total horizontal load is smaller in this case. The main difference lies at the top near where the force is applied. In this scenario the force is applied to the top left beam, where the maximum stress point of 188 MPa is located at the end point for this beam. Once again, this presents a singularity problem enhanced by the low contact area without the welding material.

Like the findings with the friction load, the dimensions of the pipe sections appear to be suitable. However, the structure would benefit from the addition of stiffening plate elements in the corners to increase contact area and assist in distributing stresses more effectively. This adjustment would enhance the overall performance and durability of the main frame structure under overpull loading conditions.

### 4.2.2 Side Hatches

To reduce the workload the analysis is limited to the front and rear hatches while assuming similarity for the side hatches. Since the side hatches share structural similarities with the front and rear ones, it's results should align. The changes made for the front and rear hatches will therefore be replicated onto the side hatches. The front and rear hatches will undergo testing for crane ship heave, temporary parking of ROV’s or equipment, and dropped objects.

#### 4.2.2.1 Crane Ship Heave

To simulate the pulling force induced by the heave motion of the crane ship operating the hatch, a static load equal to 7 tons is applied at the connection point for the ship wire. This load will be most severe when the hatch is in a completely vertical position, where the hatch is unable to rotate or move. This will causing the full pulling force to be absorbed by the elongation of the hatch. The resulting von Mises stress distribution from this analysis can be observed in Figure 42 below.

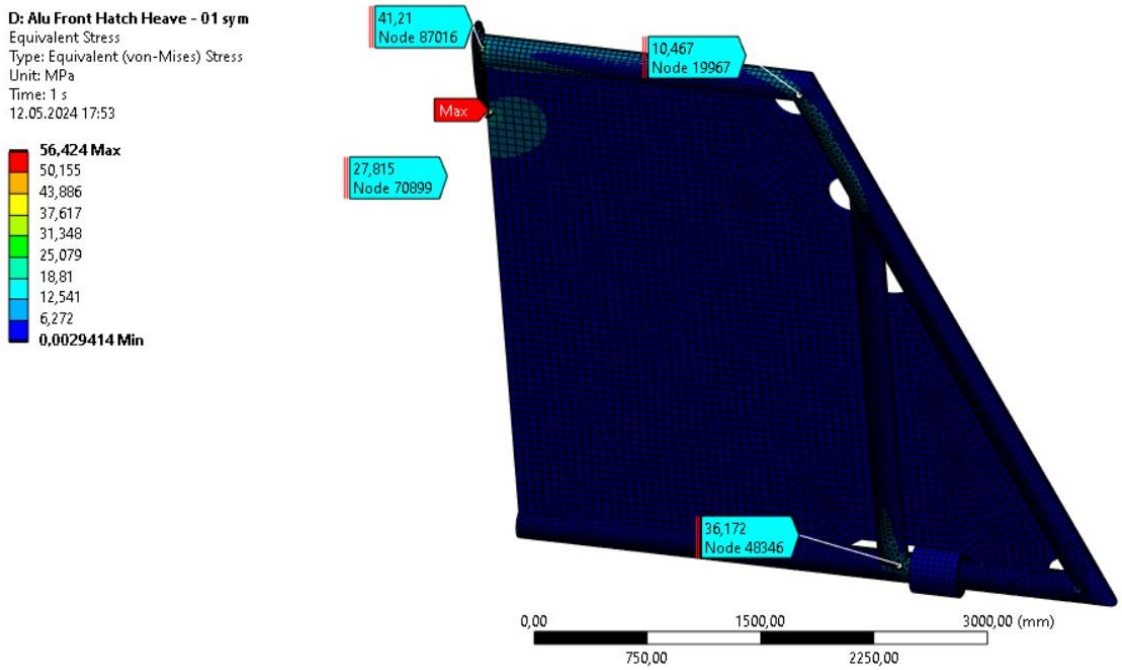


*Figure 42: Ansys Model - Front Hatch - Heave Motion and Resulting von Mises Stresses.*

As seen from the figure above the resulting stresses are relatively small and will not cause any problems for the hatch. The results showcase an opportunity to reduce the weight of both the tube- and plate elements. A detailed view of the wire connection point is shown in Figure 43, where the maximum value of 56 MPa can be seen for the bracket plate. The added welded material will also result in a larger contact area between the bracket and hatch, lowering the overall stresses in this area.

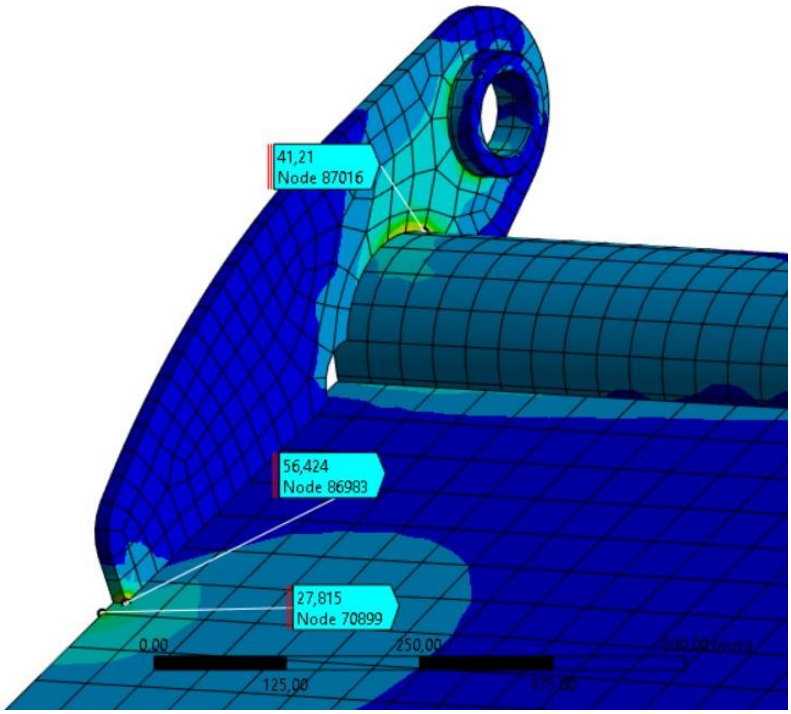


*Figure 43: Ansys Model - Bracket for the Front Hatch During Heave Motion.*

4.2.2.2 Parked ROV

To analyze the hatch for ROV parking, a contact area of 1.6 x 2.6 meters is defined at the center of the hatch. The contact area dimensions used are found in the data sheet for the Magnum Plus heavy work class ROV [68]. The force applied is equal to 7502 N, as specified in Table 15. This force results in a significant bending moment towards the hinges, as they are the only supported points on the hatch. The resulting von Mises stress distribution can be found in Figure 44 below.

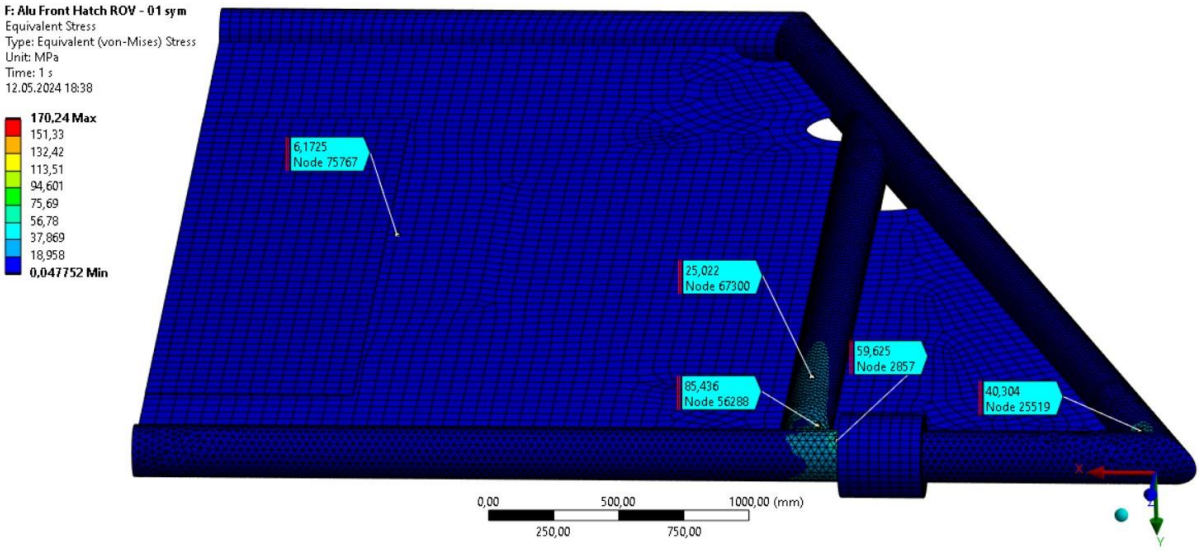


*Figure 44: Ansys Model - Front Hatch with Parked ROV.*

In this loading scenario, the stresses observed are more significant than those from the heave load. The most problematic area is the pipe sections near the hinge point, primarily due to the large bending moment caused by the added weight of the ROV. Despite the singularity problem, the pipe sections experience stresses of up to 85 MPa in HAZ areas. Figure 45 shows a more detailed view of the singularity point and nearby stresses.

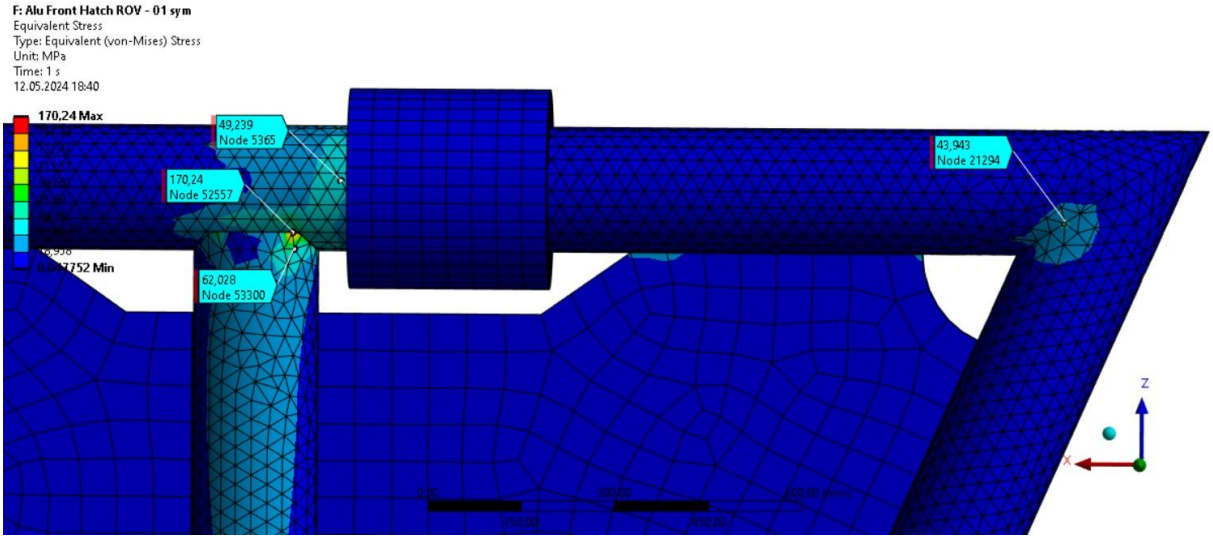


*Figure 45: Ansys Model - Hinge Area on Front Hatch During ROV Touchdown.*

Given that the pipe section handles most of the stresses, the plate element remains mostly unaffected by the loading. This shows a significant opportunity to reduce the weight of the structure, as the plate elements represent the majority of the hatches mass. It is important to still consider that if the touchdown of the ROV occurs at an angle, this will result in a more localized load with less contact area, which will affect the plate element more significantly. While reducing the weight of the structure is desirable, ensuring the structural integrity under potential variations in loading conditions remains important.

To further mitigate stress in the pipe section under this type of loading, one could consider a support option for the hatch in its fully open position. One potential solution could involve attaching a wire to the main frame structure and to the sides of the center of mass of the hatch. The wire should hang freely when the hatch is closed, without the risk of interference, and tighten when the hatch is fully open. This setup would help alleviate the large bending moment at the hinges, thereby drastically reducing the associated stresses. By distributing the load more evenly along the frame, this support mechanism would enhance the structural integrity of the hatch and improve its performance under various loading conditions.

#### 4.2.2.3 Dropped Objects

To test the structure for accidental falls of varying objects when lifted over the template structure, two loading cases will be considered. The estimated values of the static loads caused by this are 40 kN and 50 kN, applied on circular contact areas with diameters of 500 mm and 100 mm, respectively. As the 50 kN load with the smaller contact area clearly induces the highest stresses, this is the only case presented. The other case of 40 kN can be found in appendix C. Figure 46 illustrates the von Mises stress distribution for the 50 kN loading case.

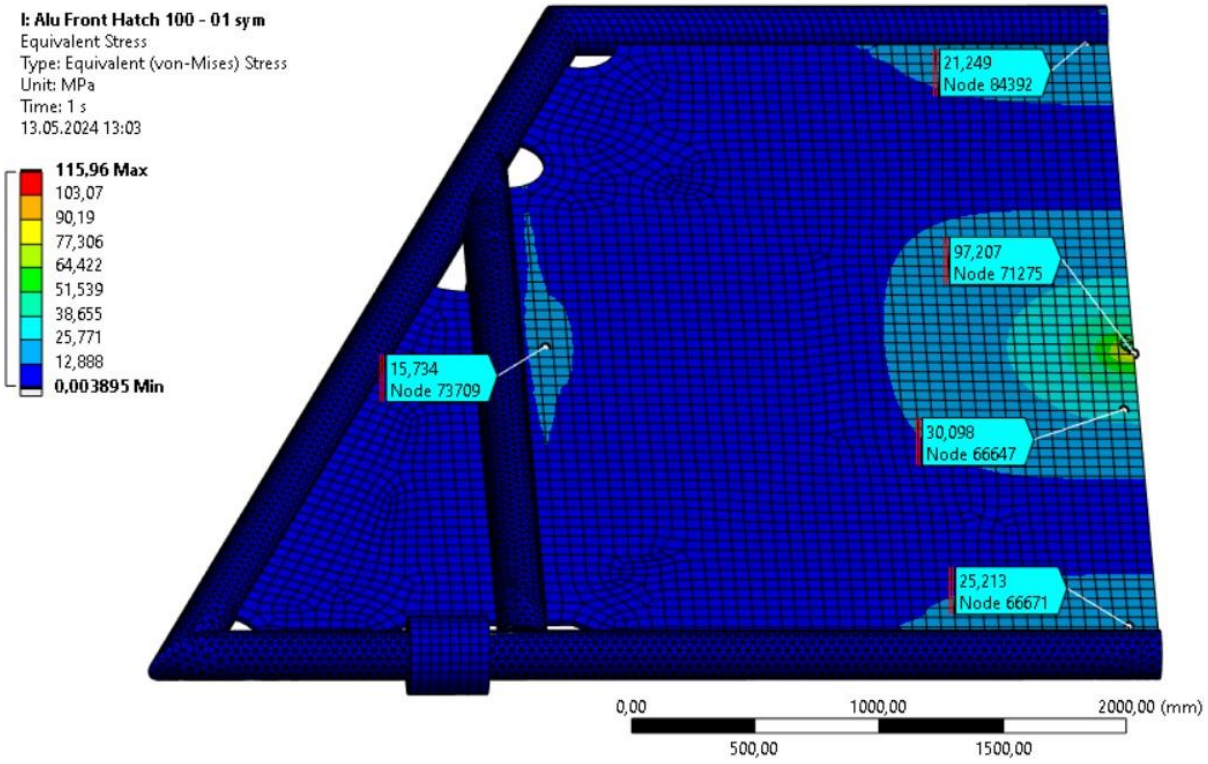


*Figure 46: Ansys Model - Front Hatch with von Mises Stresses - 100 mm Dropped Object.*

The load is applied at the middle of the hatch, where the highest stresses are observed. Here it is important to note that in reality the entirety of the load would not be absorbed directly into the hatch. The loading case occurs while the hatch is in its closed position with a steep incline. Objects hitting the plate will only transfer a certain amount of energy to the hatch before being deflected and changing direction as they continue down the hatch. Despite this the full load is used as an extra safety factor for the hatch, ensuring that it can withstand accidental impacts under conservative assumptions.

Figure 47 provides a detailed view of the impact area. It shows that the maximum stress in the plate element of the hatch is 97 MPa, while the attached part to simulate the falling object shows a maximum value of 116 MPa. Given that the hatch is the area of interest, the maximum stress of 97 MPa is considered. Since this stress is not in a HAZ area, it is well below the specified yield strength of 143 MPa. Consequently, the thickness of the hatch elements can be deemed somewhat excessive, suggesting potential opportunities for weight reduction without compromising the structural integrity.

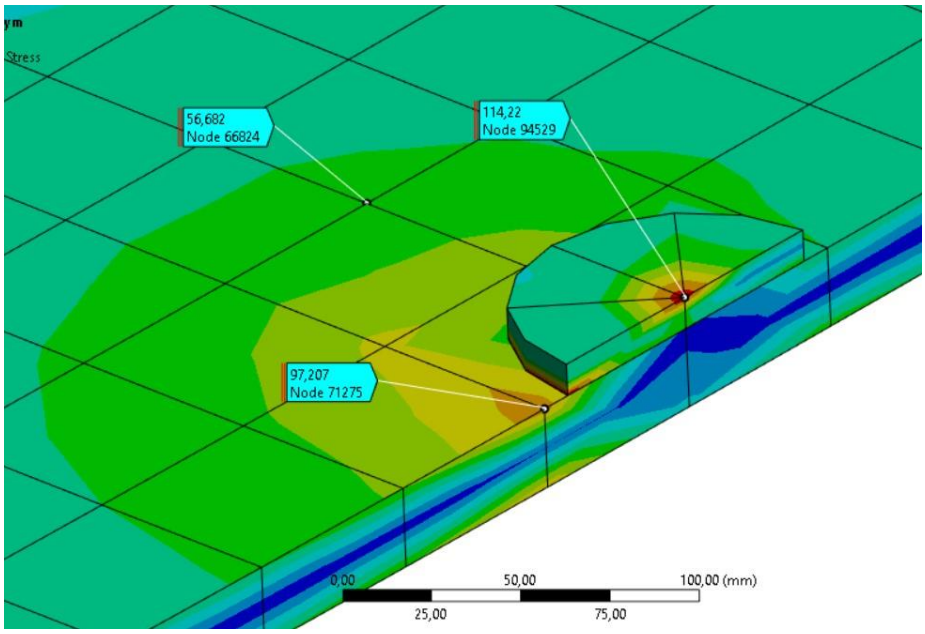


*Figure 47: Ansys Model - Front Hatch with Closeup of Dropped Object 100 mm.*

### 4.2.3 Top Hatch

Since the top hatch is structurally different from the side hatches, an independent analysis of is considered necessary. The placement of the hatch will also affect the loading case concerning dropped objects, as it lies horizontal in its closed position. Therefore, the top hatch will be analyzed separately for crane ship heave and dropped objects. However, the parked ROV analysis is excluded from this assessment as it is not intended for this application. The analysis for trawlnet friction will also be excluded due to the low stresses experienced by the hatch but can be found in appendix C.9.

#### 4.2.3.1 Crane Ship Heave

To simulate the top hatch's response to the heave motion of the crane ship, a vertical load of 7 tons is applied at the bolt housing for the wire connection. The hatch will also be positioned vertically as it will be most affected in this position due to the limited ability to move. The resulting von Mises stress distribution can be observed in Figure 48 below.

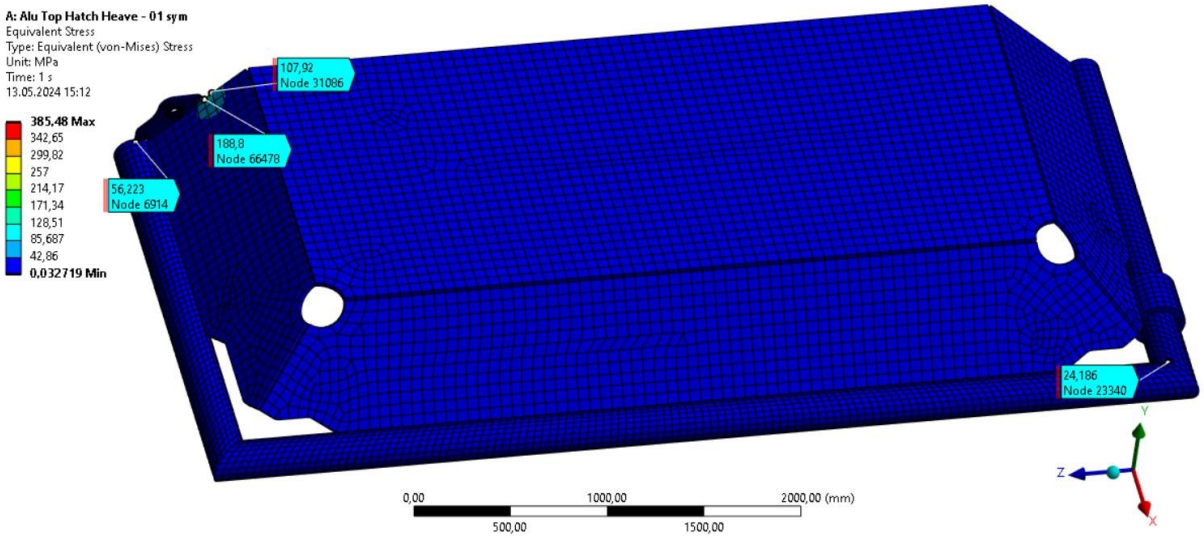


*Figure 48: Ansys Model - Top Hatch with Resulting von Mises Stress from Heave Motion.*

The stresses observed are highly localized around the bracket for the bolt housing, affecting primarily the plate element welded to the bracket and the corresponding pipe section. A detailed view of the bracket can be seen in Figure 49. The maximum stress value of 385 MPa is indicative of a singularity point, but it's evident that the bracket is still experiencing high stresses near this point. Meanwhile, the corresponding plate element of the hatch exhibits a maximum stress value of 108 MPa.

Including the welded material for the bracket and plate element would likely help reduce the stress values. However, it's apparent that the stresses are still too high, particularly since they occur in a HAZ area. This indicates a need for design modifications or reinforcements to ensure that the bracket and plate element can withstand the applied loads without exceeding safe stress limits.

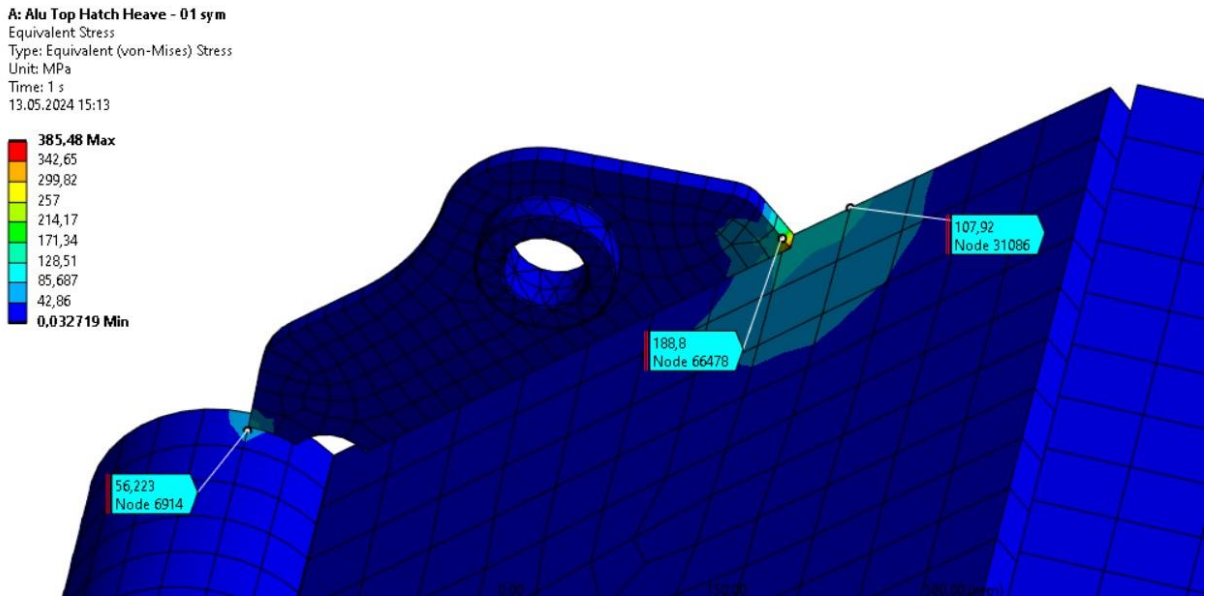


*Figure 49: Ansys Model - Detailed view of Top Hatch with Heave Motion.*

### 4.2.3.2 Dropped Objects

The same two loads as those applied to the front hatch to simulate dropped objects will be tested on the top hatch. These loads consist of 40 kN and 50 kN, with corresponding circular contact areas having diameters of 500 mm and 100 mm, respectively. As with the front hatch, only the load of 50 kN will be presented in the report. Figure 50 shown below, illustrates the corresponding von Mises stress distribution for the 50 kN loading case.

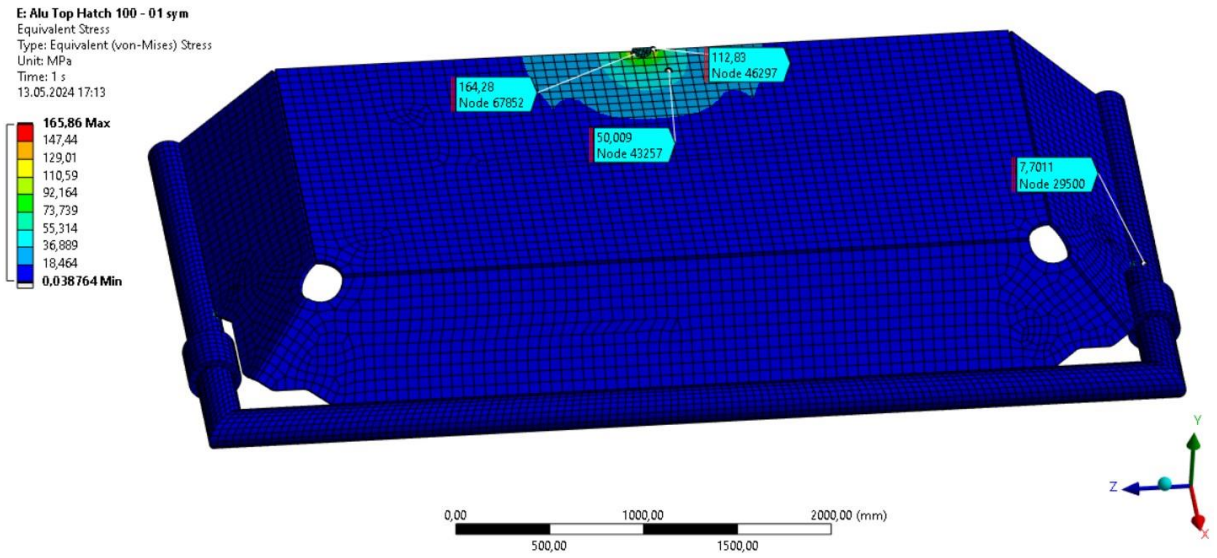


*Figure 50: Ansys Model - Top Hatch with von Mises stresses for 100 mm Dropped Object.*

The stresses are highly localized in the center of the hatch around the impact area. The only parts showing significant strain are the center top plate element and the nearby beam stiffeners beneath it. The rapid decline in stresses away from the impact area indicates that the stiffeners effectively absorb the tension. As seen in more detail in Figure 51, the maximum stress of 166 MPa is observed in the part placed to simulate the falling object. The maximum stress in the plate element of the hatch is 113 MPa, which will define the limiting load. Since this is not a HAZ area, the load is well within the limit of 143 MPa. This suggests a clear indication of potential reduction in the top plate element. While the stiffeners effectively distribute the stresses, with a maximum stress of 52 MPa they also show potential for weight reduction.

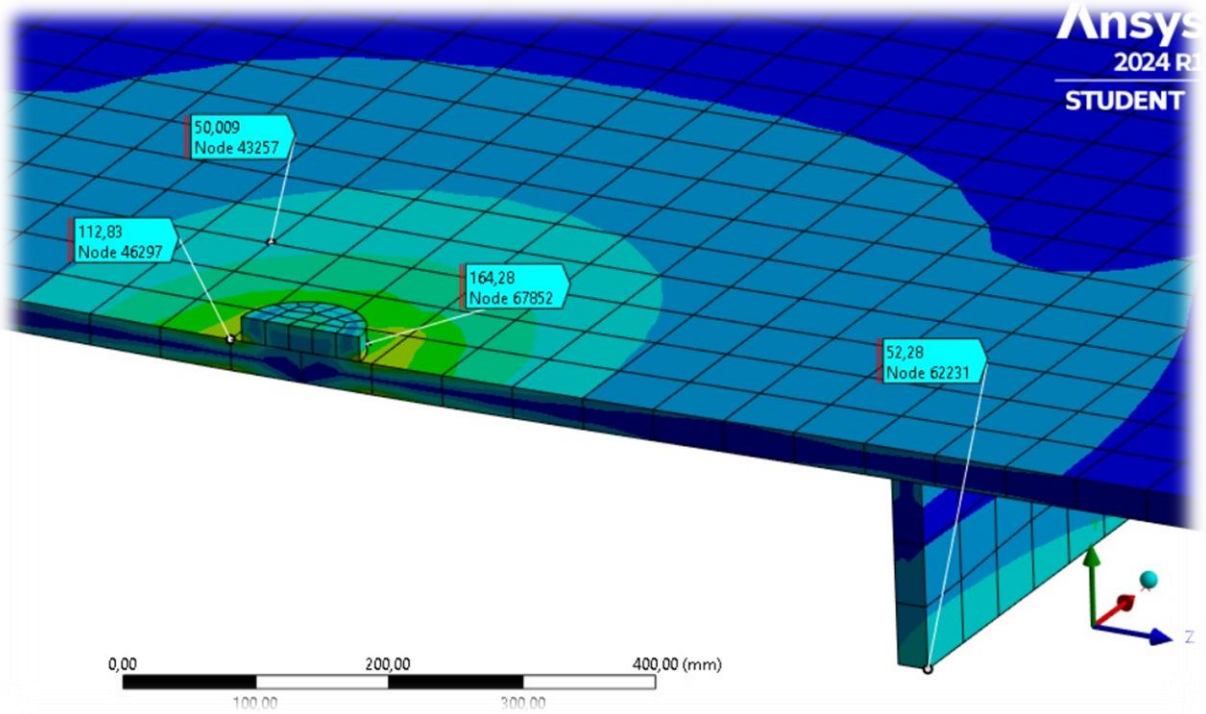


*Figure 51: Ansys Model - Detailed Impact Area with 100 mm Dropped Object.*

## 4.3 Steel Module

The steel module is positioned in the middle of the aluminum module, meaning it does not experience direct loading effects. To obtain realistic loads for the steel module, a probe function is utilized at the flanges of the aluminum structure to capture the loading cases it experiences. The load cases with the greatest stress will be utilized to determine the loading conditions for the steel module.

### 4.3.1 Trawlnet Friction

The loading case that induces the most stress for the steel module is the trawlnet friction, with a force of 2 x 200 kN applied on the top hatch of the template. This force is transferred to the steel module, resulting in twisting and displacement of the flanges. The reaction force obtained from the aluminum frame can be found in Table 21.

*Table 21: Reaction Forces Obtained from Aluminum Module Flange.*

| | **X AXIS** | **Y AXIS** | **Z AXIS** | **TOTAL** |
|---|---|---|---|---|
| | | [N] | | |
| **FLANGE A** | 25 138 | -61 082 | -97 773 | 117 990 |
| **FLANGE B** | 29 632 | 93 236 | -102 230 | 141 500 |

The forces presented in the table correspond to the coordinate system shown in Figure 52. Here the forces are shown with red arrows indicating the direction of the force. It's important to note that the opposite direction from the table above has been used to accurately represent the direction of the force action on the module.

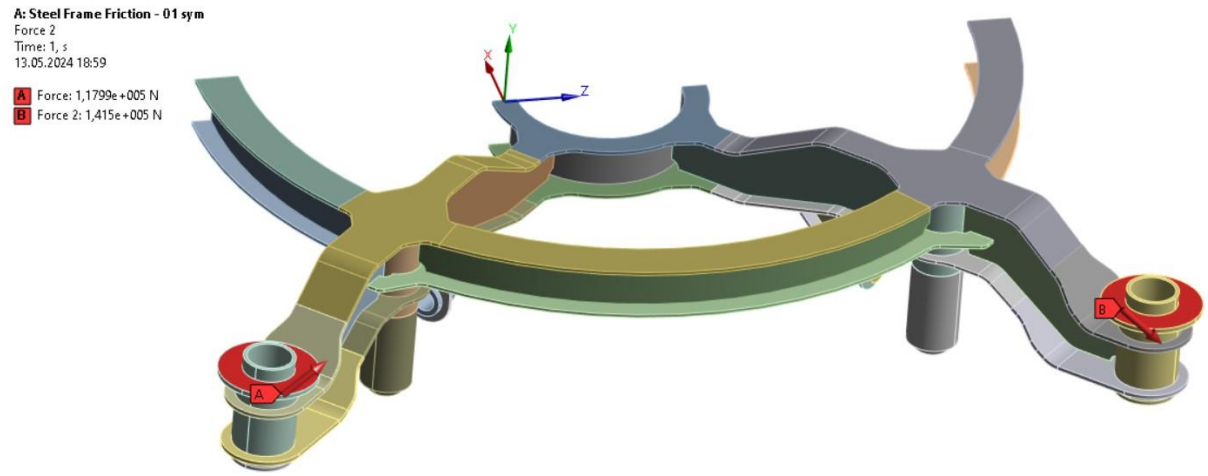


*Figure 52: Ansys Model - Steel Frame with Corresponding Loads from Trawlnet Friction.*

Figure 53 displays the von Mises stress distribution on the steel module. The maximum stress of 321 MPa occurs at a singular point, with the actual value significantly lower. The frame exhibits generally high stresses from the flanges down to the connection point to the suction anchor. In this area stresses close to the yield limit of 237 MPa can be seen, including the SF of 1.5. The remainder of the module is nearly unaffected, indicating a poorly designed model in terms of fully utilizing the strength potential of the system. This highlights the need for design optimization to ensure a more balanced distribution of stresses throughout the steel module, thereby maximizing its structural efficiency and performance.

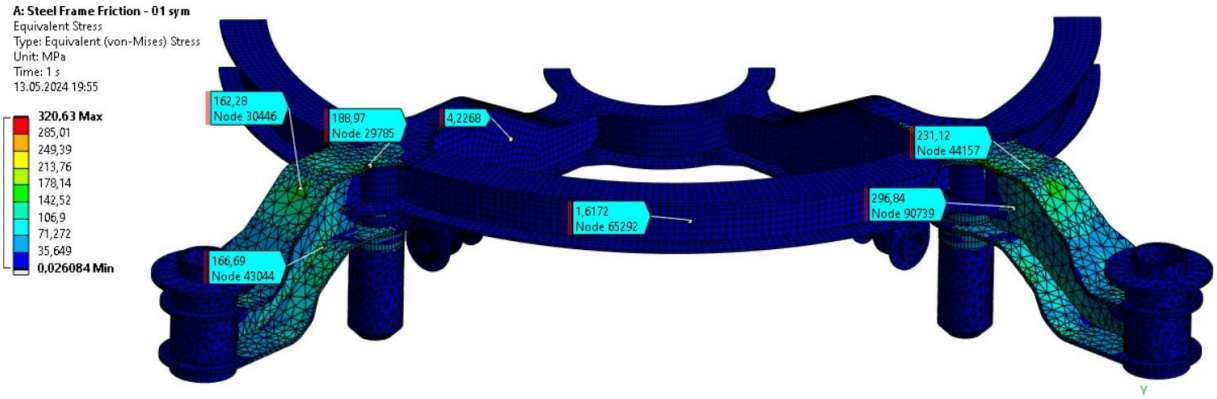


*Figure 53: Ansys Model - Steel Module for Trawlnet Friction Load.*

One solution to this problem involves adding additional bracing between the flanges and the circular beam element. Given that there is sufficient space in that area, this solution can drastically reduce stresses and deformation while adding only a limited amount of weight. With the more efficient strength profile achieved through this bracing, it's likely that the thickness of some plate elements can be reduced. This will be resulting in an overall reduction in the weight of the structure despite the addition of the bracing beam elements. The deformation of the structure can be observed in Figure 54, with a magnification of x 64 to clearly illustrate the deformation pattern.

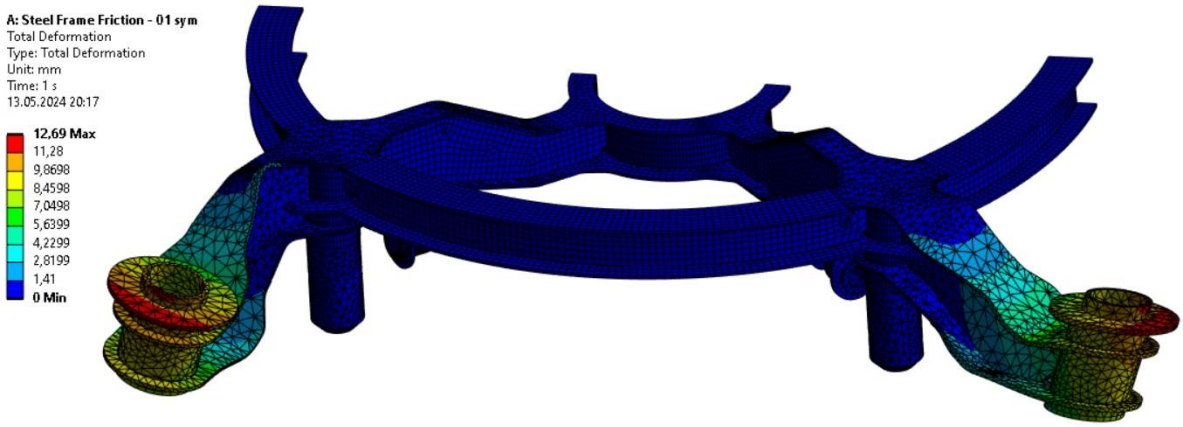


*Figure 54: Ansys Model - Deformation of Steel Module for Trawlnet Friction Load.*

The deformed model clearly exhibits twisting of the flanges, which can be addressed through the addition of bracing beams. Given the varying displacement behavior of the flanges, utilizing a tubing section for the bracing beam would be an optimal choice due to its versatile strength profile.

## 4.4 Corrosion Protection

The complete modular template structure consists of two main components, the aluminum frame and connecting steel frame. Since the components are built using two different materials with different electrode potential, it is important to consider the galvanic corrosion effect this could purpose. A solution to protect the components from corrosion and strength losses will be covered in this sub-chapter.

### 4.4.1 Steel Module Protection

The entire subsea operation station is intended to be freestanding on the seafloor and likely controlled from an onshore facility, such as the Northern Lights facility. Because of this the practicality of employing GACP or ICCP is deemed limited due to maintenance and changeability requirements. Consequently, the chosen approach is to employ a protective coating for the steel module.

Following the NORSOK M501 Standard, which states that any steel material that are subject to surface preparations, shall as a minimum requirement be coated with a primer as a temporary corrosion protection with rust grade B, following ISO 8501-1. This coating must also be removed before the application of the actual corrosion coating system [70].

The Norwegian standard specifies that any carbon steel operating at temperatures below 120 degrees Celsius must undergo a pre-qualification. This involves approval of the topcoat, intermediate coating, and film thickness for each coat. Additionally, the steel module must have a Coating Procedure Specification (CPS) and coating procedure test (CPT) before it can be deemed suitable for immersed installation [70]. The required surface preparation, coating system, number of coats and minimum dry film thickness (MDFT) are shown below in table 22.

*Table 22: Surface Preparation and Coating - Carbon Steel [70].*

| | | Surface Preparation | | | MDFT |
|---|---|---|---|---|---|
| **Application** | Temperature | Cleanliness: | Roughness: | Coating | [µm] |
| **Carbon Steel** | < 120° C | ISO 8501-1 Sa 2 1/2 | ISO 8503 Grade Medium G | 1 coat zinc rich primer | 60 |
| | | | | Minimum Coats: 3 | - |
| | | | | Complete Coat | 280 |
| **Submerged Carbon Steel** | - | | | Two Component Epoxy | - |
| | | | | Complete Coat | 350 |

### 4.4.2 Aluminum Module Protection

The frame module is constructed using an aluminum alloy 5083-H116, approved for submerged applications as referenced in section 2.5.1. While the alloy itself possess good corrosion resistance, challenges arise with the inclusion of the steel module. As carbon steel and aluminum have different electrode potentials, introducing the risk of galvanic corrosion.

While aluminum alloys generally do not require corrosion protection coatings, exceptions arise when considering potential contact with carbon steel. NORSOK M-501 addresses this concern:

*"If stainless steel is connected to carbon steel, the stainless steel part shall be coated 50mm beyond the weld zone onto the stainless steel."* [70]

5083-H116 is not technically considered a stainless steel but can be regarded as such when considering the high corrosion resistance the alloy possess. The two modules are to remain separated by a flange, as detailed in section 4.4.3. Although direct contact between the modules is prevented with this flange, it is decided that the aluminum module shall be coated following guidelines covered by the NORSOK Standard. This precaution serves as a safety measure in case of flange deterioration or malfunction. The coating system specified for submerged stainless steel is outlined in Table 23.

*Table 23: Surface Preparation and Coating - Stainless Steel [70].*

| APPLICATION | SURFACE PREPARATION | COATING | MDFT [µM] |
|---|---|---|---|
| **SUBMERGED STAINLESS STEEL** | Sweep Blasting w/ non-metallic and chloride free grit to obtain profile of 25-45 µm | Two Component Epoxy Coats : minimum 2 | 350 |

### 4.4.3 Isolating Gasket

To prevent galvanic corrosion when submerged, it's essential to maintain separation between aluminum alloy and carbon steel. According to NORSOK M-001 (2014), any connections between aluminum and steel must adhere to the following guidelines:

*"Direct contact between aluminium and carbon steel shall be prevented in marine environments. Aluminium and steel (carbon steel and stainless steel) surfaces shall in general be segregated with pads made of non-metallic materials such as rubber. For combinations carrying high loads type 316 SS shims can be used in between carbon steel and aluminium. Fasteners shall be made of type 316 SS grade 70 or 80 with type 316 SS plate washers used under both bolt head and nut. The plate washer shall not be thinner than 4 mm."* [71]

The implementation of such gasket is therefore regarded as necessary for the structure established within the thesis to prevent the risk of galvanic corrosion.

#### *4.4.3.1 Bolts and Washers:*

All bolts and washers must be of type 316 SS as stated by the Norwegian Standard, adhering to ISO 3506-1 grade A4-80 and ISO 7090 [72]. Additionally, the washers require a coating of Polytetrafluoroethylene (PTFE) to serve as an insulating layer. Before applying this coating, the washer surface must undergo cleaning and blasting to achieve a roughness level of 6-12 μm [73].

The PTFE layer should then be applied with a thickness ranging from 10-20 μm, followed by subjecting the washer to a baking process at temperatures between 120-180 degrees Celsius for a minimum of 15 minutes. To ensure the washer's operational integrity for over 20 years, a second layer must be applied, resulting in a complete coating thickness of 20-38 μm [73].

The compressive yield strength of PTFE is approximately 12 MPa, while steel structures are typically tightened with bolts to about 100-150 MPa for secure installation. Due to the PTFE covering a larger surface area than the bolted region, the compressive force is regarded as negligible.

As an additional safety measure, it's recommended that any horizontal surface employs two washers, one on the top surface and one on the bottom surface. This precaution ensures that any localized damage to the PTFE-coated washers during tightening does not pose significant risks [73].

*4.4.3.2 Insulation Gasket:*

The two modules must remain separated at all times, this can be achieved by applying a non-metallic barrier between the connection points. This barrier, made from either rubber or a PTFE material, should be 3-4mm thick [73].

After the installation of the two modules, with separation barrier, a sealing compound must be applied over the two metals, gasket, bolt holes, and external corners to prevent water ingression. The insulation material's lifespan must match or exceed the design lifetime of the structure to be considered applicable for use [73]. A description of components and seals are provided in Figure 55.

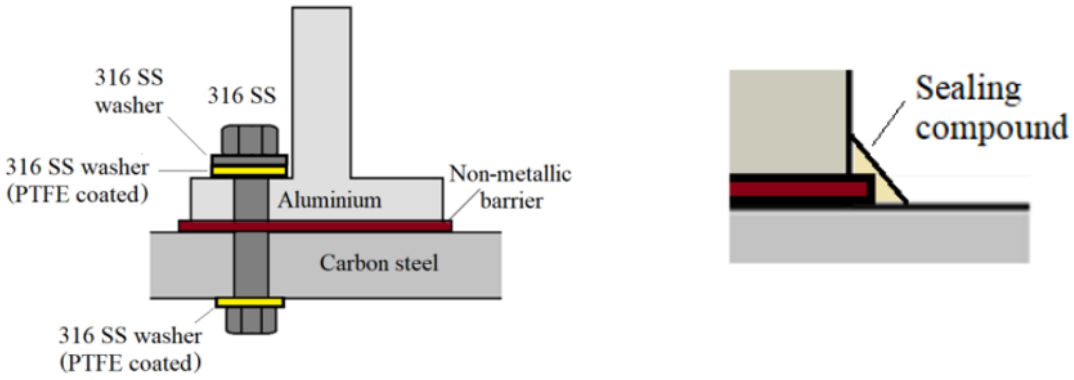


*Figure 55: Aluminum and Carbon Steel Separation [73].*

## 4.5 Design of Flange and Bolts

The bolts used in the flanges connecting the steel and aluminum modules must withstand various loading scenarios. To prevent pure shear stress in the bolts, the flange is designed to restrict horizontal movement. By doing this the bolts will only experience vertical tensile forces, which they are much more capable of handling. This will result in the need of overall fever bolt with a smaller dimensions.

To ensure the structural integrity of the bolts a conservative approach has been used, utilizing a maximum load of 2 x 200 kN as specified in NORSOK U-001 for trawlnet friction [64]. This load is considered to be concentrated at one of the four flanges, representing a worst-case scenario where the entire friction force is focused in one corner with an upward pulling force. With a safety factor of 2.0, the total uplifting force becomes 800 kN. Given that each flange uses 5 bolts, the resulting force per bolt, $F_t$, is 160 kN. Using the equation below, the nominal stress area, $A_s$, can be determined.

$$F_t = \frac{k_2 * f_{ub} * A_s}{Y_{M2}} \Rightarrow$$

$$A_s = \frac{F_t * Y_{M2}}{k_2 * f_{ub}}$$

*Equation 7: Calculation of Bolt Dimensions from EN 1993-1-8 [74].*

Where the variables are listed below and in Table 24:

$k_2$ = coefficient.

$f_{ub}$ = ultimate tensile strength of the bolt with grade A3 or A4.

$A_s$ = nominal stress area.

$Y_{M2}$ = Steel partial material safety factor.

*Table 24: List of Variables for Bolt Design [75].*

| $F_T$ | $F_{UB}$ | $K_2$ | $Y_{M2}$ |
|---|---|---|---|
| 160 kN | 700 MPa | 0.9 | 1.25 |

As specified in section 4.4.3.1, a 316 SS (stainless steel) bolt of grade A3 or A4 is required. Using Equation 7, the resulting nominal stress area is then 317.5 $mm^2$. Table 25 below shows the corresponding bolt thread diameter and nominal stress area. Since the calculated value exceeds that of an M22 bolt, five M24 bolts should be used for the flanges.

*Table 25: Nominal Stress Areas with Thread Diameters from ISO-898-1-2013 [76].*

| THREAD DIAMETER | NOMINAL STRESS AREA |
|---|---|
| **M20** | 245 |
| **M22** | 303 |
| **M24** | 353 |

### 4.5.1 Complete Design of Flanges

By combining the data obtained in this and the previous chapter, a complete flange design has been created. This design includes a full set of specified components and materials, exemplifying a structurally robust flange with isolation capabilities. Figure 56 illustrates the finished design.

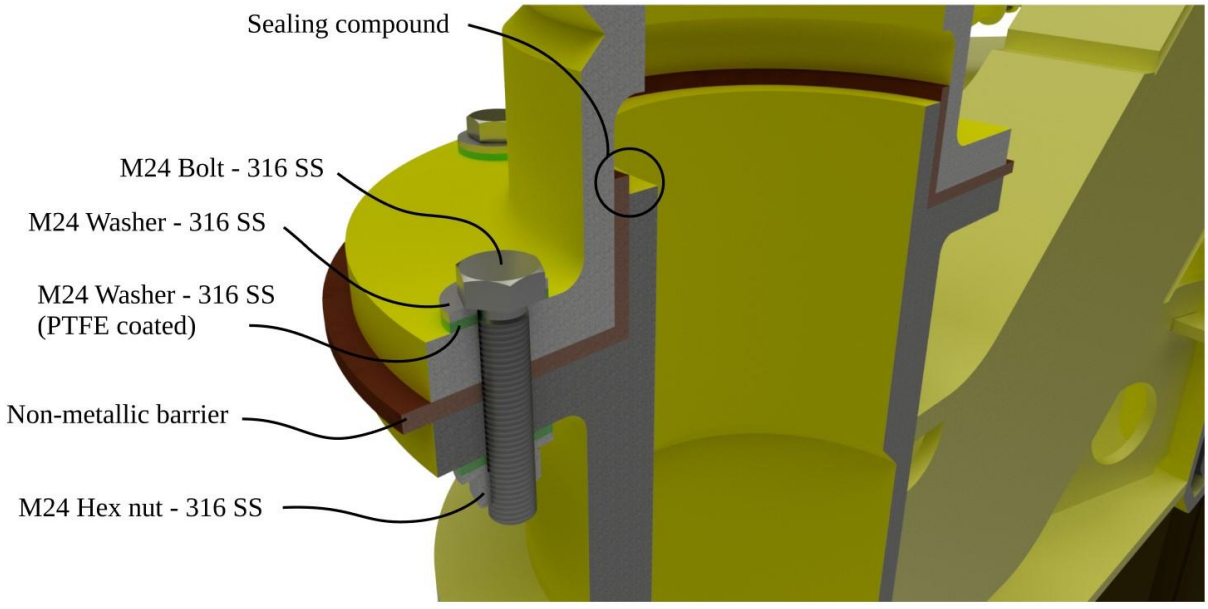


*Figure 56: CAD Model - Flange Design Between the Steel- and Aluminum Module.*

In the figure, green represents coated parts, red non-metallic parts, dark gray indicates the steel module, and light gray the aluminum module. The steel segment of the flange extends into the aluminum part to lock it in place, preventing horizontal displacement. To achieve this, the non-metallic barrier also extends upward by 10 mm past the steel module. This top section must then be sealed with a sealing compound to minimize the risk of galvanic corrosion in this area.

# 5. Presentation and Comparison of Final Model

In this chapter the final model will be presented with the latest changes made based on the preceding analysis. This model represents the finished concept model where the template itself, installed equipment, and the installation process will be discussed. The model will also be compared to the solution utilized by the Northern Lights project, as presented in chapter 2. This comparison will focus on cost, installation phase, intervention work, and potential parts reuse.

## 5.1 Presentation of Final Model Concept

The modifications applied to the final model is based on the outcomes of the structural analysis. The templates original design demonstrated promising potential, with minimal adjustments required for the dimensions of the tube and plate elements. The structure's geometry also showed good capabilities at handling various loading scenarios, simplifying the dimensioning process as major design alterations were unnecessary.

### 5.1.1 Aluminum Frame

The tubing sections utilized in the aluminum frame exhibited stress levels within acceptable limits, and the cross-sections of the beam elements remain unchanged. The most significant stress concentrations were observed near the corner connections, primarily due to the limited contact area between the beam elements. To distribute the stresses more efficiently and better utilize the material's strength away from the joint sections, bracing plate elements have been incorporated. These elements are highlighted in green in Figure 57 below, illustrating the new frame configurations.

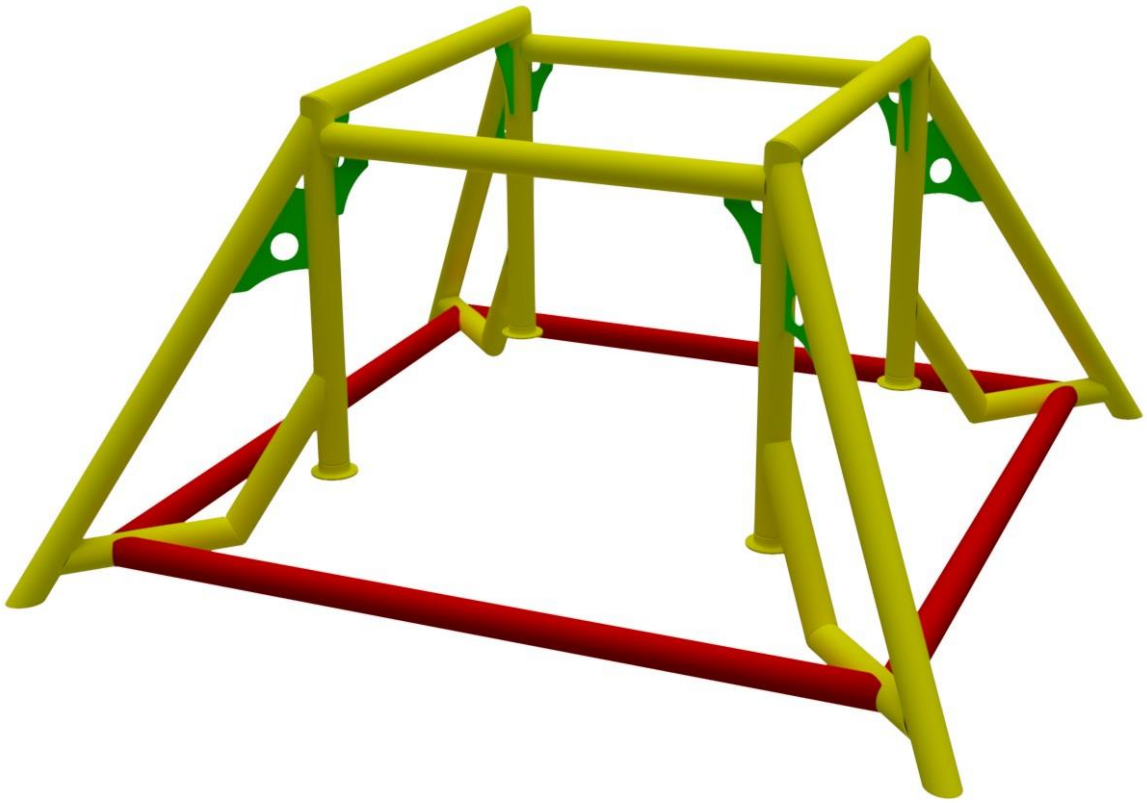

*Figure 57: CAD Model - Finished Aluminum Frame.*

The inclusion of the bracing plate elements has significantly influenced the results, where the structural analysis with the corresponding von Mises stress distribution can be found in appendix C.1 and C.2. Due to spacing limitations caused by the hinge brackets for the top hatch, the sizing of the bracing plate elements should be further optimized. An effective solution would be to merge the bracket and bracing elements of the frame to create a stronger and more space-efficient design. This integration has not been incorporated into the current design due to time constraints but could be considered in the future to further optimize the structure.

The beams highlighted in red in Figure 57 have been lengthened and moved further from the center of the frame. This adjustment is done to optimize the geometry of the brackets for the front and rear hatch hinges. By moving this beam, a more compact bracket design has been achieved, resulting in fewer parts and an overall cleaner design.

### 5.1.2 Front and Rear Hatch

The frame elements of the front and side hatches demonstrated an overall good performance across the full range of loading cases. Consequently, the main frame configuration and the dimensions of the tubing section remain unchanged. For the plate elements both the inner and outer plates showed lower stress levels, allowing for a reduction in their thickness. The most significant change has been made to the two outer corner plates, reducing their thickness from 25 mm to 12 mm. This reduction is possible due to the smaller size of the plates, where the framing absorbs most of the local loading. Additionally, the two plates in the middle of the hatch have been reduced from 25 mm to 20 mm, with the primary constraint being the need to withstand the impact of dropped objects. The changed plate elements are highlighted in red in Figure 58 below.

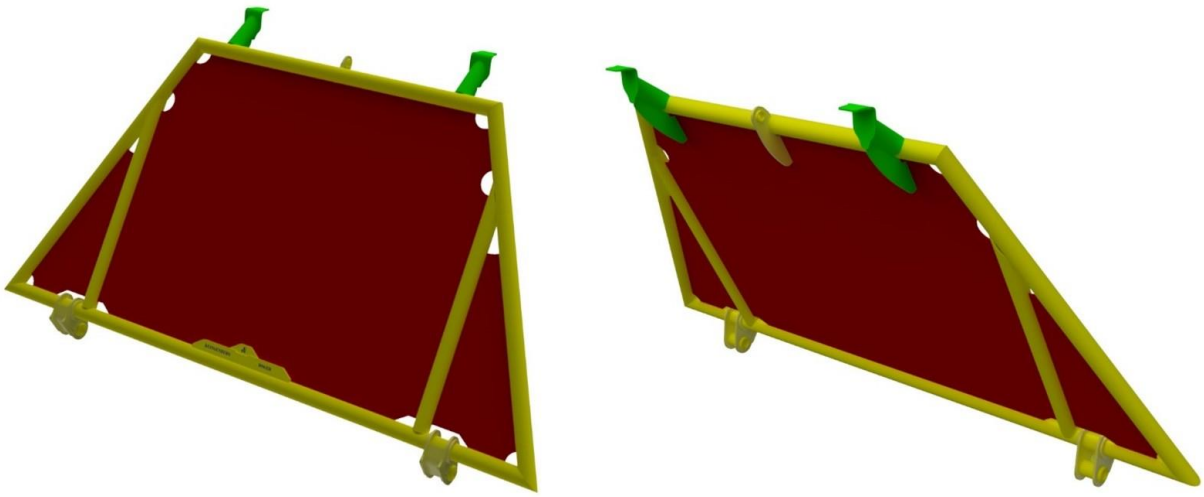

*Figure 58: CAD Model - Finished Front and Rear Hatch.*

In an effort to achieve smaller support arms, the arms have been relocated to the top of the hatch as highlighted in green in Figure 58 above. This change results in a noticeable weight reduction due to the shorter travel distance of the support arms to the structural frame. Additionally, it helps reduce the risk of interference with the ROV during operational work. When in its open position, the support arms are positioned further away from the tree, decreasing the likelihood of cable entanglement for the ROV operating on the installed equipment within the frame.

### 5.1.3 Top Hatch

Similar to the front and rear hatches the framing section remains unchanged, as it demonstrated overall good performance during the varying loading cases. The plate elements located at the top and sides have all been reduced in thickness from 25 mm to 20 mm, highlighted in red in Figure 59 below. Like the front and rear hatches, the primary limitation is the impact of dropped objects. When the thickness of the front plate element was reduced, significant stresses appeared near the connection point for the wire from the crane ship. To address this a smaller plate element with a thickness of 15 mm has been added around this bracket, as indicated in green in the figure below. This addition helps distribute the stresses, resulting in a reduction of higher local stresses.

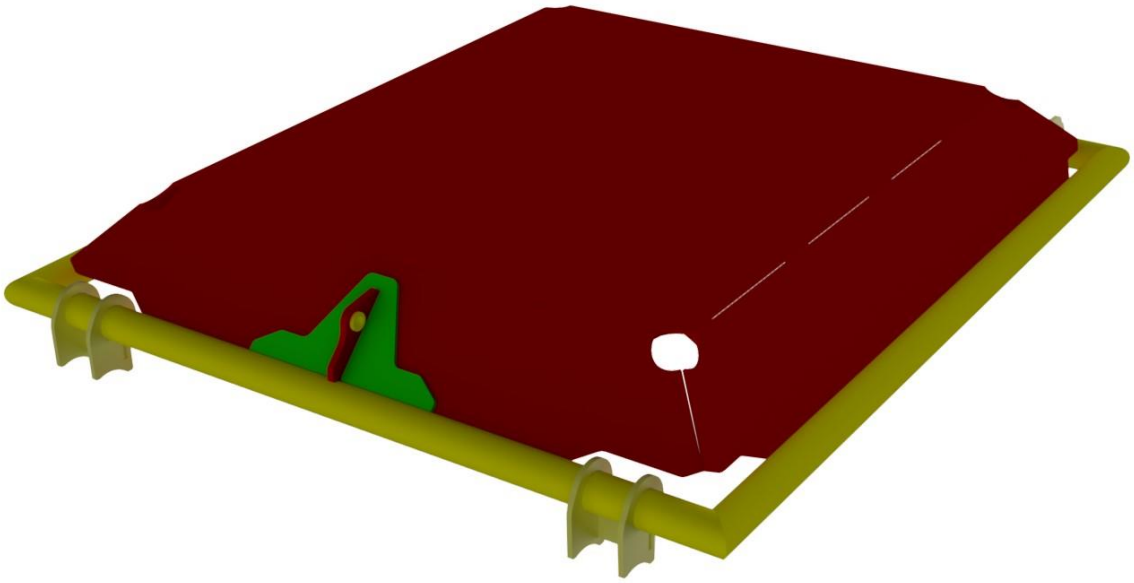

*Figure 59: CAD Model - Finished Top Hatch.*

The beams under the hatch effectively absorbed and distributed stresses during different loads, with stress levels comfortably below the limit. Due to this their thickness has been reduced from 25 mm to 15 mm. Since the exact load of dropped objects is somewhat estimated, the primary focus is ensuring the structure can handle such loads with efficient use of material. Adjusting the dimensions of both the plate and beam elements to suit the structure is relatively straightforward and can be finetuned at a later stage if dynamic simulations is done to properly simulate the impact energy. Figure 60 displays the interior of the top hatch with the stiffening beam elements.

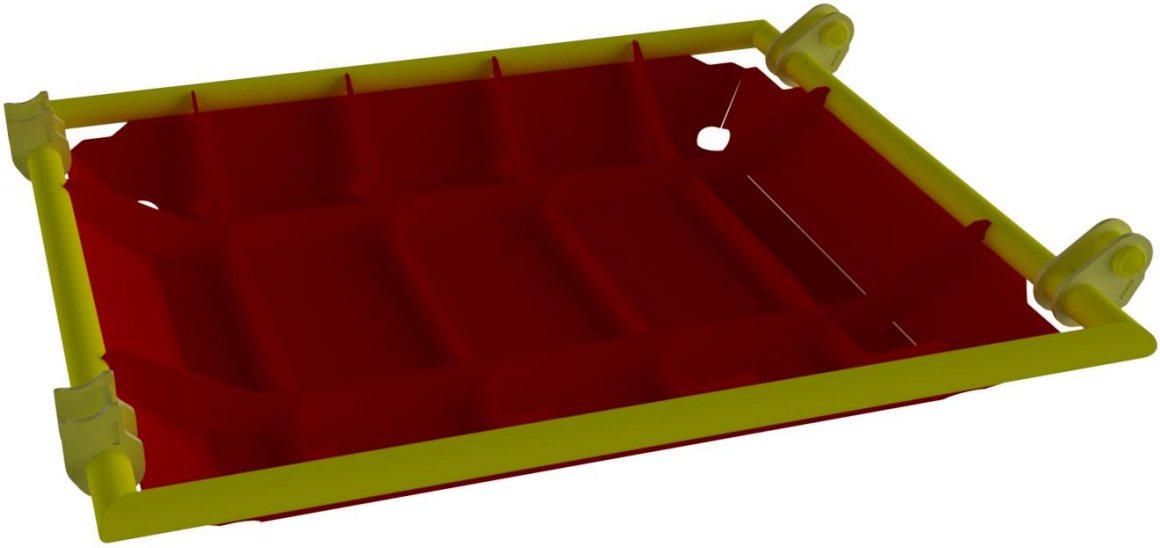

*Figure 60: CAD Model - Inside of Finished Top Hatch.*

### 5.1.4 Steel Module

The steel module showed the most compromised results. Adding bracing elements towards the flange connection was essential for achieving a functional design without excessive material usage. Stress levels were significantly higher near the flanges, while the inner part of the frame was almost unaffected. To help the structure better utilize its complete strength, bracing elements, shown in green in Figure 61, were added. Tubing beams were used for these bracing elements due to their versatile strength and sufficient spacing.

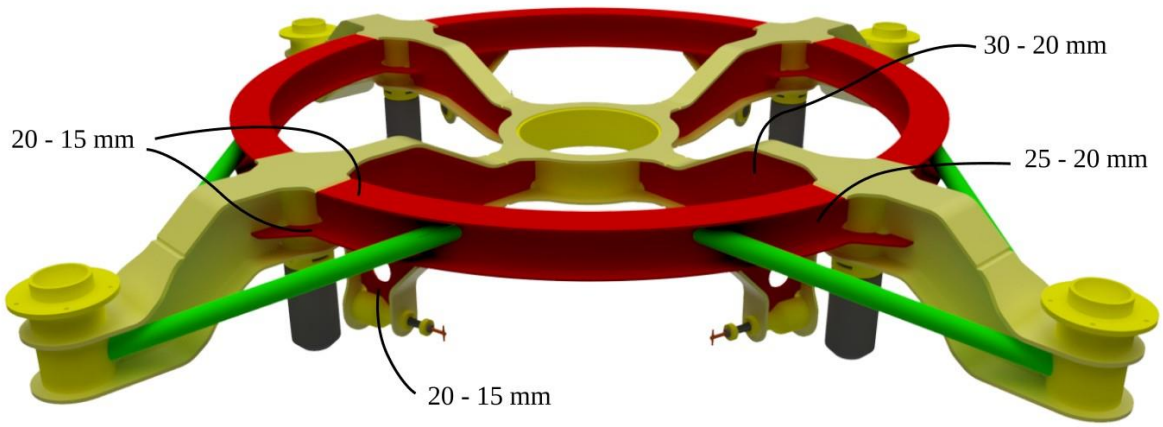


*Figure 61: CAD Model - Finished Steel Module.*

The inclusion of these bracing beams significantly increased the stiffness of the flange tip, resulting in a lower moment at the connection point towards the center of the frame. The stress levels were significantly reduced, demonstrating that the circular I-beam of the frame now contributes more to the overall strength profile. The inner segment of the frame still shows overall low stress levels, allowing for a reduction in the thickness of some plate elements. An overview of these changes can also be seen in the figure above. To ensure the frame can handle varying loading cases, such as collision loads during installation, a conservative approach has been taken when reducing the thickness of these plates.

Another major change to the steel module is relocating the horizontal connection bolts to the circular I-beam, instead of placing them towards the middle of the frame as in the initial concept model. This adjustment makes it easier for an ROV to operate during installation, as there is more space and accessibility in this area. Additionally, the structure should have strategically placed handlebars in this area for the ROV to grab when operating these bolts.

### 5.1.5 Complete Final Model

The finished model represents the complete subsea template concept for this study. Major improvements throughout the project have significantly reduced the weight of the structure and enhanced its usability. The final model has been tested against the designated loading case requirements for an overtrawlable template structure installed on the Norwegian continental shelf. Although some simplifications were made for certain loading cases, the finished model still demonstrates the realistic possibilities present within the design. The complete model is shown in Figure 62 in its fully closed position.

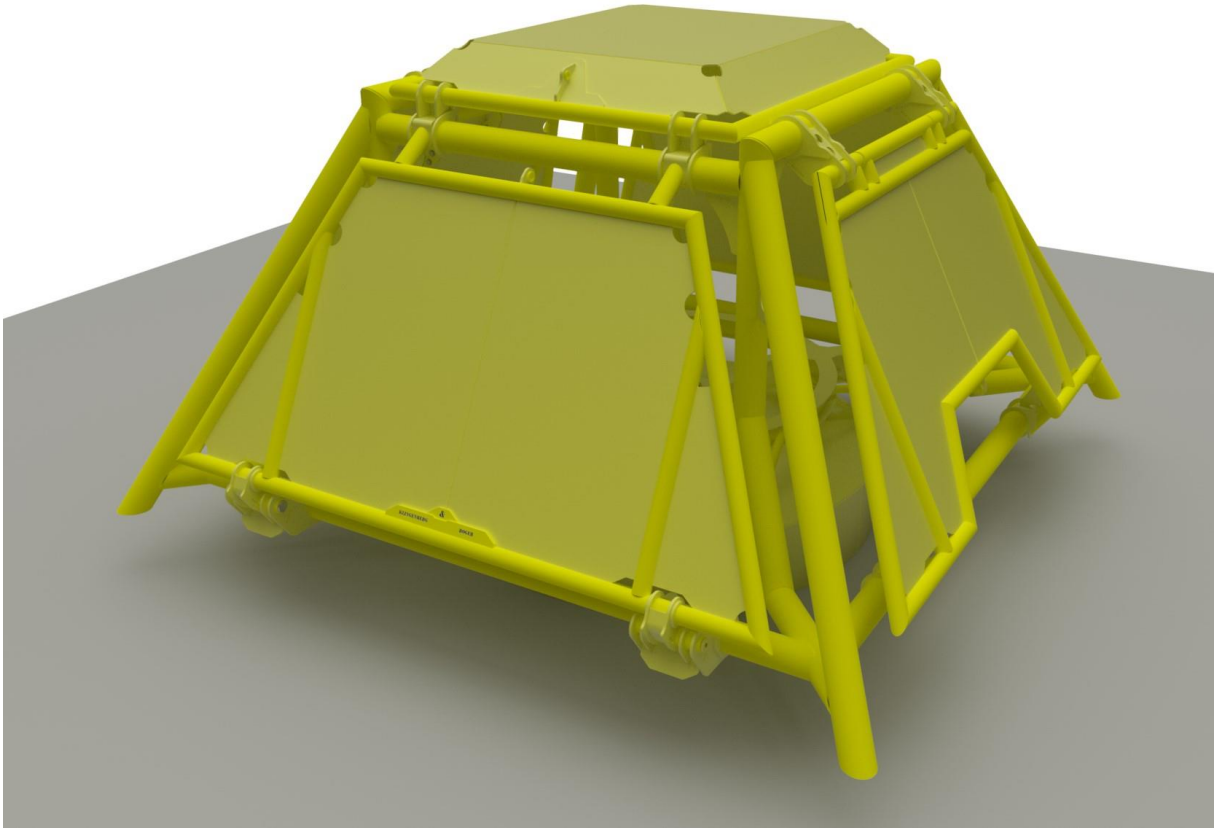

*Figure 62: CAD Model - Finished Template Structure in its Closed Position.*

One of the major improvements, along with weight reduction, has been the increased accessibility of the template for installation and intervention work. The size-reduction and relocation of the hatch arms provide more space near the installed equipment, along with easier access points for the locking mechanisms during installation. Figure 63 shows the template structure in a fully open position.

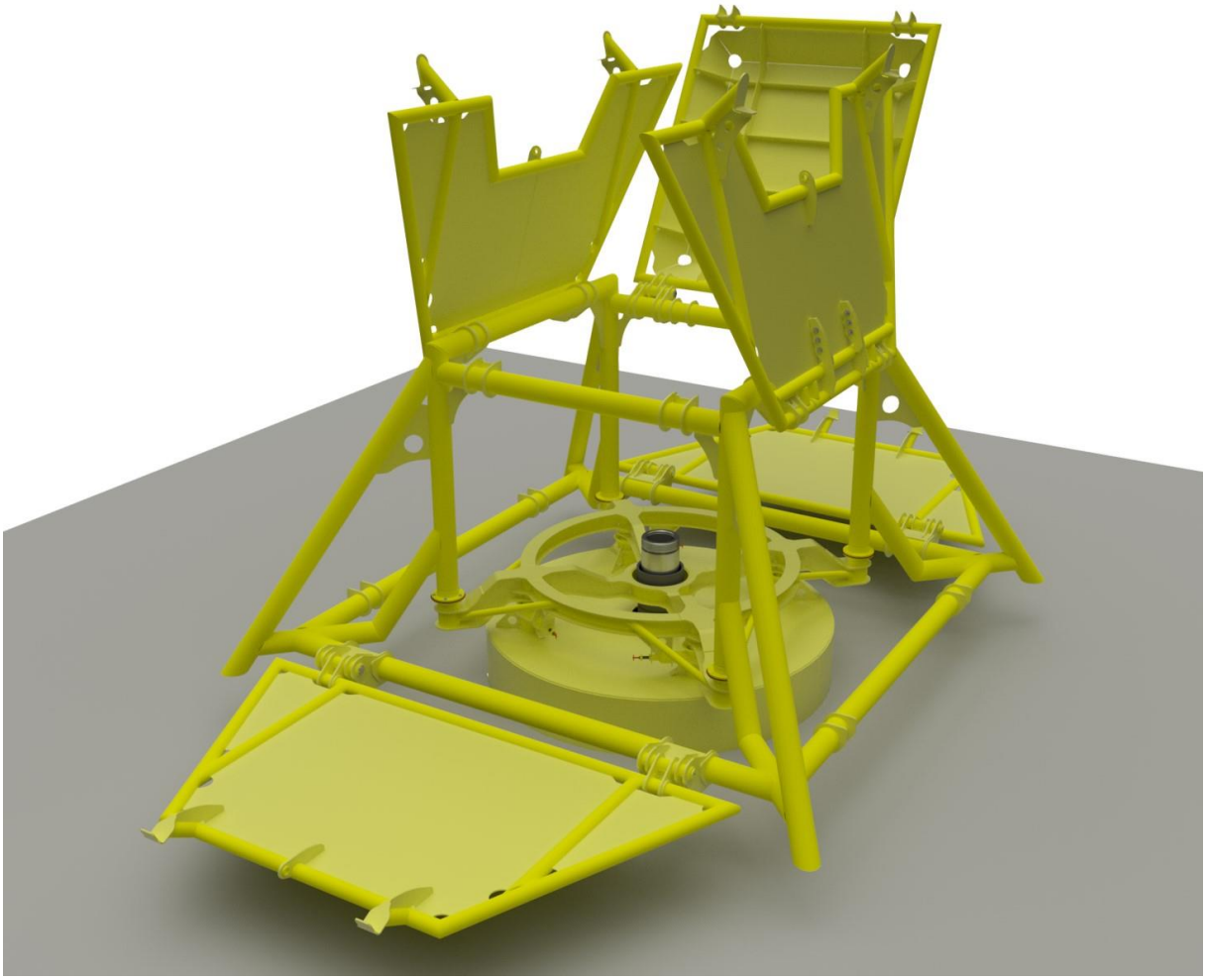

*Figure 63: CAD Model - Finished Template Structure in its Fully Open Position.*

The first concept model demonstrated good capabilities in the structural analysis, so the differences in both geometry and weight are not substantial. The total number of parts has increased by 5 due to the added bracing in both the steel and aluminum modules, despite a reduction in parts from the simplified bracket design of the front and rear hinges. However, the total weight of the structure has decreased by 2574 kg, excluding the suction anchor. A detailed overview of the properties comparing the first and final model, can be found in Table 26.

*Table 26: Component Overview First vs. Final Model.*

| | FIRST MODEL | | | FINAL MODEL | | |
|---|---|---|---|---|---|---|
| **COMPONENTS** | **Parts** | **Total Weight [kg]** | **Quantity** | **Parts** | **Total Weight [kg]** | **Quantity** |
| **ALUMINUM FRAME** | 24 | 6137 | 1 | 36 | 6688 | 1 |
| **FRONT/REAR HATCH** | 30 | 2500 | 2 | 30 | 2060 | 2 |
| **SIDE HATCH** | 38 | 2480 | 2 | 38 | 2042 | 2 |
| **TOP HATCH** | 31 | 2754 | 1 | 32 | 2286 | 1 |
| **FRONT/REAR HINGE** | 16 | 322 | 4 | 12 | 176 | 4 |
| **SIDE HINGE** | 8 | 108 | 4 | 8 | 108 | 4 |
| **TOP HINGE** | 11 | 102 | 2 | 11 | 102 | 2 |
| **STEEL MODULE** | 87 | 6397 | 1 | 95 | 6078 | 1 |
| | | | | | | |
| **TOTAL** | 396 | 27170 | - | 401 | 24596 | - |

## 5.2 Installation Process

In this chapter the installation process will be presented step by step, showcasing the complete procedure. One of the key features of the modular approach to the template structure is the two-step installation process, which involves installing the suction anchor and the template frame separately. This approach potentially minimizes the cost associated with using a larger crane ship. The focus will be on the installation process from the transportation vessel at the surface to the template is securely installed at the seabed, excluding the transportation phase to the installation site.

### 5.2.1 Installation of Suction Anchor

The suction anchor will be installed individually at the site before drilling of the well begins. The anchor's size is designed to fit through a 6x6 meter moonpool. To ensure this is feasible, necessary calculations regarding the stability of the anchor and template on the seabed must be completed in advance to confirm the anchor size is sufficient. If this is the case, installing through a moonpool allows for a more controlled lowering process, eliminating direct wave forces on the anchor through the splash zone. A detailed cost evaluation of installing through a moonpool versus the side of a crane ship should be conducted beforehand to determine the most cost-effective solution.

The anchor should have built-in ventilation holes that must remain open during the initial lowering phase through the water. Due to the large surface area of the anchor, a horizontal drift is expected, depending on the current at the installation site. An estimated horizontal drift of 32 to 304 meters is anticipated at the Northern Lights project installation site, with a water depth of 300 meters and an average current of 1 to 3 m/s. Due to the limited weight of the anchor when installed alone, the drift will quickly increase with higher current speeds. This potential drift should be evaluated beforehand to ensure safe installation of the anchor. The calculations done regarding this can be found in appendix A.3.

At the seabed the anchor will penetrate the surface using the weight of the structure. When the anchor reaches a natural stopping point, the ventilation hatches must be closed before an ROV connects its compressor to the anchor. The lower internal pressure in the anchor will be the final driving force for the anchor to reach the planned penetration depth. An estimated size of the anchor, with a diameter of 5.5 meters and a penetration depth of 6 meters has been determined. The reasoning behind the large diameter relative to the penetration depth is to maintain a higher

stability for the anchor. However, a solution with a smaller diameter and increased penetration depth could be beneficial when considering only the weight of the anchor. The required suction pressure for the anchor to reach the required penetration depth is then estimated to be 0.1 bar. Calculations for the anchor is based on the specialization project report for this thesis, where the calculation specific to this model regarding penetration depth and suction pressure can be found in appendix A.1 and A.2.

After the anchor is installed, its positioning can be read by the ROV at the site. This will be done using an integrated spirit level on the anchor, which will show the tilt angle. This information will be used to pre-adjust the leveling function of the template frame, which will be discussed in more detail later.

### 5.2.2 Installation of Template Frame

After the well is completed, the template frame will be installed on top of the anchor. The aluminum and steel module will be assembled at the workshop, ready for installation. Given the size of the template at 10.5 x 10.5 meters (L x W), it must be installed through the splash zone from the side of the crane ship. To limit the stresses experienced by the template at this stage, the side and top hatches will be open, allowing for better wave flow through the template. This configuration of the template is shown in Figure 64 below.

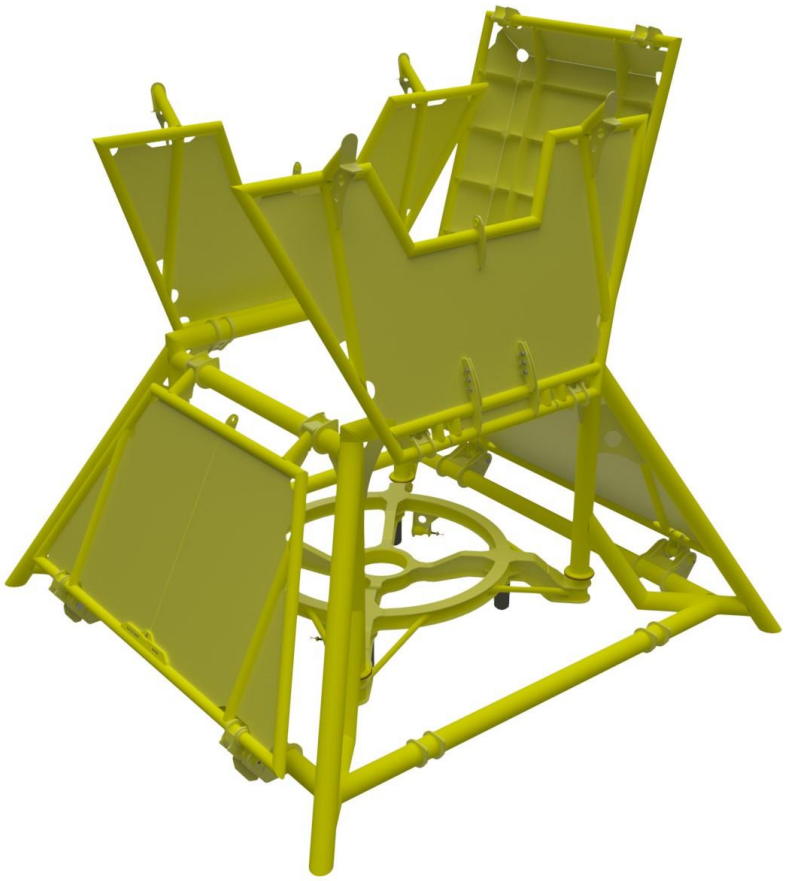

*Figure 64: Illustration - Template Frame During the Lifting Phase of the Installation.*

During the installation phase, the top and side hatches will be tied together with a tension rope. This will lock the hatches in place and allow for easy release by an ROV once the template has securely landed on the suction anchor. For the template frame to be placed correctly the connection pins illustrated in gray in Figure 65, must align with the housings on the suction anchor. The design of these pins and housings includes a 45 º incline at the top of the housing and the bottom of the pins to help guide the structure into place.

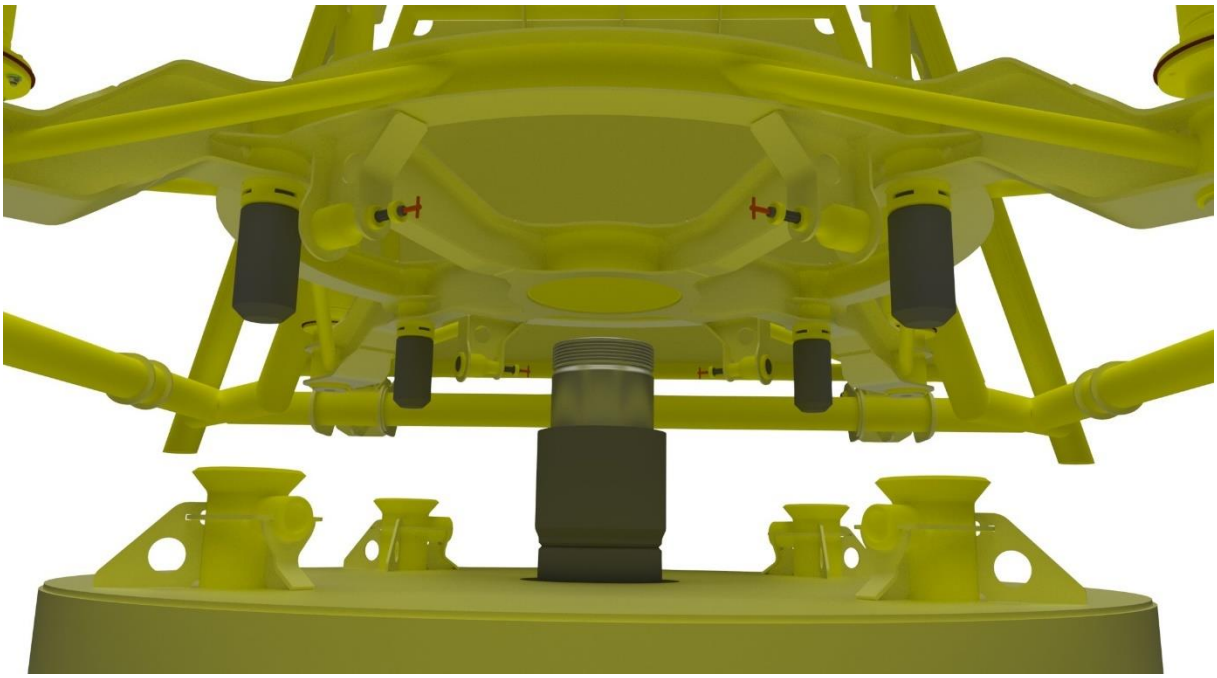

*Figure 65: Illustration - Template Frame Positioned Correctly Above the Suction Anchor.*

To ensure that the frame is level, a leveling function is incorporated into the connection pins of the frame. These pins are height-adjustable with a locking function, allowing for adjustments before the template frame leaves the workshop. This is possible because the suction anchor is installed before the drilling of the well, allowing the tilt of the anchor to be determined once it is in place. The positioning of the connection pins can then be adjusted accordingly to achieve a level frame once installed on the anchor.

To limit the risk of collision between the anchor and template, sufficient spacing has been provided for the wellhead through the center of the frame. The pins are designed with enough length to enter the housings before the frame reaches the same height as the conductor piping, ensuring sufficient clearance. Once the template has landed, the locking pins shown in Figure 66 can be operated by an ROV to secure the template in place. These pins have been repositioned in the final model to improve accessibility for the ROV. The new layout allows all four locking pins to be operated with only the front and rear hatches open.

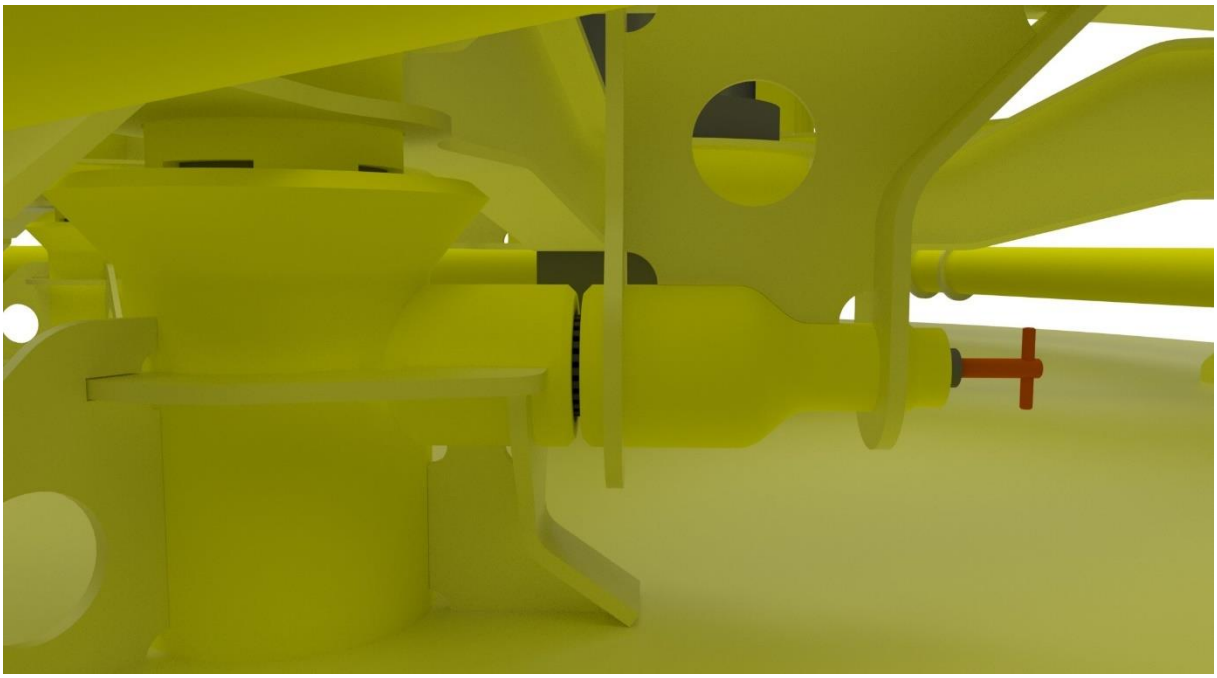

*Figure 66: Illustration - Template Frame Installed at Anchor with Attached Locking Bolt.*

Once the template frame is securely locked into place on the anchor, the required equipment can be installed. When installing the X-mas tree, the top, front, and rear hatches should be open to provide enough space for the tree to enter and sufficient access for the ROV. After the tree is installed, the side hatches can be opened to allow for the connection of the flowlines. A system similar to the horizontal tie-in system used in the Northern Lights projects discussed in Chapter 2.2.3 will be employed, where an ROV is used for the attachment. The side hatches will then be closed, with cutouts in the hatches providing sufficient space for the attached flowlines and cables.

## 5.3 Subsea X-mas Tree

The main focus of this thesis has been on the template structure, no concept modeling or analysis has been conducted for the subsea X-mas tree. To evaluate a complete subsea system for CO2 injection, this chapter will instead discuss a potential configuration of the X-mas tree to be installed in the template. This discussion will be based on one of the two ideas previously presented in chapter 5.2 in the specialization project for this thesis [62].

### 5.3.1 Size Reduction

An important factor contributing to the effectiveness of the template design is achieving smaller installed equipment. This makes the template proportionally smaller, which limits the design challenges associated with the reduced stability of a larger structure with one central suction anchor. Therefor one of the main goals for the conceptual x-mas tree is to achieve a reduced height without compromising well integrity.

As discussed in Chapter 2.4, the design parameters for a pure CO2 injection tree differ from those of a conventional production tree. The redundancy and dimensions of the valve layout on a production tree can be seen as excessive for CO2 injection purposes. For a vertical x-mas tree, the height is dependent on the number of barrier valves installed. Therefore, an effective way to achieve height reduction is to reevaluate the necessity and placement of each installed valve.

### 5.3.2 Module Based Design

Similar to the template concept, the modularization of the X-mas tree opens up new possibilities for the subsea system. The main advantage of this approach is the ability to replace individual valves and parts of the tree during interventional work. One possible configuration is presented in Figure 67 below.

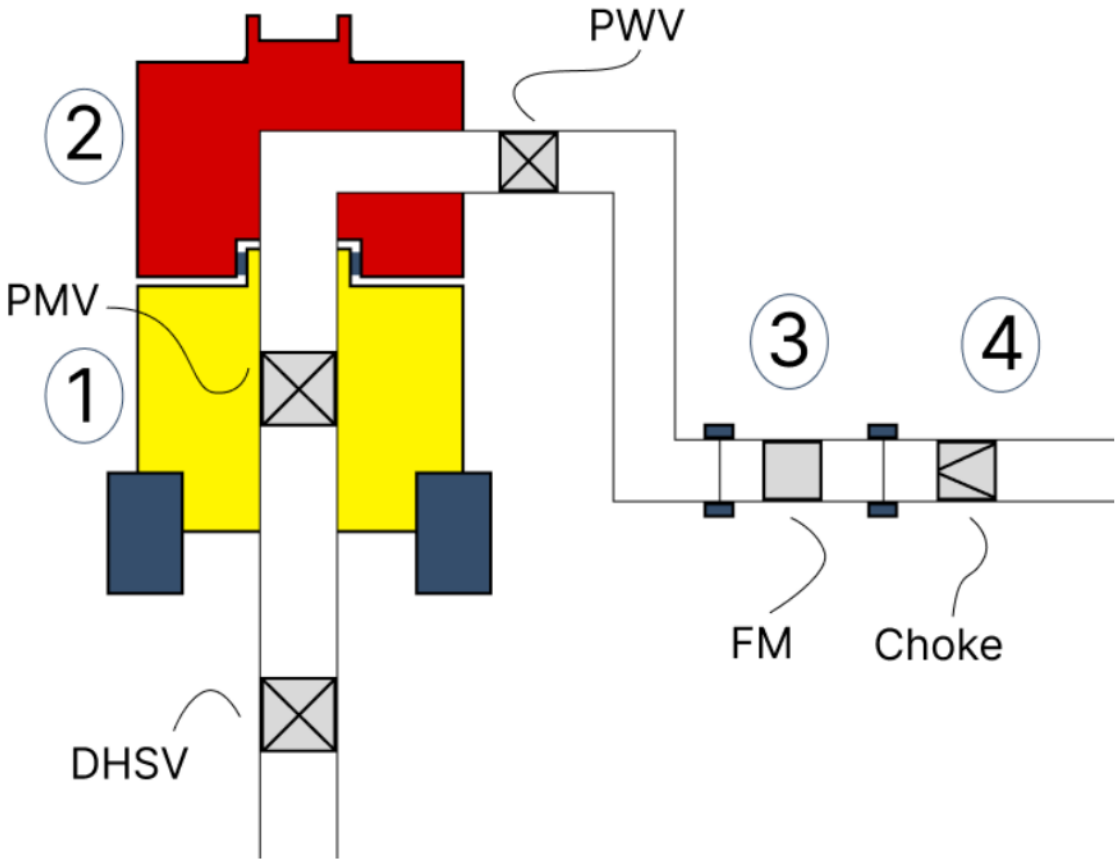


*Figure 67: Illustration - Module-based X-mas Tree Concept [62], page 26.*

Here a vertical x-mas tree is shown with a 4-module layout. The first module houses the Production Master Valve (PMV) with a Downhole Safety Valve (DHSV) placed further down the well. For the removal of Module 2 to be possible, at least two barrier valves must be present below it. Another option while achieving this is to include two PMV in the first module, making the valves more accessible for interventional work. The downside of this approach is the increased height of the tree due to the added valve in the bore hole. A detailed evaluation of the costs and compromises associated with these two layouts should be conducted before finalizing the design.

Module 2 is connected to Module 1 using hydraulic pressure, similar to the system typically used for the wellhead and tree connection. This ensures a pressure sealed connection with easy removal capabilities for potential replacement or maintenance of the module. Module 2 will house only the production wing valve (PWV). The PWV is often used for opening and closing the well, and can experience additional wear especially due to the high Joule-Thomson effect for CO2 in its gaseous state. The Joule-Thomson effect states that rapid pressure changes can

result in extremely low local temperatures, potentially shortening the lifespan of the valve material [77]. During the normal injection phase, the CO2 should be in a liquid state. This issue will therefore mainly arise during start-up or shutdown of the well, when lower flow rates can lead to short periods of gaseous CO2.

The easily accessible placement and compact size of Module 2 are therefore particularly beneficial for the injection system. Consequently, the concept excludes the use of a swab valve or tree cap at the top of the tree, with the idea that Module 2 can be easily removed if vertical access to the well is needed. A bracket should be designed on the front or rear hatch, which lays horizontally when open, to park Module 2 during interventional work if necessary.

As the expected lifespan of the PWV is assumed shorter than that of the PMV and DHSV, this arrangement can be especially beneficial. Module 2 is intended to be retrieved to the surface during interventional work, where a new module can be installed while the old one is sent back to shore for maintenance.

Modules 3 and 4 will consist of a flowmeter and choke valve, respectively. These modules are designed to be individually retrievable for easier replacement and interventional work. Their placement must be strategically around the tree to ensure sufficient space and accessibility. Given that the choke valve will also experience the Joule-Thomson effect during flow regulation, it will be beneficial to design it for easy retrieval like the PWV.

Due to time limitations, a complete conceptual CAD model of the x-mas tree design has not been created. This will need to be developed later to showcase the complete conceptual model of the subsea system. The design of the tree and template should complement each other to achieve the most effective solution in terms of size, weight, and operability.

## 5.4 Economical Drivers

In this chapter a price comparison between the two main metals shall be assessed to further set light on the economical factor that drives this to be an attractive investment for the industry. Some ideas around the installation of the complete system are included to showcase the possibilities of lowering the installation costs compared to a standard system, as well as the possibilities around reusage of the components for later installations.

### 5.4.1 Material Cost

The specific materials utilized for the Northern Lights satellite structure is not specified, but one would assume the material to be a marine grade structural steel, as this is commonly used within the industry and approved for such applications by the NORSOK standard. The price calculations are therefore based on the assumption that the NL structure is manufactured using S355 marine grade (MG) structural steel.

*Table 27: Material Costs.*

| Structure | Marine Grade Material | Price [per Ton] | Weight [Tons] | Material Cost | Total | NOK | REF |
|---|---|---|---|---|---|---|---|
| **Concept** | S355 Steel | USD 800,00 | 6,078 | USD 4 862,40 | USD 69 675,40 | NOK 736 468,98 | [78] |
| | 5083 Alu. | USD 3 500,00 | 18,518 | USD 64 813,00 | | | [79] [80] |
| **Northern Lights** | S355 Steel | USD 800,00 | 103,0 | USD 82 400,00 | USD 82 400,00 | NOK 870 968,00 | [78] |

These material costs are calculated based on the exact weight of the finished product, but the manufacturer must in reality purchase more material to sufficiently manufacture the complete structure. The cost estimation is done simply to showcase the economical savings for the material due to weight reduction. The table shows the conceptual structure to be cheaper in terms of material choice than the standard integrated steel structure utilized for the Northern Lights field.

### 5.4.2 Installation Phase

The installation phase is regarded as one of the economical drivers for this thesis. A lower total weight of the subsea equipment will result in a smaller installation cost. For a conventional subsea system, larger installation vessels must be used to handle the high-weight components. These operations are considered expensive, and a reduction in required vessel size and crane capacity would drastically reduce the cost of installation.

The total weight for the conceptual template structure is approximately 25 Tons without the suction anchor, compared to the Northern Lights structure of 103 Tons. The NL structure will also be installed with the anchors attached in contrast to the conceptual model. Excluding the anchors, the weight difference is approximately 75%. This brings into discussion the reduction of installation vessel size, where a smaller vessel is to be considered viable for installation, resulting in a lower overall cost. A table from ULSTEIN is provided in Figure 68 to set perspective on the vessel size that could be feasible for a template and suction anchor installation as described in chapter 5.2.

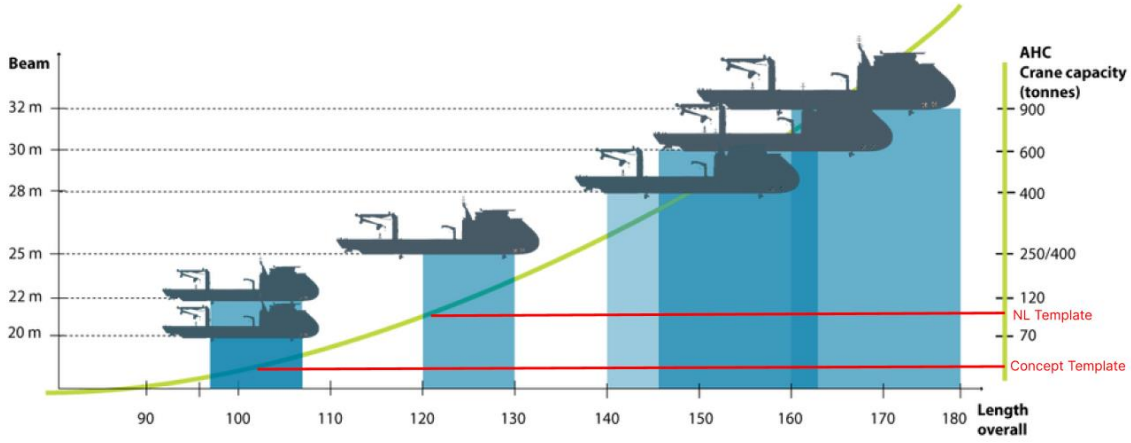


*Figure 68: Installation Vessel Size [81].*

### 5.4.3 Manufacturing Phase

Estimating the manufacturing costs for any system is challenging, especially for a structure still in its conceptual phase. The compact size of the structure will contribute to a significant reduction in manufacturing costs, as the smaller parts will be cheaper to produce, ship, and assemble.

The number of parts will be considerably larger for the modularized design compared to a fully integrated option of the same size. This generally means more welding and a more complex assembly process, which increases the overall cost. However, the modularized design allows for parallel production of the modules, reducing the overall production time.

### 5.4.4 Reuse of Components

The two separate frame modules are designed to be retrieved at the end of the injection work and provide possibility for reusage for the majority of the template structure. This excludes the suction anchor, as the possibility for reusability is limited due to varying soil condition at different installation sites. The components considered for reusage must undergo thorough testing to make sure the structure has not been subject to any corrosion or strength decreases before being approved reusable for a new injection field. This design feature opens the possibility of considerable savings, as the reusability factor will eliminate all material and manufacturing costs of producing a completely new template structure.

# 6. Discussion

In this chapter, the main elements of the material presented in this thesis will be discussed. The possibilities and design choices of the concept developed through the thesis will be elaborated on, along with an evaluation of the limitations of the structural analysis. Alternative configurations to the concept model will also be discussed.

## 6.1 Possibilities Within the Concept Design

The main goal of this thesis was to explore new design possibilities for a pure CO2 well and the associated subsea system. The presented subsea system showcases a new design with opportunities to implement alternative materials, reduce the necessary material usage and its environmental footprint, and introduce a new installation process. The installation process includes the potential use of smaller crane ships with less capacity and cost, due to the compact modularized design.

From the data presented in Chapter 4, it is clear that the new design has the potential to be deemed fit for installation on the Norwegian continental shelf without major design changes. The design offers a solution where the majority of the template can be reused without compromising the safety of the installed equipment. The implementation of a modularized design results in a template that aligns with a modernized view of what a subsea system should be, considering both environmental footprint and cost-effectiveness.

The design choices for the template show promising results, though a more detailed evaluation is needed to fully understand its complete capabilities. The goal of this template design has been to gain a better understanding of the concept and explore the possibilities of a finished product.

The presented X-mas tree design includes unique features intended to enhance the operability of a CO2 injection system and address its associated challenges. The modularization of the tree allows for easier retrieval of compromised parts, accommodating the unique demands of CO2 injection. A primary concern specific to a CO2 injection tree is the high Joule-Thomson effect during smaller flow rates, such as during start-up or shutdown of the well. The component most exposed to this effect is the Production Wing Valve, as it is used for starting up and shutting down the well. The tree design focuses on establishing an easy replacement process for this valve, implementing it as a standalone module placed at the top of the tree for easy access.

The rest of the modules are designed to facilitate the individual replacement of parts that experience wear, reducing the costs associated with the complete removal of a subsea tree. The placement of these final modules are not discussed in detail, as a complete model showcasing their configuration and placement within the template structure has not yet been made.

The size of the tree also has the potential to be reduced compared to a normal production tree due to the lower pressures experienced during its lifespan, as discussed in Chapter 2. Achieving a more compact tree despite the modularization is therefore an obtainable task, provided that the necessary calculations and simulations of the tree's integrity are conducted. Specific calculations for the tree have been outside the scope of this thesis and should be elaborated on at a later stage.

Despite the lack of data regarding the tree design, the subsea system still demonstrates many desirable solutions. This including increased operability, reduced size and weight, a more flexible installation phase, a smaller environmental footprint, and lower costs over the structure's lifespan. To achieve the best solution, the tree design should be tailored specifically to the presented template design. This approach would enhance the effectiveness and possibilities of the complete subsea system.

## 6.2 Choice of Material

The two materials chosen for the template structure are primarily based on the data presented in Chapter 2. Using an aluminum alloy for the outer frame module has presented both benefits and challenges during the construction phase. The main advantage is the reduced density of the aluminum alloy compared to structural steel, being about three times lower. Despite having a yield limit at about 60% of that of S355 steel, the aluminum alloy has provided a much more efficient structure when considering the combination of strength and weight.

As a result of this the template configuration has a highly competitive weight and operability compared to some solutions used today, with the Northern Lights projects being the main competitor. The aluminum alloy used is also considered safe for subsea applications and is approved by NORSOK standards. This means that there is sufficient data from earlier applications to better assess the reliability of the material for long-term installations ensuring that the structural integrity is not compromised.

The use of aluminum also contributes significantly to achieving a more environmentally friendly solution. This is because the production process of aluminum is more energy efficient compared to steel, requiring less energy. Aluminum can also be endlessly recycled without losing quality, making it a material much more in line with today's standards of providing environmentally friendly solutions with increased reusability capabilities [82].

The disadvantages of using an aluminum alloy primarily emerged during the structural analysis of the template structure. The yield strength of aluminum is approximately 60% of that of steel and is maintained only in areas not significantly affected by heat and cooling processes such as welding. In the HAZ areas the material strength is significantly lower, depending on the type of alloy and welding used. For the configuration used on the template, a reduction of 28% - 32% is considered. This reduction is based on plate- and tube elements ranging from 6 to 15 mm, introducing uncertainty since the template construction uses plate elements up to 25 mm. As the areas experiencing the most significant stresses often lie within the HAZ areas, this has posed a challenge throughout the dimensioning phase. This challenge is unique to the use of aluminum alloys, representing a clear disadvantage compared to structural steel.

Another disadvantage with the use of aluminum is the added initial cost compared to that of steel, while recent years have seen a decrease in aluminum prices making it a more desirable option [82]. However, it generally remains a more expensive choice due to the initial investment

required. Additionally, the need for insulation and maintenance to protect against galvanic corrosion adds to the overall cost when opting for aluminum.

Opting for steel for the inner frame module and suction anchor has proven to be a sufficient solution, mitigating some of the challenges associated with a complete aluminum structure. By using steel concerns related to galvanic corrosion on the installed tree are eliminated, making it a safer and more predictable approach. This choice also allows for a simpler design of the connection point between the frame and suction anchor, as both components are made of the same material. Significant stresses toward the flanges have been identified, where the use of aluminum would require excessively large plate and pipe elements. The extensive welding required in these areas would lead to a challenging construction phase and a suboptimal result due to the HAZ areas.

Choosing steel for the suction anchor was primarily to ensure the structural integrity during various loading cases. With a centered suction anchor, trawling loads cause significant bending moments and associated stresses. One solution to maintain the anchor's structural integrity while reducing its weight is to design it with a structural steel frame and use a non-corrosive material for the outer plating. A potential option for the outer material could be fiberglass, which could be explored more in future studies. Due to the limited scope of this thesis, this configuration of the anchor has not been elaborated on.

## 6.3 Limitations of FEM Analysis

The structural analysis of the template structure was conducted to gain a better understanding of the concept model. The primary goal was to identify potential weaknesses early on to facilitate necessary design changes. Consequently, significant time was spent optimizing the design, aiming for effective and streamlined solutions, guided by the structural analysis data.

Given that the objective of the thesis was not to develop a fully production-ready model with in-depth analysis of each component, some loading cases were simplified. Certain components, such as the hinges and suction anchor, were not analyzed in detail. Instead, their dimensions were estimated based on the overall analysis, leading to some uncertainty in the total weight and configuration of the template design. However, this uncertainty is considered minor given the dimensions of the unexamined components.

Some loading scenarios in the structural analysis were simplified to limit time usage. These scenarios included dropped objects and trawlboard impact, which require dynamic analysis for a realistic assessment of stresses in the structure. Such detailed analysis was beyond the scope of this thesis. For dropped objects, static loads were estimated to understand how the structure behaved under such conditions and to evaluate the design's effectiveness in distributing and absorbing local stresses. As a result, the dimensions of the plate elements on the hatches may need to be adjusted later for an optimal result.

Another limitation was the restricted number of elements and nodes allowed by the student license of the ANSYS software. To address this limitation, careful consideration was given to model division, the use of symmetry, and applying a more concentrated mesh in exposed areas for each analysis. The results indicate that this approach has had a minimal impact on accuracy, and the preventive measures taken have been effective. To validate this, test analyses were conducted on some loading cases, comparing results from a full model to those using symmetry. These comparisons resulted in minor differences, demonstrating that further decreasing the mesh size would not significantly influence the outcomes.

## 6.4 Alternative Configurations

The concept model developed in this thesis is one of many possible configurations for a template structure. The main objectives for the template structure have been to achieve a compact and modularized configuration, creating a competitive solution compared to similar constructions. However, the approach taken in this thesis is not necessarily the best solution to the problem.

One alternative configuration would be to combine the aluminum and steel frame modules into a single module. This idea arises from the structural analysis of the steel module, which shows low stresses toward the middle of the frame. The current design could be seen as excessive in terms of material usage, suggesting that a complete redesign could be beneficial. Some key point of this alternative approach will be discussed below.

### 6.4.1 Simplification and Material Considerations

The new combined module would ideally be made of steel to mitigate the challenges associated with corrosion and welding aluminum at the connection point between the frame and anchor. By merging the two modules, the isolated flange could be eliminated, allowing for a complete redesign of the connection point between the anchor and the template.

### 6.4.2 Design Benefits

A unified frame with no material toward the center will result in an improved space for annulus access and a reduced overall weight of the structure. Instead of a complete frame structure in the center, the frame could incorporate four brackets toward the middle, which would support the guideposts for the installed equipment. This design approach would enhance the operational space within the template while reducing excessive material usage.

### 6.4.3 Weight Considerations

Switching to an all-steel template would significantly increase the structure's weight. A detailed evaluation of the associated costs compared to the current solution presented in this thesis would be necessary to get a full understanding of the concept. Although the increased weight is a drawback, it could be somewhat offset by the simplification of the frame design due to the

merged modules. Additionally, further investigation into the integration of glass fiber panels on the suction anchor, as discussed in Section 6.2, could help reduce the structure's weight if needed.

### 6.4.4 Conclusion

The suggested alternative configuration offers several potential benefits, including material efficiency, simplified construction, and improved operational space. However, a thorough cost-benefit analysis and detailed structural evaluations would be required to determine the most effective and desirable design solution.

# 7. Conclusion

Through this thesis a detailed concept model has been developed to showcase the possibilities of a pure CO2 injection system. A set of loading cases has been conducted to obtain realistic figures regarding the geometry, part count, size, and weight of the modularized template structure. Additionally, discussions regarding the configuration of the installed x-mas tree have been included to provide a better understanding of a complete subsea injection system that could rival the solutions utilized today. From this, the following remarks can be concluded:

- The concept model achieves a compact and modularized configuration, creating a competitive solution considering size and weight compared to current subsea systems.
- The modular design will allow for easier maintenance and replacement of parts, enhancing the overall operability of the system.
- The use of aluminum for the outer frame module and steel for the inner frame module and suction anchor achieves a good balance between weight reduction and ensuring the structural integrity of the template.
- The use of steel for the inner frame and anchor will reduce concerns associated with galvanic corrosion and welding challenges.
- Aluminum's higher strength to weight ratio can significantly contribute to lowering the overall weight of the template structure.
- Aluminum's lower energy requirement for production and its recyclability align with modern standards for environmentally friendly solutions and will contribute to reducing the environmental footprint of the template structure.
- The structural analysis highlighted the challenges of using aluminum, particularly in heat-affected zones (HAZ) where material strength can be significantly reduced. This necessitates careful consideration during the design and welding processes to ensure structural integrity.
- The structural analysis provided valuable insights into the behavior of the structure under various required loading cases regarding the NORSOK standards for trawl loads, static loads and dropped objects.
- Some loading cases like dropped objects and trawlboard impact will require a dynamic analysis along with more data regarding the objects to fully evaluate the structure.
- While aluminum offers several advantages, its initial material cost along with insulation measures will require a higher initial investment compared to an all-steel structure.

- The conceptual design of the x-mas tree presents a modularized solution that will facilitate easier replacement of exposed parts tailored towards challenges associated with pure CO2 injection.
- The tree design will have to be tailored towards the presented template construction to achieve the most efficient solution and integration process.
- An alternative configuration that merges the aluminum and steel frame modules into a single steel module can be a viable option for the template structure. This solution can potentially simplify the connection point between the frame and anchor, improve annulus access, remove excess material and parts, and accomplish an overall more efficient structure.
- A thorough cost analysis comparing the aluminum-steel hybrid model to an all-steel model would be beneficial when evaluation the two options.

The thesis presents a promising concept for a pure CO2 injection system, addressing new solutions to the associated challenges for the subsea system. The findings represent the groundwork for the complete system where further research and development is needed to create an effective, environmentally friendly and cost-efficient production ready subsea injection system.

# 8. Future work

As the subsea system is in its conceptual stage there is a lot of future work involved before a production ready system with detailed data sheets can presented. In order to achieve this the following should be included in further work:

- More time spent on optimizing the design solutions for each component of the template structure to achieve an optimal design.
- Including a detailed model of the suction anchor with an added bracing frame for strengthening the connection points and overall stiffness of the anchor based on the relevant loading cases.
- A detailed analysis regarding the stability of the single anchor configuration for different soil conditions.
- Conduct experimental testing of the shell of the model in a towing tank to obtain the needed qualification for an overtrawlable template structure at the installation sites.
- Run in depth dynamic analysis for the dropped objects and impact loads with specific data for the installation sites.
- Potential required design changes to the model from the complete data obtained from model testing and dynamic analysis.
- Develop a detailed concept model of the modularized x-mas tree tailored to the template structure to fully showcase the opportunities within the subsea system.
- Develop alternative configuration for the template structure as discussed in chapter 6.4 and evaluate the benefits and weaknesses of the two approaches.
- Conduct a detail cost analysis of the modularized template structure and compare it to the solutions utilized in today’s industry.

# Bibliography


[1] Energifaktanorge, «Taxes and Emissions Trading,» 2023.

[2] Regjeringen, «Regjeringen.no,» Regjeringen, 27 09 2023. [Internett]. Available: https://www.regjeringen.no/no/tema/energi/landingssider/ny-side/ccs/id2863902/?expand=factbox2864130. [Funnet 11 02 2024].

[3] Equinor, «Smeaheia – muliggjør storskala CO2-lagring for europeisk industri,» Equinor, [Internett]. Available: https://www.equinor.com/no/energi/smeaheia. [Funnet 12 02 2024].

[4] Equinor, «CCS: Carbon capture and storage - making net zero possible,» Equinor, [Internett]. Available: https://www.equinor.com/energy/carbon-capture-utilisation-and-storage. [Funnet 12 02 2024].

[5] Global CCS Institute, «Capturing CO2,» 2018. [Internett]. Available: https://www.globalccsinstitute.com/wp-content/uploads/2018/12/Global-CCS-Institute-Fact-Sheet_Capturing-CO2.pdf. [Funnet 20 03 2024].

[6] Global CCS Institute, «CCS Explained: Transport,» Global CCS Institute, [Internett]. Available: https://www.globalccsinstitute.com/ccs-explained-transport/. [Funnet 20 03 2024].

[7] Sokkeldirektoratet, «Nye standarder for transport og lagring av CO2,» Sokkeldirektoratet, 01 11 2017. [Internett]. Available: https://www.sodir.no/aktuelt/nyheter/generelle-nyheter/2017/Nye-standarder-for-transport-og-lagring-av-CO2/. [Funnet 20 03 2024].

[8] Globas CCS Institute, «GEOLOGICAL STORAGE OF CO2: SAFE, PERMANENT, AND ABUNDANT,» 2018. [Internett]. Available: https://www.globalccsinstitute.com/wp-content/uploads/2018/12/Global-CCS-Institute-Fact-Sheet_Geological-Storage-of-CO2.pdf. [Funnet 03 20 2024].

[9] Y.-S. Jun, L. Zhang, Y. Min og Q. Li, «Nanoscale Chemical Processes Affecting Storage Capacities and Seals during Geologic CO2 Sequestration,» Research Gate, 07

2017. [Internett]. Available: https://www.researchgate.net/figure/CO-2-trapping-mechanisms-at-GCS-sites_fig1_318292323. [Funnet 20 03 2024].

[10] Equinor, «Northern Lights Project Concept Report,» Equinor, 2019.

[11] Equinor, «Northern Lights Project,» 2024. [Internett]. Available: https://www.equinor.com/energy/northern-lights. [Funnet 18 04 2024].

[12] Havtil Norwegian Ocean Industry Authority, «§ 45 Development concepts,» 01 01 2011. [Internett]. Available: https://www.havtil.no/en/regulations/all-acts/?forskrift=158. [Funnet 04 18 2024].

[13] The Commonwealth, «Oil and Gas Decommissioning Toolkit - Practical Guidance for Governments,» 2024. [Internett]. Available: https://thecommonwealth.org/oil-and-gas-decommissioning-toolkit. [Funnet 18 04 2024].

[14] Equinor, «Smeaheia - Bringing large scale CO2 storage to European Industry,» Equinor, 2023. [Internett]. Available: https://www.equinor.com/energy/smeaheia. [Funnet 18 04 2024].

[15] Sokkeldirektoratet, «The Viking Group,» Sokkeldirektoratet, [Internett]. Available: https://www.sodir.no/en/whats-new/publications/co2-atlases/co2-atlas-for-the-norwegian-continental-shelf/5-the-norwegian-sea/5.1-geology-of-the-norwegian-sea/the-viking-group/. [Funnet 18 04 2024].

[16] Oljedirektoratet, H. Fredrik, A.-K. Farouk, B. Egil, V. J. og D. A. G., «Dunlin Group,» [Internett]. Available: https://www.nhm2.uio.no/norges/litho/dunlin.php. [Funnet 19 04 2024].

[17] K. S. -. E. T. Norway, «Store ambisjoner for CCS på norsk sokkel,» ETN, 22 02 2024. [Internett]. Available: https://www.energytransitionnorway.no/blog/hoye-ambisjoner-for-ccs-pa-norsk-sokkel. [Funnet 19 04 2024].

[18] A. Gierzynski, «Implications of Permeability Uncertainty During Three-phase CO2 Flow in a Basalt Fracture Network,» ResearchGate, 12 2016. [Internett]. Available: https://www.researchgate.net/publication/326492803_Implications_of_Permeability_U

ncertainty_During_Three-phase_CO2_Flow_in_a_Basalt_Fracture_Network. [Funnet 13 04 2024].

[19] B. Wischnewski, «Calculation of thermodynamic state variables of carbon dioxide,» Peace Software, [Internett]. Available: https://www.peacesoftware.de/einigewerte/co2_e.html. [Funnet 10 04 2024].

[20] AAPG Wiki, «Pressure detection,» AAPG Wiki, 20 01 2022. [Internett]. Available: https://wiki.aapg.org/Pressure_detection. [Funnet 12 04 2024].

[21] Xometry, «Aluminium Alloy: Definition, Characteristics, Types, Properties and Applications,» Xometry, 15 04 2023. [Internett]. Available: https://www.xometry.com/resources/materials/what-is-aluminum-alloy/. [Funnet 26 04 2024].

[22] U. Rusal, «What is aluminium?,» [Internett]. Available: https://aluminiumleader.com/about_aluminium/what_is_aluminum/. [Funnet 29 04 2024].

[23] Weerg, «What are aluminium alloys,» Weerg, 13 07 2021. [Internett]. Available: https://www.weerg.com/guides/what-are-aluminium-alloys. [Funnet 29 04 2024].

[24] Norsok, «Standard M-121 - Aluminium Structural Materials,» Norsok, 2015.

[25] Engineers Edge, «Aluminium Tempers, Specifications and designation,» Engineers Edge, [Internett]. Available: https://www.engineersedge.com/aluminum_tempers.htm. [Funnet 30 04 2024].

[26] Smiths, «5083 Aluminium - Technical Datasheet,» 2023. [Internett]. Available: https://www.smithmetal.com/pdf/aluminium/5xxx/5083.pdf. [Funnet 29 04 2024].

[27] Cumberland, «Tempers - Aluminium Temper Definition,» Cumberland, [Internett]. Available: https://www.cumberlandmetals.com/aluminum/tempers/. [Funnet 29 04 2024].

[28] Yieh Corporation Limited, «Technical Data Sheet - 5083 Aluminium Alloy Plate,» Yieh, [Internett]. Available:

http://aluminum.yieh.com/Upfiles/EDUp/files/5000%20Series/TDS/AA5083/TDS-YIEH-5083-Plate.pdf. [Funnet 03 05 2024].

[29] European Aluminium, «Aluminium Automotive Manual,» 15 09 2022. [Internett]. Available: https://european-aluminium.eu/blog/aluminium-automotive-manual/. [Funnet 02 05 2024].

[30] Thyssenkrupp, «Types of Welding Used for Aluminium,» 2024. [Internett]. Available: https://www.thyssenkrupp-materials.co.uk/technical-knowledge-hub/types-of-welding-used-for-aluminium. [Funnet 02 05 2024].

[31] Welding Engineers, «Hot Crack: How it occurs and how it can be prevented,» Welding Engineers, [Internett]. Available: https://weldingengineers.co.nz/welding-assistance/hot-crack-how-it-occurs-and-how-it-can-be-prevented/. [Funnet 02 05 2024].

[32] Keyence, «Arc welding types and principles,» Keyence, [Internett]. Available: https://www.keyence.com/ss/products/measure/welding/arc/mechanism.jsp. [Funnet 02 05 2024].

[33] S. Sild, «MIG Welding Explained,» Fractory, 19 04 2022. [Internett]. Available: https://fractory.com/mig-welding-explained/. [Funnet 03 05 2024].

[34] J. Grill, «MIG vs. TIG Welding: The Main Differences,» Weld Guru, 04 01 2024. [Internett]. Available: https://weldguru.com/mig-vs-tig-welding/. [Funnet 03 05 2024].

[35] European Standard, «Eurocode 9: Design of aluminium structures - Part 1-1: General Structural rules,» European Standard, 06 2009. [Internett]. Available: https://www.phd.eng.br/wp-content/uploads/2014/11/en.1999.1.1.2007.pdf. [Funnet 10 04 2024].

[36] Migal.co, «Preheating and intermediate pass temperature,» migal.co, [Internett]. Available: https://www.migal.co/en/service/welding-of-aluminium/preheating-and-intermediate-pass-temperature. [Funnet 02 06 2024].

[37] Xometry, «Laser Welding: Definition, How it Works, Process, Types, and Advantages,» Xometry, 24 05 2023. [Internett]. Available: https://www.xometry.com/resources/sheet/laser-welding/. [Funnet 03 05 2024].

[38] C. Veilleux, «What is laser welding and how does it work?,» LaserAX, 16 04 2024. [Internett]. Available: https://www.laserax.com/blog/laser-welding. [Funnet 03 05 2024].

[39] 3Printr.com, «On nature of meltpool,» 3Printr.com, 20 07 2023. [Internett]. Available: https://www.3printr.com/on-the-nature-of-meltpool-3263630/. [Funnet 03 05 2024].

[40] TWI Global, «What are the typical defects in laser welds?,» TWI Global, [Internett]. Available: https://www.twi-global.com/technical-knowledge/faqs/faq-what-are-the-typical-defects-in-laser-welds. [Funnet 03 05 2024].

[41] Thyssenkrupp, «Advantages of Aluminium,» Thyssenkrupp, [Internett]. Available: https://www.thyssenkrupp-materials.co.uk/advantages-of-aluminium.html. [Funnet 03 05 2024].

[42] PTG, «What is friction welding?,» PTG, [Internett]. Available: https://www.holroyd.com/what-is-friction-stir-welding-fsw/. [Funnet 02 05 2024].

[43] Sunrise, «Friction Stir Welding (FSW) - Process & Applications,» Sunrise, [Internett]. Available: https://www.sunrise-metal.com/friction-stir-welding-process-and-applications/. [Funnet 03 05 2024].

[44] TWI Global, «What is Friction Stir Welding (FSW)? - Process and Applications,» TWI Global, [Internett]. Available: https://www.twi-global.com/technical-knowledge/faqs/faq-what-is-friction-stir-welding. [Funnet 04 05 2024].

[45] M. H. El-Moayed, S. Y. Ahmed, M. A. Rabou og E.-S. G. Mahmoud, «A detailed process design for conventional friction stir welding of aluminum alloys and an overview of related knowledge,» Wiley Online Library - Engineering Reports, 24 09 2020. [Internett]. Available: https://onlinelibrary.wiley.com/doi/full/10.1002/eng2.12270. [Funnet 03 05 2024].

[46] TWI Global, «Friction Stir Welding,» TWI Global, [Internett]. Available: https://www.twi-global.com/technical-knowledge/job-knowledge/friction-stir-welding-147. [Funnet 04 05 2024].

[47] Xometry, «Steel: Definition, Composition, Types, Properties, and Applications,» Xometry, 21 04 2023. [Internett]. Available: https://www.xometry.com/resources/materials/steel/. [Funnet 11 05 2024].

[48] B. Index, «The Alloy Steel Manufacturing Process,» Sciencing, 25 04 2017. [Internett]. Available: https://sciencing.com/alloy-steel-manufacturing-process-7267414.html. [Funnet 11 05 2024].

[49] D. Weinhandl, «All You Need To Know About Steel Alloys,» Mead Metals, 03 04 2024. [Internett]. Available: https://www.meadmetals.com/blog/steel-alloys. [Funnet 11 05 2024].

[50] N. Gilbert, «Structural Steel - S235, S275, S355 Chemical Composition, Mechanical Properties and Common Applications,» AZO Materials, 05 2012. [Internett]. Available: https://www.azom.com/article.aspx?ArticleID=6022. [Funnet 11 05 2024].

[51] MT Copeland, «What Is Structural Steel?,» MT Copeland, 19 01 2022. [Internett]. Available: https://mtcopeland.com/blog/what-is-structural-steel/. [Funnet 11 05 2024].

[52] Stalforbund.no, «Steel for Offshore Structures, Standards Comparison,» Sålforbundet, 2004. [Internett]. Available: https://www.stalforbund.no/steel_offshore.htm. [Funnet 11 05 2024].

[53] Murray Steel Productions, «S355 - Structural Steel / Steel Plate,» Murray Steel Productions, [Internett]. Available: https://www.murraysteelproducts.com/products/s355-low-carbon-manganese-steel. [Funnet 11 05 2024].

[54] TWI Global, «What Is Corrosion? - Definition and Prevention,» TWI Global, [Internett]. Available: https://www.twi-global.com/technical-knowledge/faqs/what-is-corrosion. [Funnet 10 05 2024].

[55] Scottish Development International, «Corrosion Protection,» [Internett]. Available: https://www.sdi.co.uk/media/2wkh0yxs/05-corrosion-protection.pdf. [Funnet 10 05 2024].

[56] AMPP, «Galvanic Corrosion,» AMPP, [Internett]. Available: https://www.ampp.org/technical-research/impact/corrosion-basics/group-1/galvanic-corrosion. [Funnet 10 05 2024].

[57] K. Nanan, «The Basics of Cathodic Protection,» Corrosionpedia, 29 06 2020. [Internett]. Available: https://www.corrosionpedia.com/2/1368/prevention/cathodic-protection/cathodic-protection-101. [Funnet 11 05 2024].

[58] STRUCTX, «Galvanic Corrosion,» STRUCTX, 04 07 2024. [Internett]. Available: https://structx.com/Material_Properties_001.html. [Funnet 11 05 2024].

[59] cathwell, «Cathodic Protection Explained,» cathwell, 20 11 2023. [Internett]. Available: https://cathwell.com/cathodic-protection-explained/. [Funnet 11 05 2024].

[60] Wolkerstorfer Co., «Subsea Coatings,» Wolkerstorfer Co., [Internett]. Available: https://wolkerstorfer.com/markets/subsea/. [Funnet 12 05 2024].

[61] Subsea Coating Technologies, «We Go Big,» Subsea Coating Technologies, [Internett]. Available: https://www.subseacoat.com/. [Funnet 12 05 2024].

[62] E. K. &. S. B. Øren, «Subsea System for CO2 Injection,» NTNU, Trondheim, 2023.

[63] I. Andersen, «TU,» 19 April 2016. [Internett]. Available: https://www.tu.no/artikler/denne-statoil-utviklede-teknologien-skal-gjore-barentshavet-lonnsomt/346459. [Funnet 12 March 2024].

[64] NTS, «NORSOK standard U-001, Rev. 3,» NTS, Oslo, 2002.

[65] NORSOK STANDARD, «NORSOK U-002 Subsea Structures and Piping System, Rev. 2,» NTS, Oslo, 1998.

[66] J. A. D. Costa, «Grabcad,» 24 October 2020. [Internett]. Available: https://grabcad.com/library/rov-workclass-1. [Funnet 29 March 2024].

[67] NTNU, «Kompendium TMR 4167 Marin teknikk 2,» NTNU, Trondheim, 2022.

[68] oceaneering, «oceaneering,» oceaneering, 2024. [Internett]. Available: https://www.oceaneering.com/rov-services/rov-systems/. [Funnet 7 04 2024].

[69] NTNU, *TMR 4190 Finite Element Methods in Structural, lecture notes,* Trondheim: NTNU, 2023.

[70] NORSOK, «NORSOK Standard M-501,» NORSOK, 05 06 2004. [Internett]. Available: https://www.stacoat.com/STACbase/Norsok%20M-501%20e.pdf. [Funnet 12 05 2024].

[71] NORSOK M-001 Materials Selection, «NORSOK STANDARD,» 05 09 2014. [Internett]. Available: http://aboutcorrosion.s3.amazonaws.com/Standards/NORSOK/m00001_2014%7B5%7Den.0115940830.pdf. [Funnet 14 05 2024].

[72] NORSOK, «M-102 Structural Aluminium Fabrication,» NORSOK, 2015.

[73] M. Langøy, «REVIEW OF STRUCTURAL CONNECTIONS OF DISSIMILAR METALS - PREVENTION OF GALANIC CORROSION; PRACTICE AND EXPERIANCE,» 02 03 2021. [Internett]. Available: https://www.havtil.no/contentassets/2be164e3a83c47a6be00badecc8d40d6/review-of-structural-connections-of-dissimilar-metals--prevention-of-galvanic-corrosion---practice-and-experience. [Funnet 15 05 2024].

[74] European Standard, «Eurocode 3: Design of steel structures - Part 1-8: Design of joints,» European Standard, Brussels, 2005.

[75] ISO, «Mechanical properties of corrosionresistant stainless-steel fasteners - Part 1: Bolts, screws and studs,» ISO, Switzerland, 1997.

[76] ISO, «ISO 898-1: Mechanical properties of fasteners made of carbon steel and alloy steel, part 1,» ISO, Switzerland, 2013.

[77] C. M. Oldenburg, «sciencedirect,» June 2007. [Internett]. Available: https://www.sciencedirect.com/science/article/abs/pii/S0196890407000349. [Funnet 15 May 2024].

[78] TMC Triton, «S355 Steel Plate,» Triton, [Internett]. Available: https://www.tritonalloysinc.com/s355-steel-plates.html. [Funnet 01 06 2024].

[79] Haomei Aluminium, «Aluminium Marine Plate 5083-H116,» Haomei, [Internett]. Available: https://www.marine-grade-aluminum-plate-sheet.com/a/aluminium-marine-plate-5083-h116.html. [Funnet 01 06 2024].

[80] A. Jie, «How Much Does Marine Aluminium Plate Cost,» 15 03 2024. [Internett]. Available: https://www.linkedin.com/pulse/how-much-does-marine-aluminum-plate-cost-august-jie-aluminum-pjrsc/. [Funnet 01 06 2024].

[81] Ulstein, «Subsea Vessel,» Ulstein, [Internett]. Available: https://ulstein.com/vessels/subsea-vessel. [Funnet 02 06 2024].

[82] Kattsafe, «Kattsafe,» 16 May 2023. [Internett]. Available: https://kattsafe.com.au/resources/blog/aluminium-versus-steel-a-comparison-of-the-pros-and-cons. [Funnet 12 May 2024].

[83] B. Pettersen, «Marin Teknikk 3 - Hydrodynamikk Kompendium,» NTNU, Trondheim, 2023.

[84] Sintef, «Sintef,» 2 December 2021. [Internett]. Available: https://www.sintef.no/en/projects/2021/marinal-safe-use-of-aluminium-in-marine-multi-material-constructions/. [Funnet 5 March 2024].

[85] Hydro, «5083 alloy,» Hydro, [Internett]. Available: https://www.hydro.com/en/aluminium/products/extruded-profiles/alloys-for-extruded-profiles/5083-alloy/. [Funnet 28 04 2024].

[86] B. D. Horbaniuc, «sciencedirect,» 2004. [Internett]. Available: https://www.sciencedirect.com/topics/earth-and-planetary-sciences/joule-thomson-effect. [Funnet 15 May 2024].

[87] B. D. Horbaniuc, «sciencedirect,» 2004. [Internett]. Available: https://www.sciencedirect.com/topics/earth-and-planetary-sciences/joule-thomson-effect. [Funnet 22 September 2023].

# Appendix A

# Calculations

## A.1 Penetration Depth Suction Anchor

These calculations are based on the procedure and data provided in the specialization project, page 35 – 38 [62]. Estimated and typical values are used to establish a baseline for the needed dimensions of the anchor.

*Table 28 - A.1: Undrained Shear Strength at Specific Penetration Depths.*

| PENETRATION DEPTH [m] | UNDRAINED SHEAR STRENGTH [kPa] |
|---|---|
| **0** | 5 |
| **1** | 5 |
| **2** | 7 |
| **3** | 6 |
| **4** | 8 |
| **5** | 10 |
| **6** | 11 |
| **7** | 11 |
| **8** | 12 |
| **9** | 11 |
| **10** | 14 |

*Table 29 - A.1: Data Properties - Calculations of Penetration Depth for Suction Anchor.*

| Factors | Unit | Value |
|---|---|---|
| Weight aluminum module | [kg] | 18 518 |
| Weigh steel module | [kg] | 6 078 |
| Diameter suction anchor | [m] | 5.5 |
| Thickness suction anchor | [m] | 0.025 |
| Penetration depth | [m] | 6 |
| Water density | [kg/m$^3$] | 1025 |
| Aluminum density | [kg/m$^3$] | 2700 |
| Steel Density | [kg/m$^3$] | 7850 |
| Design factor | [-] | 1.15 |
| Bearing capacity factor, $N_c$ | [-] | 8.0 |
| Friction factor, α | [-] | 0.3 |

Buoyancy factor for aluminum and steel:

$$BF_{Alu} = (2700 - 1025) / 2700 \approx 0.62$$

$$BF_{Steel} = (7850 - 1025) / 7850 \approx 0.87$$

*Equation 8 - A.1: Buoyancy factor for aluminum and steel.*

Total wet weight of the template structure:

$$(18518 * 0.62) + (6078 * 0.87) = 16769kg = 164.5kN$$

*Equation 9 - A.1: Total Wet Weight.*

Needed surface areas on suction anchor:

$$A_{top} = (\pi / 4) * (5.5 - 2 * 0.025)^2$$

$$A_{top} = 23.3m^2$$

*Equation 10 - A.1: Area of top section.*

$$A_{tip} = (\pi / 4) * (5.5^2 - (5.5 - 2 * 0.025)^2)$$

$$A_{tip} = 0.43m^2$$

*Equation 11 - A.1: Area of tip section.*

$$A_w = \pi * 5.5 * (6 + 1)$$

$$A_w = 155.5m^2$$

*Equation 12 - A.1: Area of outer wall section.*

$$A_{wall} = 2 * \pi * (5.5 - 0.025) * 6$$

$$A_{wall} = 275.2m^2$$

*Equation 13 - A.1: Area of wall section.*

Wet weight of suction anchor:

$$W_{wet} = (23.3 * 121) * 0.025 * 7850 * 0.87 * 9.81$$

$$W_{wet} = 251.7kN$$

*Equation 14 - A.1: Wet weight of suction anchor.*

Average undrained shear strength at a penetration depth of 6 meters:

$$S_u^{av} = (5 + 5 + 7 + 6 + 8 + 10 + 11) / 7$$

$$S_u^{av} = 7.4kPa$$

*Equation 15 - A.1: Average undrained shear strength.*

Total wet weight of template including the suction anchor:

$$W_{tot} = (164.5 + 251.7) * 1.15$$

$$W_{tot} = 478.6kN$$

*Equation 16 - A.1: Total wet weight.*

Total penetration resisting force:

$$Q_{tot} = (8 * 7.4 * 0.43) + (0.3 * 7.4 * 206.4)$$

$$Q_{tot} = 483.6kN$$

*Equation 17 - A.1: Total penetration resisting force.*

$Q_{tot} \sim W_{wet}$, which means an **estimated penetration depth of 6 meters.**

## A.2 Required Suction Pressure for Anchor

These calculations are based on the procedure provided in TPG4200 – Subsea Production System, lecture notes [83].

Needed additional force to penetrate can be found by:

$$F_{suction} = Q_{tot} - W_{wet}$$

$$F_{suction} = 483.6kN - 251.7kN$$

$$F_{suction} = 231.9kN$$

*Equation 18 – A.2: Additional Penetration Force.*

Needed suction pressure is then:

$$P_{suction} = F_{suction} / A_{top}$$

$$P_{suction} = 231.9kN / 23.3m^2$$

$$P_{suction} \approx 0.1Bar$$

*Equation 19 - A.2: Required Suction Pressure.*

Required suction pressure for the anchor is **0.1 Bar.**

# A.3 Horizontal Drift of Anchor During Installation

These calculations are based on the procedure and data provided in the specialization project, page 40-43 [62].

*Table 30 - A.3: Component and Data Properties - Calculations of Horizontal Drift.*

| Factors | Unit | Value |
|---|---|---|
| Diameter wireline | [m] | 0.1 |
| Diameter suction anchor | [m] | 5.5 |
| Current velocity | [m/s] | 1-3 |
| Crane tip height | [m] | 10 |
| Water depth | [m] | 300 |
| Water density | [kg/m$^3$] | 1025 |
| Kinematic velocity | [m$^2$/s] | 1*10$^{-6}$ |
| Weight suction anchor | [kN] | 251.7 |

Reynolds number can then be found for both the anchor and wireline for a current velocity of 1 m/s:

$$R_n(WL) = \frac{1\frac{m}{s} * 0.1m}{1*10^{-6}\frac{m^2}{s}} = 100.000$$

$$R_n(A) = \frac{1\frac{m}{s} * 5.5m}{1*10^{-6}\frac{m^2}{s}} = 5.500.000$$

*Equation 20 - A.3: Reynolds Number for Anchor and Wireline.*

Drag coefficient can be read from the table below:

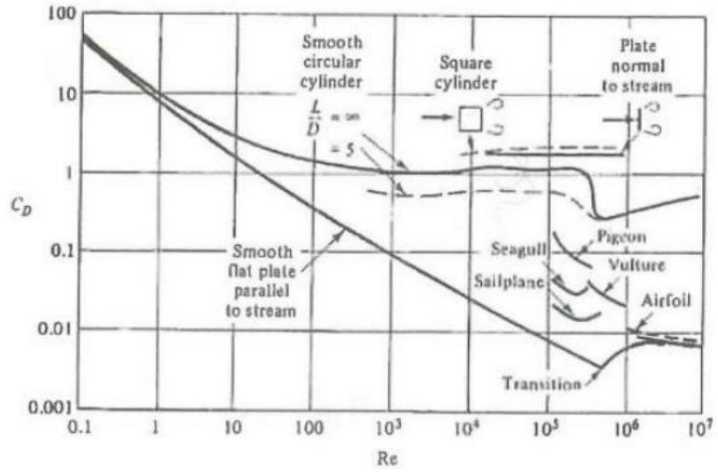


*Figure 69 - A.3: Raynolds Number with Corresponding Drag Coefficient [83].*

$$C_D(WL) = 1.5$$

$$C_D(A) = 0.7$$

Drag force for the two components can be found by:

$$F_D(WL) = \frac{1}{2} * \rho * U^2 * C_D * A_p$$

$$F_D(WL) = \frac{1}{2} * 1025 \frac{kg}{m^3} * (1m/s)^2 * 1.5 * (0.1 * 300) m^2$$

$$F_D(WL) \approx 23.1kN$$

$$F_D(A) \approx 13.8kN$$

*Equation 21 - A.3: Drag Force for Wireline (WL) and Anchor (A).*

Equilibrium equation for the crane tip:

$$M_{CT} = 0 \Rightarrow$$

$$(F_D(WL) * (10 + 150)m) + (F_D(A) * (10 + 300)m) = S * x$$

$$(23.1kN * 160m) + (13.8kN * 310m) = 251.7kN * x$$

$$x = 31.7m$$

*Equation 22 - A.3: Equilibrium of Crane Tip.*

From this one can estimate a horizontal drift of the anchor of **31.7 meters** for an average current of 1 m/s. By doing the same for 1 current of 3 m/s the estimated drift is **303.6 meters.** One contributing factor to the large drift is the small weight of the anchor. As the weight is estimated and do not include the added weight of the connection points for the template and added structural bracing to accommodate for this the assumed drift will be notably lower.

# Appendix B

# ANSYS Setup

## B.1 Aluminum Frame - Trawlnet Friction

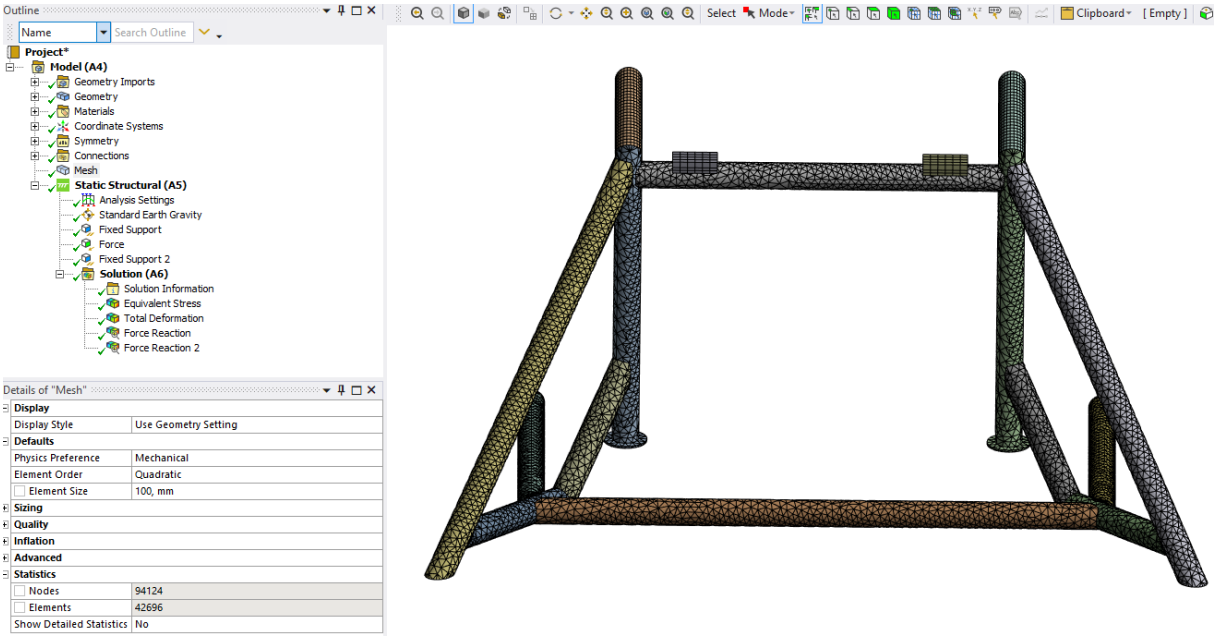


*Mesh Setting and Properties for Trawlnet Friction Analyses.*

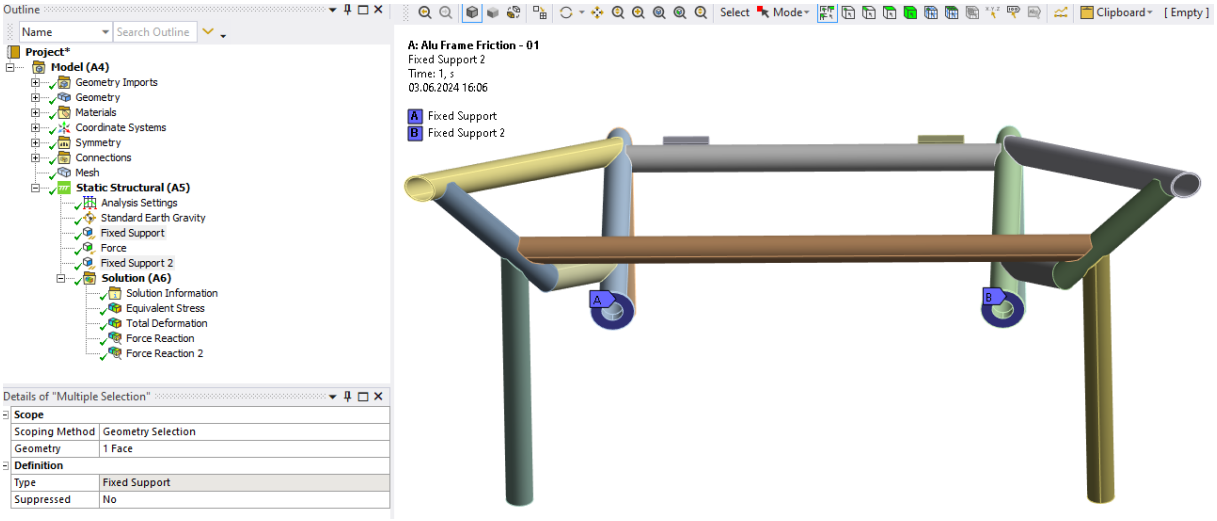


*Fixed Support Constrains for Trawlnet Friction Analyses.*

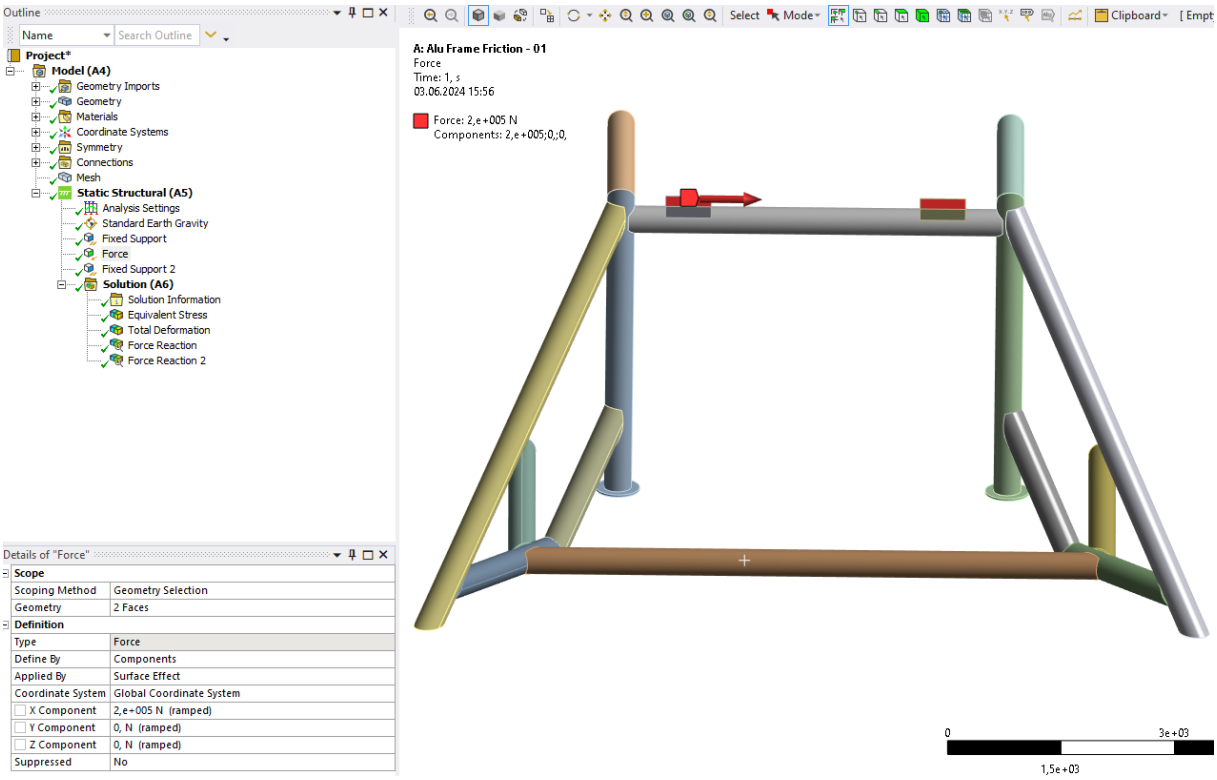


Details of "Force"

| Scope | |
|---|---|
| Scoping Method | Geometry Selection |
| Geometry | 2 Faces |
| **Definition** | |
| Type | Force |
| Define By | Components |
| Applied By | Surface Effect |
| Coordinate System | Global Coordinate System |
| X Component | 2,e+005 N (ramped) |
| Y Component | 0, N (ramped) |
| Z Component | 0, N (ramped) |
| Suppressed | No |

*Force Direction and Properties for Trawlnet Friction Analyses.*

# B.2 Aluminum Frame - Trawlboard Overpull

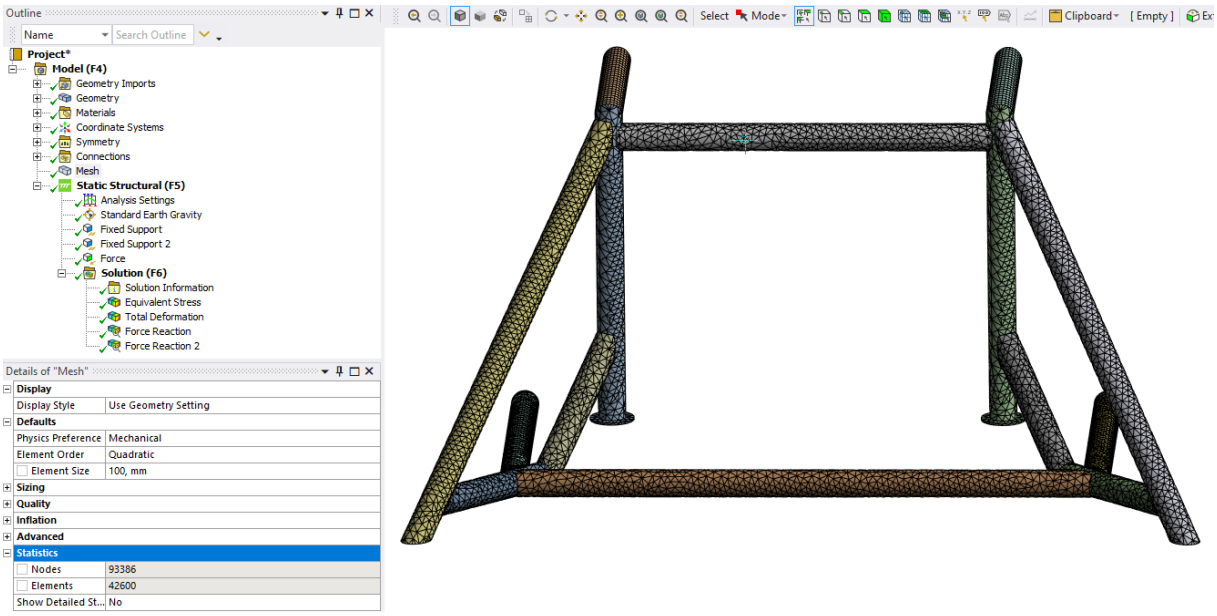


*Mesh Setting and Properties for Trawlboard Overpull Analyses.*

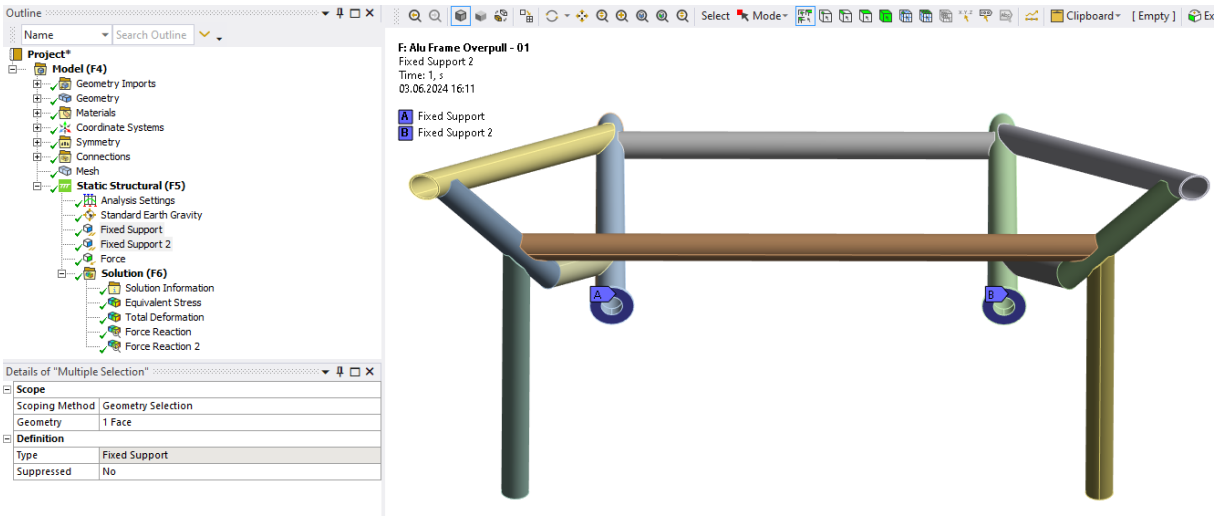


*Fixed Support Constrains for Trawlboard Overpull Analyses.*

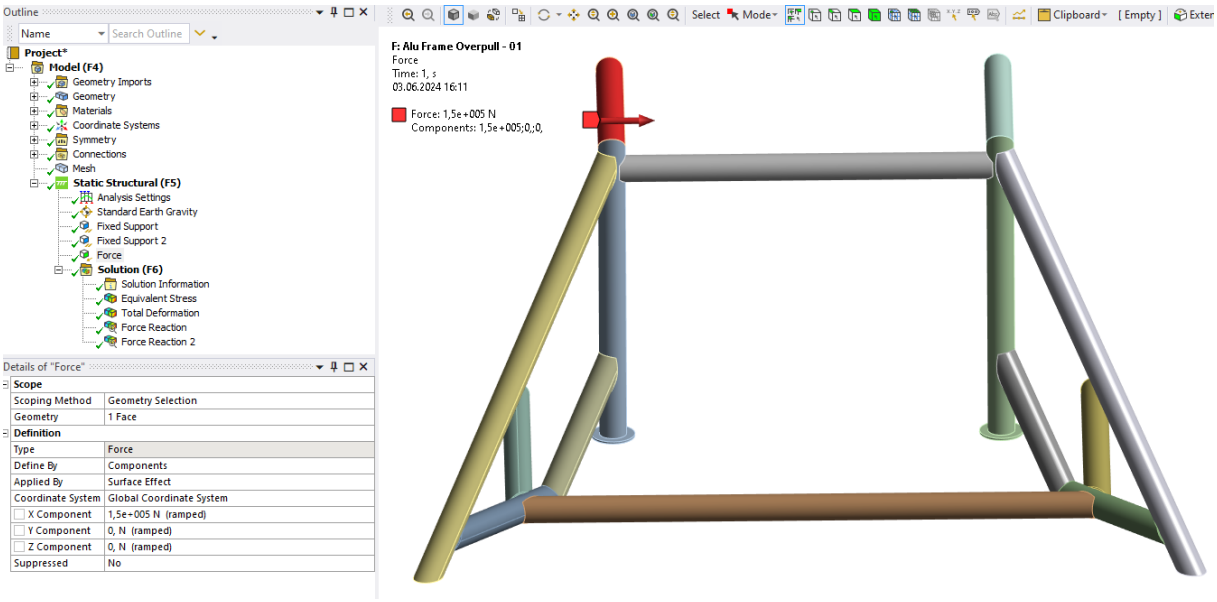


*Force Direction and Properties for Trawlboard Overpull Analyses.*

# B.3 Front Hatch - Heave Motion

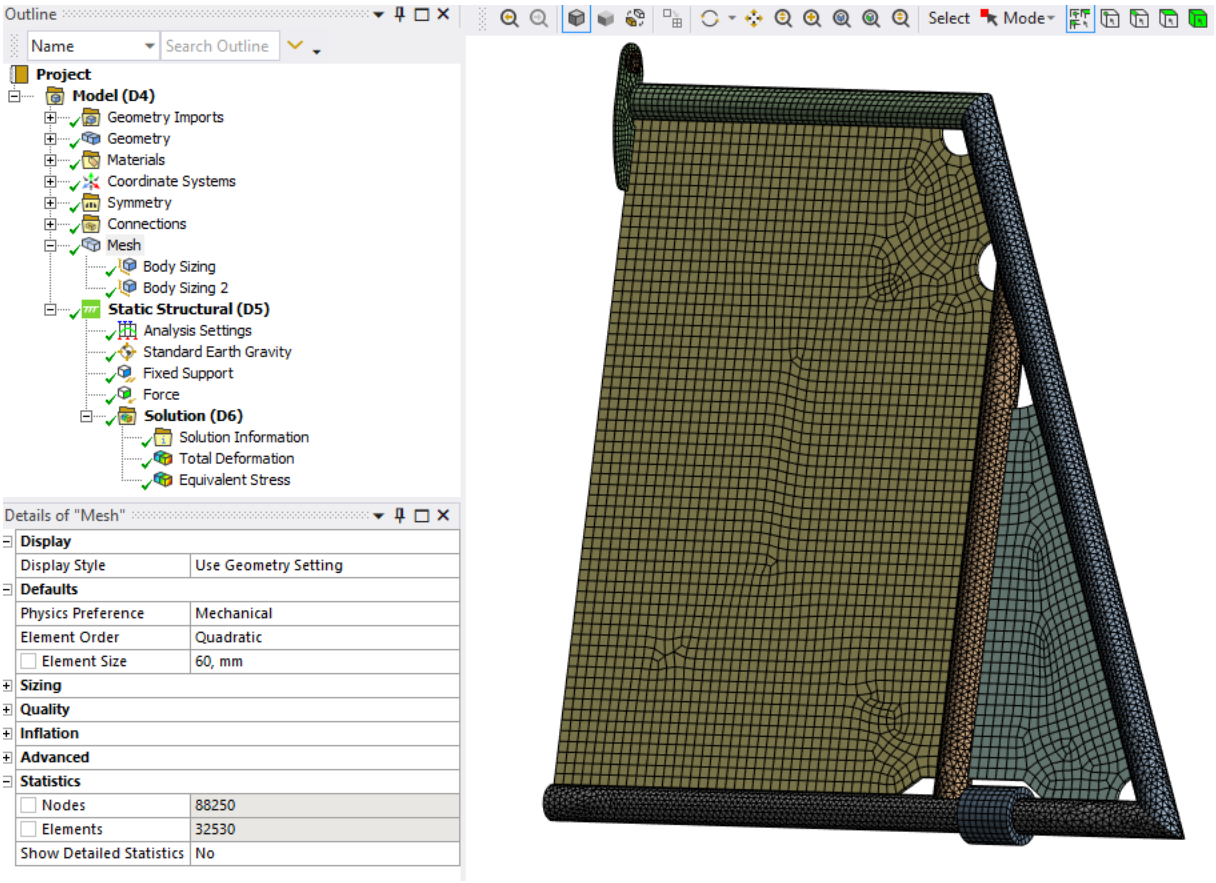


*Mesh Setting and Properties for Heave Motion Analyses.*

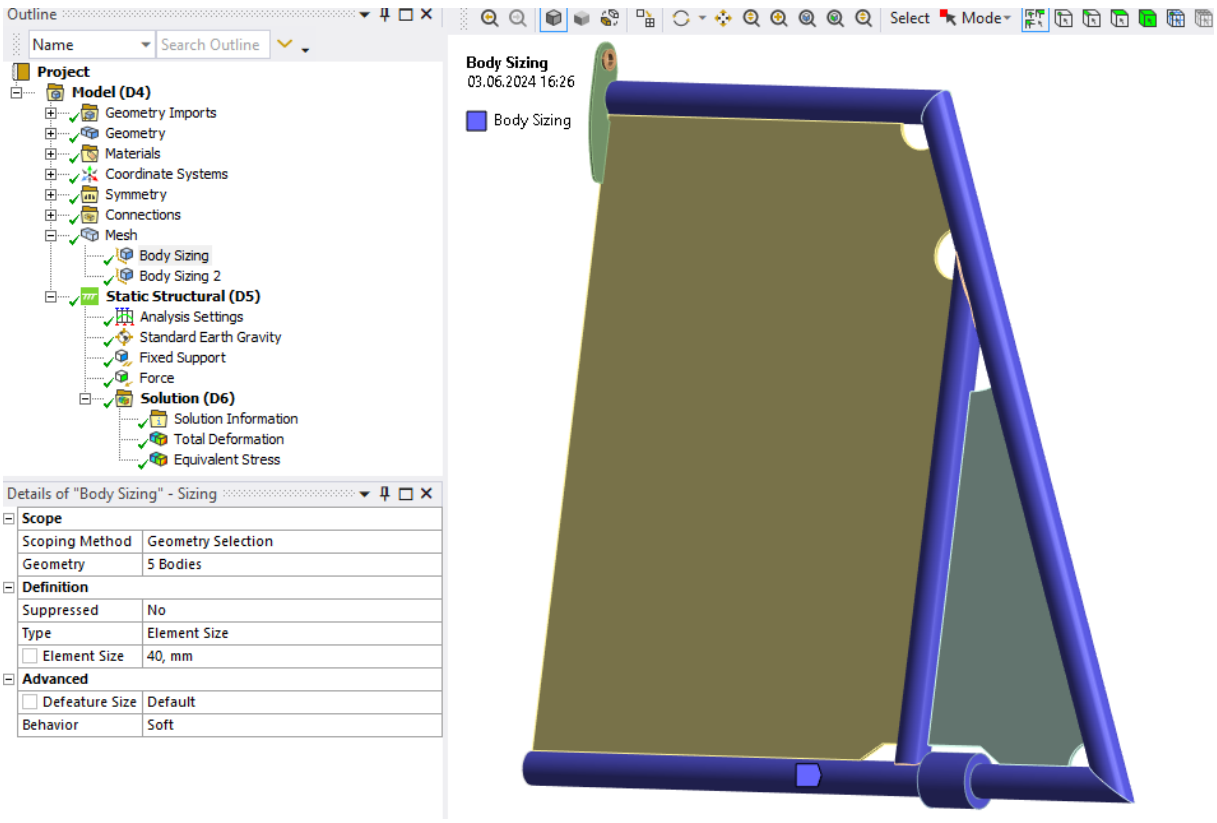


*Mesh Sizing 1 Setting and Properties for Heave Motion Analyses.*

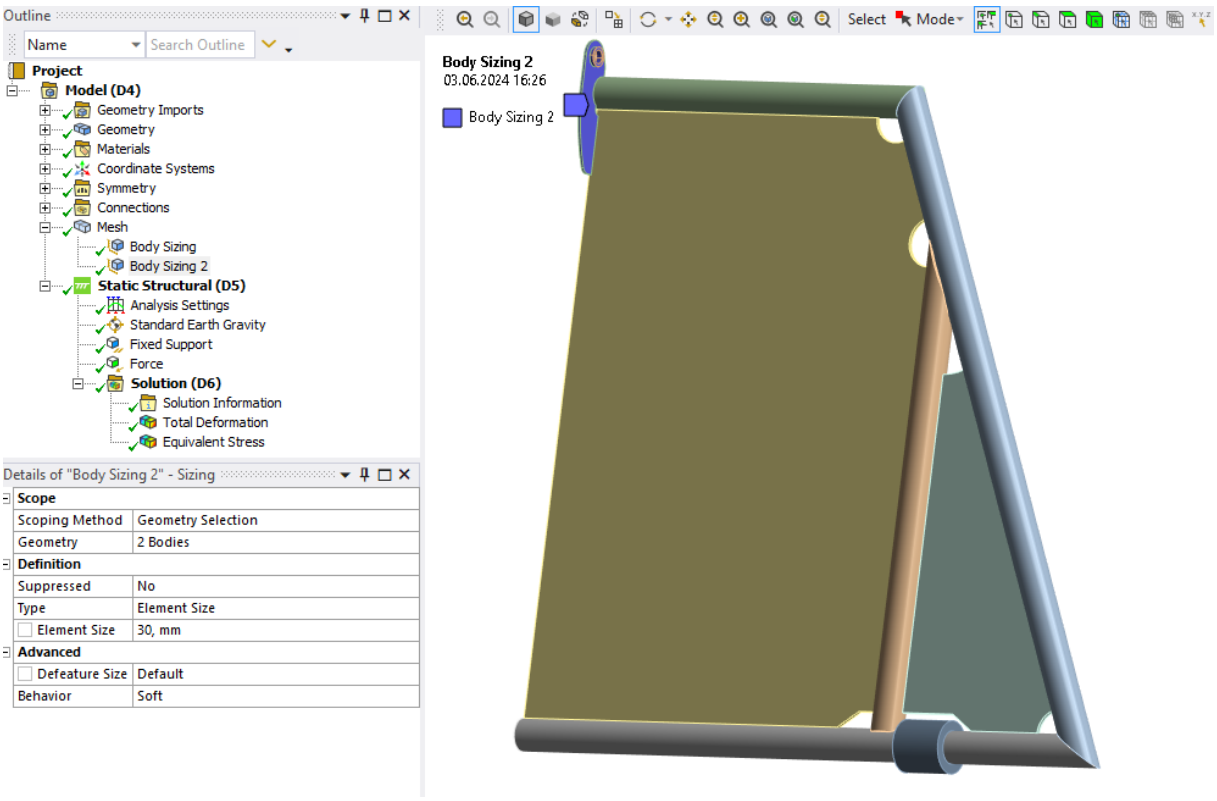


*Mesh Sizing 2 Setting and Properties for Heave Motion Analyses.*

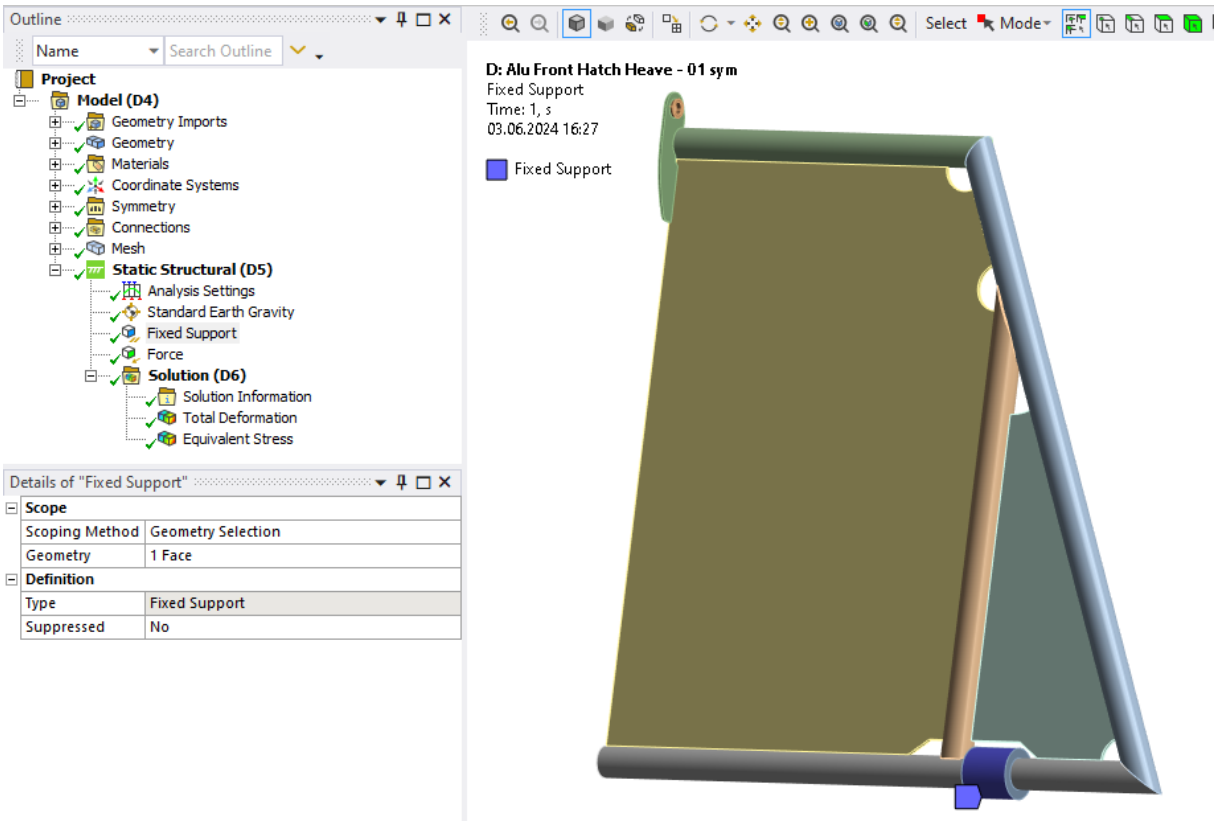


*Fixed Support Constrains for Heave Motion Analyses.*

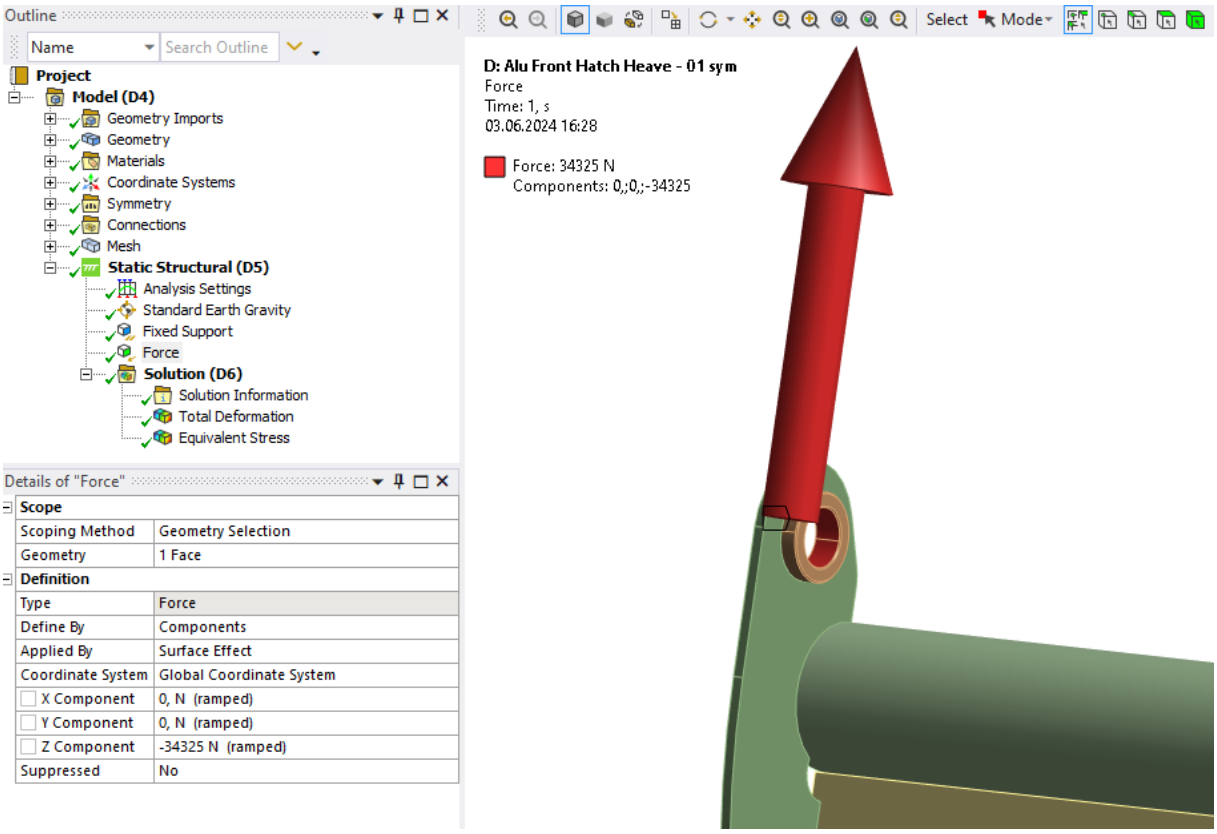


*Force Direction and Properties for Heave Motion Analyses.*

# B.4 Front Hatch – ROV Parking

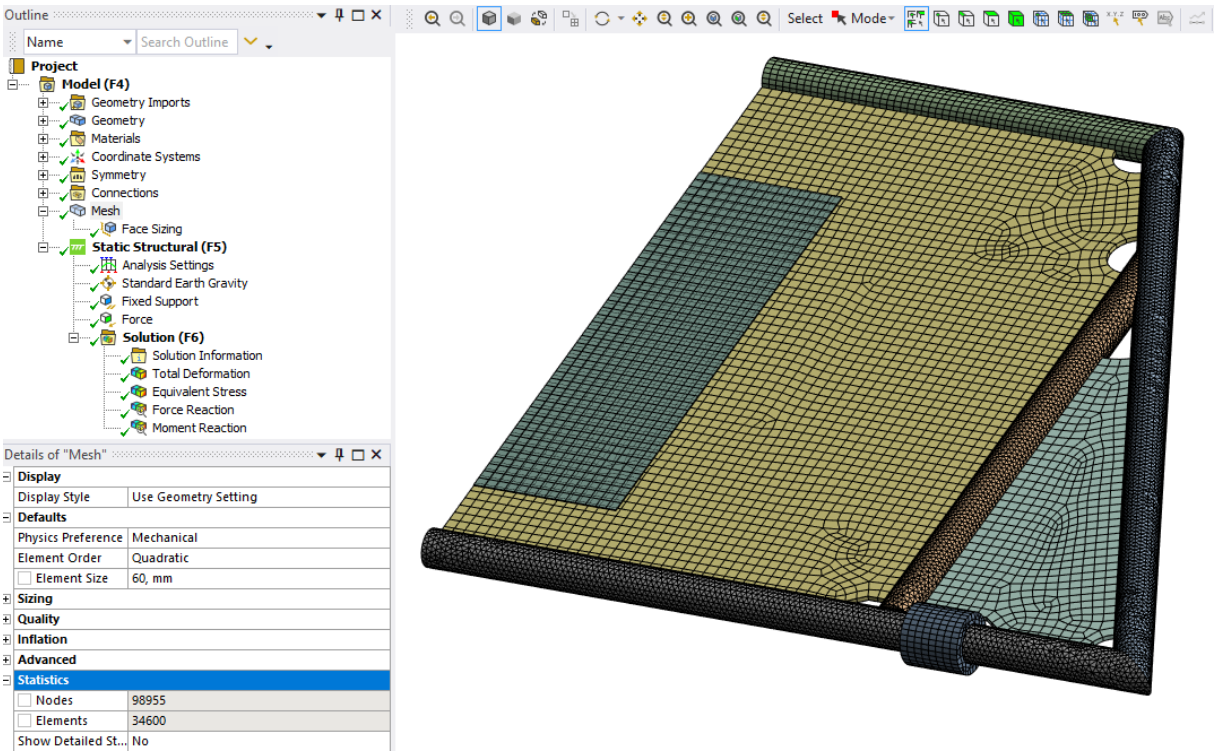


*Mesh Setting and Properties for ROV Parking Analyses.*

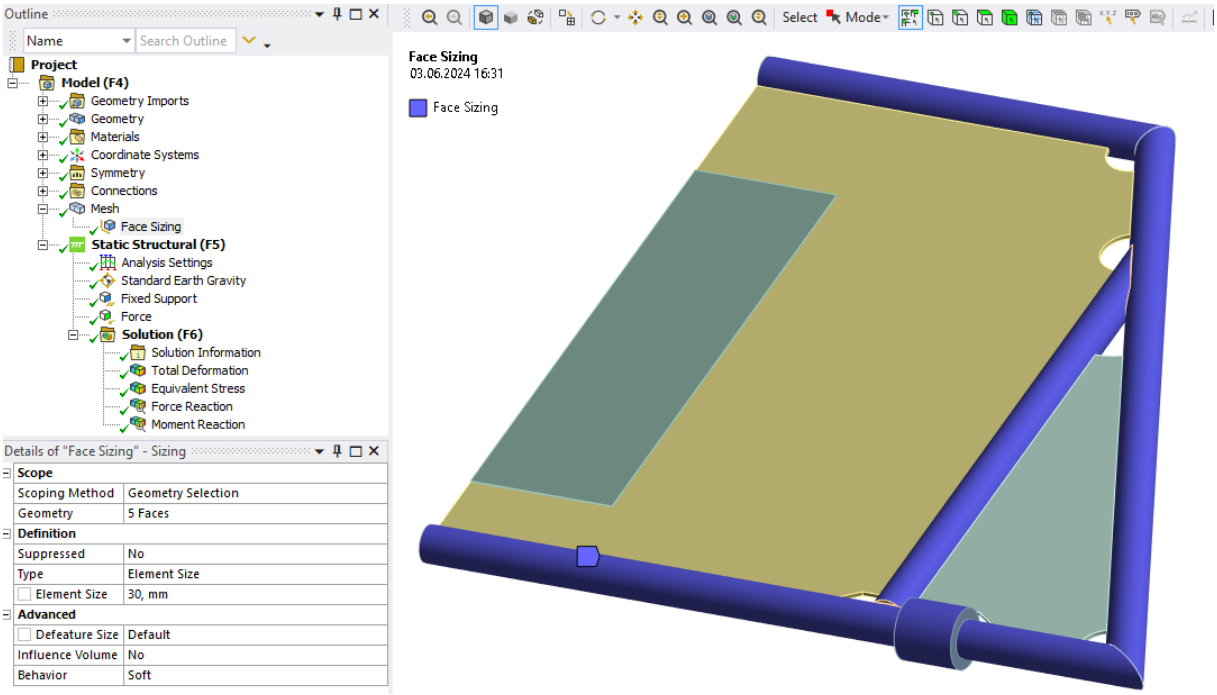


*Mesh Sizing Setting and Properties for ROV Parking Analyses.*

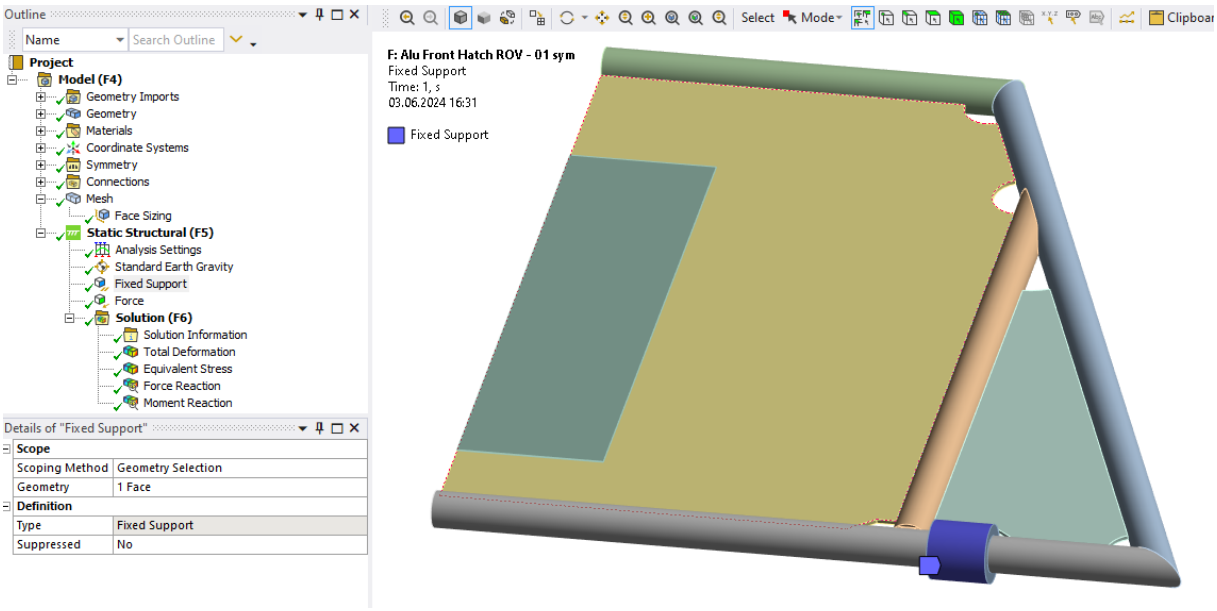


*Fixed Support Constrains for ROV Parking Analyses.*

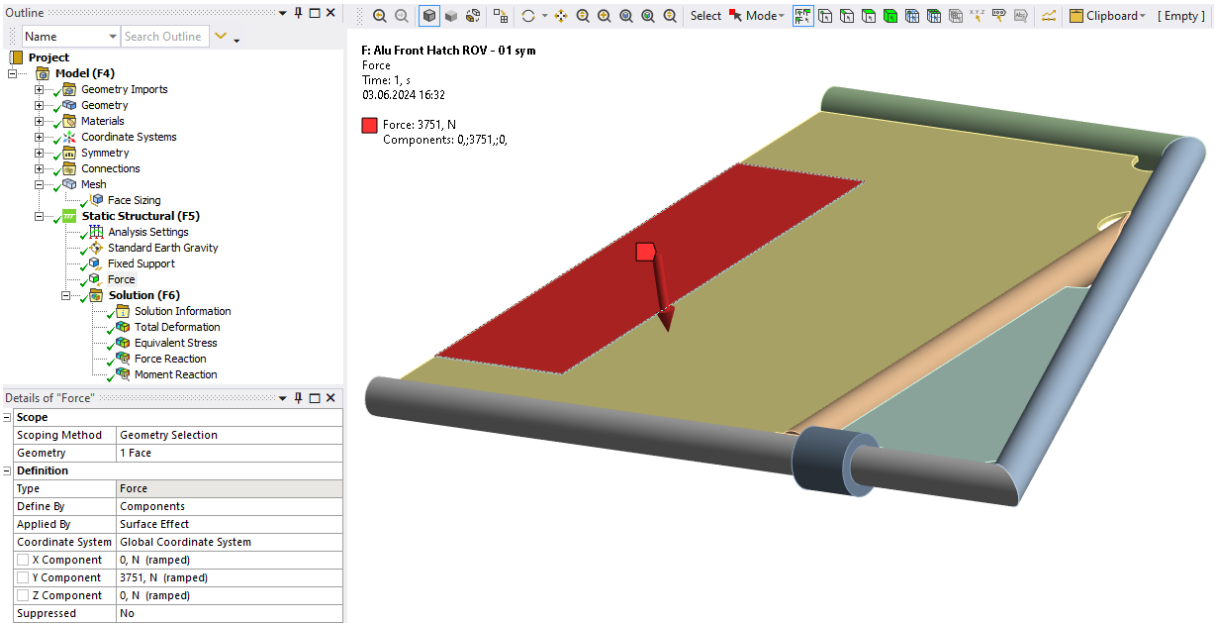


*Force Direction and Properties for ROV Parking Analyses.*

# B.5 Front Hatch – Dropped Object 100 mm

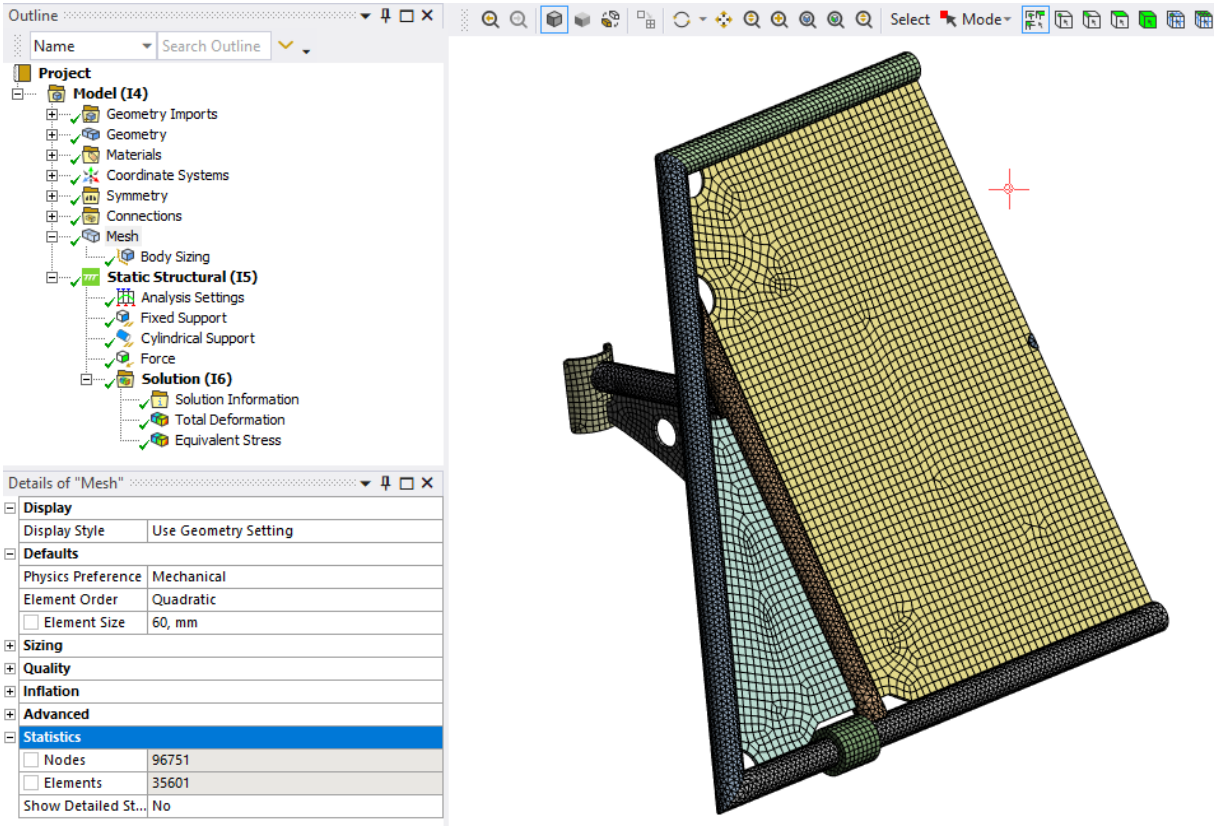


*Mesh Setting and Properties for Dropped Object 100 mm Analyses.*

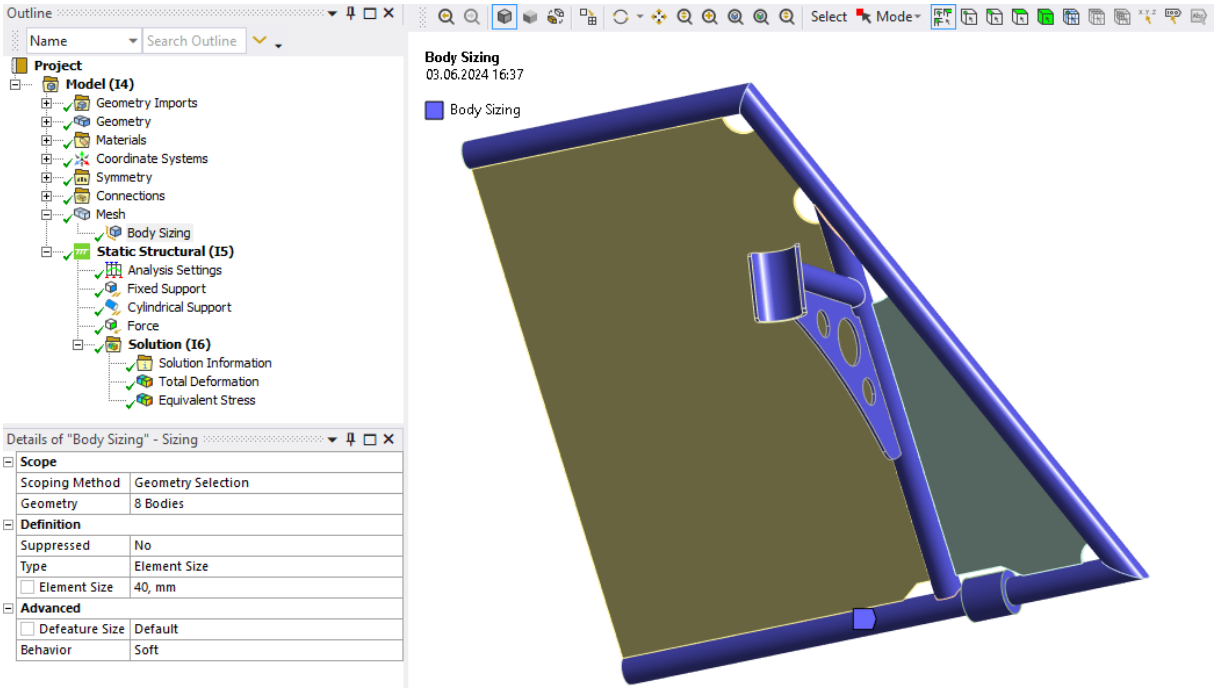


*Mesh Sizing Setting and Properties for Dropped Object 100 mm Analyses.*

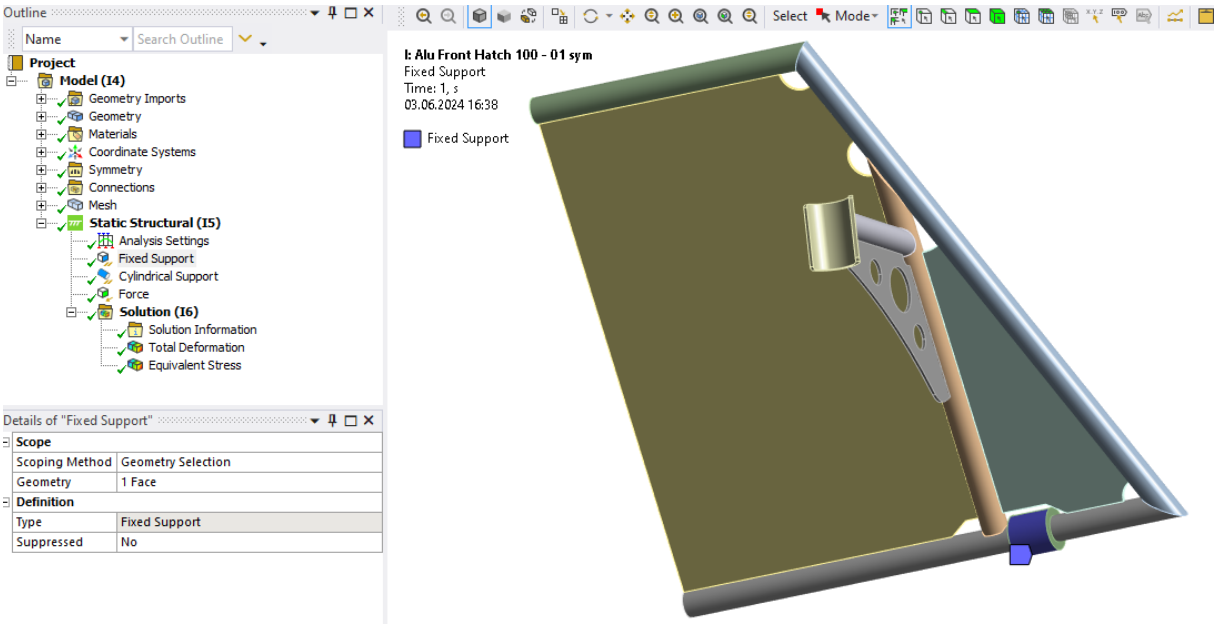


*Fixed Support Constrains for Dropped Object 100 mm Analyses.*

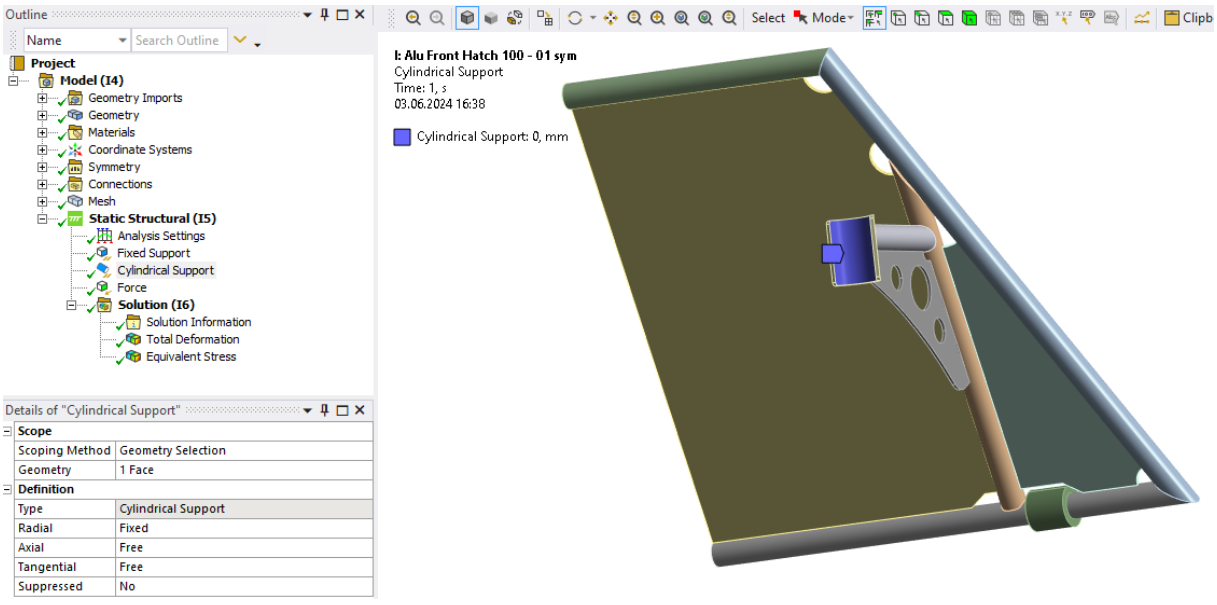


*Cylindrical Support Constrains for Dropped Object 100 mm Analyses.*

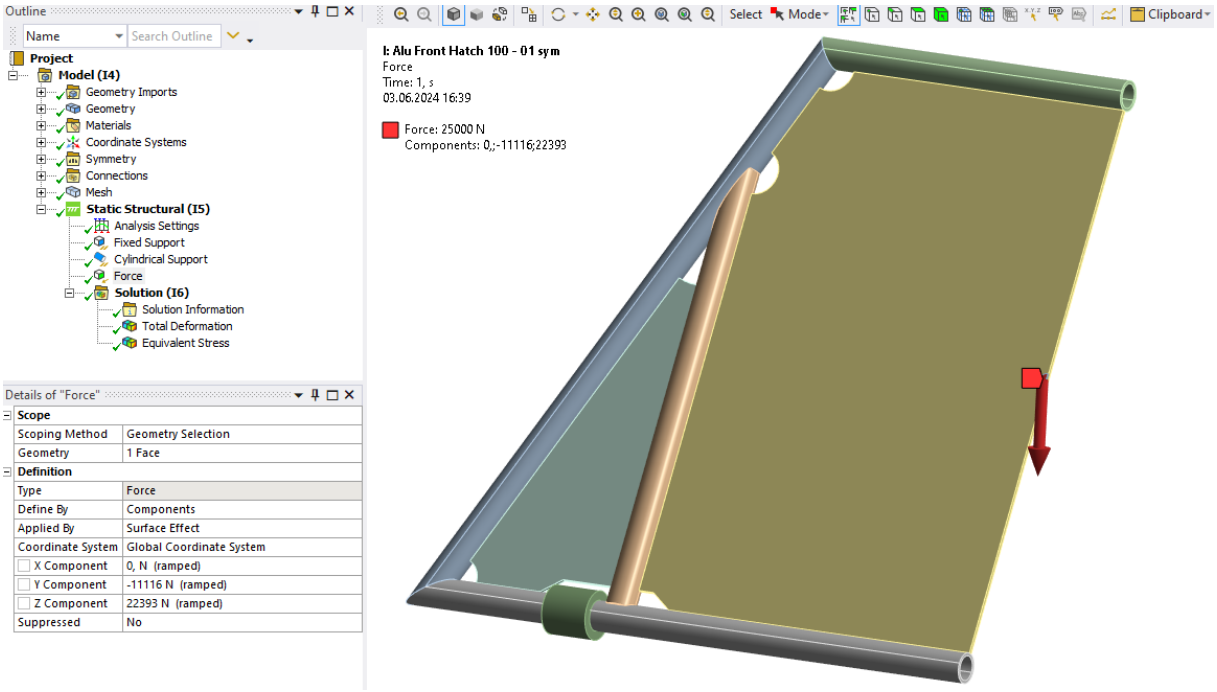


*Force Direction and Properties for Dropped Object 100 mm Analyses.*

# B.6 Top Hatch – Heave Motion

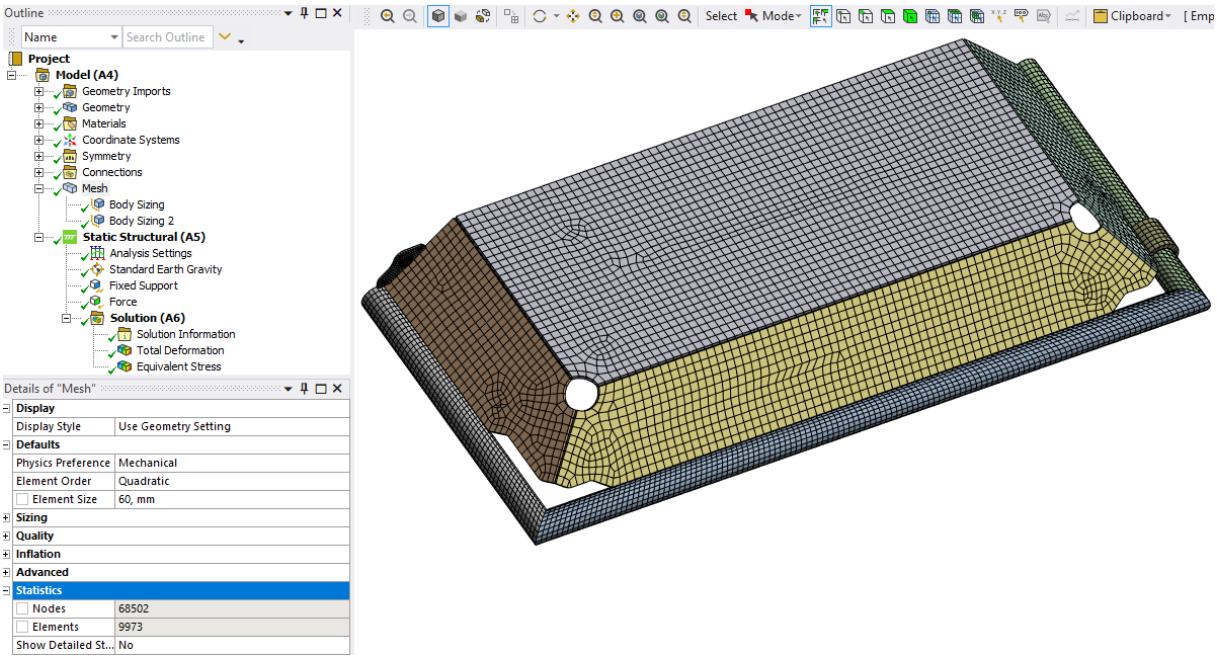


*Mesh Setting and Properties for Heave Motion Analyses.*

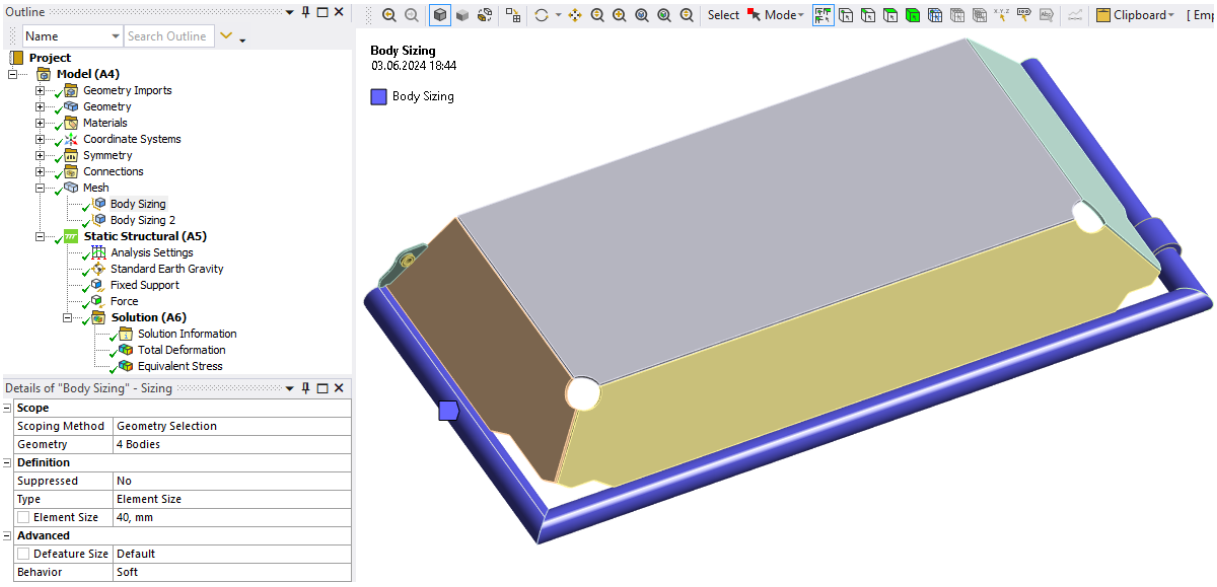


*Mesh Sizing 1 Setting and Properties for Heave Motion Analyses.*

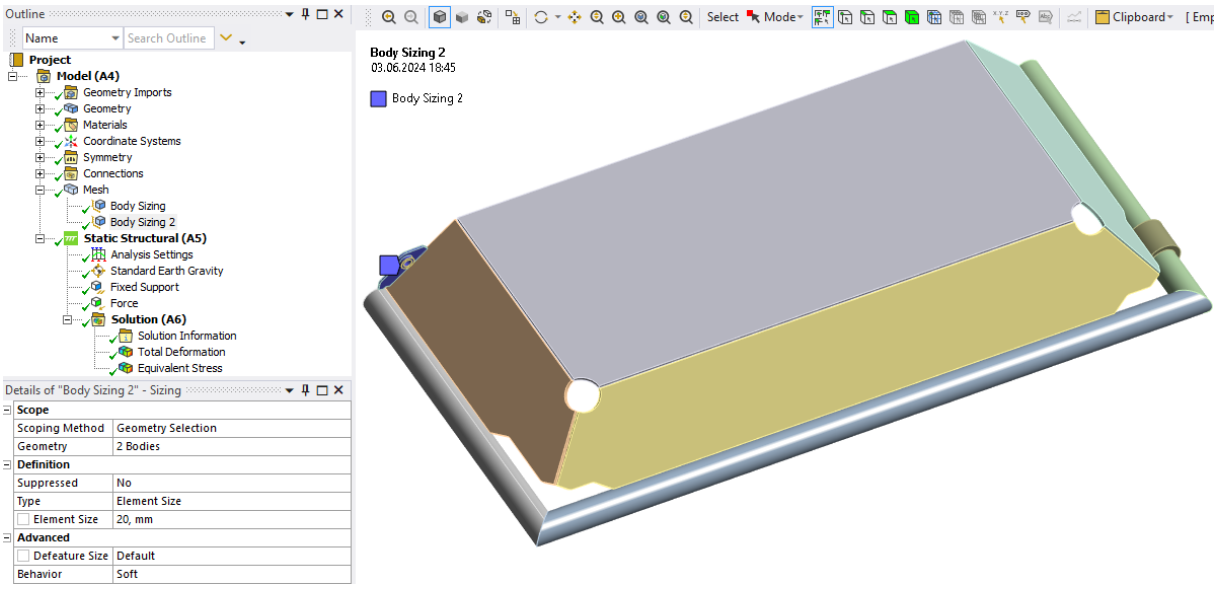


*Mesh Sizing 2 Setting and Properties for Heave Motion Analyses.*

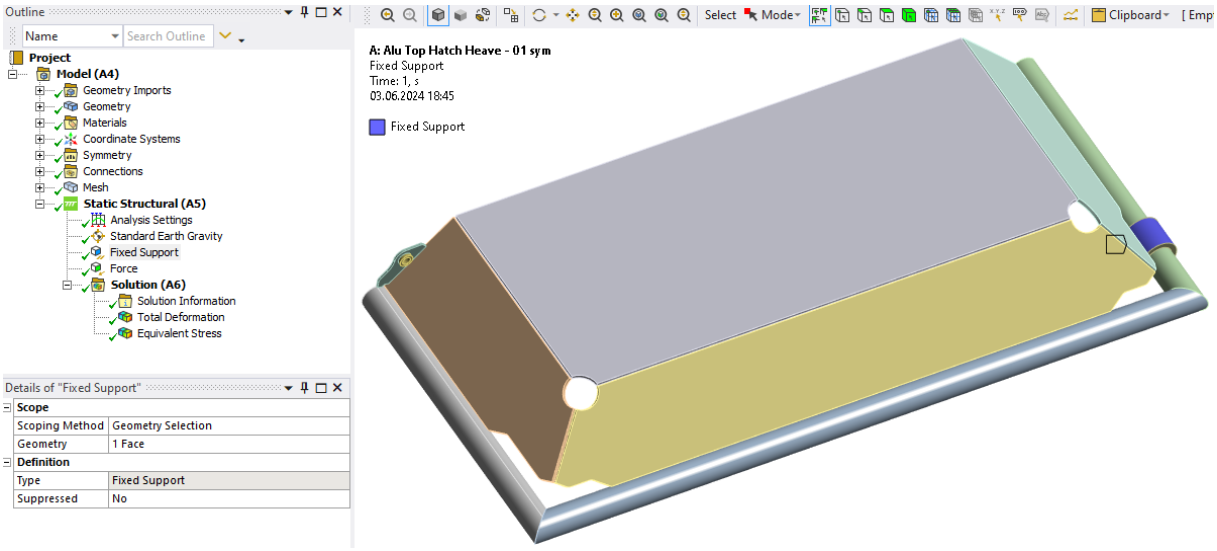


*Fixed Support Constrains for Heave Motion Analyses.*

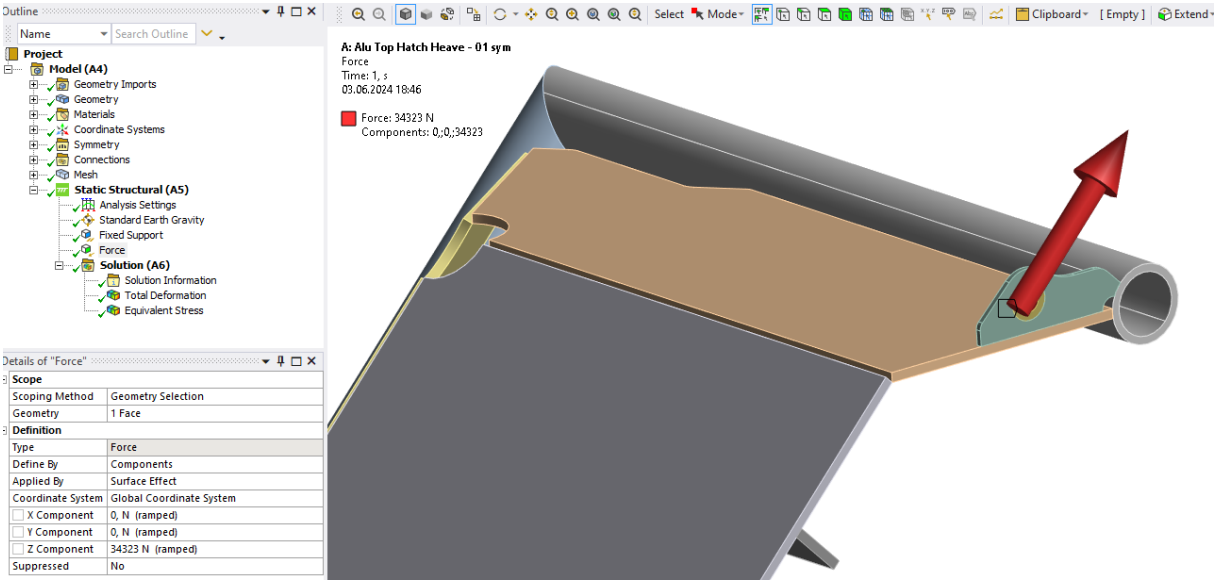


*Force Direction and Properties for Heave Motion Analyses.*

# B.7 Top Hatch – Dropped Object 100 mm

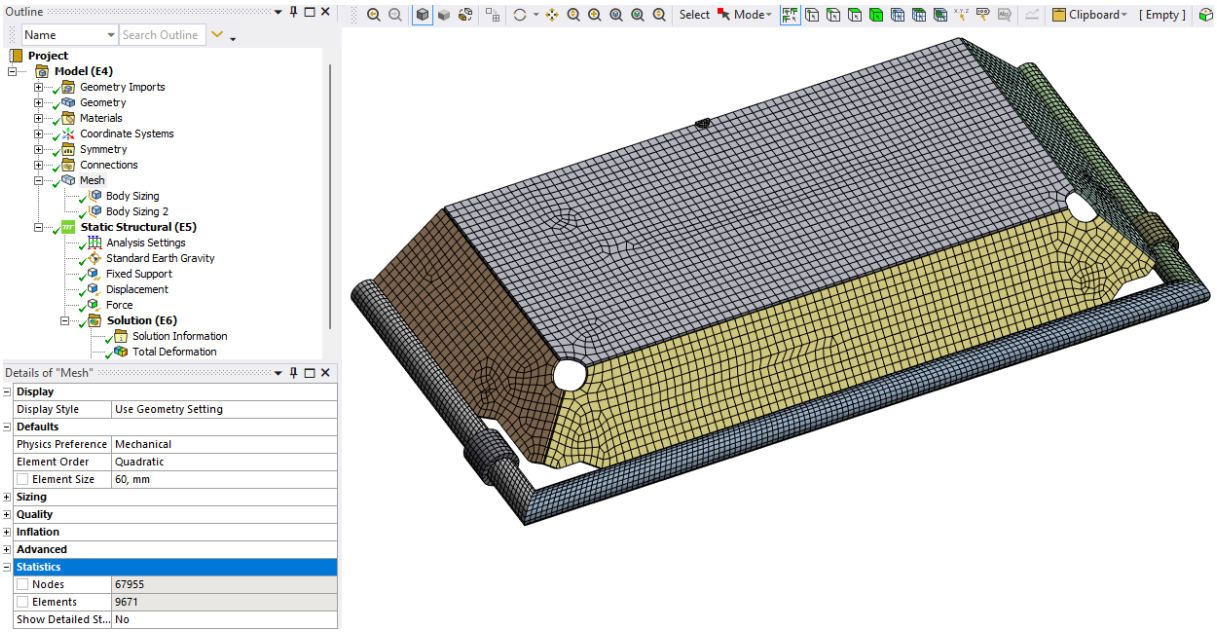


*Mesh Setting and Properties for Dropped Object 100 mm Analyses.*

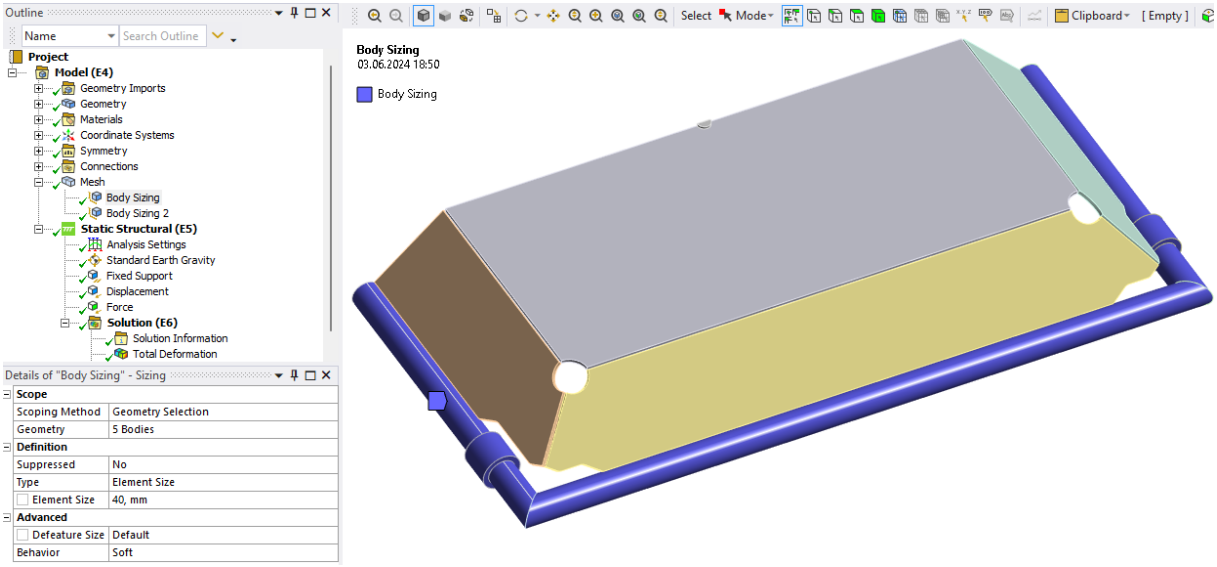


*Mesh Sizing 1 Setting and Properties for Dropped Object 100 mm Analyses.*

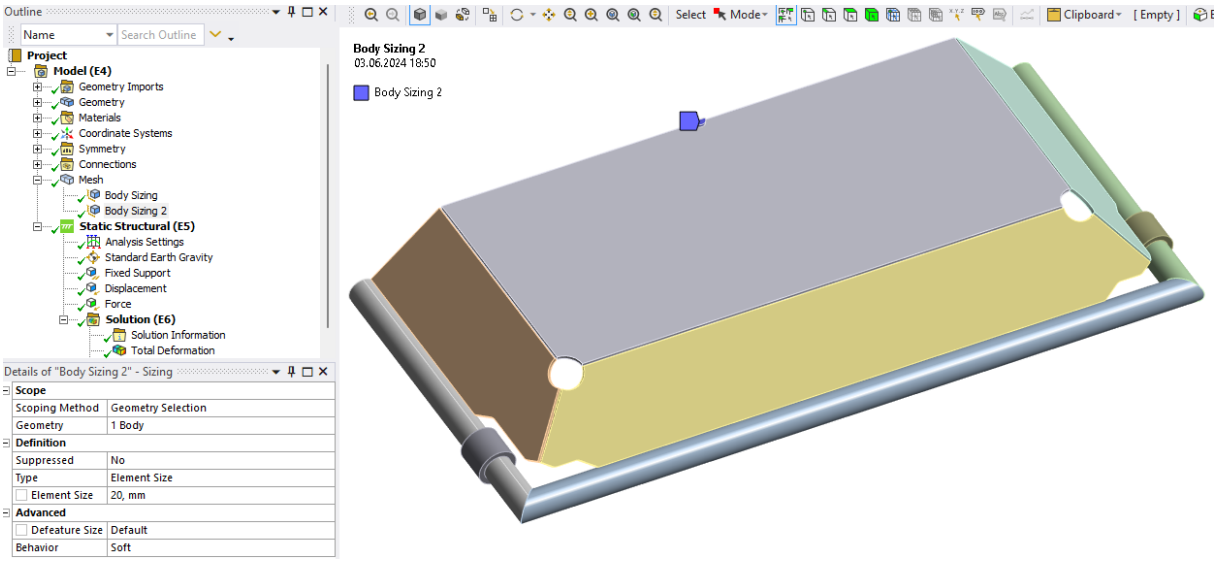


*Mesh Sizing 2 Setting and Properties for Dropped Object 100 mm Analyses.*

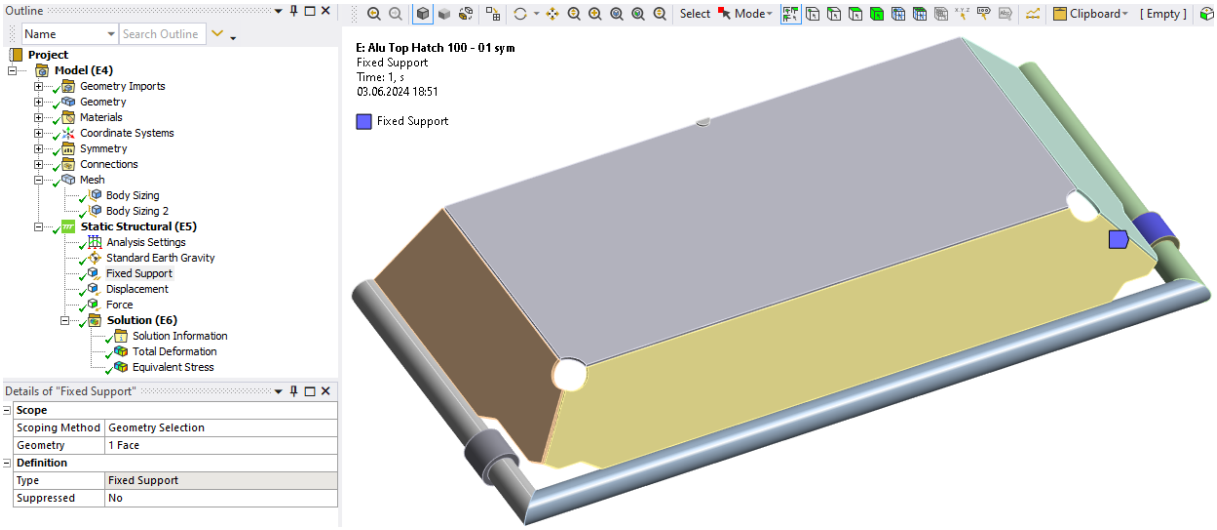


*Fixed Support Constrains for Dropped Object 100 mm Analyses.*

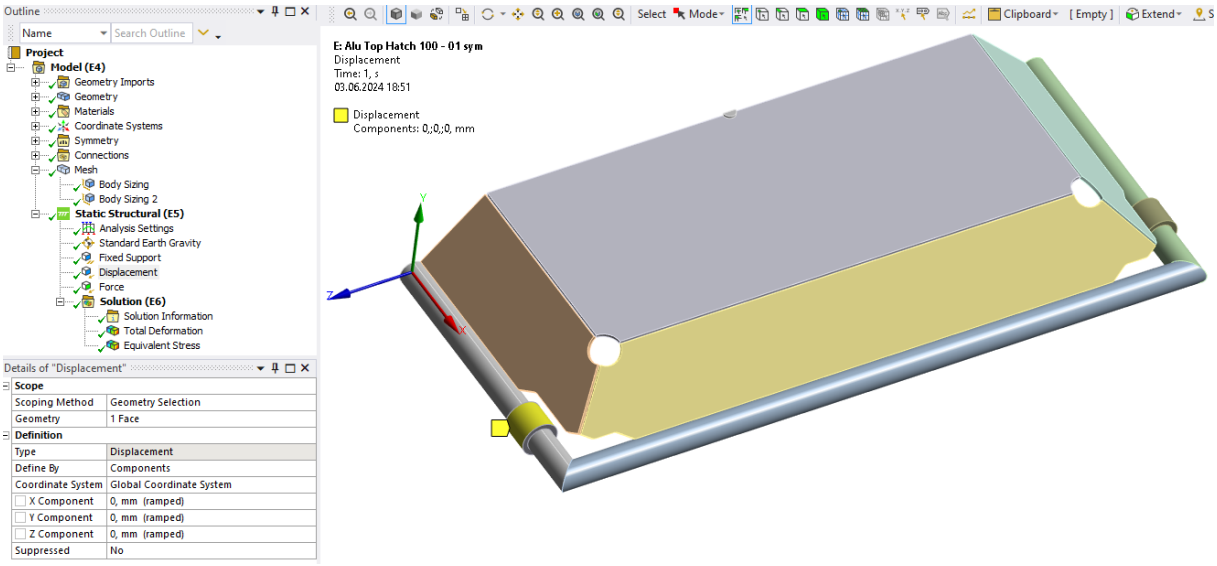


*Displacement Constrains for Dropped Object 100 mm Analyses.*

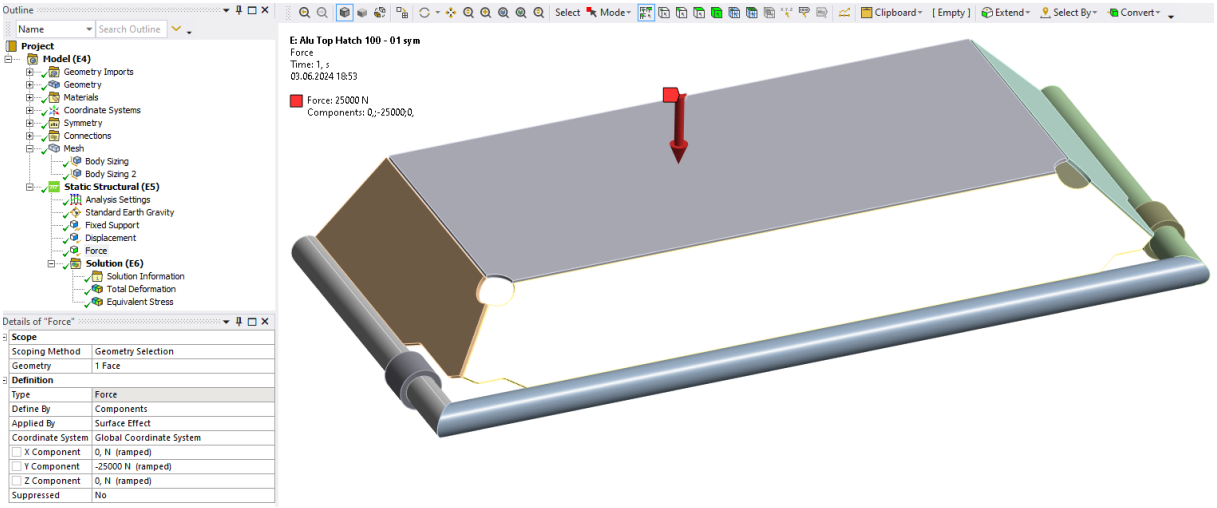


*Force Direction and Properties for Dropped Object 100 mm Analyses.*

# B.8 Top Hatch – Trawlnet Friction

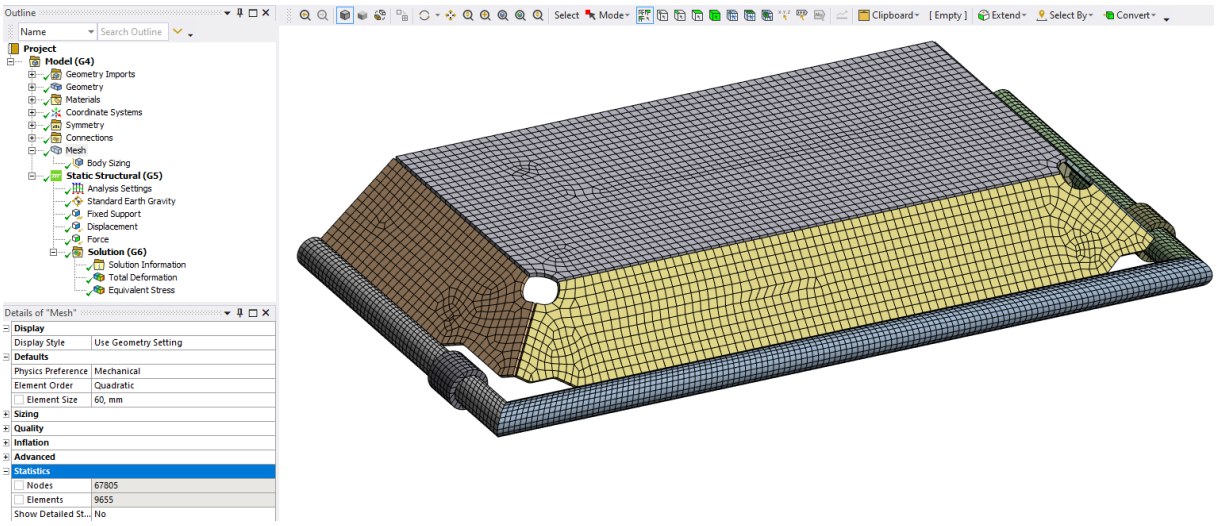


*Mesh Setting and Properties for Trawlnet Friction Analyses.*

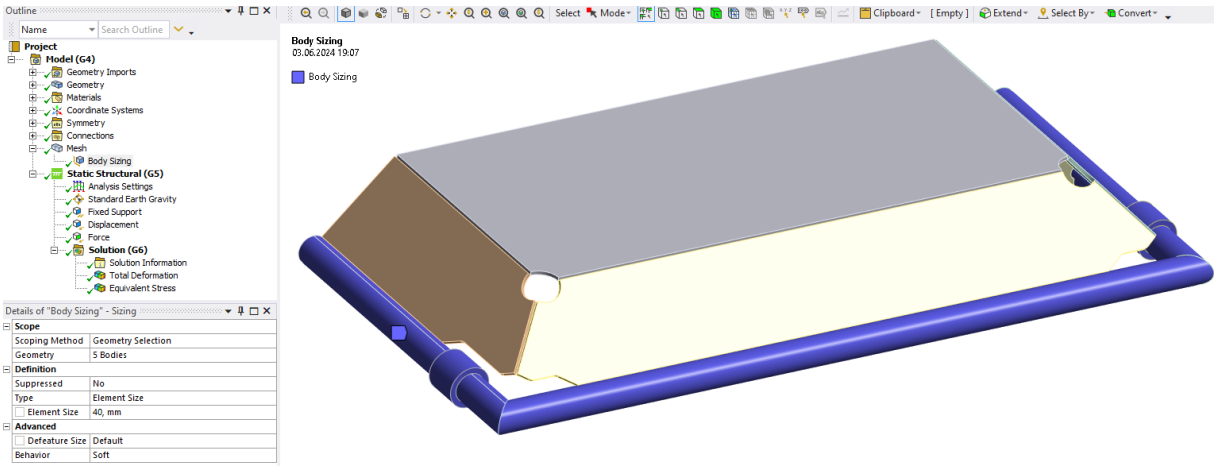


*Mesh Sizing 1 Setting and Properties for Trawlnet Friction Analyses.*

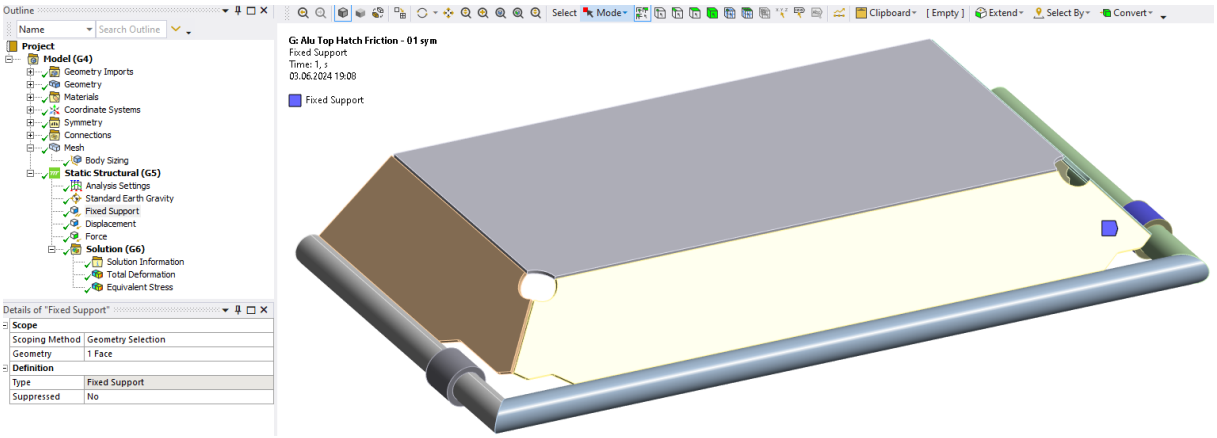


*Fixed Support Constrains for Trawlnet Friction Analyses.*

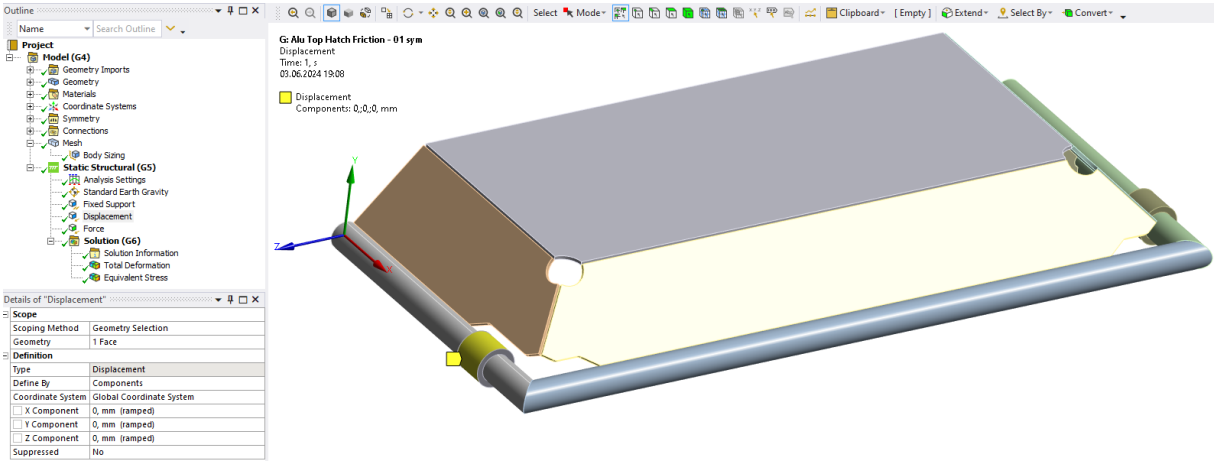


*Displacement Constrains for Trawlnet Friction Analyses.*

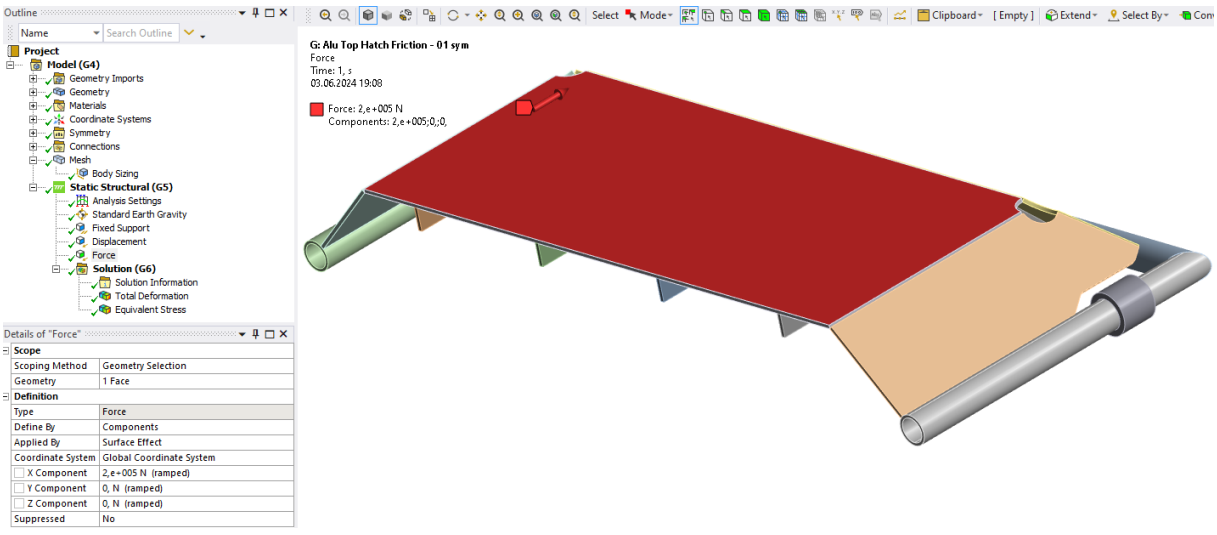


*Force Direction and Properties for Trawlnet Friction Analyses.*

# B.9 Steel frame – Trawlnet Friction

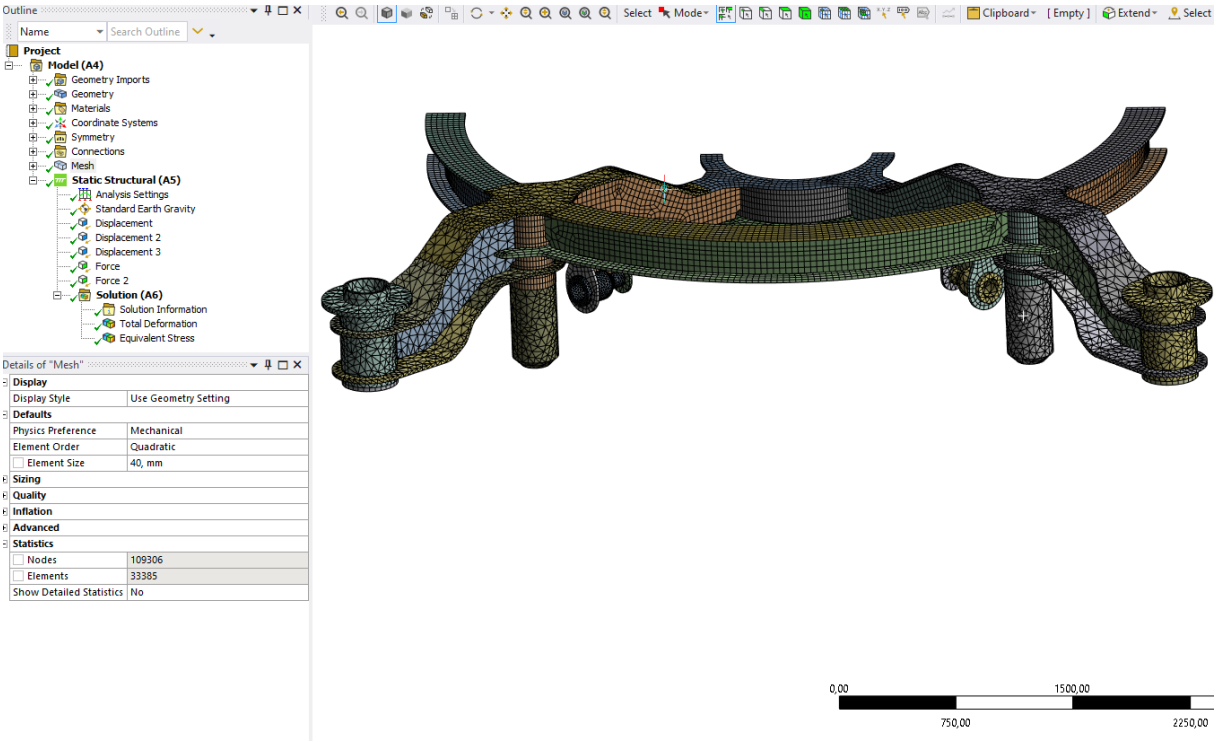


*Mesh Setting and Properties for Trawlnet Friction Analyses.*

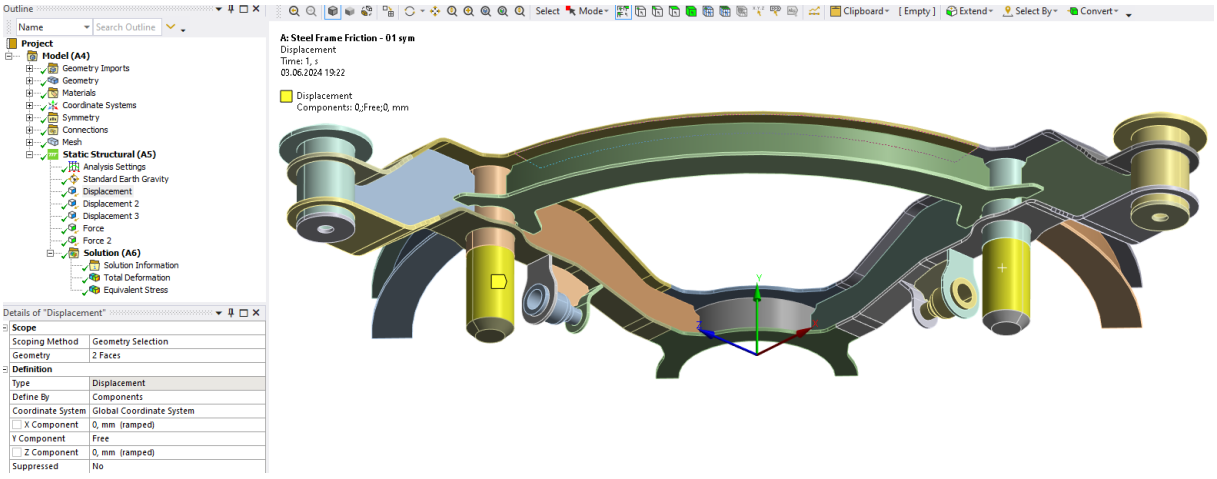


*Displacement 1 Constrains for Trawlnet Friction Analyses.*

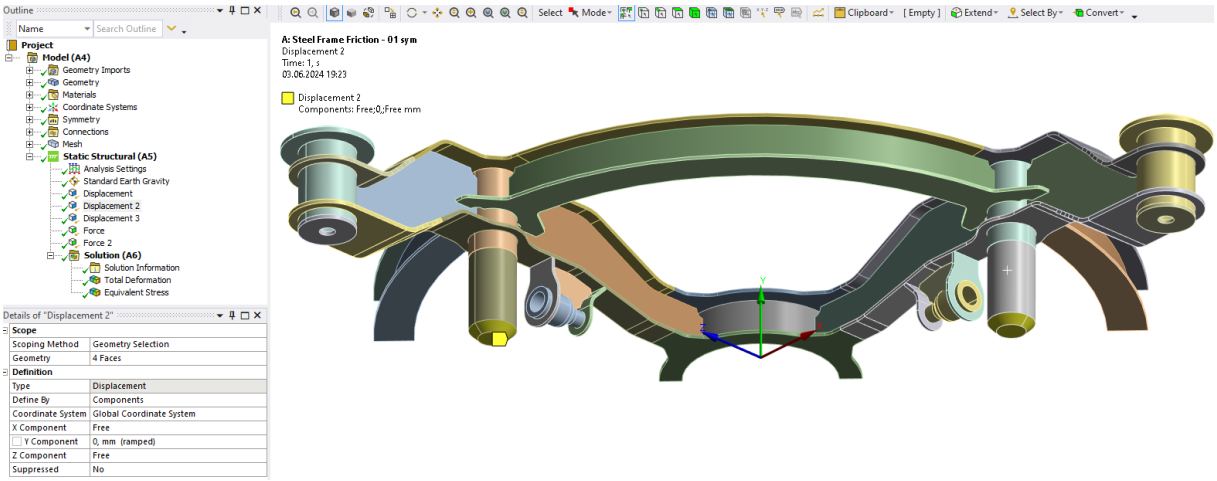


*Displacement 2 Constrains for Trawlnet Friction Analyses.*

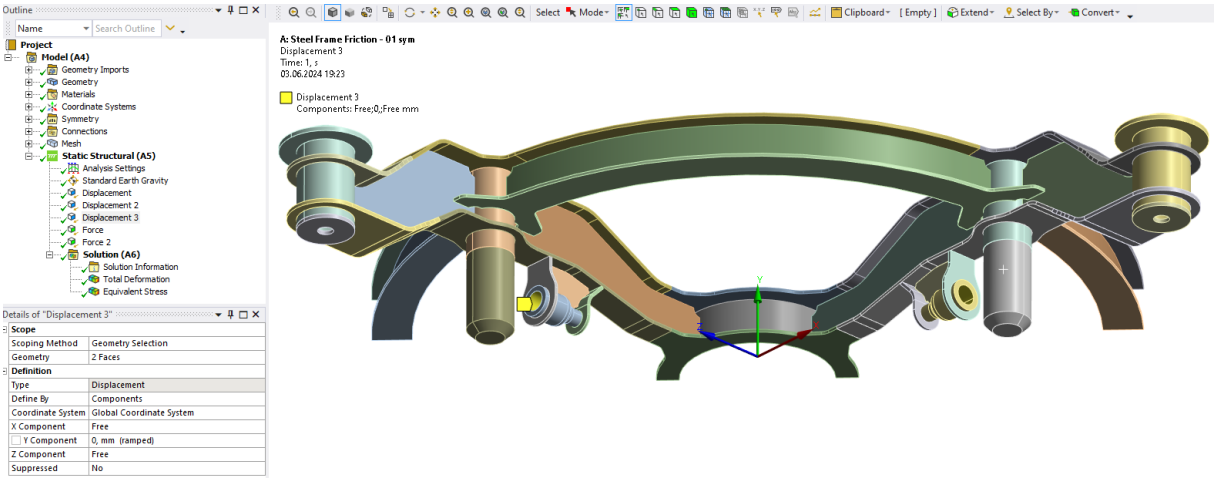


*Displacement Constrains for Trawlnet Friction Analyses.*

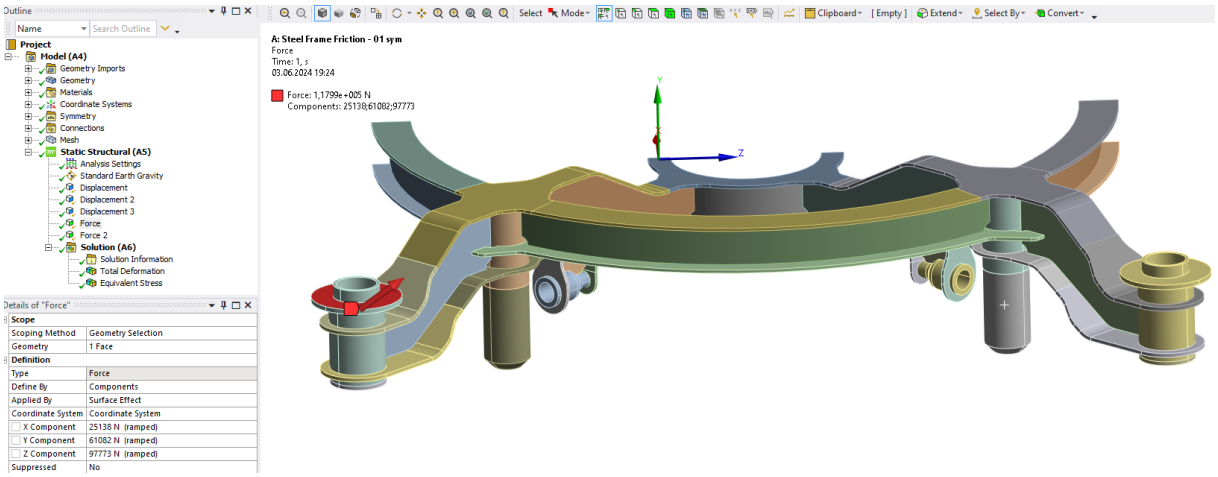


*Force 1 Direction and Properties for Trawlnet Friction Analyses.*

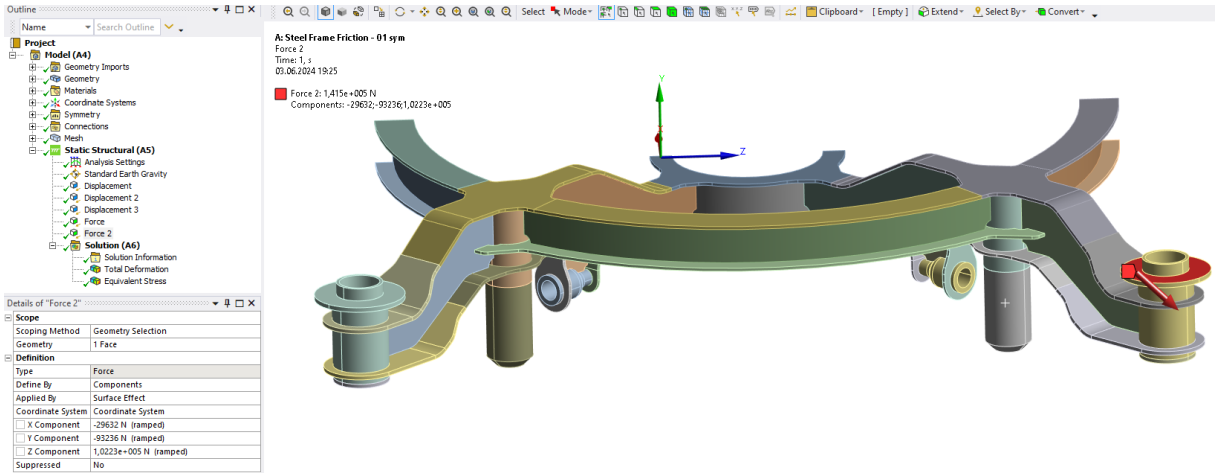


*Force 2 Direction and Properties for Trawlnet Friction Analyses.*

# Appendix C

# ANSYS Results with von Mises Stress Distribution for Final Model

## C.1 Aluminum Frame – Trawlnet Friction

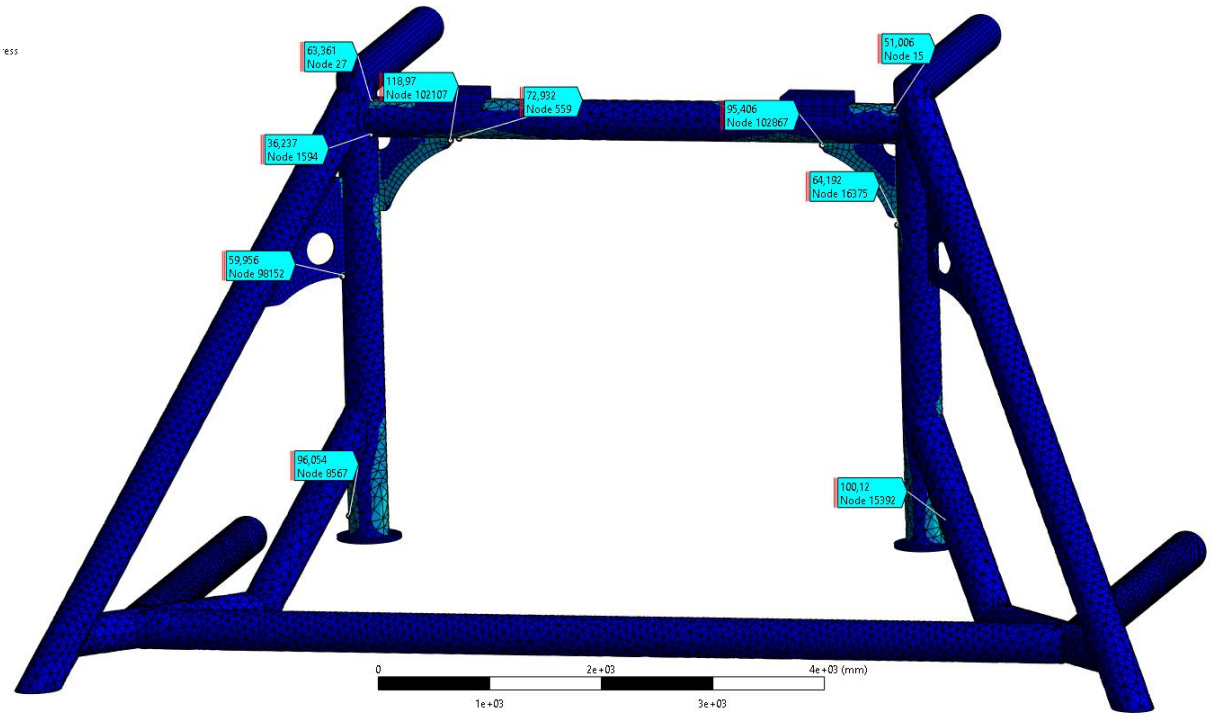


*Trawlnet Friction Load with Resulting Von-Mises Stresses.*

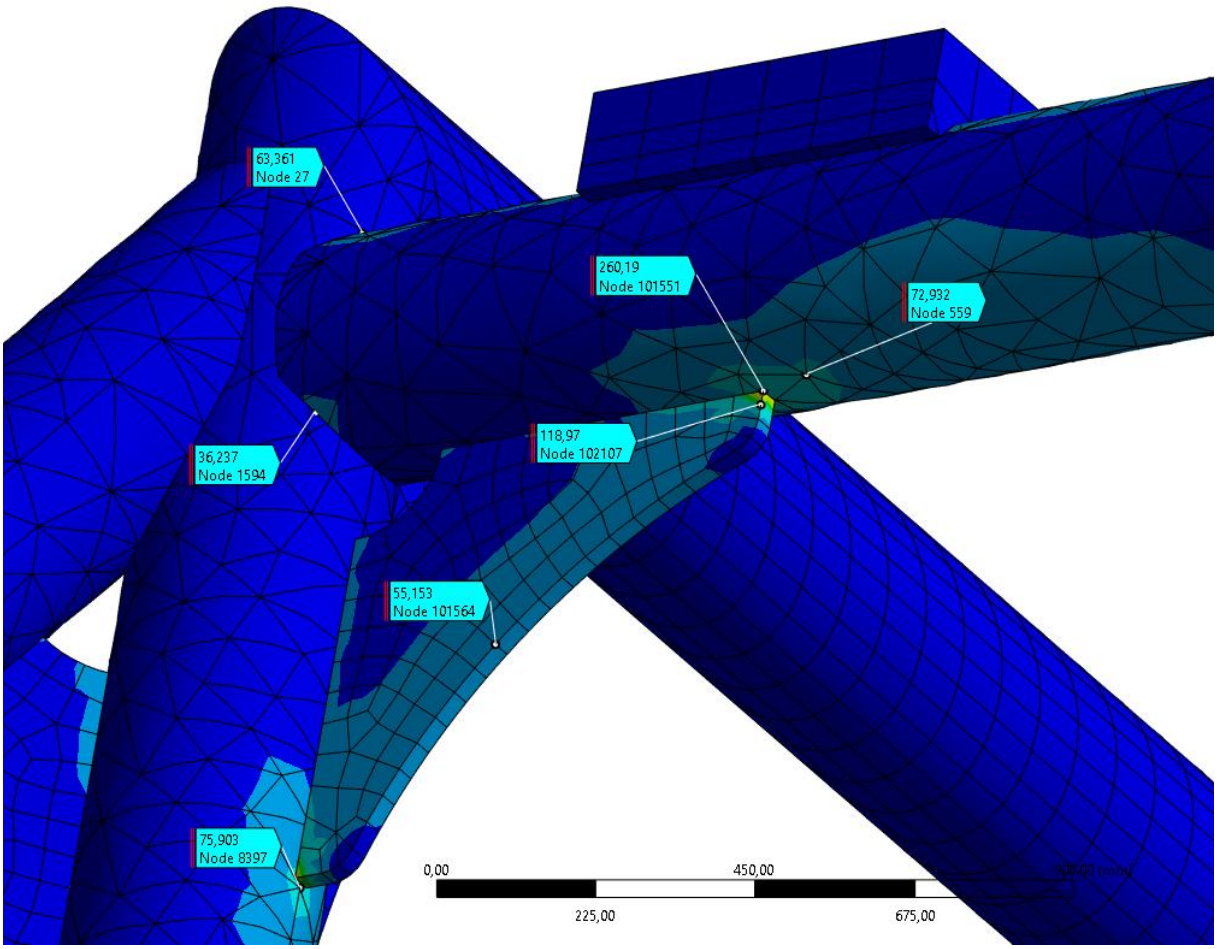


*Trawlnet Friction Load with Resulting Von-Mises Stresses.*

# C.2 Aluminum Frame – Trawlboard Overpull

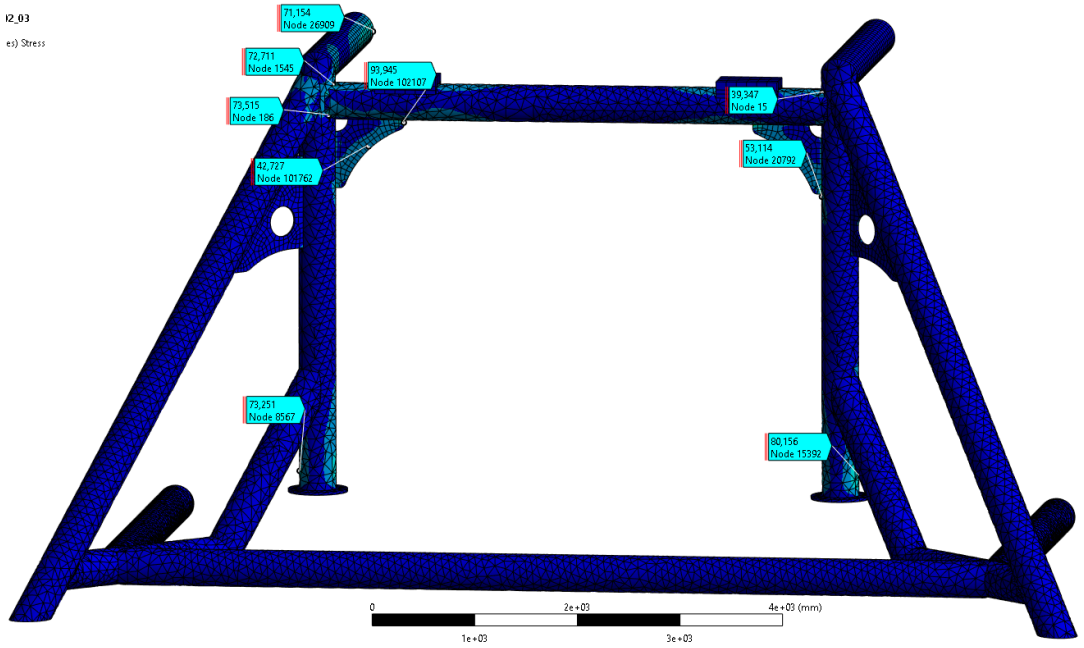


*Trawlboard Overpull Load with Resulting Von-Mises Stresses.*

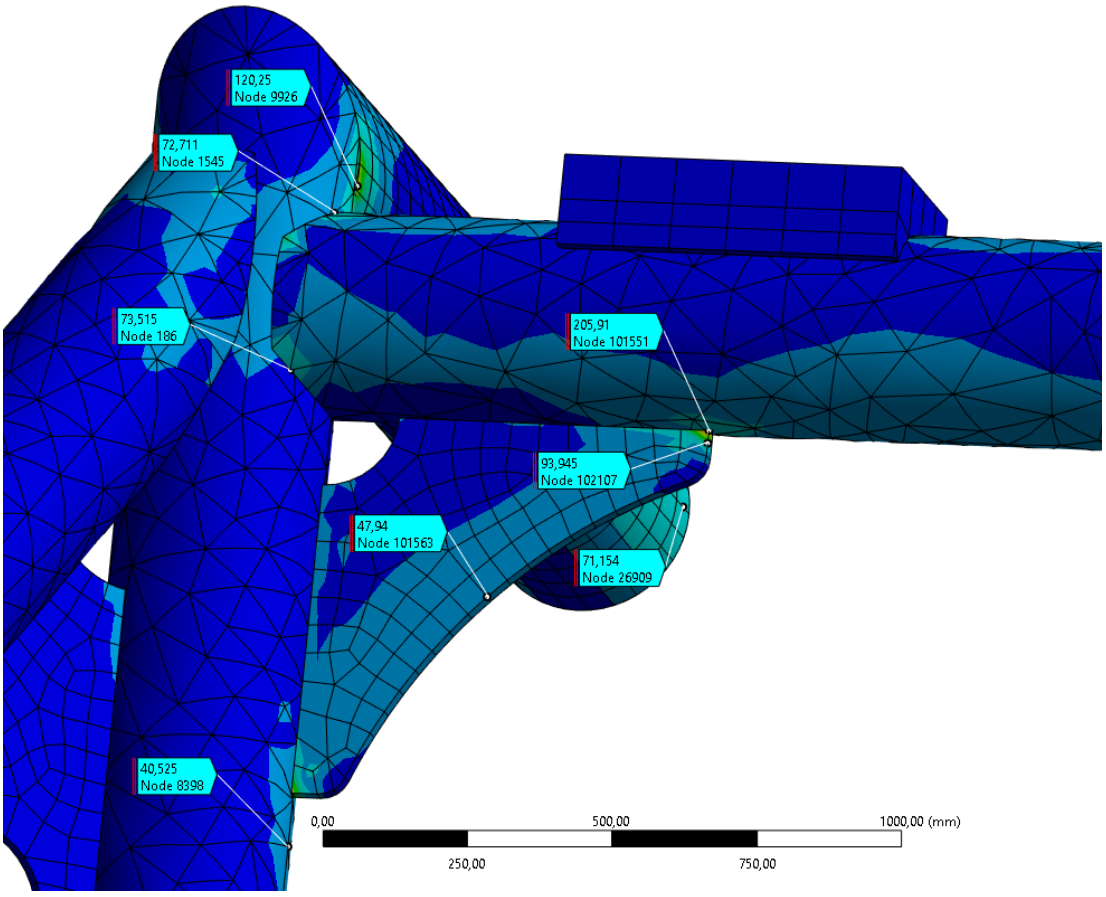


*Trawlboard Overpull Load with Resulting Von-Mises Stresses.*

## C.3 Front Hatch – Heave Motion

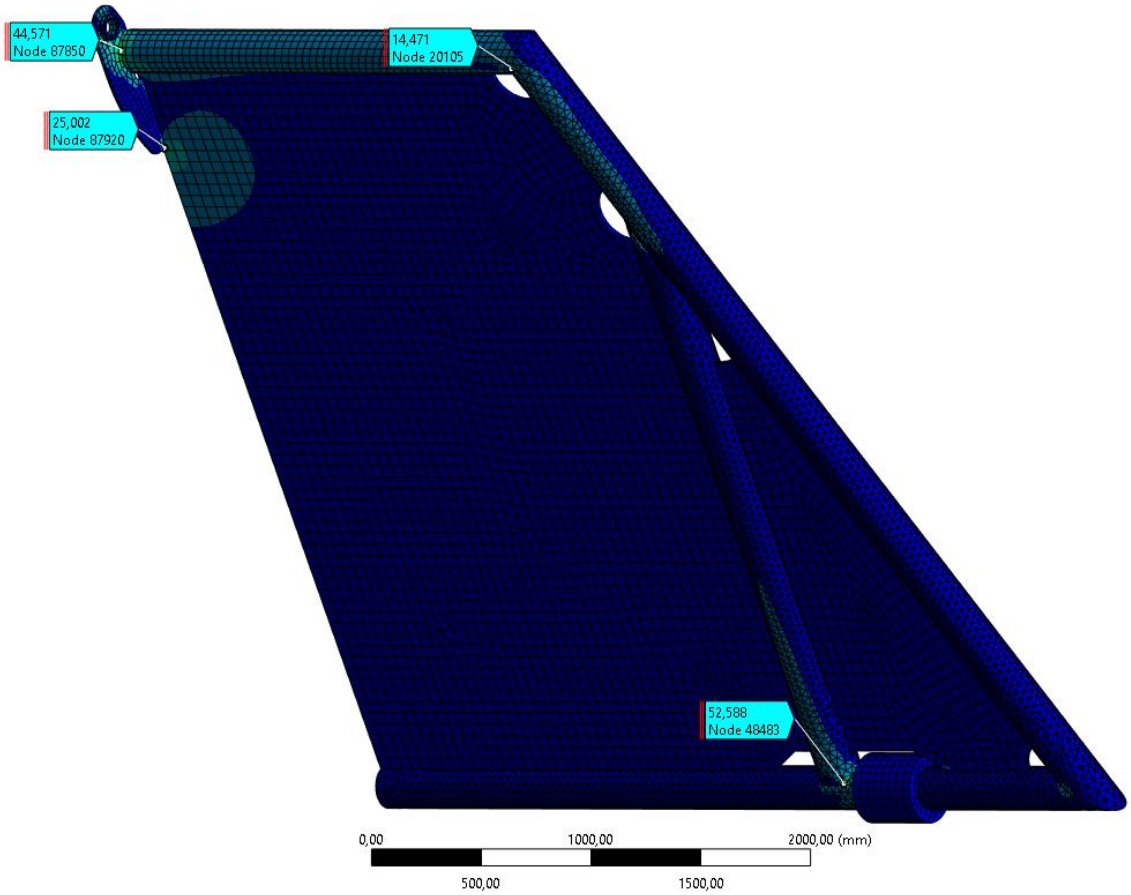


*Heave Motion Load with Resulting Von-Mises Stresses.*

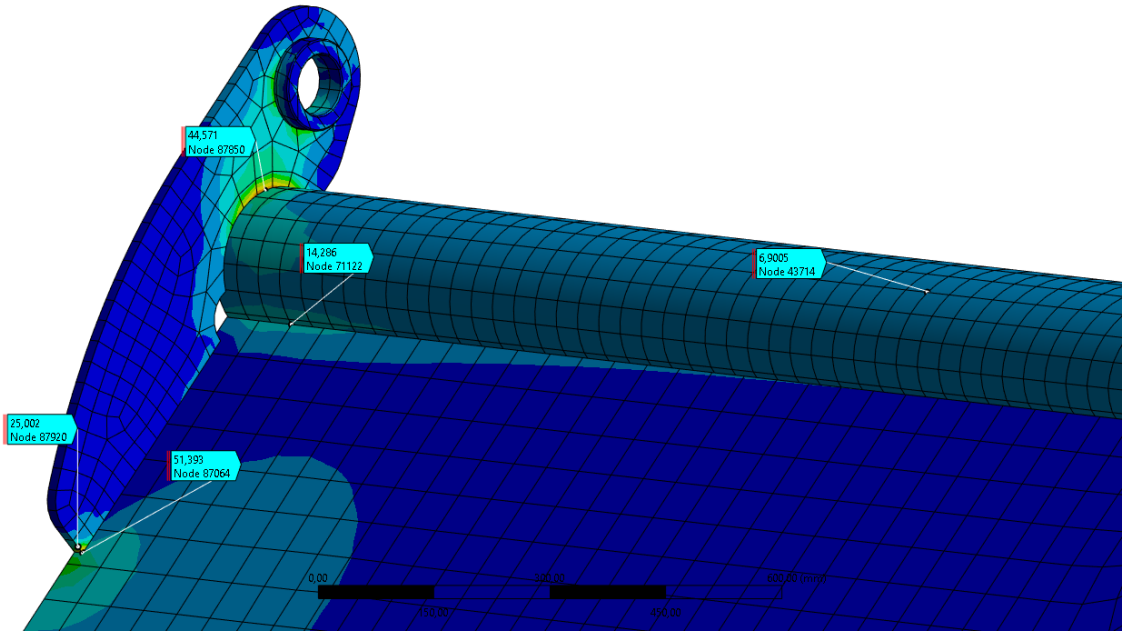


*Heave Motion Load with Resulting Von-Mises Stresses.*

# C.4 Front Hatch – ROV Parking

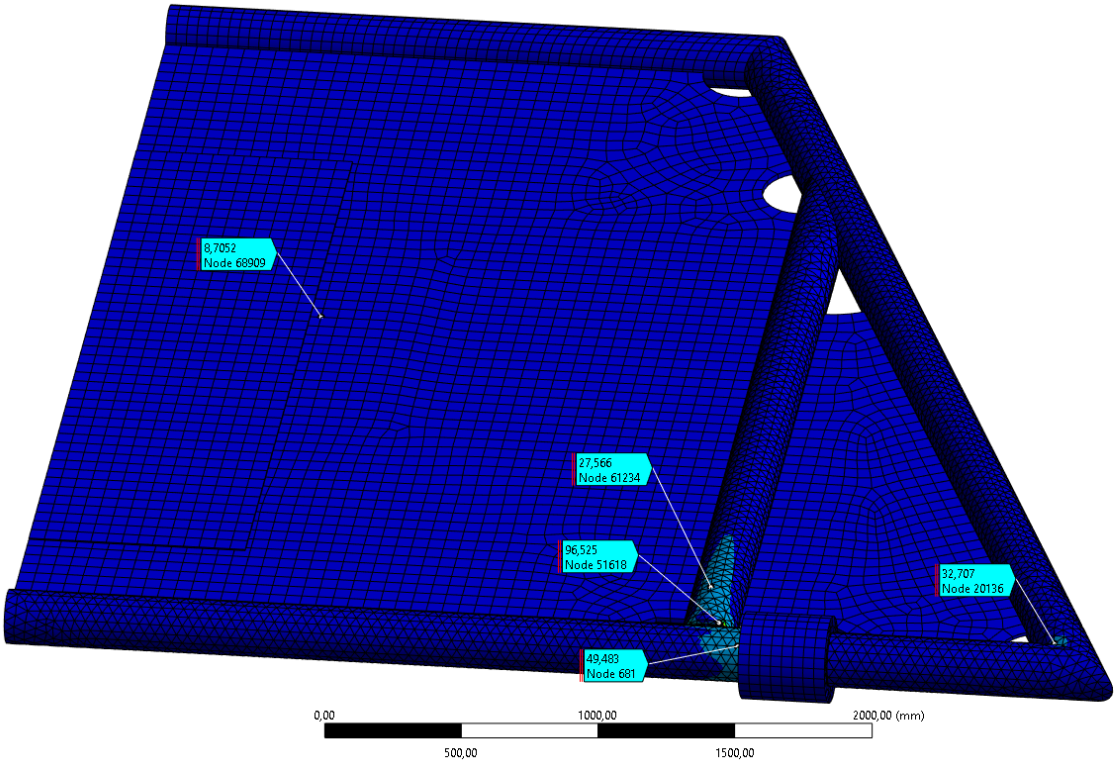


*ROV Parking Load with Resulting Von-Mises Stresses.*

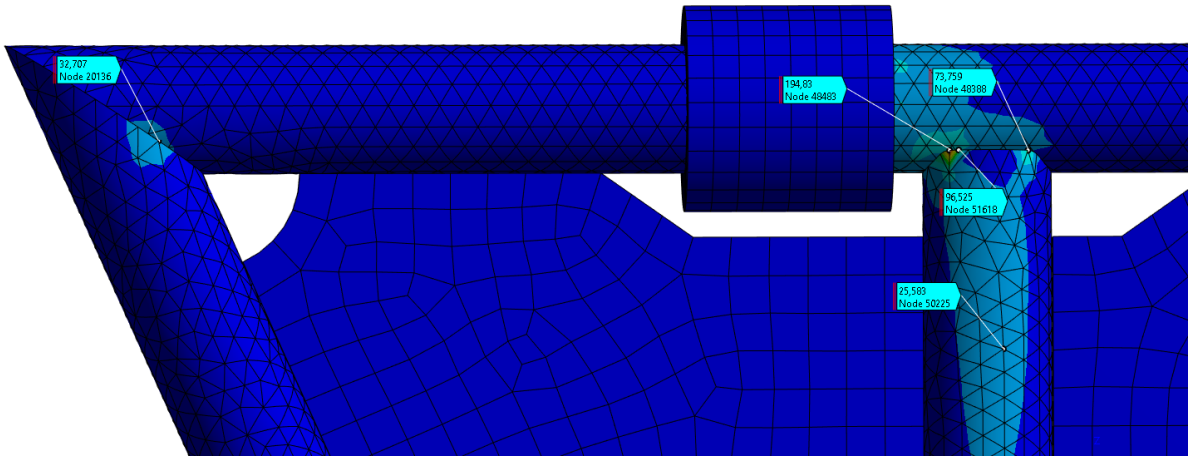


*ROV Parking Load with Resulting Von-Mises Stresses.*

# C.5 Front Hatch – Dropped Object 500 mm

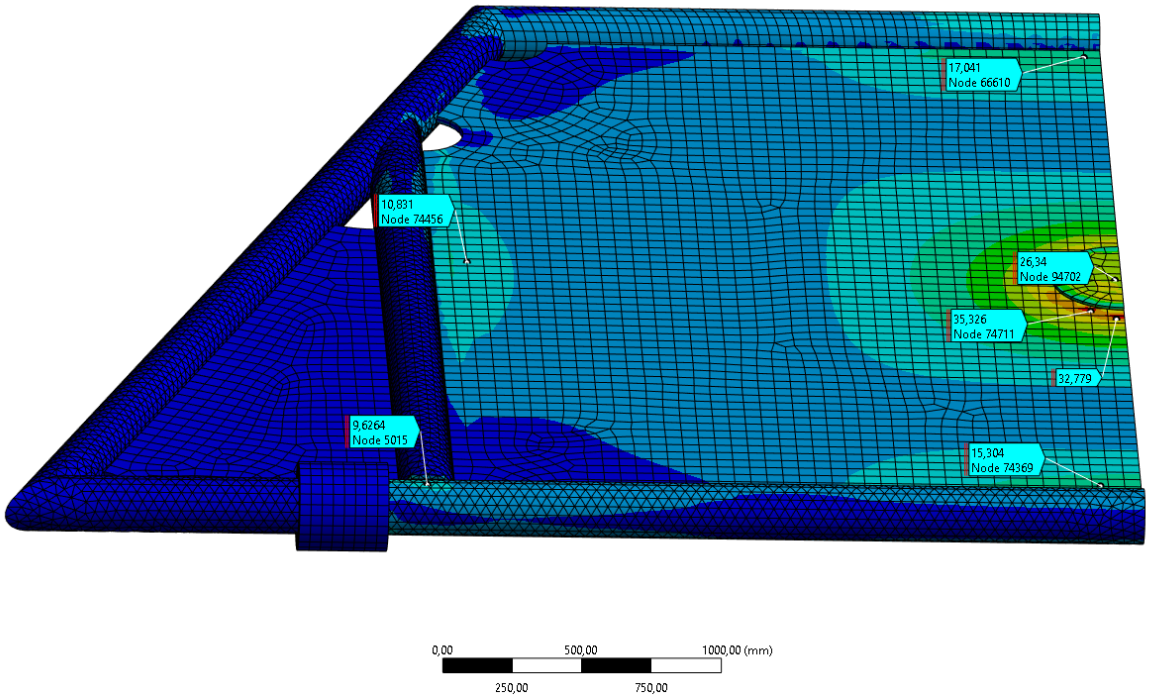


*Dropped Object 500 mm Load with Resulting Von-Mises Stresses.*

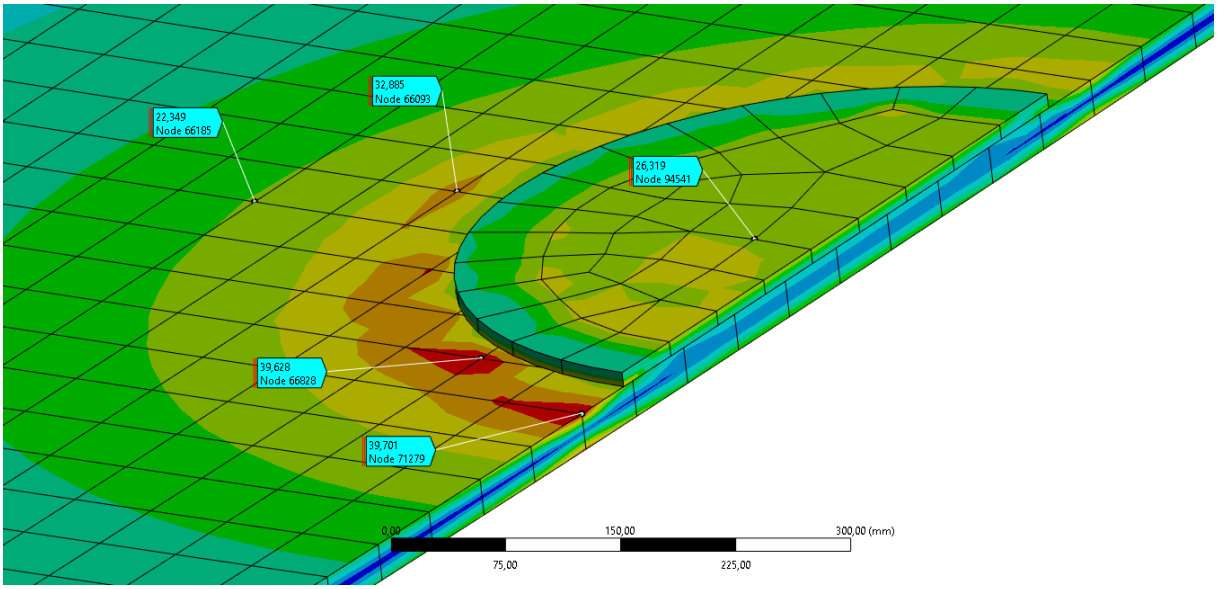


*Dropped Object 500 mm Load with Resulting Von-Mises Stresses.*

# C.6 Front Hatch – Dropped Object 100 mm

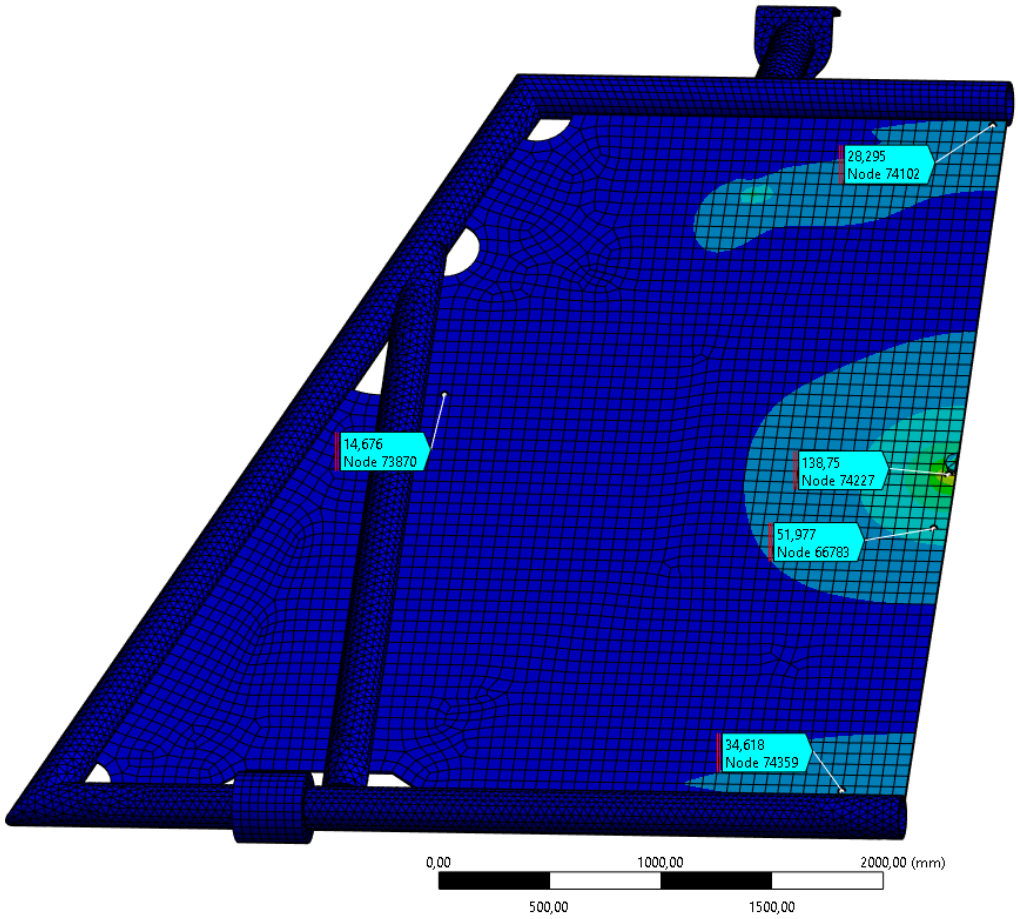


*Dropped Object 100 mm Load with Resulting Von-Mises Stresses.*

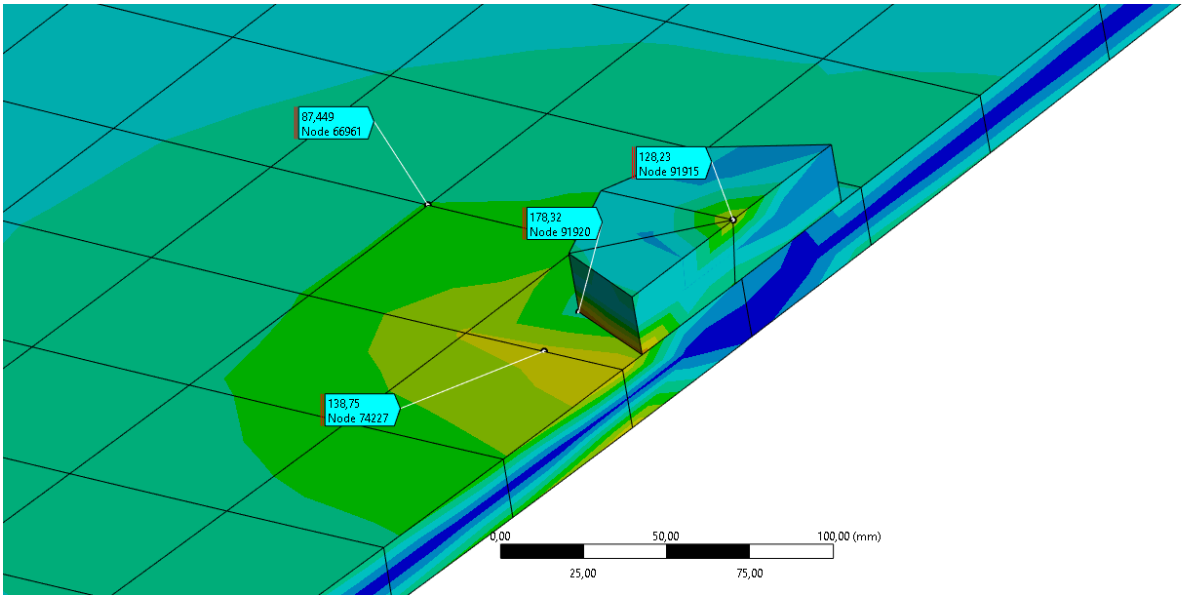


*Dropped Object 100 mm Load with Resulting Von-Mises Stresses.*

# C.7 Top Hatch – Heave Motion

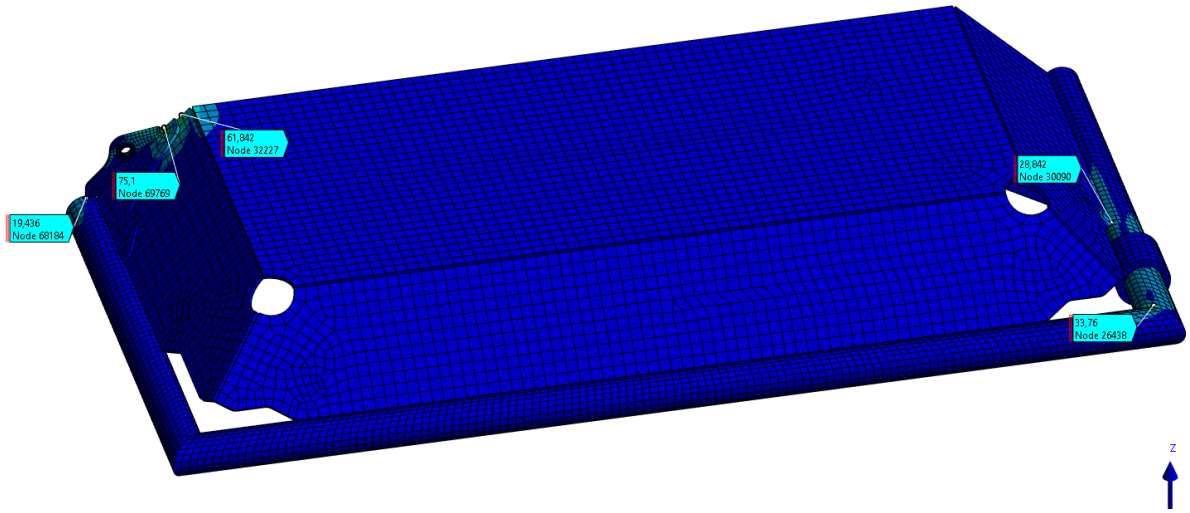


*Heave Motion Load with Resulting Von-Mises Stresses.*

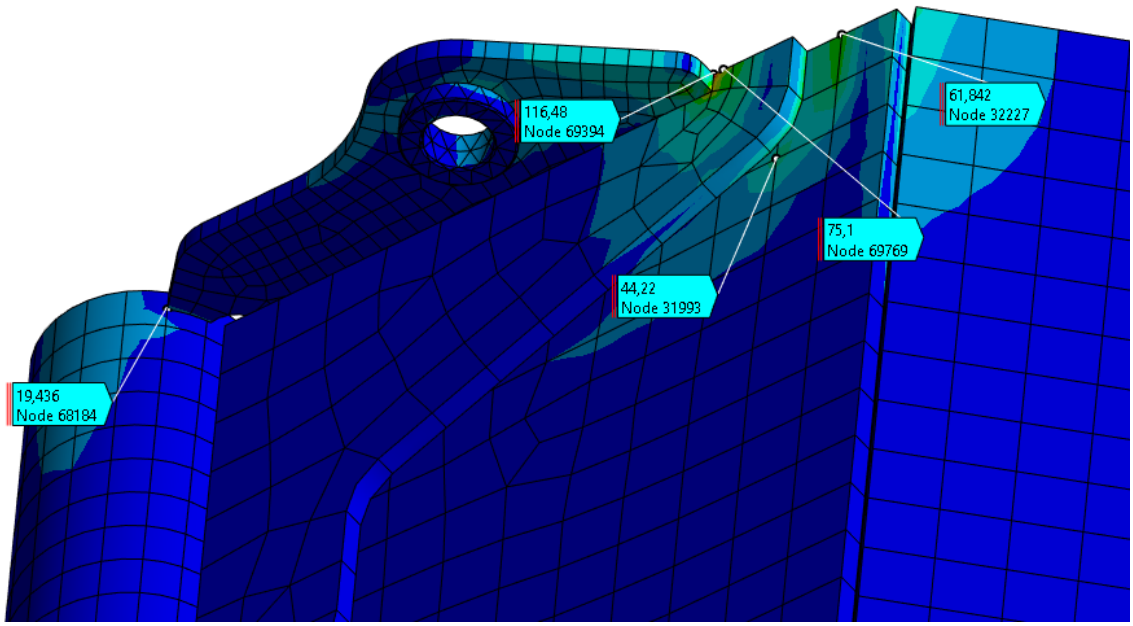


*Heave Motion Load with Resulting Von-Mises Stresses.*

# C.8 Top Hatch – Dropped object 100 mm

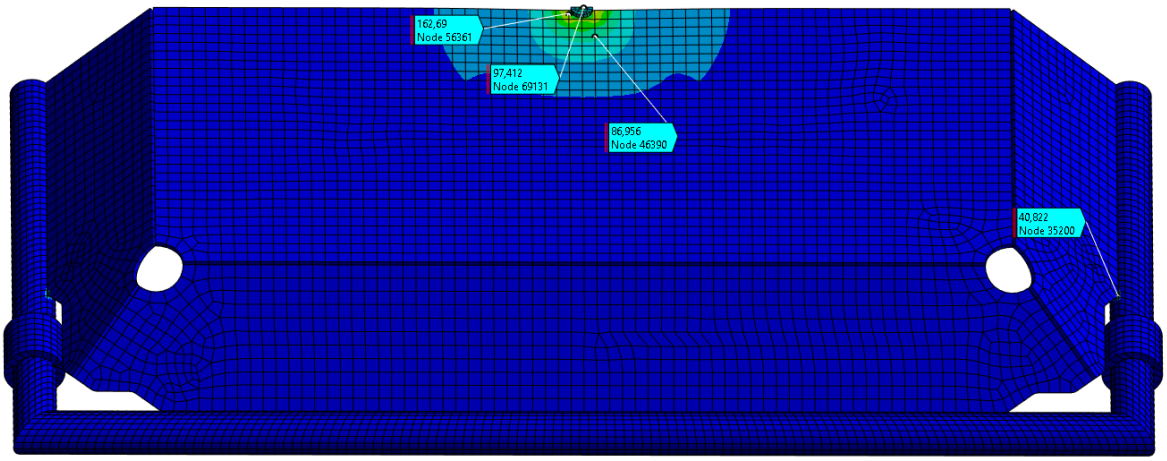


*Dropped Object 100 mm Load with Resulting Von-Mises Stresses.*

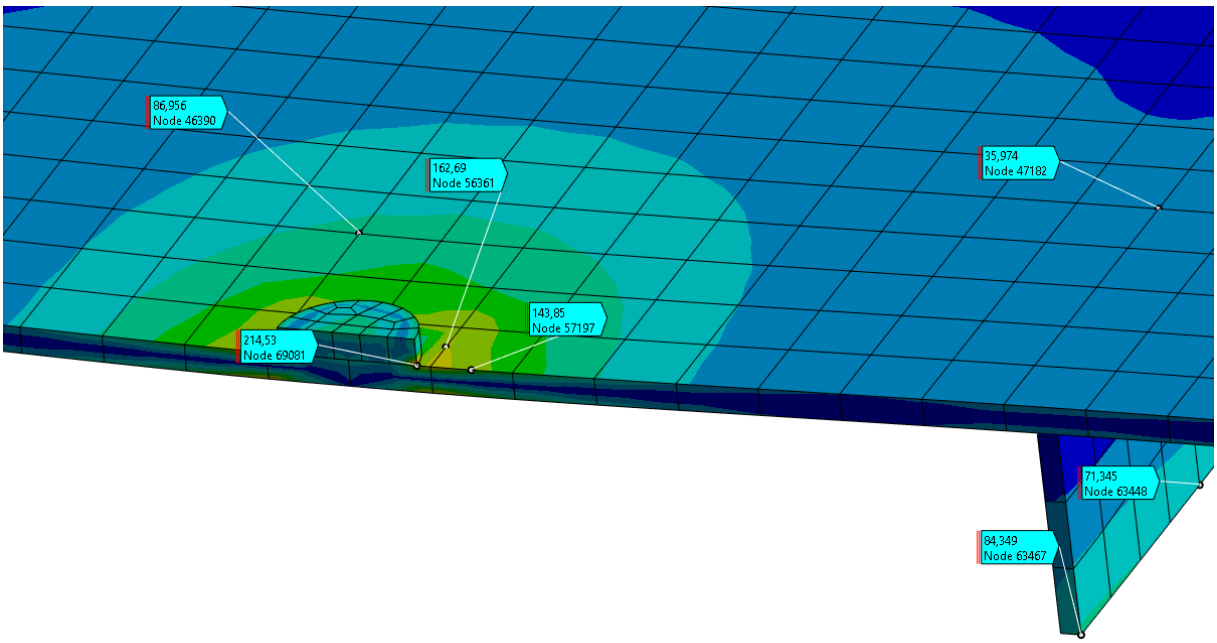


*Dropped Object 100 mm Load with Resulting Von-Mises Stresses.*

# C.9 Top Hatch – Trawlnet Friction

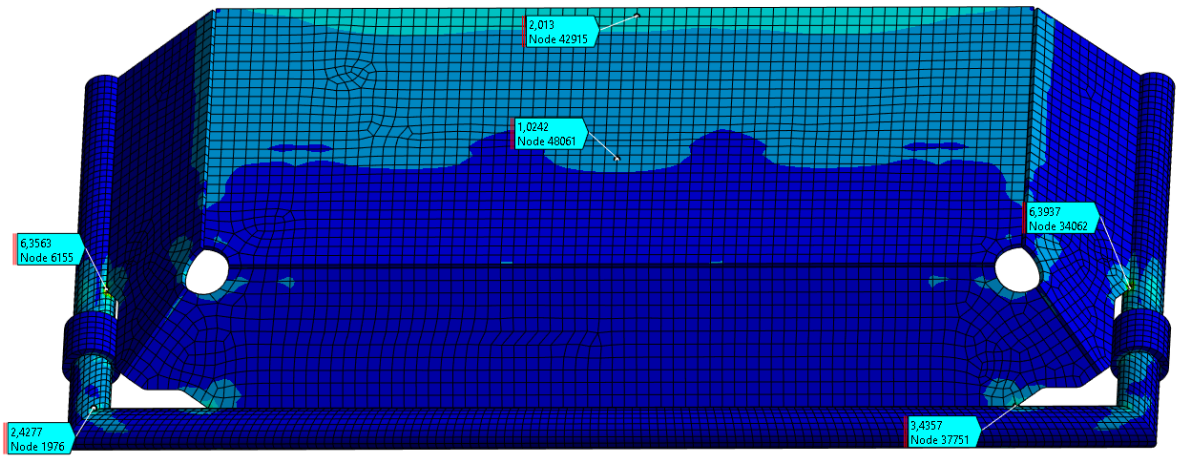


*Trawlnet Friction Load with Resulting Von-Mises Stresses.*

# C.10 Steel Frame – Trawlnet Friction

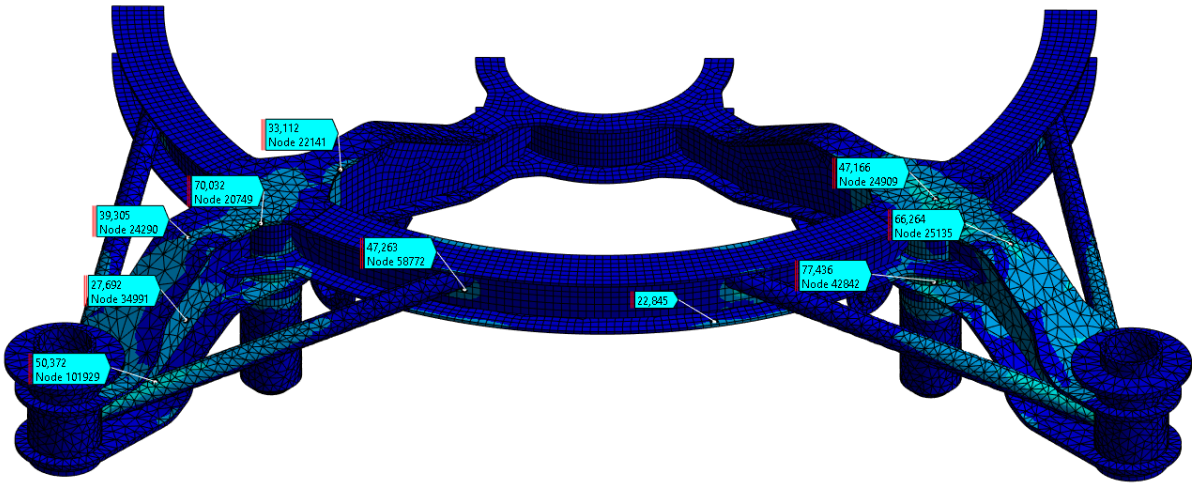


*Trawlnet Friction Load with Resulting Von-Mises Stresses.*

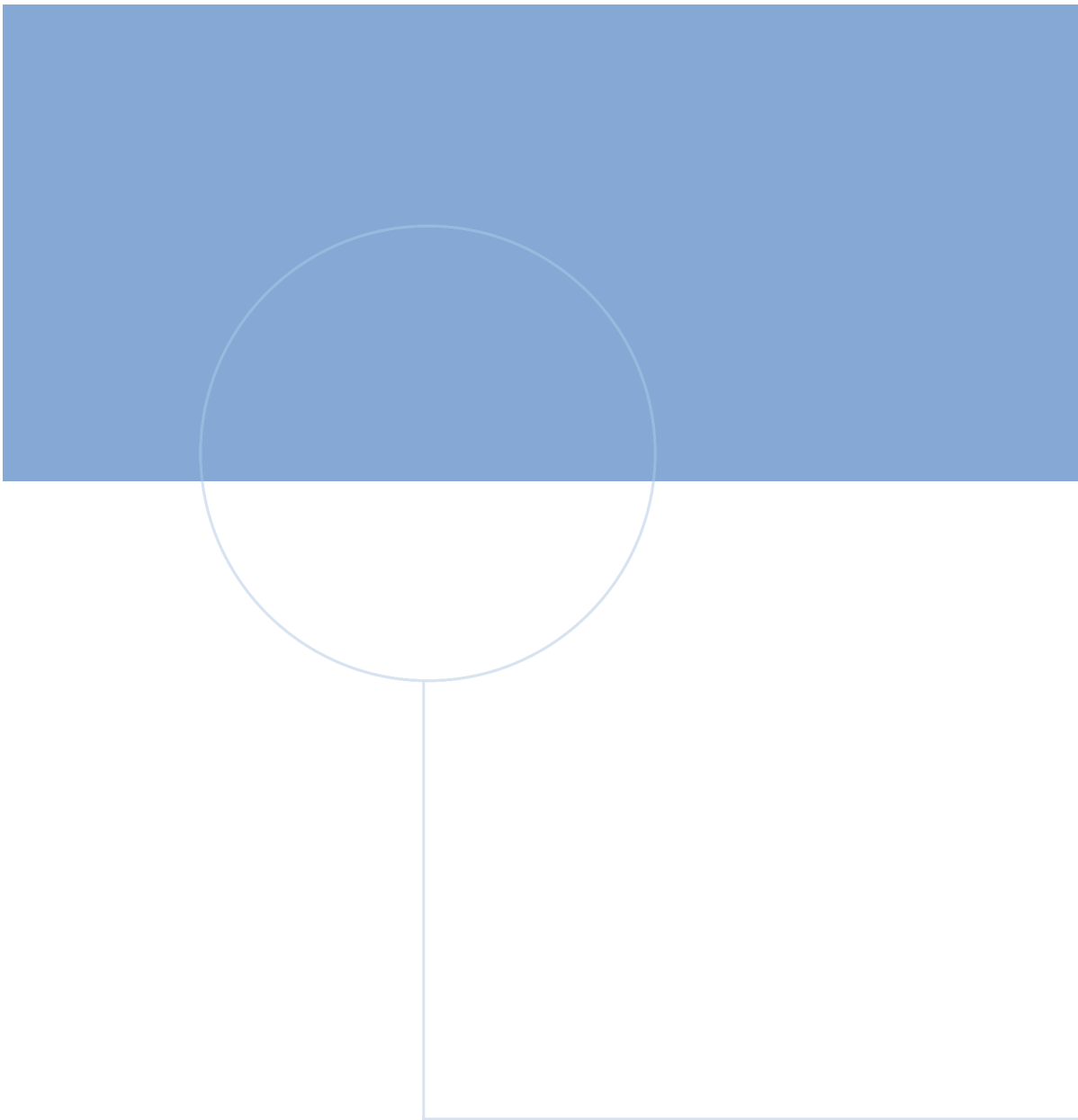

NTNU

Norwegian University of
Science and Technology